Universiteit Gent
Faculteit Wetenschappen
Vakgroep Geologie en Bodemkunde
Renard Centre of Marine Geology

The sediment dynamics along the Belgian shoreline, studied with airborne imaging spectroscopy and LIDAR

Bart Deronde

Faculteit
Wetenschappen

Scriptie voorgedragen tot het behalen van
de graad van Doctor in de Wetenschappen,
Richting Geologie

Gent, 2007

The sediment dynamics along the Belgian shoreline, studied with airborne imaging spectroscopy and LIDAR

Bart Deronde

Promotor
Prof. Dr. Jean-Pierre Henriet
Vakgroep Geologie en Bodemkunde
Renard Centre of Marine Geology
Krijgslaan 281- S8
9000 Gent

Co-promotor
Dr. Vera Van Lancker
Vakgroep Geologie en Bodemkunde
Renard Centre of Marine Geology
Krijgslaan 281- S8
9000 Gent

Co-promotor
Dr. Rik Houthuys
Zelfstandig Geograaf
Suikerkaai 8
1500 Halle

Dankwoord

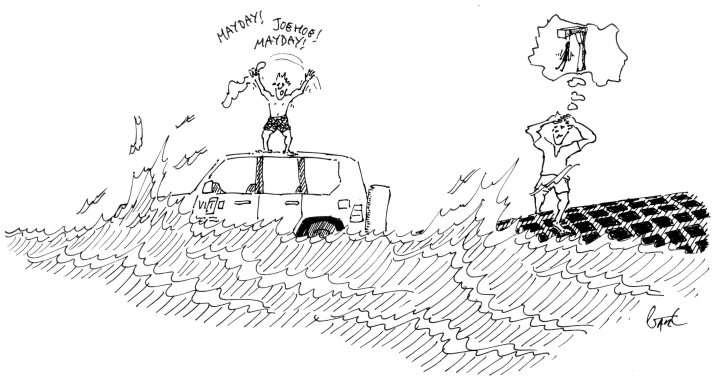

September 2000, een mooie nazomerdag, ergens in duinen van Oostduinkerke…

Ik zat de doctoraatsthesis van Valéry Gond te lezen, een boeiend werk over het gebruik van lage resolutie teledetectie voor de opvolging van de Afrikaanse Savanne. Als logisch vervolg op mijn licentiaatverhandeling zou ik ook een doctoraat maken, toegepast op de vegetatie in Afrika. Nu ik zeven jaar later in diezelfde duinen rondloop, kan ik niet anders dan erom glimlachen. Van de vegetatie in Zuidoost-Afrika naar het strand aan onze Belgische kust. Van de verre droom terug stevig met mijn voeten op de grond, de grond waar ik als kleine rakker graag rondliep. Het kan verkeren…

Eén en ander heb ik te danken aan een aantal mensen bij de Afdeling Kust (Vlaamse Overheid) in Oostende. Ik denk hierbij in het bijzonder aan ir. Peter De Wolf, ir. Toon Verwaest, ir. Stefaan Gysens, en ir. Kevin Delecluyse, die VITO een aantal jaren onderzoeksopdrachten toevertrouwden i.v.m. de opvolging van onze stranden d.m.v.

hyperspectrale teledetectie. Dit onderzoek vormde de basis voor deze thesis en ik ben deze personen daar dan ook oprecht dankbaar voor. Maar, mijn collega's zullen het beamen, vooraleer je op VITO een leuk onderzoeksproject kan uitvoeren, moet je het eerst zien binnen te halen! De onderzoeker als sales manager… dit ware echter nooit gelukt zonder de steun van een aantal gedreven VITO'ers; ik denk hierbij in de eerste plaats aan Dirk Fransaer die ondanks zijn functie van afgevaardigd bestuurder steeds de tijd vond om me te helpen dit onderzoek naar VITO te halen en het met interesse op te volgen. Maar op VITO zijn er nog veel meer mensen die ik van harte wil danken en zonder wie dit werk er nooit was geweest. Het is een cliché zo hoog als de appartementen op de zeedijk, maar het is de enige waarheid. In de eerste plaats mijn schitterende collega's van de hyperspectrale groep, Koen, Els, Sindy, Ils, Luc, Pieter, Marcel en Johan. Hun vakkennis heeft mij vaak de nodige duw in de rug gegeven op de punten waar ik tekort schoot. Mijn zeer sterke appreciatie hiervoor. Ook Walter, die aan de basis ligt van het hyperspectrale gebeuren in VITO, verdient een bijzonder woord van dank, net als Jurgen, Gil en Dirk. Stuk voor stuk steengoede en fijne collega's waar ik dagelijks veel van opsteek en die ik erg waardeer.

Een bijzondere vermelding in dit rijtje verdient Rik Houthuys. Deze halve VITO'er, die net iets te ver van VITO woont om een hele VITO'er te worden, heeft me eenvoudigweg álles over de kust geleerd. Als er al iemand is waarmee dit doctoraat staat of valt, is het zeker Rik. Rik, ik ben je hiervoor als collega en als vriend uiterst dankbaar.

Maar, -vergeef me de volgorde, in een verhaal staat de 'clou' ook nooit vooraan- er is nog een belangrijke schakel in dit verhaal. En ik zou geen goede geograaf zijn als ik deze niet halverwege tussen VITO en de kust zou hebben gezocht. Prof. Jean-Pierre Henriet en dr. Vera Van Lancker van het Renard Centre of Marine Geology in Gent ben ik erg dankbaar omdat zij me de kans hebben geboden dit doctoraat uit te werken. Ondanks het feit dat ik niet volledig in het plaatje van de vakgroep paste -ik zat immers in een vliegtuig en niet op een boot-, hebben zij dit doctoraat steeds loyaal gesteund. Een oprechte dank u, Vera en Prof. Henriet!

En dan, "Doe er toch maar mee voort", "Je weet nooit waarvoor dat goed kan zijn", "Je hebt er nu al zo veel voor gedaan", "Komaan Bart!". Zonder twijfel waren mijn ouders, mijn kameraden (dank voor de leuke cartoon, Bart!) en vooral mijn Liesbetje in dit werk de belangrijkste schakels. Hen voldoende bedanken is niet eens mogelijk op dit A4'tje…

Tot slot dank ik alle nalezers van dit werk en alle leden van de lees- en examencommissie voor hun waardevolle bijdrage.

Mol, juni 2007

Contents

List of Acronyms

AISA	Airborne Imaging Spectrometer for Applications
ASD	Analytical Spectral Devices, Inc.
BSI	Beach State Index
CAR	Carbonates
CASI	Compact Airborne Spectrographic Imager
D50	Median Grain Size
DEM	Digital Elevation Model
DTM	Digital Terrain Model
ED-XRF	Energy Dispersive X-Ray Fluorescence
FA	Factor Analysis
FWHM	Full Width at Half of Maximum
GPS	Global Positioning System

HALE-UAV	High Altitude Long Endurance – Unmanned Aerial Vehicle
HyMap	Hyperspectral Mapper
ICZM	Integrated Coastal Zone Management
IMU	Inertial Measurement Unit
INS	Inertial Navigation System
IPCC	Intergovernmental Panel on Climate Change
IS	Imaging Spectroscopy
LDA	Linear Discriminant Analysis
LDC	Linear Discriminant Classifier
LIDAR	LIght Detection And Ranging
ORG	Organic Matter
NAP	Nieuw Amsterdams Peil
PCA	Principal Component Analysis
PDF	Probability Density Function
S	Sorting
SAM	Spectral Angle Mapper
SFFS	Sequential Floating Forward Search
SWIR	Short-Wave InfraRed light
TAW	Tweede Algemene Waterpassing
VIS	VISible light
VNIR	Visible and Near InfraRed light

Summary

Recent indications and model predictions leave little room for argument that the sea level worldwide is rising and that the rising will continue and will even be accelerated in the next decades. Many factors have been identified in causing the sea level rise, with warming of the oceans and melting of land ice as the dominant players. The anthropogenic influence in this process has recently been confirmed by the Intergovernmental Panel on Climate Change (IPCC). The rising of the sea level goes hand in hand with climate changes that are expected to cause more storminess along the western European coastline, as well as along many other coastlines. Even without an intensified storminess and an accelerated sea level rise, the western European coastline, and more in particular the Belgian shoreline, needs permanent attention as this shoreline is highly prone to erosion. The huge socio-economic value of the Belgian shoreline, which asks for a stable and save shoreface, is not compatible with the dynamic nature of the system. Therefore man has strived to keep the shoreline at its position for many decades. As a result of all this, the regular monitoring of the Belgian shoreline is absolutely necessary. In this thesis, two state-of-the-art remote sensing techniques have been explored to monitor the Belgian shoreline in the period 2000 – 2006. Airborne LIDAR or laserscanning is a well-known technique that allows making accurate Digital Terrain Models (DTMs) of the beach environment. Successive DTMs were used to calculate the amount of sediment that was eroded or deposited. As a novel technique, airborne hyperspectral remote sensing or airborne imaging spectroscopy, was applied to classify the sediment of the beach and the foredunes in seven sand type classes. Several classification strategies were tried out; a comparison was made between the non-statistical Spectral Angle Mapper (SAM) and a statistical classifier based on Linear Discriminant Analysis (LDA), making use of AISA-Eagle imagery.

The best classification results were obtained applying LDA in combination with a feature selection based on Sequential Floating Forward Search (SFFS). The latter is a band selection technique that chooses the sub-optimal combination of spectral bands from the hyperspectral data in order to obtain the best classification accuracy. Classifications were performed with the original bands as well as with wavelet coefficients. The latter significantly enhanced the classification accuracy obtained. The combination of LDA with SFFS resulted in an overall classification accuracy of 82%, using three wavelet coefficients. Replacing the LDA with the non-statistical SAM algorithm reduced the overall classification accuracy to 74%, using all bands or wavelet coefficients. Tests pointed out that, as a result of the limited number of training samples available, using more than two to three bands or wavelet coefficients did not result in higher classification accuracies. HyMap data, featuring 126 bands in the Visible till Shortwave Infrared part of the spectrum, were used to demonstrate that the Visible and the Near-Infrared part of the spectrum outperform the Shortwave Infrared part for classification purposes in this application.

As a side-step, airborne hyperspectral data acquired over the Molenplaat in the Westerschelde, were classified applying the LDA and SFFS algorithms. The aim of this study was to investigate whether this classification methodology could be used to identify sediment habitat types on tidal sand shoals. High classification accuracies were obtained for the water content (88%), the median grain size (88%) and the chlorophyll-a concentration (84%). The organic matter content scored somewhat lower but still reached 80% overall accuracy. The four parameters classified allowed to define the general sediment habitat types which could consequently be used in more detailed biological or sedimentological studies.

However, the main goal of this thesis was the application of the airborne hyperspectral data and the airborne LIDAR data to map and analyse the sediment dynamics along the Belgian shoreline in the period 2000 – 2006. While the LIDAR data served to calculate the amount of sediment eroded or deposited (Figure 1), the classified hyperspectral data served to interpret the sand dynamics and more specifically the sediment transport directions. The classes were used as tracer for the sediment transport. The methodology was applied in five distinct units, most of them limited by harbour dams or harbour channels, which allowed treating each unit as a more or less closed system.

In summary, it could be concluded that the beach in the period studied was in most places stable (i.e., less that 25 cm accretion or erosion) or erosive. The beaches which were most affected by erosion are mainly situated along the Middle and East Coast, among which the beaches of Knokke-Zoute, the Duinse Polders, and a large area around De Haan featured the most severe erosion. The only accretional beaches were found in Zeebrugge, Sint-Laureins and the centre of Koksijde. However, the accretion on each of these beaches could be linked to human interventions. The overall natural tendency was erosive. The dune area in Figure 1 contains the foredunes, i.e., the dunes immediately landward of the beach. Contrary to the beach, they grew in many places or remained stable. Only along the Middle Coast, between Westende and Oostende, the

foredunes were erosive. A detailed analysis was performed for each unit separately and particular attention was paid to the sediment transport directions; hereto all available data layers originating from the LIDAR and hyperspectral data were combined in a GIS and an integrated analysis was made.

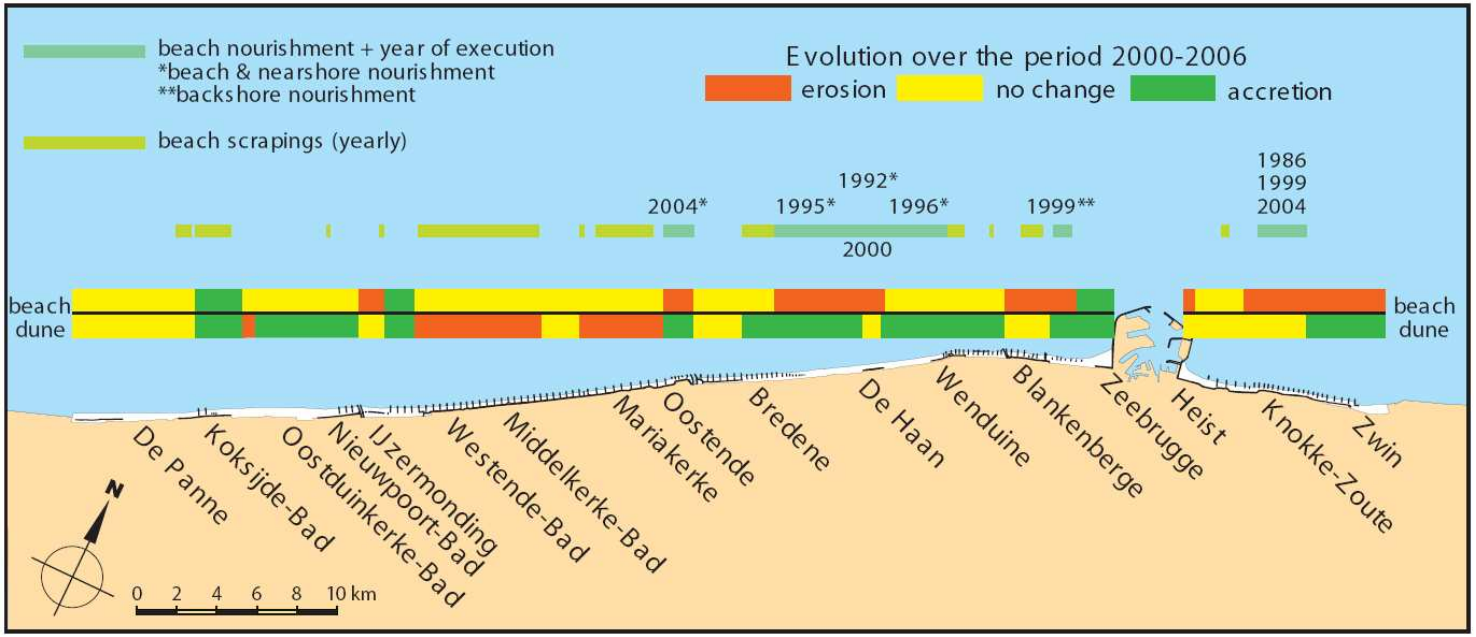

Figure 1: Schematic representation indicating the areas with erosion and accretion on the beach and in the foredunes ('dune') for the period 2000 – 2006. The major beach nourishments and beach scrapings are indicated as well.

Samenvatting

Recent onderzoek laat er geen twijfel over bestaan; het zeeniveau stijgt wereldwijd en de snelheid van de stijging neemt toe. De belangrijkste oorzaken hiervoor zijn de opwarming van de zeeën en oceanen en het smelten van sneeuw en ijs op het land. De menselijke invloed op de versnelde klimaatsverandering werd recentelijk bevestigd door het Intergovernmental Panel on Climate Change (IPCC). Onderzoek toont eveneens aan dat het toekomstige klimaat aan de Belgische kust zal gekenmerkt worden door meer extreme weersverschijnselen waaronder een toename van het aantal stormen alsook de kracht van de stormen. Maar zelfs zonder toenemende stormactiviteit, is onze kust sterk dynamisch en treedt er op veel plaatsen erosie op. De vele economische activiteiten langsheen de Belgische kust laten geen natuurlijke dynamiek toe en ze zijn aldus mede verantwoordelijk voor het erosief karakter van onze kust. Al deze zaken maken dat een regelmatige opvolging van onze kustlijn onontbeerlijk is om te kunnen oordelen over de stabiliteit en veiligheid van onze zeewering. In deze thesis worden twee vliegtuig-gebaseerde teledetectie technieken gebruikt om de dynamiek van onze kust in kaart te brengen en te analyseren voor de periode van 2000 tot 2006. Vliegtuig-gebaseerde LIDAR of laserscanning is een bekende techniek die gebruikt wordt om accurate Digitale Terrein Modellen (DTMs) te maken van het strand en de (onbegroeide) duinen. Door opeenvolgende DTMs te vergelijken kunnen zones met erosie of aangroei afgebakend worden. Vliegtuig-gebaseerde hyperspectrale teledetectie daarentegen, is een recente techniek die toelaat om d.m.v. analyse van het gereflecteerd zonlicht het zand op het strand en in de duinen in te delen in een aantal zandtype klassen. Kleine verschillen in de samenstelling, het vochtgehalte of de korrelgrootte laten toe spectraal een onderscheid te maken tussen verschillende zandtypen. Alvorens het zandtransport in kaart te brengen en te

analyseren, werden twee classificatietechnieken uitgetest; de niet-statistische Spectral Angle Mapper (SAM) en een statistische classificatie methode gebaseerd op Lineaire Discriminant Analyse (LDA). De hyperspectrale data die hiervoor gebruikt werden, zijn afkomstig van de AISA-Eagle sensor. De beste classificatieresultaten werden behaald met LDA, in combinatie met een methode (Sequential Floating Forward Search of SFFS) die uit het groot aantal spectrale banden de sub-optimale combinatie voor classificatie kiest. Testen toonden eveneens aan dat -voor deze applicatie- betere classificatieresultaten kunnen behaald worden wanneer de spectrale banden worden omgezet naar wavelets. De combinatie van LDA en SFFS, toegepast op wavelet coëfficiënten, resulteerde in een classificatie accuraatheid van 82%. Bij gebruik van SAM daalde de accuraatheid naar 74%. Door het beperkt aantal trainingssamples kon slechts een beperkt aantal (twee tot drie) spectrale banden of wavelets gebruikt worden. HyMap data werden gebruikt om na te gaan welk spectraal domein het best geschikt is om strandzand te klasseren. Hieruit bleek dat visueel en nabij-infrarood licht betere classificatieresultaten opleveren dan kort-golvig infrarood licht.

Als nevenstudie, werd dezelfde classificatiemethode (LDA in combinatie met SFFS) gebruikt om de sedimenten op de Molenplaat in de Westerschelde te klasseren in een aantal sediment habitat klassen. Vier parameters werden hiertoe afzonderlijk en met hoge accuraatheid geklasseerd: het watergehalte (88%), de mediane korrelgrootte (88%), de chlorofyl-a concentratie (84%) en het gehalte aan organisch materiaal (80%). Hiermee kon aangetoond worden dat deze methode eveneens geschikt is om sediment habitat klassen af te bakenen hetgeen als basis kan dienen voor meer gedetailleerd biologisch of sedimentair onderzoek.

Het hoofddoel van deze thesis was echter de analyse van het zandtransport langsheen de Belgische kust in de periode 2000 – 2006. Daar waar de LIDAR data gebruikt werden om het sedimenttransport kwantitatief te begroten, werden de hyperspectrale data gebruikt om de transportrichtingen te bepalen. De zandtype klassen werden bijgevolg gebruikt als ‘tracer’ voor het zandtransport. De methode werd toegepast in 5 ruimtelijke eenheden die meestal begrensd worden door havengeulen. Deze laatste vormen immers een barrière voor het langstransport waardoor elke eenheid kan beschouwd worden als een quasi gesloten systeem.

Samenvattend kan men stellen dat de Belgische kust op de meeste plaatsen erosief of stabiel is (stabiel wil zeggen dat er minder dan 25 cm erosie of aangroei optrad); zie Figuur 2. De meest erosieve stranden bevinden zich aan de Midden- en Oostkust. Vooral het strand van Knokke-Zoute, het strand aan de Duinse Polders en dat rond De Haan waren sterk erosief. De enige stranden die aangroei kenden zijn deze van Zeebrugge, Sint-Laureins en Koksijde. Het moet echter opgemerkt worden dat al deze aangroeiende stranden het gevolg zijn van menselijke ingrepen. In tegenstelling tot de overheersende erosieve trend van de stranden, groeiden de zeewerende duinen in de bestudeerde periode op veel plaatsen aan. Enkel aan de Middenkust, tussen Westende en Oostende, waren de zeewerende duinen erosief. Elke eenheid werd in detail geanalyseerd waarbij bijzondere aandacht werd besteed aan de zandtransportrichtingen,

gebruik makend van alle datalagen die werden afgeleid van de LIDAR data en de hyperspectrale data.

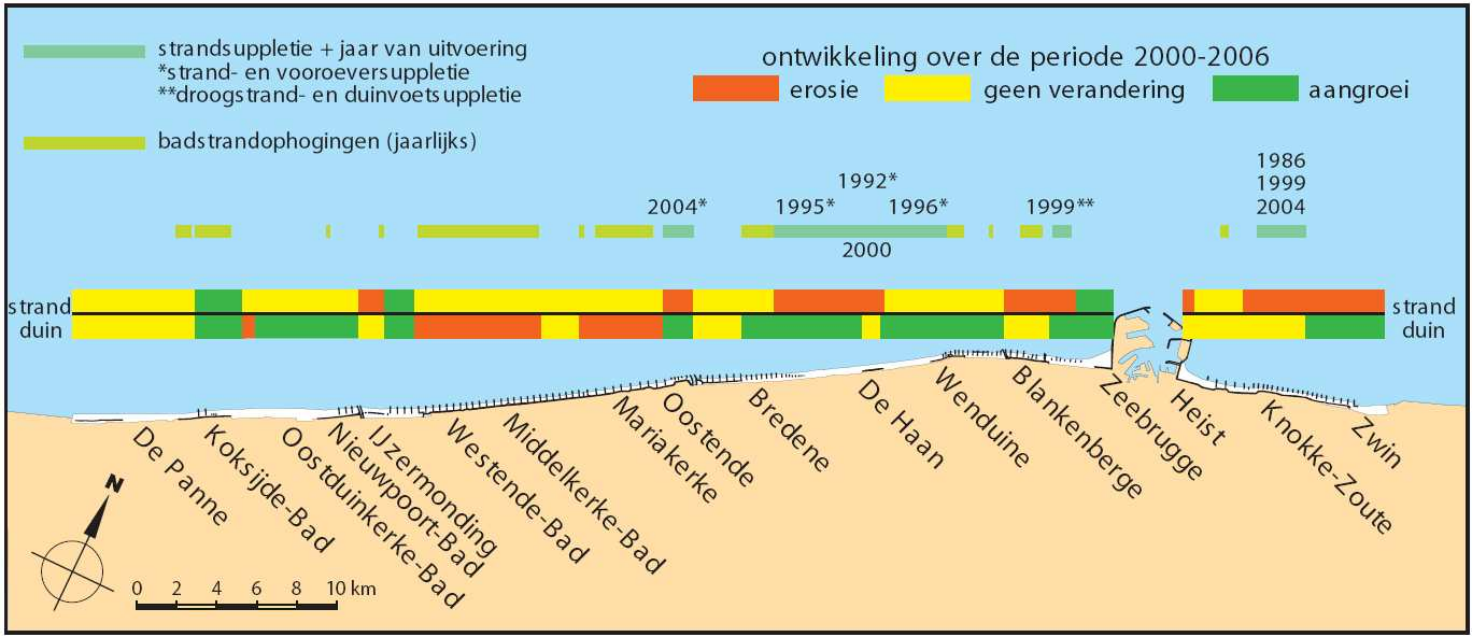

Figuur 2: Schematische voorstelling van de zones met erosie en aangroei in de periode 2000 – 2006. Er werd een onderscheid gemaakt tussen het strand en de voorste zeewerende duinen ('duin'). De belangrijkste suppleties en badstrandophogingen worden eveneens weergegeven.

Structure of the thesis

The emphasis of this thesis is on the use of two airborne remote sensing techniques, airborne hyperspectral remote sensing and airborne laserscanning, to map and monitor the sediment dynamics along the Belgian shoreline. The final goal is the classification of the beach in sand type classes, making use of the hyperspectral data, and consequently the analysis of the sediment transport. The latter is based on the sand class maps and on differential height maps which are derived from the laserscan data.

The reader will notice that the topic of the thesis balances between coastal geomorphology and 'pure' remote sensing. Remote sensing is used as a tool to analyse the geomorphology and the dynamic behaviour of the beach, but in some chapters a more fundamental analysis of the remote sensing data is performed. However, the latter always frames in a thematic end-goal. Hence, this thesis does not fit in the corner of fundamental remote sensing research, but rather in remote sensing applied to coastal zone monitoring and in particular the follow-up of the dynamic behaviour of the sandy beaches along the Belgian shoreline. The choice of this study area was based on the possibility to achieve new and repetitive remote sensing data over this area, the extensive field knowledge available, the accessibility of the site, and last but not least the fascination for this highly dynamic area with its conflicting activities and interests (see Chapter 2).

The thesis is structured as follows:

- **Chapter 1** – An introductory chapter provides the reader with the necessary background knowledge to understand and interpret the thesis. After a general background and motivation, an introduction is given to airborne hyperspectral remote sensing and airborne laserscanning, as well as to classification techniques.
- **Chapter 2** - This chapter contains an introduction to the study area, starting with the geological background, followed by the present-day geomorphological characteristics and the man-made structures and interventions. Finally, some reference TAW levels are listed.
- **Chapter 3** - The third chapter provides an overview of the available airborne and ground truth data. After a brief overview of both types of data, a more detailed analysis is made of the sedimentological characteristics of the beach. This analysis is based on ground truth data collected in 2001 and 2002.
- **Chapter 4** till **Chapter 7** - Consequently, four peer-reviewed journal papers are listed. They were modified to avoid overlap with the introductory chapters and to attain consistency throughout the thesis.
    - The first paper focuses on the use of the SAM classification algorithm for the classification of the beach sediments and a first attempt was made to combine hyperspectral data and laserscan data to analyse the sediment transport. This paper, published in the *Journal of Coastal Research*, was the first paper written in the framework of this thesis and therefore it is limited to the data captured in 2000 and 2001.
    - The second paper, published in *Estuarine Coastal and Shelf Science*, has a somewhat different scope. In this paper, a linear discriminant classifier (LDA), in combination with feature selection, was used to classify the sandy and muddy sediments on the Molenplaat (Westerschelde) into sediment habitat types. Here, specific attention was paid to the biological value of the sediment and it was shown how the technique used is suited to classify sediment habitat types.
    - After the small-scale test of the linear discriminant classification algorithm and the feature selection approach on the Molenplaat, the same methodology was applied to the entire Belgian shoreline. Additionally, tests were performed to investigate the influence on the classification accuracy of transforming bands into wavelet coefficients; the SAM algorithm (applied in the first paper) was compared with LDA, and the influence on the classification accuracy of the band width and the band range used was analysed. Hence, in contrast with the other papers, this paper is focusing on classification

techniques rather than on the application itself. It is currently under review (*International Journal of Remote Sensing*).

- The fourth paper uses all available data from 2000 till 2006 to demonstrate how the combination of airborne hyperspectral remote sensing and airborne laserscanning can be used to analyse the sediment transport along the Belgian shoreline. The methodology was demonstrated on three sites: Koksijde, located at the West Coast and characterised by wide accretional beaches, influenced by dry berm replenishment works and the construction of groynes. Zeebrugge, at the Middle Coast, where a beach nourishment was executed one year before the remote sensing acquisitions started and where the dams of the harbour of Zeebrugge are responsible for the formation of a large accretional beach, and Knokke-Heist, located at the East Coast and characterised by narrow, locally reflective, beaches, heavily influenced by nourishment activities. This paper is accepted and will be published in *Earth Surface Processes and Landforms*.

- **Chapter 8** - As the fourth paper was meant as a demonstration of the methodology to an international audience, it did not allow to describe and analyse the sediment transport in each coastal unit. Therefore this chapter handles in detail the sediment transport along our shoreline between 2000 and 2006. It can be considered as the final thematic product of this thesis utilising all remote sensing (and field) data available. The chapter is divided in 5 parts, each of them covering a distinct unit of the shoreline.
- **Chapter 9** - In the last major chapter, the results obtained during the sediment transport analysis are commented and remarks on the technique used and methodology applied are formulated. Finally, recommendations are made regarding future monitoring strategies.

To conclude this section, here are the questions that are addressed in this thesis:

From a methodological point of view, it was investigated which type of hyperspectral data is most suited to classify a sandy beach in sand type classes. Hereto, several questions were tackled:

- Do we need a hyperspectral sensor capturing both the VNIR and SWIR spectrum, or is a VNIR sensor sufficient to obtain accurate classification results?
- Do we need many narrow spectral bands to achieve this goal? Or is there a possibility to use broader and fewer bands (cf. multispectral remote sensing)?
- Is it useful to transform the original spectral bands into wavelet coefficients; does this decomposition result in a higher classification accuracy?
- Is a common SAM classifier adequate? Or can better results be achieved applying a parametric classifier?

All these methodological questions frame in the thematic end-goal of this thesis, i.e., the monitoring of the sediment dynamics along the Belgian shoreline in the period 2000 – 2006. With respect to this, an answer to the following questions was sought:

- Was the Belgian beach and foredune area in the previous years erosive, stable or rather accretional? And which spatial variation can be observed?
- Is it possible to detect on hyperspectral data areas where beach nourishments have been executed? And which other sand types can be distinguished?
- Can hyperspectral data be of value in the monitoring of the sediment transport directions?
- How can nourished areas be monitored with a combination of hyperspectral and LIDAR data? And can we derive information on the life time of beach nourishments?
- And finally, can the classification methodology be applied to map certain parameters indicative for the biological value of the sediment (cf. sediment ecotope mapping)?

Note that the aim of this thesis is not to analyse the processes of sediment dynamics. Though, existing knowledge on transport processes and human interventions provided necessary background for interpreting the actual detected changes.

Chapter 1

Introduction

1.1 Background and motivation

The challenge of this thesis was to apply state-of-the-art remote sensing techniques to analyse the dynamic behaviour of the Belgian coastline. The latter is situated at the southern edge of the North Sea basin and has a length of 65 km from De Panne in the Southwest till Knokke-Heist in the Northeast. The economical and social importance of the Belgian shoreline is hardly to overrate. Belgium and especially Flanders is among the most densely populated regions in Europe (447 inhabitants/km² in 2005[1]). The 65 km long coastline has a major economic value thanks to its attractive beaches (cf. tourism industry) and the presence of two important sea ports (Zeebrugge and Oostende). However, this valuable coastline is highly dynamic and this dynamic behaviour interferes with the economic activities along the shoreline. Because the direction of this coastline is almost identical to the prevailing wind direction, sand tends to move parallel to the beach instead of from the sea to the dunes. However, man has strived, ever since the Middle ages, to keep the shoreline at its position and even to move it seaward. The first attempts to limit the natural dynamics of the Belgian beach were, without exception, hard defence structures: seawalls, reinforced dune bases, groynes, beach groynes, and Longard tubes. However, since the 70s, one is convinced that so-called soft defence structures like beach nourishments and beach scrapings (or beach replenish works) are to be preferred to hard defence structures (see Section 2.3).

To follow up the dynamic behaviour of the beach and to evaluate the effects caused by the artificial interventions, several monitoring strategies can be adopted. A good but labour-intensive strategy is to measure the beach topography along transects oriented

[1] http://statbel.fgov.be/figures/dsp_nl.asp

perpendicular to the coastline (with a theodolite or GPS). This technique can deliver accurate data in the measured points, but one has to interpolate to cover the area between the measurements. To overcome this, remote sensing techniques can be applied. Remote sensing is a very powerful tool for beach monitoring and investigation, since it allows collecting spatially continuous information over a wide area in a short time frame. The latter is highly important in coastal areas as this environment is subject to fast changes in time. Moreover, the technique is not hampered by the (in)accessibility of the site, what often is a problem in coastal areas. The common spaceborne platforms, making use of sun-synchronous satellites, are limited by their fixed orbit. This implies that acquisitions can not be planned in time; hence, tides and weather are often prohibiting successful acquisitions. Airborne remote sensing on the other hand, although often more expensive, is much more flexible. It allows planning the missions carefully taking into account all possible constraints. Cracknell (1999) and consequently Malthus and Mumby (2003) provided an overview of the capacities of remote sensing for estuarine and coastal zone studies. While the focus in these review articles is mainly on low-resolution remote sensing, Mumby and Edwards (2002) investigated the additional value of very high resolution data (IKONOS) and hyperspectral data (CASI, see Section 1.2). In the Netherlands, interesting research was conducted by Eleveld *et al.* (2000) who explored the possibilities of aerial video camera to derive relief maps of coastal landscapes and by Van Zuidam et al. (1998) and Eleveld (1999) who combined remote sensing techniques, GIS and dynamic modelling for a better management of the coastal zone.

The novel aspect of this thesis is the combination of two techniques of airborne remote sensing for the monitoring of a sandy shoreline: airborne hyperspectral remote sensing (or airborne imaging spectroscopy) and airborne LIDAR (or airborne laserscanning). The development of LIDAR represented a technological breakthrough in topographic monitoring. A number of studies have demonstrated the ability of LIDAR data to accurately measure the topography over large sections of the coastline (Revell *et al*., 2002; Sallenger *et al*., 2003; White and Wang, 2003), and sequential LIDAR surveys have shown that shoreline changes can be monitored over time (Stockdon *et al*., 2002). In Belgium, LIDAR has been applied since 1999 to map the beach topography and to make differential height maps (from the mid 1970s till 1998, stereographic aerial photographs were used for this purpose). The vertical accuracy of the LIDAR measurements proved to be between 5 and 10 cm, allowing a detailed budgeting of the volumetric changes between consecutive observations. Hence, LIDAR measurements provide very valuable input data for the study of the coastal morphodynamics. But, as these data do not provide any information on the type of sand, it is not possible to gain direct knowledge on the directions of the sediment transport. Therefore, LIDAR was combined with hyperspectral remote sensing. The latter allowed us to classify the beach in several sand type classes and these classes can be used as tracers to monitor the sediment transport. This technique proved to be appropriate to map and monitor areas where beach nourishments or beach scrapings had been executed. Indeed, the type of sand used for these soft defence works is often borrowed from banks offshore

and, due to its different mineralogical composition and grain size, it can be distinguished spectrally from the sand, naturally found on the beach. The combination of the LIDAR data and the hyperspectral data is a new approach in beach monitoring and proved to be suited to improve the knowledge on the sediment transport along the Belgian shoreline.

As stated earlier, the economic importance of the Belgian shoreline is very high, resulting in a difficult equilibrium between economic development and conservation of the landscape and the ecology. As such, the research presented is linked to the concept of Integrated Coastal Zone Management (ICZM) (Post and Lundin, 1996). This concept, consistent with principles 1 through 19 of the 1992 United Nations Conference on Environment and Development (Rio) Declaration[2] and chapter 17 of Agenda 21[3], is most concisely defined in the so-called Noordwijk guidelines, set out at the 1993 World Coast Conference:

> *ICZM involves the comprehensive assessment, setting of objectives, and planning and management of coastal systems and resources, taking into account traditional, cultural and historical perspectives and conflicting interests and uses; it is a continuous and evolutionary process for achieving sustainable development.*

The core objective of ICZM is to balance socio-economic development and ecological conservation (Post and Lundin, 1996; Kelleher, 1999). For a comprehensive overview of the literature on ICZM, the reader is referred to Vanderstraete (2007). Despite the dual, and sometimes conflicting interest in the management of the Belgian shoreline, it should be noted that the first aim of coastal morphological monitoring in Belgium is to determine the safety level of the sea-defence and to steer the measures needed to keep the safety at this level. The coastal barrier indeed protects an up to 20 km wide strip of coastal lowland from flooding. In the context of global warming, an effective management of the coastline is increasingly important (COMRISK, 2004). For the low-lying countries, such as Belgium, an efficient monitoring is a prerequisite in the view of an expected sea-level rise of 3-4 mm/year (IPCC, 2001). Moreover, the return period of heavy storms is expected to reduce drastically (IPCC, 2001), causing important economic losses for many coastal nations (Mills, 2005). The combination of higher sea levels with more extreme weather events necessitates a regular and detailed mapping of the affected shorelines, applying the most suited techniques. In addition, if data can be obtained on the state and the dynamics of the coastal sediment budget, it can better be estimated how well beach sections recover from erosive events and whether there is sufficient sediment available to cope with sea-level rise.

[2] http://www.un.org/documents/ga/conf151/aconf15126-1annex1.htm

[3] http//www.un.org/esa/sustdev/documents/agenda21/english/agenda21chapter17.htm

1.2 Introduction to airborne imaging spectroscopy

1.2.1 Historical development

Remote sensing[4] is, broadly but logically speaking, the collection of information about an object without making physical contact with it (Campbell, 1996). This is a simple definition, but too vague to be really useful, therefore we restrict it to the Earth's surface and atmosphere, viewed from above, using electromagnetic radiation. This narrower definition excludes techniques as seismic, geomagnetic and sonar investigations, as well as (for example) medical and planetary imaging, all of which could otherwise be described as remote sensing (Rees, 2001). Nowadays, the type of remote sensing we refer to is often described by the alternative name *Earth Observation*.

Although significant developments in the theory of optics began to be made in the seventeenth century, and glass lenses were known much earlier than this, the first real advance towards our modern conception of remote sensing came in the first half of the nineteenth century with the invention of photography. For the first time, it became possible to record an image permanently and objectively. Also during the nineteenth century, forms of electromagnetic radiation were discovered beyond the visible part of the spectrum: infrared radiation by Herschel, ultraviolet by Ritter and radio waves by Hertz, and in 1863, Maxwell developed the electromagnetic theory on which so much of our understanding of these phenomena depends.

Aerial photography followed almost immediately on the discovery of the photographic method. The first aerial photograph, unfortunately no longer in existence, was probably made in 1858 by Gaspard Félix Tournachon (known as 'Nadar', °Paris 1820 – 1910), taken from a balloon at an altitude of about 80 m. The next step towards what we now recognise as remote sensing was taken with the development of practicable airplanes in the early twentieth century. Again, the potential applications were quickly recognised and aerial photographs were taken recorded from airplanes from 1909. During the two World Wars, the techniques developed further and the first applications in cartography, geology, agriculture and forestry emerged. By the 1950s, false-colour infrared film, originally developed for military use, was finding applications in vegetation mapping, and high resolution imaging radars were being developed. As these developments continued through the 1960s, sensors began to be launched in space. This was originally part of the programme to observe the Moon, but the advantages of applying the same techniques to the observation of the Earth were soon recognised and the first multispectral spaceborne image of the Earth was acquired from *Apollo 6* (1968).

[4] See Campbell (1996) for a summary of the main definitions of remote sensing that have been adopted over the last few decades. The term 'remote sensing' itself was first used by the U.S. Office of Naval Research in the 1960s (Cracknell and Hayes, 1991).

Although there were earlier unmanned remote sensing satellites[5], the opening of the modern era of spaceborne remote sensing ought probably to be dated to July 1972 with the successful operation of ERTS, the Earth Resources Technology Satellite, by the U.S. National Aeronautics and Space Administration (NASA). The ERTS was renamed *Landsat-1*, and after seven satellites (with some variation in sensors on the different satellites) the Landsat programme still continues today. In 1999, the first truly commercial remote sensing satellite was launched: the Ikonos satellite acquires images with a panchromatic resolution of 1 m and a multispectral resolution of 4 m, with a capacity of acquiring images every 3 to 4 days (Mumby and Edwards, 2002). Since then, several high resolution commercial satellites have been launched, showing clearly that the commercial sector is focusing on the acquisition of high resolution, short response time imagery, suitable for many commercial and disaster monitoring purposes.

The most recent and novel development in this direction is the design of High Altitude Long Endurance Unmanned Aerial Vehicles (HALE-UAV) which will be able to acquire almost continuously very high resolution imagery (app. 20-30 m pixel resolution) at a much lower cost than conventional satellites or manned airplanes (see for instance http://www.pegasus4europe.com). Peterson *et al.* (2003) investigated the possibilities of UAV platforms for coastal zone monitoring.

With the desire to acquire more information from remote sensing, the interest in the technique of *imaging spectroscopy* increased. Imaging spectroscopy is the acquisition of image data in many (typically a few tens to a few hundreds) contiguous (i.e., adjacent and not overlapping) spectral bands. Different names have been given to this field of remote sensing including 'imaging spectroscopy', 'imaging spectrometry', 'spectroradiometry' and '*hyperspectral remote sensing*'. Although they have a different meaning in the sense of a direct translation of the term (i.e., spectroscopy = seeing, spectrometry = measuring, hyperspectral = too many bands), the significance and the perception to the remote sensing community is the same: "the acquisition of images in tens to hundreds of registered, contiguous spectral bands such that for each picture element of an image it is possible to derive a complete reflectance spectrum (Goetz, 1992a).

The first step beyond laboratory and field spectrometry was airborne and spaceborne profiling in many spectral bands simultaneously. In 1976, the Shuttle Multispectral Infrared Radiometer (SMIRR), a 10-channel spinning filter wheel radiometer, was flown on the second flight of the space shuttle in 1981. Data from this instrument provided the first direct identification of clay, kaolinite and limestone from the orbit (Goetz *et al.*, 1982). In the late 1970s an airborne 500-channel profiler was developed by Geophysical Environmental Research and used to develop mineralogical maps, as well as to identify trees stressed by excess copper in the soil. This profiler led to the

[5] The first was TIROS-1, launched in April 1960.

discovery of the 'blue shift' in the red edge of the chlorophyll well at 0.68 μm (Collins *et al*., 1983).

In 1981, an imaging spectrometer program was started at the NASA Jet Propulsion Laboratory. This program had as its goal two different imaging spectrometer systems, a shuttle experiment, and the free-flying version known as the High Resolution Imaging Spectrometer (HIRIS) (Goetz and Davis, 1991). Unfortunately, HIRIS was cancelled due to funding issues. The first airborne system was the Airborne Imaging Spectrometer (AIS) which was in fact a detector test bed covering 128 bands in either the 400 to 1 200 nm or 1 200 to 2 400 nm range (see Section 1.2.2). The second, and nowadays still operated, airborne system was AVIRIS (Airborne Visible and Infrared Imaging Spectrometer). This opto-mechanical whiskbroom scanner preluded the era of the modern airborne imaging spectroscopy.

Today, two spaceborne imaging spectrometers are operational: the test instrument CHRIS (the Compact High Resolution Imaging Spectrometer) on board the micro-satellite Proba (the PRoject for On-Board Autonomy, designed by a consortium led by Verhaert in Belgium), and the Hyperion satellite on board EO-1 (Earth Observing-1). CHRIS captures the reflected light in 18 spectral bands covering the visible and near-infrared part of the spectrum (i.e., 400 – 1 050 nm) at a pixel resolution of 17 m ('Land Mode with full swath width'), while Hyperion has 220 bands from the visible to the shortwave infrared (400 – 2 400 nm) and a pixel resolution of 30 m. It is expected that by 2009 – 2010, a new generation of spaceborne hyperspectral systems will be launched, which is strongly hoped for as both CHRIS and Hyperion are advancing in years. The airborne market is much more covered with several commercial manufacturers delivering state-of-the-art instruments. Among many others, we mention the CASI instruments (covering the visual and near-infrared part of the spectrum) and the SASI (covering the short-wave infrared), both manufactured by ITRES Research Ltd (based in Calgary, Canada). In Europe, the most important manufacturer of commercial hyperspectral sensors is SPECIM Ltd. who designed the AISA Eagle (visual and near-infrared range) and the AISA Hawk (short-wave infrared range). Last but not least, we mention the new airborne hyperspectral sensor, APEX, which has been designed and is today being built by a Swiss-Belgian consortium under the authority of ESA (http://www.apex-esa.org). This scientific instrument will be operational from 2008 onwards and is expected to set the new standard in airborne hyperspectral remote sensing.

1.2.2 Fundamental principles

The key of deriving information from spectroscopy data is the understanding of the interactions between electromagnetic energy, emitted by the sun, and the surface being observed. Electromagnetic energy treated as a stream of discrete particles (photons or quanta), carries a fixed amount of energy which causes energy transfer between individual atoms or molecules whenever a photon interacts with an atom or molecule

(Hunt, 1980). All physical bodies, at temperatures above absolute zero (0 K or -273°C) radiate electromagnetic energy. A blackbody is a perfect absorber and emitter of radiation and will look absolutely black to the human eye. The energy emitted by the sun has a spectral distribution similar to that of a blackbody at a temperature of 6 000 K. The temperature at the Earth's surface varies, but is on average at about 27°C or 300 K. Hence, according to Wien's law, which gives the wavelength of the peak energy radiated by a body, the peak radiance from the sun is at about 500 nm, coinciding with the part of the spectrum visible to the human eye as green light:

$$\lambda_p = \frac{a}{T} \qquad \textit{Eq 1-1}$$

where λ_p is the peak wavelength in nm and a is the constant 2.898 x 10^6 nm K.

A comprehensive introduction to the basic laws and principles of remote sensing is beyond the scope of this thesis; for this, the reader is referred to Rees (2001), Landgrebe (2003) or McCloy (2006).

When photons enter an absorbing medium, they are absorbed according to Beer's law:

$$I = I_0 e^{-kx} \qquad \textit{Eq 1-2}$$

where I is the observed intensity, I_o is the original light intensity, k is an absorption coefficient and x is the distance travelled through the medium. Eq 1-2 holds true for a single wavelength. At other wavelengths, the absorption coefficient is different, and the observed intensity varies. The absorption coefficient as a function of wavelength is a fundamental parameter describing the interaction of photons with a material. Due to the absorption of specific wavelengths (i.e., amounts of energy) it is possible to distinguish between different minerals, different plant species, different water constituents, etc. Indeed, the wavelength specific absorption is the basis for any analysis in imaging spectroscopy.

There are several causes of absorption (Goetz, 1992b). At the level of individual atoms *electronic processes* take place, which occur at shorter wavelengths (0.40 to 1.10 µm, i.e., in the visible and near-infrared part of the spectrum, see Figure 1-1). Here, the energy needed to lift an electron into a higher energy level is high. Absorption bands can also be caused by charge transfer, or inter-element transition where the absorption of a photon causes an electron to move between ions or between ions and ligands. Or the transition can occur between the same metal in different valence states, such as between Fe^{2+} and Fe^{3+}. In general, absorption bands caused by charge transfer are diagnostic of mineralogy. They produce broad absorption features that require high energy levels. For more detailed discussions of electronic processes reference is made to the review paper of Hunt (1977) or the book of Burns (1970).

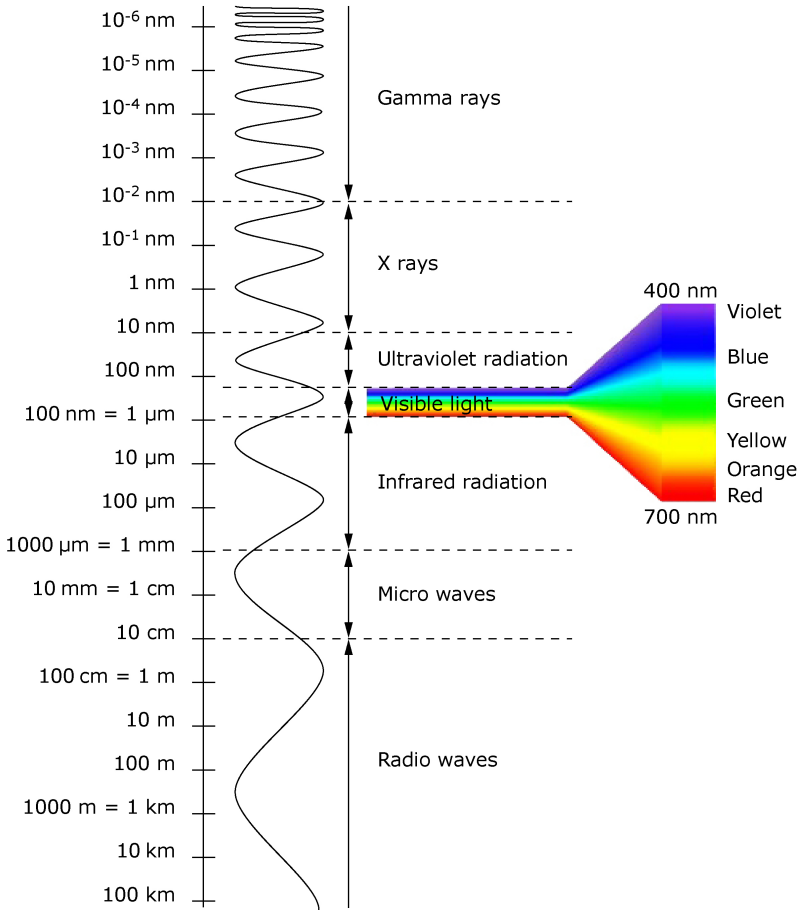

Figure 1-1: The electromagnetic spectrum. The diagram shows those parts of the electromagnetic spectrum that are important in remote sensing, together with the conventional names of the various regions of the spectrum.

A second cause of absorption are *vibrational processes*. The bonds in a molecule or crystal lattice are like springs with attached weights: the whole system can vibrate. The frequency of vibration depends on the strength of each spring and their masses. For a molecule with N atoms, there are 3N-6 normal modes of vibrations called *fundamentals*. Each vibration can also occur at roughly multiples of the original fundamental frequency. The additional vibrations are called *overtones* when involving multiples of a single fundamental, and *combinations* when involving different types of vibrations (Hunt and Salisbury, 1970).

1.2.3 Applications

It is not the goal of this chapter to provide a complete overview of the literature on all applications of hyperspectral remote sensing; however, a brief overview is given with reference to some of the interesting papers in this field.

Through measurement of the solar reflected spectrum, imaging spectroscopy was introduced in a wide range of scientific research and applications during the last three decades. Van der Meer and de Jong (2001) and Toselli and Bodechtel (1992) provide a comprehensive overview of the prospective applications. Imaging spectroscopy originated largely in geology (e.g., Clark *et al*., 1990) and today, the applied geology (e.g., the mineral industry, lithological and structural mapping) hosts still the main operational applications of imaging spectroscopy. A good example of this was the development of the Autralian HyMap sensor, an airborne whiskbroom sensor (developed by Integrated Spectronics), that was specifically designed to meet the needs of De Beers, a South African mining company. During several years De Beers used the HyMap for mineralogical exploration surveys. The petroleum industry on the other hand is developing methods for implementation of imaging spectroscopy at a reconnaissance stage as well. The main targets are hydrocarbon seeps and microseeps. For an overview of the studies conducted in the field of (applied) geology reference is made to Van der Meer *et al.* (2001).

In soil science, much emphasis has been placed on the use of spectroscopy for soil surface properties and soil compositional analysis to aid in land degradation studies (e.g., Bowers and Hanks, 1964; Baumgardner *et al*., 1985; Ben Dor and Banin, 1994; Ben Dor *et al*., 2002; Goldshleger *et al*. 2002; Chabrillat *et al*., 2004; among others). An important remark that should be made when applying imaging spectroscopy to soil science (and beach monitoring) is that this technique is limited to the upper millimeters of the soil or the substrate. The reflected optical radiation is either reflected at the top of the surface or absorbed; the amount of radiation that is reflected by deeper soil or substrate layers is negligible. Hence, conclusions on the deeper layers are difficult to draw; see e.g., Figure 1-2 where the top layer of a dune pan is clearly different from the deeper layers rendering a different reflectance spectrum. This is an important element that had to be taken into account throughout the whole of this research. Field knowledge and knowledge of the processes acting in the longer term are needed to interpret the top layer and to know whether the top layer contains the same type of sediment as the deeper layers. The same top layer can be the result of different processes, e.g., a shell-rich coarse-grained top layer is often found in nourished areas where the deeper layers contain the same type of sediment, but the same top layer is also observed as a deflation pavement where it is caused by beach lowering processes that result in a concentration of the heavier and coarse-grained fractions. There is no straightforward methodology to judge on the deeper layers, but expert field knowledge helps to extrapolate the observations made at the surface to the deeper layers.

In a more regional context, imaging spectroscopy has been used to monitor agricultural areas, covering both the soil component and the crops (e.g., Ben Dor *et al*., 2004). This

brings us to the vegetation studies wherein spectroscopy has been applied to analyse leaf biochemistry and structure as well as canopy structure. Estimates of plant material and structure and biophysical parameters include: carbon balance, yield/volume, nitrogen, cellulose, chlorophyll, etc. Additionally, the technique is often used to distinguish between plant species (or crop species) and to define the vegetation health status (O'Neill and Ustin, 2000; Okin *et al.*, 2001; Armitage *et al.*, 2004; Kempeneers *et al.*, 2004; among others).

Figure 1-2: Photograph of the top layer of a dune pan at the Belgian shoreline. The surface has a different composition than the deeper layers rendering a different reflectance spectrum.

Another application that should be mentioned is the monitoring and analysis of water bodies, including both the water column and, if visible, the substratum. Unlike applications focusing on hard substrates (e.g., soil), it is possible to derive certain information from the water column as electromagnetic radiation partly transmits the water column, is scattered in the water and is partly reflected back into the atmosphere. Thanks to this, it is possible to derive certain water quality parameters like dissolved organic substances and inorganic suspended particles. On the other hand, if the water column is sufficiently clear, it is possible to study the substratum. An example of the latter is the mapping and monitoring of coral reefs (e.g., Mumby *et al.*, 2001). Imaging spectroscopy provides a synoptic view of the spatial distribution of different biological, chemical and physical variables. This knowledge is essential in environmental water studies as well as for resource management. Therefore, recent years have seen increasing interest and research in remote sensing of water quality of inland and coastal waters. Dekker *et al.* (2001) and the review papers of Cracknell (1999) and Malthus and Mumby (2003) provide a good overview of the applications in this field.

Finally, some smaller application fields exist in urban mapping, archaeological exploration, atmospheric research and, last but not least, in military survey operations.

1.3 Introduction to LIDAR

In the previous section, a *passive* technique in airborne remote sensing was introduced. Indeed, airborne imaging spectroscopy depends completely on the reflected solar radiation. LIDAR (LIght Detection And Ranging) on the other hand is an *active* technique which measures properties of scattered light to find the range and/or other information of a distant target. The prevalent method to determine distance to an object or surface is to use optical laser pulses. Like the similar radar technology, which uses radio waves instead of light, the range to an object is determined by measuring the time delay between transmission of a pulse and detection of the reflected signal. Figure 1-3 illustrates the principle of airborne laserscanning.

Other terms for LIDAR include Airborne Laser Swath Mapping (ALSM), Airborne Laser Surveying (ALS), Airborne Laser Terrain Mapping (ALTM), and Laser Altimetry. The acronym LADAR (LAser Detection And Ranging) is often used in military context.

The advent of laser scanning as a new method for the direct, high density measurement of decimeter accuracy elevation from aircraft has been enabled by the parallel development of several incorporated techniques. Kinematic differential Global Positioning Systems (GPS) methods now enable the positioning of aircraft to within cm precision. Inertial Navigation Systems (INS) or Inertial Measurement Units (IMU) can now provide three-dimensional aircraft orientation at 50 Hz within 0.01 degree (after post-processing) (Bufton, 1989; http://www. applanix.com). Combined within contemporary airborne laser mapping systems, these fastly developing technologies now enable geomorphic surveys at decimetre (and even better, see Chapter 3) vertical accuracy and at spatial densities of several elevation measurements per square meter.

A good introduction to airborne laserscanning, including the basic methods and governing equations, can be found in Baltsavias (2004) and Brock *et al*. (2002). Kidner *et al.* (2004) focus on the challenges, problems and pitfalls when applying LIDAR to coastal zone monitoring. Another interesting reference is the work of Su and Bork (2006); they investigated the influence of vegetation cover, slope and the LIDAR sampling angle on DEM (Digital Elevation Model) accuracy. Lee and Shan (2003) illustrate how LIDAR-derived DEMs can be used as an expert layer to improve the classification accuracy of high resolution IKONOS data, applied over a coastal area. Closely in line with our research is the work of Gares *et al.* (2006) who applied LIDAR to monitor the topographic and volumetric evolution of a beach nourishment in North Carolina (USA).

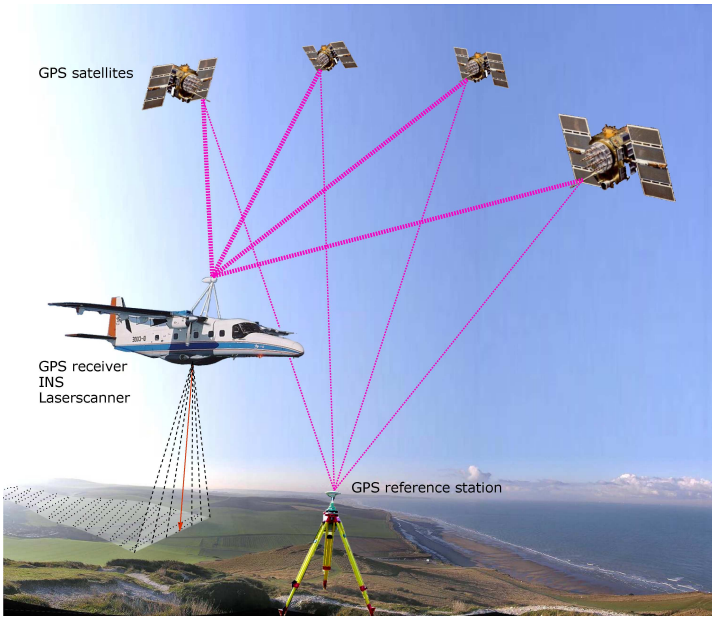

Figure 1-3: Principle of Airborne Laserscanning or LIDAR. An optical pulse is emitted by the scanner mounted in an aircraft, reflected by the surface and again received by the collector. The time difference between the emitted and received pulse permits to calculate the distance to the target.

Without going into detail, we briefly mention the basic equations relevant for laser ranging. The following equations assume that the aircraft is perfectly horizontal, in other words that the aircraft's roll and pitch angles are zero (Baltsavias, 1999; Wehr and Lohr, 1999). The travel time t_L for an individual laser light pulse is:

$$t_L = 2.\frac{R}{c} \qquad \textit{Eq 1-3}$$

where R is the distance between the laser transmitter and the object surface, and c is the speed of light in the medium. Given that neither the transmitted or received pulses are perfect step functions, the travel time is measured relative to a specific point on the pulse, typically a threshold amplitude on the pulse leading edge. From Eq 1-3, the range R to the target is:

$$R = \frac{1}{2}.c.t_L \qquad \textit{Eq 1-4}$$

The time resolution Δt_L directly controls the range resolution ΔR, which is given by:

$$\Delta R = \frac{1}{2}.c.\Delta t_L \qquad \textit{Eq 1-5}$$

The minimum detectable separation between reflecting targets along the pulse path, or the multiple target range resolution R_{min},

$$R_{\min} = c.\frac{t_{\min}}{2} \qquad \textit{Eq 1-6}$$

is similarly a function of the minimum time difference t_{min} between two received echoes. In general, very short duration, high amplitude laser pulses with a short pulse rise-time enhance multiple target discrimination in the reflected laser waveform. The absolute ranging accuracy σ_R depends on the pulse rise time t_{rise} and the overall system signal-to-noise ratio *S/N* (Wehr and Lohr, 1999):

$$\sigma_R \sim \frac{c}{2}.t_{rise}.\frac{1}{\sqrt{\frac{S}{N}}} \qquad \textit{Eq 1-7}$$

And, without deriving the equation, the pulse power received at the collector, P_{rec}, with an optical receiving area A_{rec}, is:

$$P_{rec} = \rho.\frac{M^2.A_{rec}}{\pi.R^2}.P_T \qquad \textit{Eq 1-8}$$

where ρ is the target reflectance, M is the atmospheric transmission, R is the range and P_T is the transmitted power.

For more detailed equations on the minimum detectable object, the laser footprint diameter, the across track point spacing and some operational aspects like the required number of strips, the area covered, or the amount of data collected, the reader is referred to Baltsavias (1999).

To conclude the sections on airborne imaging spectroscopy and airborne LIDAR, it is important to draw attention to the *mission planning*. Proper mission planning is a crucial key to success in any research based on airborne data. The mission planner must not only consider all technical aspects of the aircraft and the sensor(s) involved, but also local weather patterns, solar ephemeris data, and the coordination with the field campaigns which are often coinciding with the airborne survey. Each technique and each instrument asks for a customised planning. Missions that are not carefully planned and executed, result in unusable data and an important loss of financial means. Read and Graham (2002) provide an introduction to the techniques and methods of

aerial survey, while Myers and Miller (2005) focus on mission planning for optical airborne remote sensing in coastal and aquatic environments.

1.4 Introduction to classification techniques

Each pixel of an image contains a numerical or physical value that characterises that pixel. The value of pixels with a similar physical content will also be similar but, due to the variety in natural systems, they are seldom completely the same. Hence, an image consists of pixels with many different values which represent the true physical content of each pixel but to interpret the image as a whole, a simplification of the pixel values is needed. To achieve this, the image is classified into a discrete number of classes in accordance with specific criteria that are based, in part, on the individual pixel values. *Classification* is the process of using the pixel data values to allocate each pixel to one of a discrete number of classes (McCloy, 2006). Classification is related to *pattern recognition* (Duda *et al*., 2001; Landgrebe, 2003). The patterns that can be found in the pixel values of the image are represented by classes.

There are several classification strategies that can be followed; the analyst must develop a plan or strategy that allows him or her to extract the required information from the data, and this in the most cost-effective manner. Classification can be conducted by means of *supervised and unsupervised classification* techniques. Supervised classification uses training data to form class statistics as the basis of the classification. Hence, one starts with identifying informational classes (each with a certain label) that are of interest to the user. Unsupervised classification clusters the image data to create classes that form the basis of the classification. Some common unsupervised classification schemes are: Interative Self Organising Data Analysis Technique (ISODATA, Jensen and Qiu, 2001) and hierarchical clustering (Johnson, 1967). In this thesis, two supervised classification approaches are applied: the Spectral Angle Mapper (SAM), which is a non-statistical classifier, and a statistical classifier based on Linear Discriminant Analysis (LDA). For the *statistical classifier*, a Probability Density Function (PDF) that characterises the class distribution is estimated. In a *non-statistical classifier*, one does not use the training samples to estimate the PDF for each class. In case of SAM, each pixel spectrum is considered as an N-dimensional vector in an N-dimensional space, where N is the number of spectral bands. Each pixel vector is compared with pre-defined library spectra/vectors (Kruse *et al*., 1990;). The angles between each pixel spectrum and the library spectra are calculated and the pixel is assigned to the class corresponding to the smallest angle.

A statistical or parametric classifier estimates the form of the underlying density function that characterises the class distribution. The PDF is then represented in terms of a specific functional form which contains a number of adjustable parameters. During the training of the classifier, the values of the parameters are optimised to give the best fit to the data (Kempeneers, 2007). In this thesis, a Linear Discriminant Analysis

(LDA) is used as statistical or parametric classifier. It assumes that all classes have PDFs with a common covariance, specified by Σ, and that the PDFs for all classes are normally distributed. The classes do not have the same variance in all features (or spectral bands), the features are not necessarily uncorrelated, but all classes do have the same covariance and correlation structure.

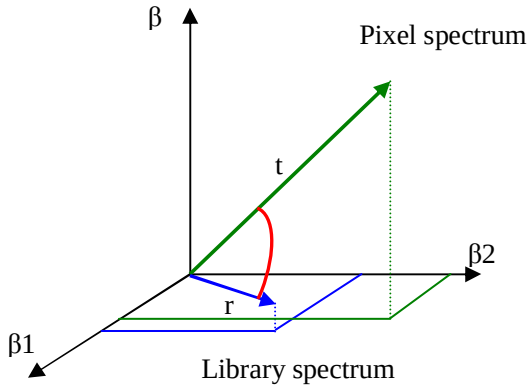

Figure 1-4: Schematic representation of the principle of the Spectral Angle Mapper classifier.

In LDA, new features are calculated as a linear combination of the original spectral bands. The decision boundary separating the classes depends on the location of the class mean values as well as on Σ, the common covariance for all the classes. The linear decision boundary is chosen in such a way that it optimises class separation. Note that LDA is also closely related to Principal Component Analysis (PCA) and Factor Analysis (FA) in that both look for linear combinations of variables. However, where PCA seeks directions or decision boundaries that are efficient for representation, LDA seeks decision boundaries that are efficient for class discrimination (Duda, 2001).

A more sophisticated classifier is a quadratic classifier; in this case the classes are not assumed to have the same covariance. The decision boundary in the feature space will be a second-order hypersurface. In theory and with an unlimited number of training samples, a quadratic classifier yields better classification results than a linear classifier but due to the class specific covariances, many more ($d + d(d-1)/2$, with d the number of bands) parameters have to be estimated for each class (assuming Gaussian distributions for all classes). In practice, for a hyperspectral sensor with a moderate number of 32 bands, one needs to estimate 528 parameters for each class. For most practical problems, with a limited number of training samples, this is not feasible.

Finally, classifiers can be divided in *pixel based and object based classifiers*. While pixel based classifiers base the assignment of each pixel to a certain class solely on the

(spectral) information of that particular pixel, object based classifiers use contextual information to segment the image into meaningful areas or objects, which are then classified. Due to the evolution in remote sensing towards smaller pixels (i.e., more detailed spatial information), they have gained a lot of attention as the need to aggregate pixels into meaningful objects increases when the pixel size decreases.

Chapter 2

Study area: the Belgian North Sea Beach

2.1 Geological background

2.1.1 Introduction and literature overview

The Belgian shoreline is situated at the southern edge of the North Sea basin (Figure 2-1). It has a length of 65 km from De Panne in the Southwest till Knokke-Heist in the Northeast and it forms an almost straight line directed 60°E. From a geological point of view, this coastline is part of the Flemish Coastal Plain, a depositional system at the southern edge of the North Sea Basin which is commonly known as the southern Bight (Rottier and Arnoldus, 1984). The first geological studies of the coastal plain date back to the 19th century (Belpaire, 1855; Rutot, 1897). Later pioneer work included the definition of the former well-known stratigraphic units such as the Calais and the Dunkerque Formations (Dubois, 1924; Briquet, 1930; Halet, 1931). However, the theory of a sequence of regressions and transgressions has recently been abandoned (see further). Tavernier (1947) and Tavernier and Moorman (1954) initiated modern geological and morphological research in the Belgian coastal plain. Verhulst (1959) started historical research on the Dunkerque transgressions and on the impact of man. For a summary of their results reference is made to Tavernier *et al.* (1970). An overview of more recent research can be found in De Moor and Pissart (1992), Maréchal (1992) and Sommé (1988). In the 80s and 90s, Baeteman (1981, 1991) concentrated on the western part of the Belgian coastal plain; while Mostaert (1985) and De Moor *et al.* (1992) focused on the eastern part, and De Ceunynck (1985) studied the dunes. For the first attempt to investigate the geology offshore Belgium, the reader is referred to Bastin (1974). The study of De Batist and Henriet (1995), of which some preliminary results have been presented by Henriet *et al.* (1989a and b) and De

Batist *et al.* (1989), represents the first comprehensive investigation of the stratigraphy and structural setting of the Belgian Continental Shelf.

Figure 2-1: The Belgian shoreline between De Panne in the Southwest and Knokke-Heist in the Northeast. Inset: situation map of the southern North Sea. Coordinates are in Belgian Lambert 2005 (x100 m).

2.1.2 Palaeogene Deposits

The substratum of the Belgian shoreline is composed of solid layers of various ages. The Palaeozoic basement, composed of solid rocks, is found at a depth of app. 250 m near the French border to 450 m near the Dutch border. It is a relatively stable continental block called the London-Brabant Massif which was only flooded since Late Cretaceous times. During this period, a chalk layer was deposited on top of the Massif with a minimal thickness of 50 m between Nieuwpoort and Oostende, increasing rapidly offshore to a maximum of 220 m in the area of the Hinder Banks. On top of this layer, one finds the Palaeogene deposits[6].

[6] Note that the conventional naming 'Tertiary and Quaternary' for the sub-era's in the era of the Cenozoic are no longer in use. Because of the historically ambiguous way in which the boundary between the Tertiary and Quaternary has been defined, these terms have fallen out of favour for

Laga *et al.* (2001) summarise the present knowledge of the Palaeogene lithostratigraphy, whilst Le Bot *et al.* (2003) provides a comprehensive overview of the offshore Palaeogene (as well as the Neogene) deposits.

Detailed seismic interpretation following Mitchum *et al.* (1977), allowed De Batist (1989) and De Batist and Henriet (1995) to identify 8 seismo-stratigraphical units and a number of subunits within the Belgian Palaeogene succession, based on geometry and facies characteristics. Erosional truncation and valley incisions are common features at the top of the units. Most of the units have a pronounced sheet-like shape, with planar dipping boundaries at their base and top, and show only minor thickness variation within the unit. Each unit is also characterised by a distinct seismic facies and/or by typical facies variations, indicative for the depositional environment and its evolution. The major seismo-stratigraphical units have been labelled with a character-digit symbol, indicating their most probable chronostratigraphical position: Y1 to Y5 from Ypresian age, L1 and L2 from Lutetian age, B1 from Bartonian age and P1 from Priabonian age. The characteristics of these units can be found in De Batist and Henriet (1995).

At the Belgian shoreline, the surface which truncates the sequence of the Palaeogene strata coincides with the base of the Quaternary deposits. Hence, the lower Neogene (Miocene and Pliocene) is not represented.

2.1.3 Quaternary Sediments

The Quaternary deposits are non-cemented sediments. A part of them is relict, but most of the surface part is currently mobile under the action of currents, waves and wind. The Quaternary in the study area is characterised by a laterally as well as vertically complex and heterogeneous facies assemblage. Quaternary deposits occur in individual morphological subunits characterised by a very distinct stratigraphical built-up and lithological complexity (Bastin, 1974; Eisma *et al.*, 1979).

Most of the preserved Quaternary sediments have been deposited during the Holocene flooding of the southern North Sea (the formerly called Flandrian transgression) which started app. 10 000 years cal BP. Nevertheless, although weakly extended, some thick deposits originate from the Pleistocene period. This epoch is characterised by the succession of glacial and interglacial stages. During the glacial stages, large amounts of sediments were carried out into the southern North Sea basin by large rivers such as the Thames, Meuse and the Rhine. On the Belgian Continental Shelf, most of the

formal scientific use, and the International Commission on Stratigraphy no longer endorses them (http://www.stratigraphy.org/). Instead, the terms Palaeogene and Neogene, in their modern form, are the preferred way to subdivide the Cenozoic Era. However, as much of the literature on the geology of the Belgian shoreline still refers to the Quaternary, both the new and the old terminology are used in this overview.

Pleistocene sediments originate from the discharge of the Rhine-Meuse system and the Flemish Valley (Houbolt, 1968). On the continental shelf only few sediments are considered of Pleistocene age; however, along the shoreline they are widespread. The supposed Pleistocene deposits consist mainly of infilling of scour hollows and palaeovalleys, burrowed in the top of the Palaeogene deposits (Le Bot *et al*., 2003).

The present-day coastal barrier, whose position and shape were conditioned by the pre-existing topography, have been shaped in a very recent and short time, at least geologically speaking, known as the Holocene (Beets and Van Der Spek, 2000; Baeteman and Declercq, 2002). The total tickness of the Holocene sediment body may locally exceed 50 m, more particularly in the dune belt. In most of the coastal plain however, the top surface of the Holocene is so flat that the relief of the Holocene base provides a good image of its thickness. Since the end of the last Ice Age, especially between 10 000 and 7 800 years cal BP, the global sea level underwent a rapid rise (Köhn, 1989; Baeteman, 1999). As a result of this, the gently sloping northern part of the coastal plain and the incised river mouths were flooded. The deceleration in the rate of the sea-level rise (from 7 800 cal BP onwards) was responsible for the formation of the first sandy coastal barrier. Landwards from this barrier, frequent alternations of mud, peat and gyttja[7] in the sedimentary sequence deposited between ca. 7 800 and 6 000 cal BP. The facies changes are determined by a sedimentological control related to the tidal channel and creek network, and not by sea-level fluctuations, as it was assumed before (Baeteman, 2007). Periods of peat growth lasted longer and the lateral extension became more widespread as deceleration of the sea-level rise and filling of the plain continued. This was associated with progradation of the shoreface from ca. 6 000 cal BP onwards. Tidal conditions returned to the area from ca. 4 000 cal BP onwards. This return was accompanied by erosion and landward migration of the sandy shoreface and channel network. The stratigraphy using Dunkerque and Calais as units has been abandoned in favour of lithological and sedimentological descriptions and age determinations together with environmental interpretations (Baeteman, 1999; Baeteman, 2007).

The sea level rise continues today. Over the period 1925-2004, the mean high water level in Oostende increased with 15 cm, i.e., almost 2 mm/year. However, the increase is not steady, it is a combination of a linear increase of 18 cm per century and a sinusoidal cycle with an amplitude of app. 3.5 cm and a period of 18.61 year (this is the Saros cycle which is due to the change in angle between the sun, moon and Earth). As a result of both trends, the sea level rises with 10 mm/year when the Saros cycle is in an upward phase and the sea level lowers with 6 mm/year when it is in the downward phase (Verwaest *et al*., 2005). The other causes of the sea level rise are complex and will not be discussed in this thesis. The main components are generally agreed to be the melting of the Weichselian ice caps and the corresponding increase of seawater volume, the thermal expansion of sea water due to higher temperatures, and, locally in

[7] Gyttja is a Swedish term for mud rich in organic matter.

northwestern Europe, a relative subsidence of the land surface to compensate for the glacio-isostatic rebound of Scandinavia after the end of the glaciation when the pressure of the ice cap was taken away. Other reasons for a local relative sea level rise include compaction of unconsolidated sediments such as clay and peat, and the continuation of restricted tectonic movements such as those related to the North Sea – Rhine graben system. Land movements during the Holocene, due to tectonics or glacio-isostatics appear to be negligible in the Belgian coastal plain (De Moor and De Breuck, 1973). Though the rate of sea-level rise decreases on a geological time scale (Köhn, 1989), many scientists nowadays believe that rates may increase again as a result of the ongoing global warming (see also Section 1.1).

2.2 Present-day geomorphological characteristics

The Belgian coastal barrier is essentially a long, almost rectilinear sandbody whose geomorphological units are the dunes, the beach, and the nearshore (Houthuys, 1993). In cross section, this sandbody is typically a few hundreds of meter to a maximum of about 2 km wide, while its surface may reach heights of 15 to 25 m TAW (Tweede Algemene Waterpassing). At irregular distances, the coastal barrier was interrupted by tidal inlets and river mouths; most of them are nowadays transformed to harbour access or drainage channels. Figure 2-2 illustrates the different morphological coastal units as they are used throughout this thesis, as well as their relative position.

The present-day position of the coastal barrier is the result of a dynamic equilibrium between coast-building and coast-destructing forces. These are supplied by coastal currents, winds and waves. As explained before, the position and shape of the coastal barrier has changed significantly throughout geological and historical time. The main factor triggering these changes appears to be the interplay of sand availability with changes in sea level, i.e., both the Holocene sea level rise and the changes in tidal range. Sea level strongly determines the impact of the forces acting directly on the coast: waves, wave driven currents, tidal currents and wind. Most of these factors have a dual action, i.e., they can be both destructive and constructive forces, depending on their magnitude, frequency, direction, etc.

It is believed that after the last Ice Age (app. 10 000 cal BP), no coastal barrier was present at the Belgian coast until the rate of sea level rise slowed down around 7 800 cal BP. The reasons for sediment accretion at the Southeast side of the southern North Sea, including the formation of a coastal barrier, inshore sediment accumulation, and the development of offshore sand banks, are complex. According to Eisma (1980), the following conditions explain the trend of accretion during the Holocene:

- the presence of large amounts of unconsolidated material, predominantly sand, deposited on the emerged shelf surface during the Ice Age low stand;

- the continuing supply of sand and mud by the rivers (Beets and Van Der Spek, 2000);
- the net easterly direction of coastal sediment transport

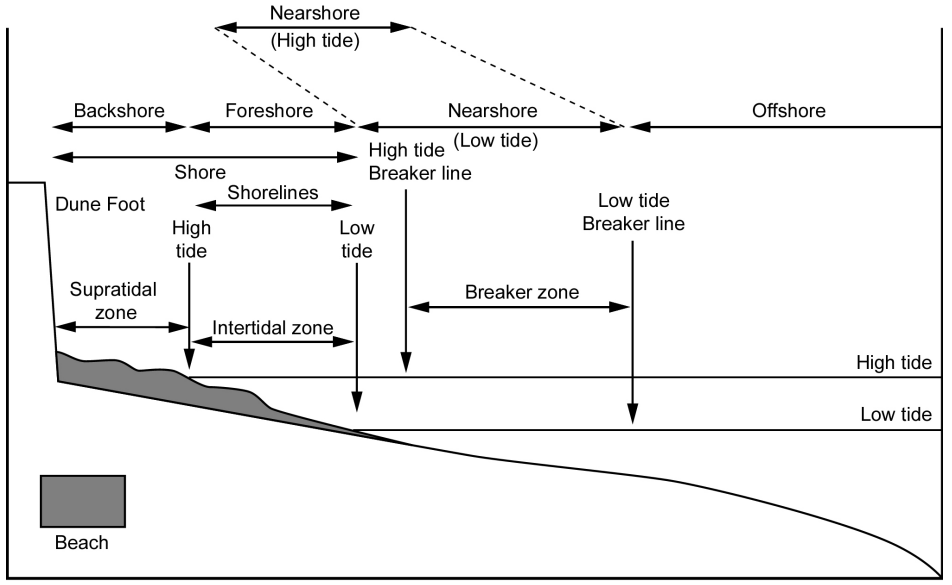

Figure 2-2: Coastal terminology, modified from Bird (2000).

Today, the sandy beach is up to 600 m wide at the West Coast in De Panne and Koksijde. These beaches are characterised by low gradient surf zones across which spilling breakers dissipate their energy. According to the Beach State Index (BSI) of McLachlan *et al.* (1993), which indicates the ability of waves and tides to move sand, these beaches can be classified as ultra-dissipative. This means that the tidal range is large and the wave energy high. Figure 2-3A shows a profile of the beach in De Panne obtained with airborne laserscanning (acquisitions in Sept. 2004). The intertidal part of the beach contains several parallel ridges and runnels which pass into the supratidal beach. The mean slope is between 1 - 1.5%.

The Middle Coast, i.e., the coastal strip between Middelkerke and Zeebrugge (Figure 2-1), is characterised by less wide beaches; on average between 200-400 m. Although they still qualify as ultra-dissipative beaches, their geomorphology is completely different from the geomorphology of the beaches along the West Coast. This is mainly due to the groynes that are present along the entire Middle Coast, except for the coastal strip around De Haan. The resulting profile is rather smooth between the low and high water mark and has an average slope of 1.5 - 2.0%, while the backshore is much steeper (more than 5%). The beach has a concave profile around the high water mark (Figure 2-3B).

A. Beach profile in De Panne (West Coast)

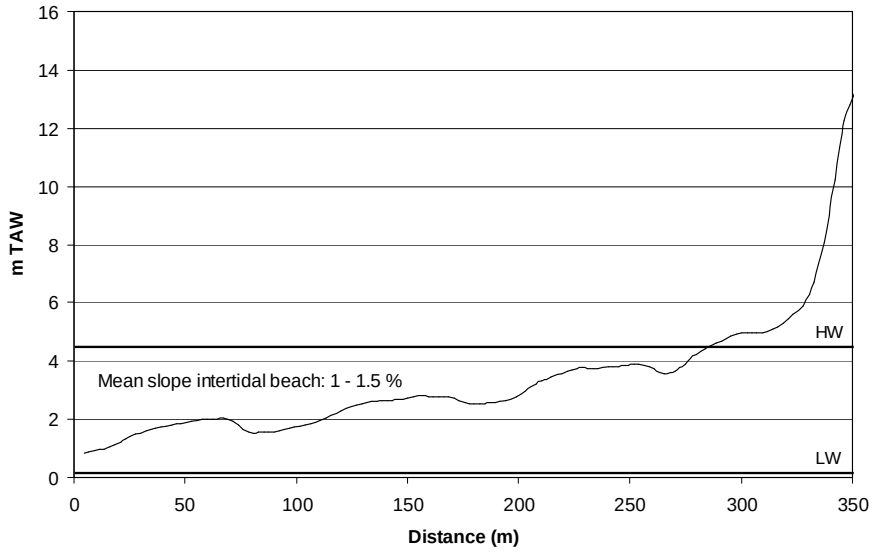

B. Beach profile in Middelkerke (Middle Coast)

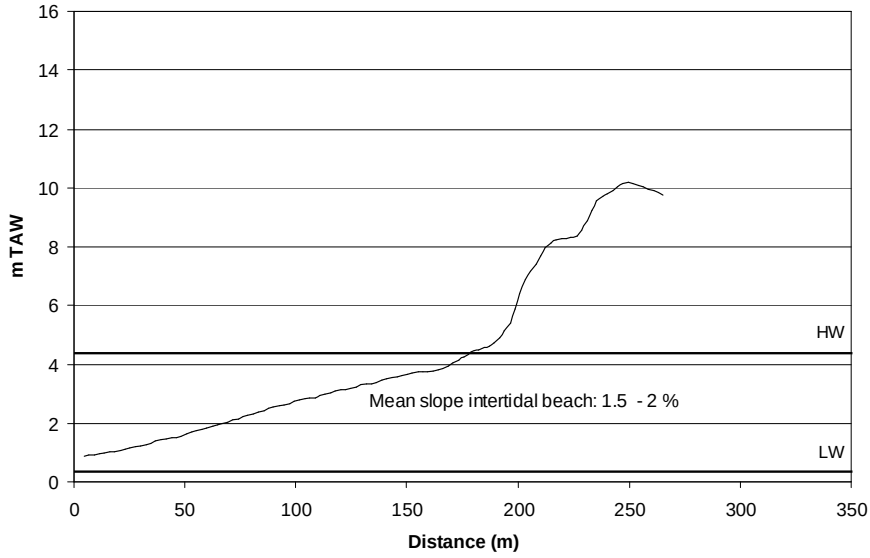

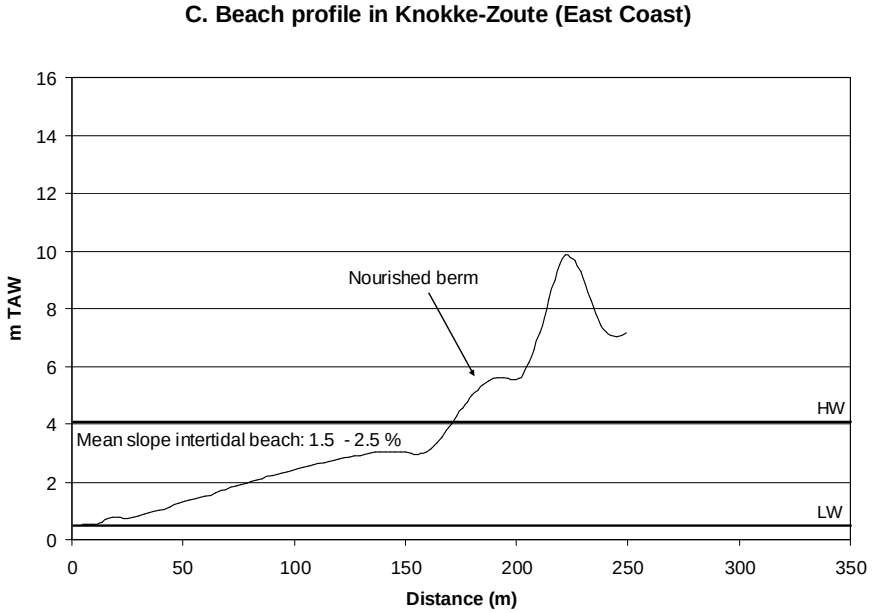

Figure 2-3: Beach profile in De Panne (A), Middelkerke (B) and Knokke-Zoute (C). The data are derived from an airborne LIDAR survey in September 2004. The upper black line indicates the local mean high water level (HW), the lower black line indicates the local mean low water level (LW).

The East Coast and especially Knokke-Heist, features the most narrow beaches in Belgium. They are only 100-300 m wide with a mean slope of 1.5 – 2.5% on the intertidal part. According to the Beach State Index, they are classified as dissipative, although local reflective conditions occur around the high water mark. The beaches of the East Coast have, in the last decades, been prone to severe erosion. Therefore, man has strived to keep this shoreline at its position since the late 70s, making use of large-scale beach nourishments in combination with groynes (the latter were already constructed before the 70s). The effect of the beach nourishments on the dry beach is clearly visible in Figure 2-3C as a berm around the high water mark.

De Moor (2006) provides a comprehensive field guide, describing the present-day geomorphology and dynamics of the Belgian beach as well as many small-scale notes.

2.3 Man made structures and interventions

The economical and social importance of the Belgian beach can hardly be overrated. Belgium, and especially Flanders is among the most densely populated regions in Europe (447 inhabitants/km² in 2005). The 65 km long coastline has a major economic

value due to its attractive beaches (cf. tourism industry) and the presence of a few important sea ports (Zeebrugge and Oostende). Therefore, a 'laissez-faire' attitude, allowing a natural dynamic behaviour of the coastline, is not an option.

The first attempts to limit the natural dynamics of the Belgian beach were, without exception, the hard defence works: seawalls, reinforced dune bases, groynes, beach groynes, and Longard tubes. However, since the 70s, one is convinced that so-called soft defence structures such as beach nourishments and beach scrapings (or beach elevation works) are to be preferred to hard defence structures. Hard coastal protection may lead to increased erosion, often at downdrift locations rather than where the actual construction took place (through longshore transport of the sediment) (Peterson *et al.*, 2000). An example of a higher risk of erosion is the disappearance of the dry beach section on many beaches along the East Coast after the construction of seawalls at the foot of the coastal dunes about a century ago (Charlier and De Meyer, 1995, 2000). Beach nourishment gives rise to smaller changes in the natural dynamics of both sediment and water, favouring a sooner and more easy equilibrium that keeps its effect for a longer time (Peterson *et al*., 2000). Negative aspects are the higher costs, as a consequence of the need of replenishment every few years, the lower applicability on beaches with high wave energy (Esteves and Finkl, 1998), and the negative ecological consequences (Speybroeck *et al*., 2006). Raudkivi and Dette (2002) discuss some cost efficiency options.

Figure 2-4 shows the spatial distribution of all soft and hard defence works along our coastline. For more information on the different types of beach nourishments, the reader is referred to Huygens (2001); this author studied a beach nourishment at the Belgian East Coast comparing field measurements, physical laboratory tests and mathematical simulations.

Today, the beaches of the West Coast are the most 'natural' beaches along the Belgian shoreline; they are not influenced by large-scale nourishment works although a few groynes, beach groynes and yearly dry beach replenishments influence the profile locally. The latter is especially the case in Koksijde. The Middle Coast has been the scene for large-scale nourishment works, especially around De Haan where in the 90s a classical dry beach nourishment was combined with the deposition of a nearshore feeder berm (De Wolf and Houthuys, 1997). Recently, in the spring of 2004, a beach nourishment took place in the centre of Oostende (also combined with the deposition of a nearshore berm). Before the nourishment, there was no dry beach anymore in the centre of the city, which implies that during high tide the seawall immediately served as sea-defence. Many places at the Middle Coast are also subject to dry beach elevation works. The East Coast (Knokke-Heist), features the most narrow beaches in Belgium. These beaches have for many decades been prone to severe erosion. Therefore, man has strived to keep this shoreline at its position since the late 70s, making use of large-scale dry beach nourishments in combination with groynes. The effect of the beach nourishments on the dry beach is clearly visible in Figure 2-3 as a berm around the high water level. Another remarkable feature at the East Coast is the beach nature

reserve in the Bay of Heist (for location, see Figure 2-5). This large beach is mainly the result of nourishments that were executed to compensate for the erosion that was expected after the construction of the harbour dams of Zeebrugge. Today, the beach in the bay is characterised by a shallow, rather muddy lagoon separated from the lower parts of the beach by a sandy ridge. However, through two openings, the lagoon is flooded twice daily. In and around the lagoon a halophytic salt marsh vegetation developed with typical species as *Crambe maritima* (Sea Kale), *Cakile maritima* (Sea Rocket), *Honckenya peploides* (Sea Sandwort), and *Atriplex littoralis* (Grass-leaved Orache). Less abundant but also present are *Apium graveolens* (Celery), *Triglochin maritimum* (Sea Arrowgrass), *Plantago maritima* (Sea Plantain) and *Crithmum maritimum* (Rock Samphire), while on the embryonic dunes, *Elymus farctus* (Sand Couch-grass) is found. Next to its botanical value, the bay is also from an ornithological point of view of high interest: it is a breeding place for *Sterna albifrons* (Little Terns), while *Haematopus ostralegus* (Oystercatchers), *Charadrius alexandrinus* (Kentish Plover) and *Charadrius hiaticula* (Great Ringed Plover) like foraging in this area. In the embryonic dunes, the *Oenanthe oenanthe* (Northern Wheatear) and the *Galerida cristata* (Crested Lark) are among the regular visitors.

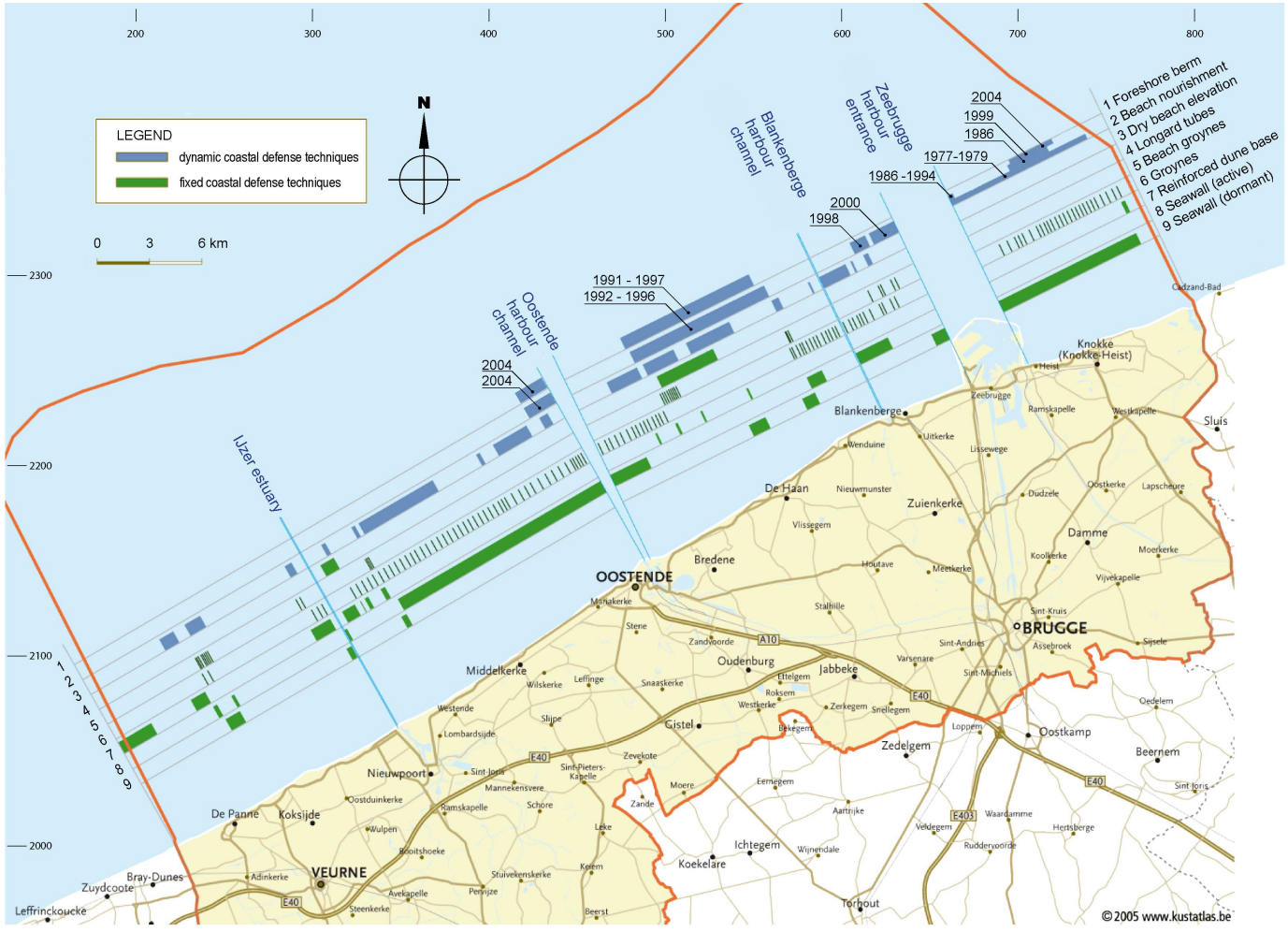

Figure 2-4: Schematic overview of the man made structures and interventions (with their corresponding date) along the Belgian shoreline (modified from Kustatlas, VLIZ, 2005). Coordinates are in Belgian Lambert 2005 (x100 m).

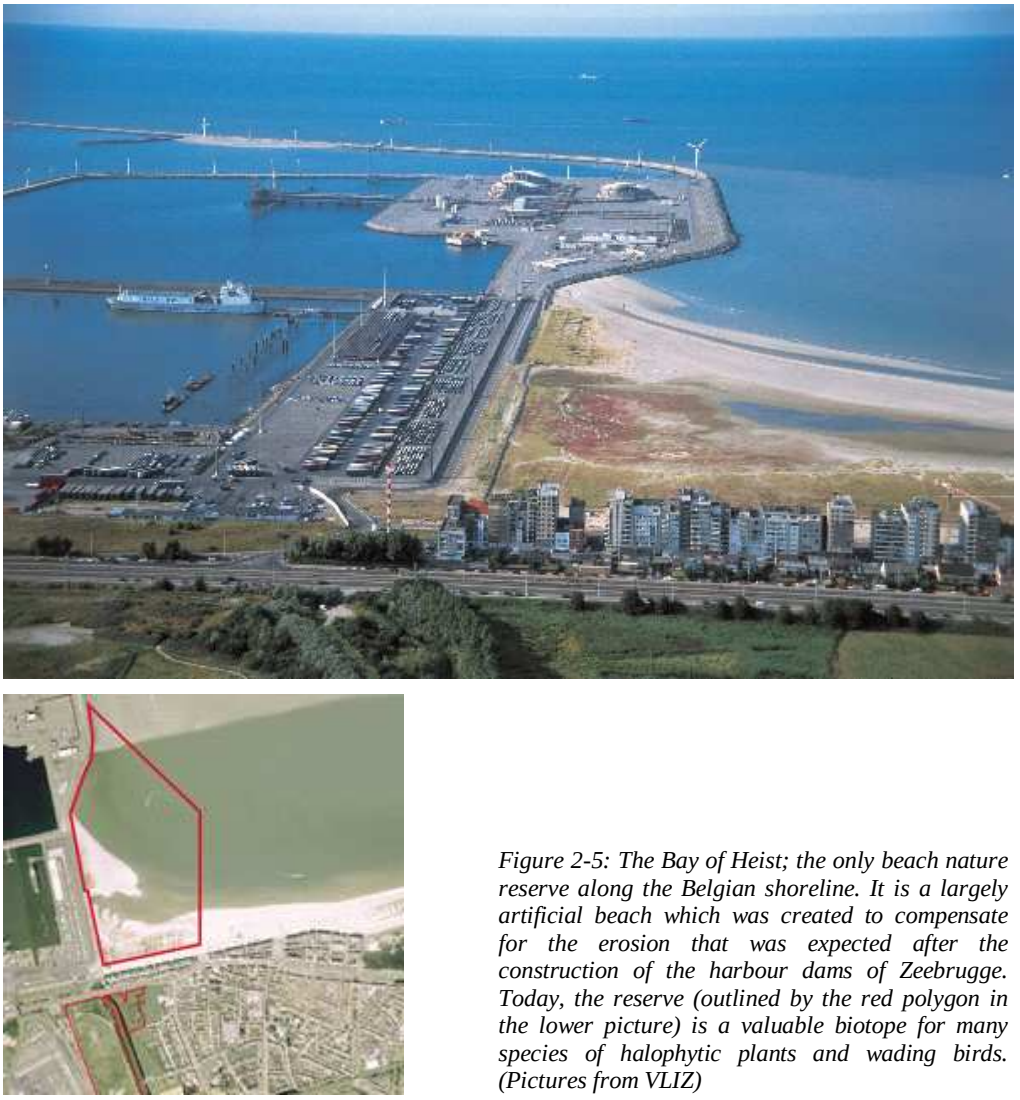

Figure 2-5: The Bay of Heist; the only beach nature reserve along the Belgian shoreline. It is a largely artificial beach which was created to compensate for the erosion that was expected after the construction of the harbour dams of Zeebrugge. Today, the reserve (outlined by the red polygon in the lower picture) is a valuable biotope for many species of halophytic plants and wading birds. (Pictures from VLIZ)

2.4 Reference TAW levels

In the next chapters, altitude with respect to the local height datum (TAW = Tweede Algemene Waterpassing) will often be mentioned. To allow the reader to interpret these numbers, this chapter provides a concise overview of the most important reference levels in use along the Belgian shoreline (expressed in TAW).

Classification of tides in Oostende (Middle Coast):

- Mean low water during spring tide: + 0.02 m
- Mean low water during neap tide: + 0.75 m
- Mean high water during spring tide: + 4.65 m
- Mean high water during neap tide: + 3.78 m
- Mean high water during extreme spring tide: + 5.08 m

Storm surge warnings (Oostende):

- High tide: + 5.60 m
- Dangerous storm surge: + 5.90 m
- Measured extreme storm surge (1 feb 1953): + 6.66 m

Elements of the beach (defined in the context of public works):

- Nearshore front (VO): - 4.11 m
- Low water level (LW): + 1.39 m
- High water level (HW): + 4.39 m
- Dune foot (DV): + 6.89 m

Height levels of existing infrastructures:

- Seawall in Knokke-Heist: + 9.60 m
- Seawall in De Haan: + 11.00 m / + 11.29 m
- Seawall in Oostende: + 8.60 till + 9.60 m
- Seawall in De Panne: + 9.60 m
- Harbour quays of Zeebrugge: + 7.89 m

The tidal wave at the Belgian coast runs from the Southwest to the Northeast, it has a mean cycle of 12 h 27 min and a mean vertical amplitude of 3.90 m (at the West Coast the amplitude is larger than at the East Coast; e.g., 4.10 m in Nieuwpoort compared to 3.68 m in Zeebrugge). The time difference between a tidal level at the French border and the Dutch border is app. 50 min.

Chapter 3

Airborne and ground truth data

3.1 Airborne data

Table 3-1 lists the available airborne hyperspectral and LIDAR data[8]. One will notice that in some years (2003 and 2005), there were no acquisitions or only one sensor was deployed (2006). This was due to financial and organisational constraints. However, the gaps in the time series do not prohibit the analysis at the longer term, although some more interpretation was needed. Another difficulty was the time lag between the hyperspectral recordings and the LIDAR campaigns. Ideally, they should be performed simultaneously, but this was not always possible from an organisational point of view.

Table 3-1: Overview of the available airborne remote sensing data.

	2000	**2001**	**2002**	**2004**	**2006**
Hyperspectral					
Sensor	CASI	CASI	CASI	AISA-Eagle	---
Date of acquisition	23/08/2000	27/08/2001	11/10/2002	6/07/2004	
LIDAR					
Sensor	ALTM 1225	ALTM 1225	ALTM 1225	ALTM 2050	ALS-40
Date of acquisition	11/09/2000	28/09/2001	18/12/2002	2/09/2004	18/04/2006

[8] All airborne data were acquired and financed under the authority of the Agency for Maritime and Coastal Services (Flemish Government). They allowed the use of these data for this PhD study but remain the only and full owner of the data and the derived products.

The hydro-meteorological conditions were verified between the observations to ensure that no major storms had taken place. As such, it is assumed that the beach was in the same morphological state during both acquisitions.

3.2 Ground truth data

Each hyperspectral campaign was accompanied by field measurements which served to train (calibrate) and validate the classifications. In the same period as the airborne acquisitions, samples from the top layer of the beach (about 200 g) were collected and afterwards analysed in the lab. At the same time, the geomorphological characteristics of the area around each sample point were described. The samples were spread over the entire coastline in order to have a representative set of training data. This implies that no systematic sampling was performed as this would result in abundant samples delivering no extra information. On the other hand, a systematic sampling scheme would omit certain interesting areas on the beach (e.g., small nourishment areas). Therefore, a non-systematic sampling was performed, based on existing field knowledge.

The number of samples used for training and validation of the classifications was:

Year	Number of samples
2000	36
2001	258
2002	99
2004	100

It should be noted that in some cases the available ground truth data was not sufficient to obtain statistical meaningful classification results. To overcome this, extra training and validation points were selected on the images. In these points, no samples could be taken, but the class they belong to was known as a result of the field knowledge.

To validate the LIDAR data, reference sites were surveyed terrestrially. The points measured were not exactly at the same locations as the DTM laser points, but all reference sites were selected on flat surfaces (e.g., flat and wide seawall tops). Hence, by spatial interpolation of the laserscan data, it was possible to calculate the height at the points measured. The validation pointed out that the DTMs have a mean absolute error of 5 cm (with a standard deviation of 7 cm). Note that the horizontal or planimetric accuracy is more difficult than vertical accuracy to assess in LIDAR datasets. This is because the land surface often lacks distinct (well defined) topographic features necessary for such tests or because the resolution of the elevation data is too coarse for precisely locating distinct surface features. Nevertheless, a frequently used rule of thumb is that the planimetric accuracy is roughly the double of the footprint size. In our observations, this results in a horizontal accuracy at nadir of 30-50 cm.

Taking into account that the point vector data were rasterised to pixels of 2 by 2 m, it can be concluded that the horizontal accuracy of the laser footprints is sufficient to obtain accurately located pixels, i.e., a horizontal accuracy often better than one pixel.

3.2.1 Sedimentological analysis of the ground truth data

The field samples, collected along the entire shoreline, were used to describe the sedimentological composition of the beach. The following parameters were measured through lab analysis:

- the total carbonates content: by adding 300 ml 2N HCl to the sample, the carbonates are removed according to the reaction (Loeppert and Suarez, 1996):

$$CaCO_3 + 2\ HCl <=> Ca^{2+} + CO_2 + H_2O + 2\ Cl^- \qquad \textit{Eq 3-1}$$

- the total organic matter content: adding 50-100 ml H_2O_2 removes the organic content.

- the granulometry: the classical dry sieving method (sieves: 500, 315, 200, 160, 100 and 63 μm) was applied to retrieve the granulometric characteristics. The main parameters derived from the granulometric analysis are the median grain size (D_{50}) and the sorting (S). As many sediment populations feature a log-normal distribution, the grain size is converted into phi (Φ) values according to (Krumbein, 1936):

$$\Phi = -\log_2 D / D_0 \qquad \textit{Eq 3-2}$$

Where D is the diameter of the particle in mm and D_0 is the diameter of a 1 mm particle (to make the equation dimensionless)

The sorting (S) is a measure for the distribution of the grain sizes around the average; it is calculated according to (Inman, 1952):

$$S = (\Phi_{84} - \Phi_{16}) / 2 \qquad \textit{Eq 3-3}$$

Where Φ_{16} and Φ_{84} are the grain sizes in the 16^{th} and 84^{th} percentile.

Hence, in a perfect log-normal distribution, the sorting corresponds to the standard deviation. In general, badly sorted sediments have an S value close to or exceeding 1, while the S value of very well sorted sediments is close to 0.

Figure 3-1 illustrates that the correlation between the D_{50} and the S is very weak. Hence, both parameters are complementary and were both taken into account.

- the total iron content: was determined using the Energy Dispersive X-Ray Fluorescence (ED-XRF) technique (Jenkins, 1999), applying an X-LAB 2000 spectrometer of Spectro. This analysis technique allows determining individual elements and molecules; however, in our description of the sedimentological

composition of the beach sand, only the total iron content was retained because of the important contribution of Fe-ions to the sediment colour.

- the microscopic mineral composition: was obtained by counting a sub-sample of 500 grains under the microscope. The following grains were distinguished: bright quartz, opaque (and coated) quartz, silex, glauconite, shell (and shell fragments), and a rest class 'other' (containing dark minerals, small pieces of concrete, sponge spicules). The proportion of each mineral is expressed as a percentage of the counted grains.

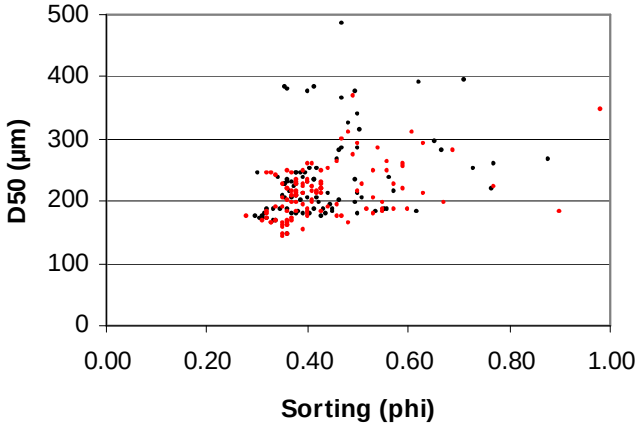

Figure 3-1: Correlation between the median grain size (D50) and the sorting (S); obtained with the samples collected in 2001 (red) and 2002 (black).

To summarise the sedimentological composition of the beach in the period studied, the analysis results of the individual samples are combined in a few graphs illustrating the spatial variation, both in the longshore and cross-shore direction. However, before looking at these results, it is worthwhile to mention the work of Depuydt (1972) who analysed systematically the sedimentological composition of the Belgian beach and dunes in the 60s. Since Depuydt conducted his research prior to the large-scale nourishment activities, which started in the 70s (cf. Section 2.3), his results are very valuable as they witness the original sedimentological characteristics of our shoreline. He concluded that the Belgian beach consisted for more than 85% of fine sand with a D_{50} between 175 and 250 µm. In De Panne, the grain size varied in the cross-shore direction from ca. 170 µm at the low water mark to ca. 210 µm at the high water mark. The sorting was very good (often better than 0.3 phi) and remained more or less the same in the cross-shore direction, although the sediment was slightly better sorted at the low water mark. In the longshore direction on the other hand, the sorting was very good (0.25 – 0.30 phi) and showed little or no variation. Also the grain size was the same along the entire Belgian shoreline (ca. 210 µm at the high water mark) with the exception of Koksijde-Bad (300 µm), De Haan (230 µm) and Knokke-Zoute

(250 μm). In the 60s, the beach in Koksijde-Bad featured severe erosion, probably due to the strong currents in the Potje, a tidal gully immediately offshore from Koksijde-Bad. Since the beaches around De Haan and Knokke-Zoute were also prone to erosion, it could be concluded that the grain size was linked to the rate of erosion (see the chapter below for our present-day results) although Depuydt's analysis in Knokke-Zoute was already hampered by the first beach nourishments there.

The analysis results mentioned in the next chapters (Section 3.2.2 till Section 3.2.6) are based on samples collected in 2001 (258 samples) and 2002 (99 samples).

3.2.2 The spatial variation of the median grain size

Back to our recent observations; Figure 3-2 illustrates the longshore variation of the median grain size for three different positions on the beach: at the low water level, just below the high water level, and on the dry beach. In general, one can see that there is a gradient from fine-grained sand at the low water level to coarser sand on the dry beach. This gradient is observed almost everywhere. In areas where beach scrapings or beach nourishments are executed, the grain size tends to be coarser, not only in the nourished zones of the beach, but along the entire transect. The most coarse sediments (close to 400 μm) were found in the nourishment area around De Haan and in Knokke-Zoute. Note that in the western part of the nourished area around De Haan, coarser sand (376 – 388 μm) was used than in De Haan-Oost. Despite the huge impact of the human interventions, a gradient from fine-grained sediments at the West Coast to coarser-grained sediments at the East Coast can be distinguished. Hence, the areas with coarser sediments correspond to the areas delineated by Depuydt (see the section above). The coarser sand in the nourished areas is both the result of the artificial nourishments where for preference coarse-grained sand is used and of the natural occurrence of coarse-grained sand in areas which are known to be subject to erosion. The reason why coarse-grained sand (often sea sand dredged on sand banks offshore) is preferred for beach nourishments and beach elevation works, is that coarse-grained sand is less subject to erosion than fine-grained sand. As such, it is possible to construct steeper slopes with coarse-grained sand.

3.2.3 The spatial variation of the sorting

In contrast with the median grain size, the cross-shore and longshore variation of the sorting is less pronounced. In general, the sorting is good (on average between 0.25 and 0.50 phi), but there are some exceptions, often related to human interventions. The sand used for nourishments is often poorly sorted, however, after a certain time the sediment is sorted out by the working of water and wind. Poorly sorted sand was found around Koksijde, on the dry beach West of the IJzermonding, along the low water level in Westende and Mariakerke, on the dry beach of De Haan and the Duinse Polders, and on the entire beach of Knokke-Zoute.

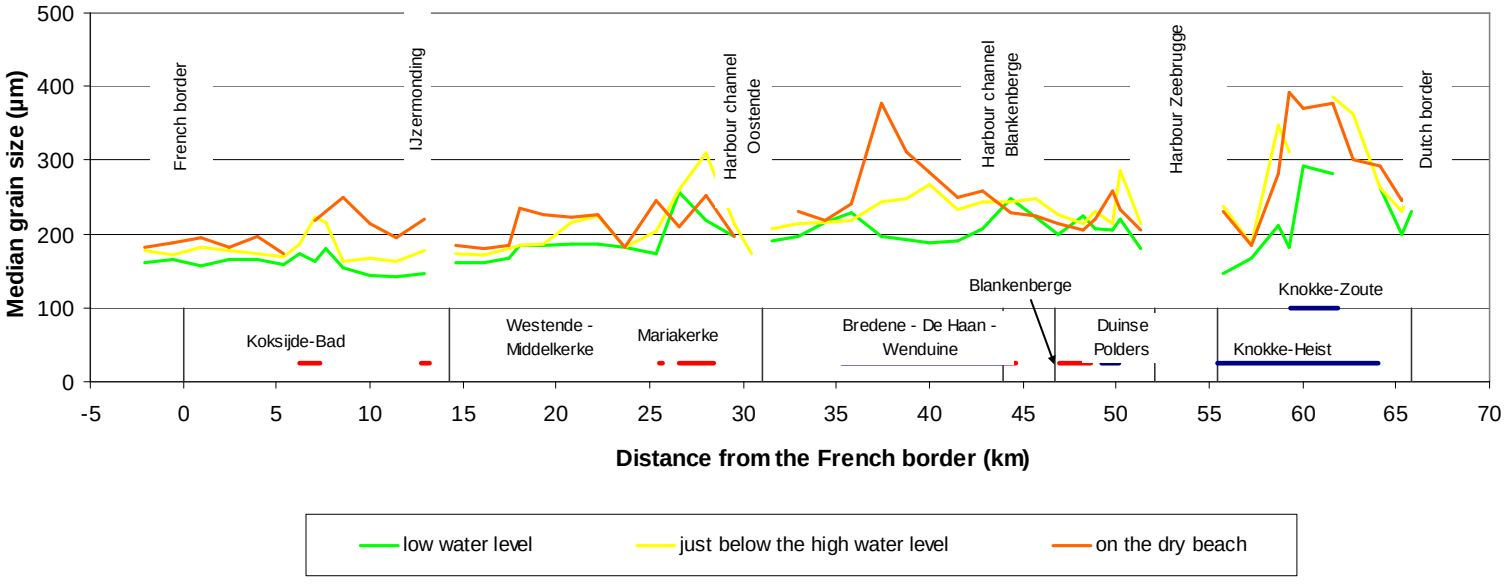

Figure 3-2: Longshore variation of the median grain size for three positions on the beach. Below in the graph, the beach nourishment areas (blue) and the beach scraping areas (red) are indicated. The analysis is based on the samples collected in 2001 and 2002. The small vertical lines indicate the coastal units as they are treated in Chapter 8.

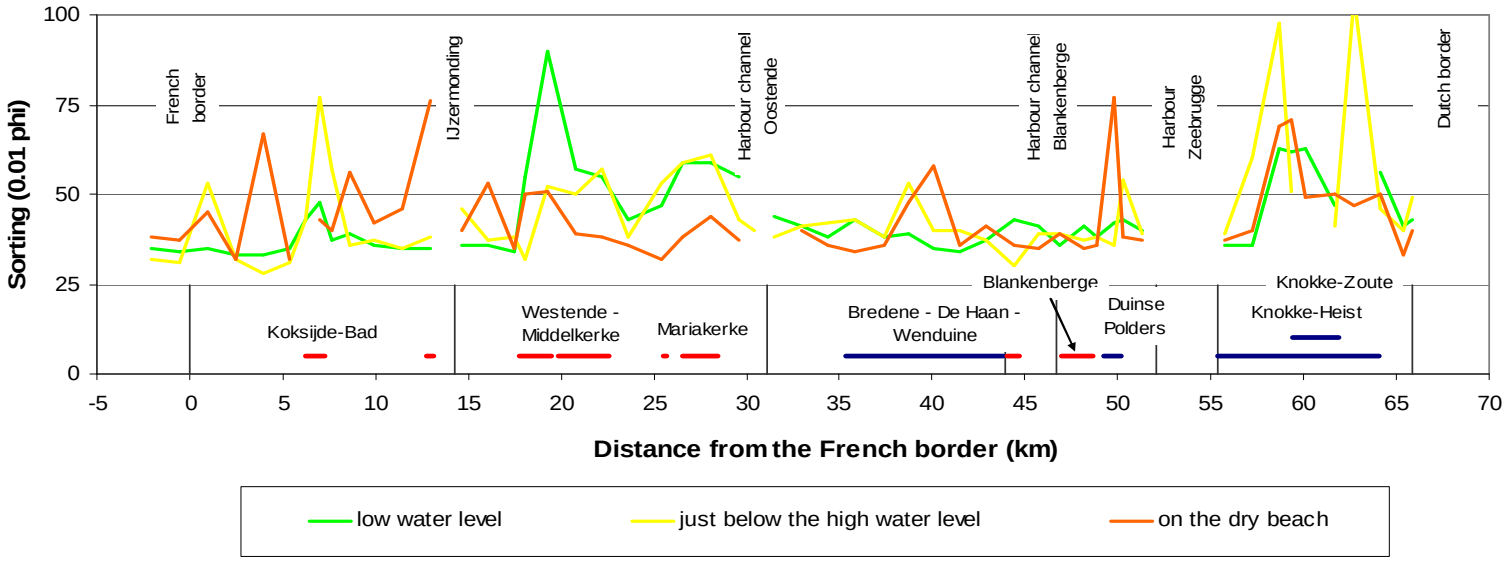

Figure 3-3: Longshore variation of the sorting for three positions on the beach. Below in the graph, the beach nourishment areas (blue) and the beach scraping areas (red) are indicated. The analysis is based on the samples collected in 2001 and 2002. The small vertical lines indicate the coastal units as they are treated in Chapter 8.

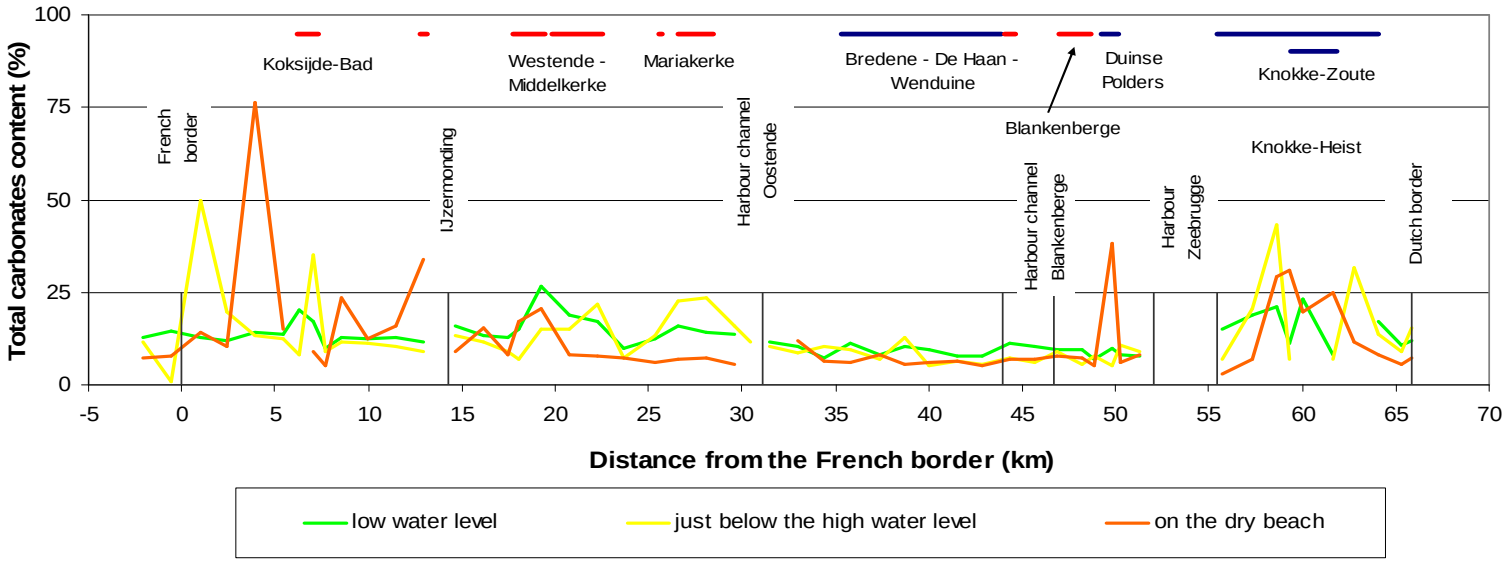

Figure 3-4: Longshore variation of the carbonates for three positions on the beach. Below in the graph, the beach nourishment areas (blue) and the beach scraping areas (red) are indicated. The analysis is based on the samples collected in 2001 and 2002. The small vertical lines indicate the coastal units as they are treated in Chapter 8.

3.2.4 The spatial variation of the total carbonates content

The carbonates in the beach sand originate from the chalk in the shells of molluscs. In the samples collected in 2001 and 2002, the weight percentage of the total carbonates content was mostly between 5 and 15%. However, shells tend to concentrate in strips on the beach; when a sample was collected in such a strip, the carbonates content may be close to 100% (this explains the very high value in Koksijde-West). On average, the carbonates content decreases from the low water level (ca. 11%) to the high water level (ca. 8%). However, a large variation was observed in this pattern. On the dry beach, the carbonates content is again somewhat higher (ca. 10%). In nourished areas, the carbonates content is everywhere higher than 13% and especially in recently nourished areas, the carbonates content is often more than 20%. Note that in the nourishment area around De Haan, shell-poor sand was used, the latter is rather exceptional for nourishment sand.

3.2.5 The spatial variation of the total organic matter content

The organic matter content is very low in all samples collected; most samples feature an organic matter content lower than 0.1%. Only the shell-rich samples show a slightly higher organic matter content of 0.2 – 0.4%. Also samples that were collected in muddy or silty areas (mostly on the lower parts of the beach and often in the runnels) show a somewhat higher organic matter content of ca. 0.3%.

3.2.6 The spatial variation of the total iron content

The iron represented in the sand samples is dominated by oxidised iron (Fe^{3+}); this has an orange-reddish colour and is found in the shells of molluscs as well as in thin coatings around quartz grains (often orange limonite). In areas where there is no influence from beach nourishments or beach elevation works, the average total iron content is 3 – 4 g/kg dry matter. The amount is stable in the across-shore direction and does not vary from the West to the East. However, sand used for beach nourishments or beach elevation works shows a higher total iron content of ca. 5 g/kg. The highest concentration is found in shell-rich areas, both in the shell strips found along the topzone of sand banks as in the shell-rich sand used for beach nourishments or beach elevation works; here, the amount is ca 10 g/kg.

Chapter 4

SAM classifier applied to beach sand classification and combination of imaging spectroscopy & LIDAR for sediment transport monitoring

This chapter is based on:

Deronde B., Houthuys R., Debruyn W., Fransaer D., Van Lancker V. and J.-P. Henriet, 2006, Using airborne hyperspectral data and laserscan data to study beach morphodynamics along the Belgian coast. Journal of coastal research, 22(5): 1108-1118.

4.1 Abstract

This paper addresses the possibilities of the combined use of airborne hyperspectral data and airborne laserscanning data to study sand dynamics on the Belgian backshore and foreshore. In August 2000, August 2001 and October 2002 airborne hyperspectral imagery was acquired with a CASI-2 sensor from the entire Belgian beach at low tide. Hyperspectral images contain for each pixel a reflectance spectrum. The characteristics of this spectrum are influenced by the state, the composition and the structure of the topsoil of the beach. After radiometric, geometric and atmospheric correction of the images a normalisation of the spectral signatures was necessary to allow the comparison of wet and dry pixels. Consequently, the first derivative of the normalised spectra was taken, followed by a Spectral Angle Mapper algorithm which was used to

perform a supervised classification. The beach was classified in eight different sand classes. Almost simultaneously to the first two CASI campaigns (in September 2000 and September 2001), a laserscan survey was performed to generate digital terrain models with a mean vertical accuracy of 5 cm. By differencing both digital terrain models, a map with sedimentation and erosion zones could be extracted. The combined interpretation of the erosion/sedimentation map and the classified hyperspectral data yields an appropriate method for studying the processes of sand transport along the Belgian coastline. The method was tried out with success on the Belgian East coast.

4.2 Introduction

One way of gaining insight in the coastal dynamics is the follow-up of the beach by airborne multispectral or hyperspectral observations and by airborne LIDAR (LIght Detection And Ranging) measurements. Bryant et al. (1996) and Rainey *et al*. (2000 and 2003) explored the possibilities of the Daedalus 1268 Airborne Thematic Mapper (ATM) to map sandy and clayey sediments in the Ribble estuary (UK), focussing on the different grain sizes as influencing parameter on the spectral reflectance. Lee and Shan (2003) combined IKONOS data and LIDAR data to classify a coastal strip in North Carolina in six classes: road, water, marsh, roof, tree and sand. Thomson *et al*. (1998) used the CASI scanner in a mode with 14 spectral bands to classify the vegetation and sediments in the Wash bay at the East Coast of England in 10 classes. In the same study area, Yates *et a*l. (1993) tried to classify sandy and muddy sediments with spaceborne Landsat TM data; the poorer spatial resolution inspired them to try a sub-pixel classification which was performed with success. However, the common experience is that the fine spectral and spatial resolution of airborne sensors offer superior capabilities for sediment monitoring. Additionally, several authors analysed the relationship between the reflected sunlight and soil properties like organic matter, soil moisture, soil salinity and grain size distribution (Bedidi *et al*., 1992; Ben Dor *et al*., 2002; among others).

4.3 Methodology

In the presented study two types of data are used: airborne hyperspectral imagery is applied to classify the sandy beach in 8 different sand types. LIDAR-derived digital terrain models (DTMs) are used to calculate erosion/sedimentation maps. The combination of the sand classification maps and the erosion/sedimentation maps provides the material for a semi-quantitative, semi-qualitative method for the regular monitoring of sandy coastlines. In the next paragraphs, the different steps of this method are explained.

On August 23, 2000 a first flight over the entire coastline was performed with a CASI-2 sensor measuring the reflected light in a 545 nm spectral range (410-955 nm) configured in the VNIR range. The original spatial resolution of the pixels after acquisition was 1.0 m by 2.2 m (1 m across-track and 2.2 m along-track). These were resampled with a bi-linear resampling algorithm to 2 m by 2 m pixels. The geometrically corrected and radiometrically calibrated data were corrected for atmospheric influences using ATCOR-4 which is based on the radiometric transfer model MODTRAN-4 (Richter and Schläpfer, 2002). Simultaneously to the flight, differential GPS measurements, sunphotometer measurements and reflectance measurements were performed. The differential GPS is used in combination with the attitude data (i.e., roll, pitch and yaw) of the aircraft to georeference the data as accurately as possible, while the data collected with the sunphotometer and the reflectance measurements of a dark and bright reference target were used in the atmospheric correction. On August 27, 2001 a second acquisition was performed yielding pixels of 1 m by 4 m, and on October 11, 2002 a third registration took place with pixels of 2.5 m by 2.5 m. All three datasets were resampled in the same way to 2 m by 2 m. The positional accuracy after the geometric correction varies from correctly positioned to a misregistration of 2 pixels.

During the three acquisitions, the CASI-2 was configured in enhanced spectral mode measuring the reflected light in 96 spectral bands. Due to the absorption by water vapor, the last 13 bands of the acquisitions had to be eliminated. Moreover, in the datasets of 2000 and 2001 the first 19 bands, and in the one of 2002 the first 16 bands, could not be used because of across-track striping. This effect has a technical cause but it is reinforced by the limited number of photons in the blue range caused by atmospheric Raleigh scattering. Finally, the analysis was performed on 64 bands for the data of 2000 and 2001 and on 67 bands for the data of 2002.

After the radiometric calibration and the geometric and atmospheric correction, the hyperspectral data were smoothed with a weighted averaging algorithm developed by Bertels (2005).

Consequently, the smoothed data were normalised in order to be able to compare wet to dry spectra. The reflectance of wet samples is much lower than the one from dry samples and since the flight was performed at low tide, a normalisation was necessary to be able to compare all reflectance curves. Figure 4-1 illustrates that the spectral reflectance curves of two different samples, regardless whether they are in dry or wet state, are more similar than the wet and dry state curves of one sample.

In Figure 4-2 the principle of normalisation is illustrated. For each wavelength a factor F is calculated which gives the ratio between the moving average through a smooth curve with high reflectance (R_{hs}) and the smoothed original curve (R_{0s}). The original curves are smoothed with a moving average over 35 values (bands). The number of bands used in the smoothing is high to retain only the general shape of the curve, not the absorption features. The ‘smooth curve with high reflectance’ is the spectrum with

the highest overall reflectance present in the scene raised with 10% reflectance. This curve is also smoothed over 35 values.

For each wavelength, F is multiplied by the difference between the original curve (R_0) and the moving average through the original curve (R_{0s}); R_n, the resulting normalised reflectance, is obtained as follows:

$$R_n(\lambda) = \left(R_0(\lambda) - R_{0s}(\lambda)\right) * F(\lambda) + R_{hs}(\lambda) \qquad \text{Eq 4-1}$$

$$\text{with } F(\lambda) = \left(R_{hs}(\lambda) / R_{0s}(\lambda)\right)$$

Note that this method preserves the shape of the spectra while the absolute value of the reflectance is lost; all spectra are raised till the reflectance level of the chosen high spectrum. Hence, it is assumed that soil moisture has a homothetic effect on the soil spectral properties. This assumption can be made when working with soils which have quasi-featureless reflectance spectra, i.e., without clear absorption bands (Bedidi *et al.* 1992).

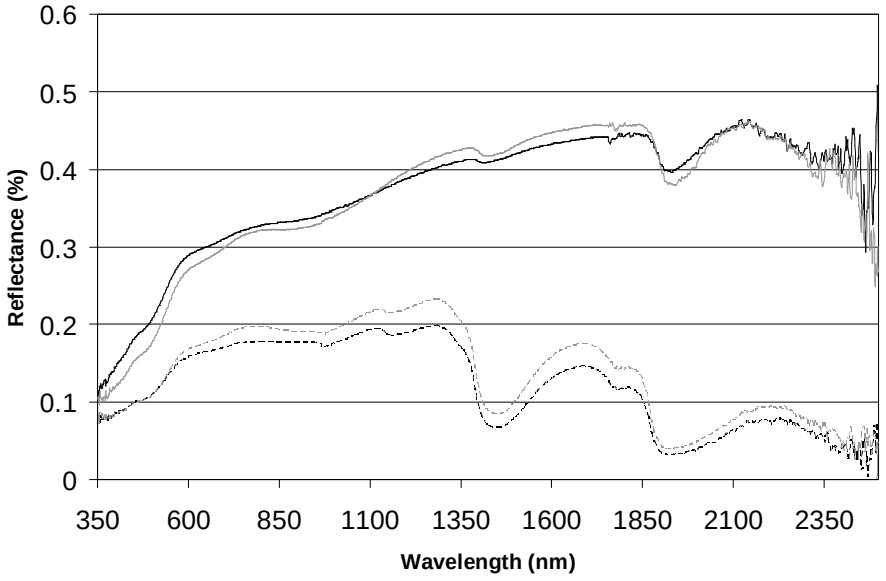

Figure 4-1: Spectral reflectance measured between 350 and 2 500 nm with an ASD (Fieldspec Pro Fr) spectroradiometer. The dashed curves are the spectra for wet, saturated samples and the full lines for dry spectra. Black and grey represent the spectra of two arbitrary samples.

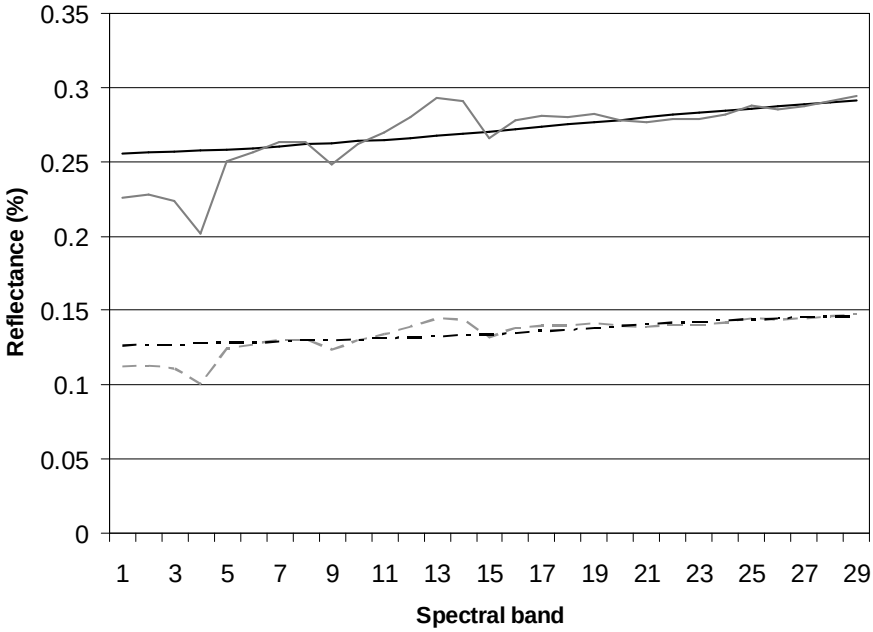

Figure 4-2: The dotted grey curve is the original spectral signal (R_o) recorded by the CASI-2 sensor. The full grey curve (R_n) is the normalised spectrum 'lifted' to the level of the full black curve (R_{hs}) which is a predefined spectrum. The dashed black curve (R_{os}) is a moving average through the dotted grey curve.

After the normalisation, the first derivative of the spectra was calculated in order to accentuate the subtle absorption features present in the data. Finally, a supervised SAM (Spectral Angle Mapper) algorithm was applied to classify the pixels. SAM considers each spectrum as an N-dimensional vector in an N-dimensional space, where N is the number of bands, and compares this vector with pre-defined library spectra (Kruse *et al.*, 1990). In this case the library spectra were retrieved from the CASI data; they are the mean spectra calculated from points and polygons measured on the ground with d-GPS. More precisely, during a field trip, in the same period as the flight, positions where specific sand types occur were recorded. The typology was worked out prior to the classifications, based on almost 20 years of field knowledge. The positions measured on the ground were retrieved in the georeferenced images what allowed to calculate the mean spectra for each sand type. The field work and the calculation of the reference spectra (or library spectra) was performed for each image set (i.e., once for the imagery of 2000, once for 2001 and once for 2002).

The result of this processing chain is a classified map showing 8 different sand classes.

Secondly, the LIDAR data were analysed. In aerial laserscanning, the scanner deflects a laser beam across the flight line and detects its reflection, so that a swath of ground

along the flight line is sampled. The distance to the Earth's surface is determined by measuring the pulse return time. The position and attitude of the sensor is calculated from d-GPS and INS (Inertial Navigation System) data. In combination with the scan angle, the 3D position of each laser beam spot on the surface can be determined. In this case, an ALTM 1225, designed by Optech Inc., was used. This is an infrared laser operating at the wavelength of 1047 nm with a pulse frequency of 25 000 Hz. The point density of the raw data is 1 point every 4 m². The elements which do not belong to the Earth's surface, e.g., beach cabins, were eliminated using a morphological filter (developed by Terraimaging B.V., http://www.terraimaging.nl). After the filtering, the point density is reduced to 1 point every 16 m². To verify the accuracy of the laser DTM, 10 reference sites were terrestrially surveyed. The individual points were not exactly at the same locations as the DTM points, but all reference sites were selected on flat surfaces, e.g., flat and wide seawall tops. Hence, by spatial interpolation of the laserscan data, it was possible to calculate the height at the points that were measured by the surveyor. This validation pointed out that the DTMs have a mean absolute height accuracy of 5 cm (with a standard deviation of 7 cm).

The first laserscanning was performed on September 11, 2000, the second on September 28, 2001. Analoguous to the CASI campaigns, a third laserscanning took place in 2002 but these data could not be included yet. By subtracting the 2000 DTM from the 2001 DTM, a map with erosion and sedimentation (or accretion) zones was derived. To resume, the laserscan data give quantitative information on the morphological changes while the hyperspectral data indicate the type of sand which was transported.

4.4 Results of hyperspectral data analysis

Applying the SAM algorithm, different numbers of classes can be obtained. It was found that the sand occurring along the Belgian coast can –for this purpose– optimally be divided in 8 classes according to their physical appearance in the field. The supervised classification is based on library spectra which were defined after extensive field work. Along the entire coast, the positions of spots with a specific type of sand were recorded so that they could be retrieved on the hyperspectral images. The mean spectral signatures for these regions were used as library spectra (see above).

Figure 4-3 illustrates a classification of the beach near Zeebrugge; in the West the image is bounded by the Pier of Blankenberge, in the East by the harbour of Zeebrugge. eastward of the Pier of Blankenberge, a beach nourishment zone stands out. Between October 1998 and April 1999, nearly 500 000 m³ of sea sand were put on the backshore. The sea sand is coarser grained than the original sand, contains a large amount of shells and even some gravel. Because of its different composition, it can spectrally be distinguished from other types of sand. Classes 7 and 8 correspond to relatively coarse-grained sand containing a lot of shell fragments. Both classes are

mostly found in the beach nourishment zone of the Duinse Polders but they are also present in patches East of the nourished area. This is an indication of erosion at the nourishment site and eastward longshore transport. It is the same transport that has caused the very wide beach at Zeebrugge, immediately West of the harbour dam. The beach started to grow after the completion of the harbour dam (late 1970s), but the sand accumulation goes on to the present day. Class 2 corresponds to fine-grained and even slightly muddy sand; it is present on the lowest parts of the beach in the swales. At the eastern lee of the Pier of Blankenberge the same type of sand is found. Classes 3 and 4 represent fine sand types on the intertidal part of the beach. On the highest parts of the beach, one finds a fine sand type which was probably transported and deposited by the wind (class 9). Class 6 is typically found in a small strip at the high water mark; along this line there is a steep slope between the intertidal part of the beach and the dry beach. Class 5 is omnipresent on the dry part of the beach. It can be considered as the original sand of the dry beach, which in some places is prone to erosion. If the dunes behind the dry beach are not wide and high enough, the erosion can be a real danger for the low polders behind the dune wall; therefore man performs beach nourishments on some parts of the dry beach, e.g., in the 'Duinse Polders'.

During the third CASI campaign, 99 field samples were collected from the upper soil layer (by scraping off the upper millimeters of sand). They were located using d-GPS so that, after classifying the 2002 images, the corresponding class could be found for each of the 99 analysed samples. This allows to define a physical identity card for each class. The following parameters have been derived on the samples: percentage of organic matter, percentage of carbonates, median grain size, sorting, total content of iron oxides and percentage of grains of glauconite, silex, quartz, and shell fragments (See Table 4-1). The effect of these different soil constituents on soil reflectance is very well explained by Baumgardner *et al.* (1985). The work of Leu (1977) provides some specific spectral analysis on beach sands focusing on the effect of soil moisture, iron content and grain size.

The lowest row in Table 4-1 indicates the "number of samples". However, the sum of the row exceeds the number of samples (99). This is caused by the following rule: if all pixels in a 3x3 window around a certain sample location are assigned to the same sediment class, then this sample is linked with that class. However, it often occurs that the pixel coinciding with the GPS position of the sample belongs to a certain class, but that the surrounding pixels belong to another class. In this case it would be wrong to link only that class to this sample since we have to take the positional error of the images into account. As explained before, there is often a mismatch of 0-2 pixels. Therefore, it was decided to look also at the classes of the pixels in a 3x3 window around the central pixel. The class that is assigned (in the classified images of 2002) to the pixel coinciding with the GPS position counts always and if there are other classes in the 3x3 window, then the class which is most occurring also counts for that sample (hence, the sample can be assigned to one or to two classes). Therefore the number of "samples" in Table 4-1 is higher than the real number of analysed samples. This is not

a standardised procedure but since it would be wrong to consider the images as perfectly located it is a justified way of working.

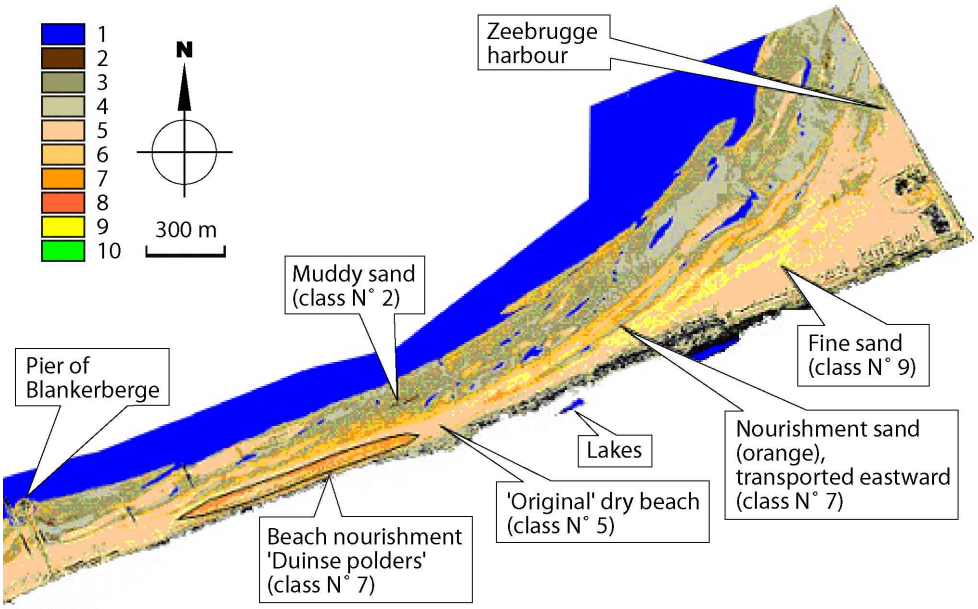

Figure 4-3: Classified image (2000 Survey) of the beach between Blankenberge and Zeebrugge, derived by SAM classification. Eight different sand types could be distinguished (labelled 2 – 9 in the legend; class 1 is water and class 10 is vegetation).

The mean grain size on the Belgian beach varies between 170 and 250 μm (Hillen and Verhagen, 1993). In general, the grain size increases from the low water mark to the high water mark which is a typical pattern for a beach characterised by accretion. In erosive areas, the grain size is coarser due to the fact that fine grains tend to be eroded first. Moreover, since the 1980s, large-scale beach nourishments have been carried out using coarser grains than those present in the natural environment in order to allow steeper beach slopes in the transition area of the lower pre-existing profile and the upper nourished berm. Classes 2 to 8 represent a succession from a fine-grained, well sorted facies to a coarser-grained, poorly sorted facies. In general the % of carbonates and iron increases in the same order. Classes 2 to 5 represent the sediments which constituted the 'original' beach; they contain only a small amount of carbonates and iron. Classes 6 and 7 on the other hand contain sand which was borrowed from banks offshore; they are coarse-grained, poorly sorted, and they contain few glauconite and silex particles but high amounts of iron and shell fragments. Class 9 is the best sorted class and contains the lowest percentage of iron.

The small amount of samples and the inherent limited accuracy of the measuring procedures result in an over-estimation of the true standard deviation, which results in

a large concentration of extreme values for some of the parameters (including negative values); e.g., %CAR for class 6. An arbitrary pixel will be assigned to a certain class with a probability determined by the statistical distribution of the parameters in Table 4-1.

For each class the following definition can be derived:

- Class 2: Sand mixed with silt and clay
- Class 3: Fine sand from the intertidal beach
- Class 4: Fine-Medium sand from the intertidal beach
- Class 5: Sand from the supratidal beach
- Class 6: Sand from the man-made beach barrier
- Class 7: Sand used in artificial beach nourishments
- Class 8: Sand with a large amount of shell fragments
- Class 9: Fine sand which was deposited after aeolian transport

Table 4-1 summarises the measured parameters for the 8 sand classes.

Table 4-1: Means and standard deviations (between brackets) for the percentage of carbonates (% CAR), the percentage of organic matter (% ORG), the median grain size (D50), the sorting (S), the total content of iron oxides (Fe) and the content of glauconite (% gl), silex (% sil) and shells (% sh). Class numbers 2 to 9 represent the 8 sand classes. The lowest row provides the 'number of samples' assigned to each class. The analysis is based on samples collected in 2002.

Sand Class	**% CAR**	**% ORG**	**D50 (mm)**	**S (phi)**	**Fe (mg/kg dry matter)**	**% Gl**	**% Sil**	**% Sh**	**No. of samples**
	8.4	0.22	230.7	0.40	4 445.7	0.9	3.9	0.4	
2	(1.3)	(0.2)	(21.6)	(0.01)	(302.0)	(0.2)	(1.4)	(0.6)	3
	11.3	0.02	187.4	0.42	4 356.6	0.6	2.0	1.6	
3	(3.4)	(0.0)	(27.2)	(0.08)	(696.0)	(0.6)	(1.4)	(1.3)	23
	13.5	0.05	239.00	0.43	4 024.3	0.6	2.0	6.1	
4	(15.2)	(0.1)	(146.4)	(0.11)	(1505.5)	(0.5)	(1.6)	(15.8)	38
	13.3	0.04	246.4	0.48	4 400.6	0.5	2.4	2.2	
5	(12.7)	(0.1)	(71.3)	(0.26)	(1702.4)	(0.6)	(1.4)	(2.4)	61
	16.1	0.05	228.4	0.53	5 266.1	0.5	2.5	2.5	
6	(16.7)	(0.1)	(54.3)	(0.40)	(2017.9)	(0.6)	(1.1)	(2.3)	23
	15.6	0.03	327.8	0.57	4 983.9	0.2	1.3	4.0	
7	(11.7)	(0.0)	(70.9)	(0.24)	(1964.3)	(0.4)	(1.1)	(3.3)	16
	26.0	0.12	715.5	0.89	6 349.9	0.2	1.8	19.4	
8	(28.8)	(0.2)	(1054.4)	(0.92)	(4791.2)	(0.4)	(1.4)	(34.4)	17
	5.7	0.01	280.9	0.37	3 181.5	0.6	2.2	0.2	
9	(0.3)	(0.0)	(133.0)	(0.05)	(450.4)	(0.8)	(0.4)	(0.3)	2

4.5 Results of LIDAR data analysis

Figure 4-4 is a 3D-elevation map of the 2000 DTM near the seaside resort of Oostduinkerke. One can see clearly the ridges and runnels on the foreshore (between the high and low water level). The red rectangular shapes are high buildings in the seaside resort of Oostduinkerke. The undulating parts bordering the beach and occurring in some inland areas are mainly dunes. The highest dunes in this area are approximately 20 m TAW.

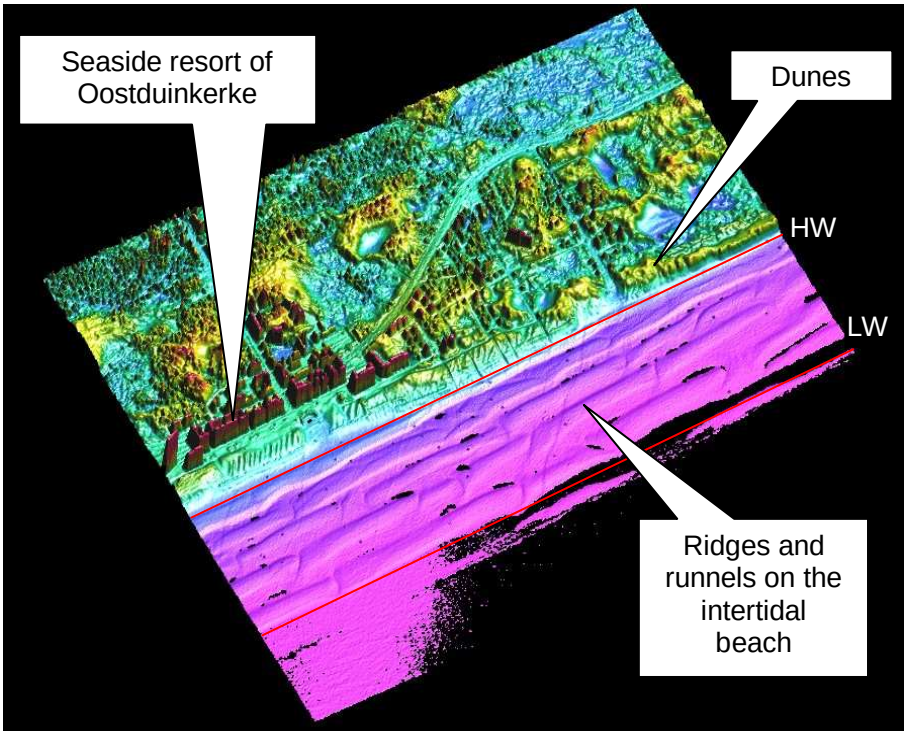

Figure 4-4: 3D representation of a DTM recorded on September 11, 2000 near the seaside resort of Oostduinkerke. HW and LW indicate resp. the high and low water mark.

When subtracting the 2000 DTM from the 2001 DTM one generates a height difference map where elevation loss corresponds to erosion and positive elevation changes indicate sedimentation or accretion. Since the vertical and horizontal accuracy of the DTM is very high, it is possible to calculate with high precision the amounts of sand transported. Figure 4-5 shows the erosion/accretion map of Knokke-Heist. The dark (black) zones were subject to erosion, the bright (white) zones are characterised by accretion, while in the grey zones no important erosion or accretion was measured. In front of the urban area of Knokke-Zoute a beach nourishment has been carried out in 1999. It is clear that the major erosion took place at the seaward side of the nourished area (indicated by the polygon on the left of the map); 41 500 m³ sand was eroded in

one year. More to the East, erosion is seen along the high water mark, while just below the high water mark, an accretion or deposition zone stands out (+ 16 300 m³); see the polygon on the right of the map. The numbers in Figure 4-5 label beach survey sections. To be able to link the erosion and accretion to the different sand classes present in this area, Figure 4-6 shows the classification result.

4.6 Combination of LIDAR data and hyperspectral data

The erosion/accretion maps can be better interpreted if they are combined with the sand type maps, established using the hyperspectral recordings (See Figure 4-7 and Figure 4-8; Figure 4-7 is made from the left part of Figure 4-5 and Figure 4-6, while Figure 4-8 focuses on the right part).

The combination of the erosion/accretion maps and the classified image results in a map with 6 types of areas:

- area without significant (< 25 cm) height difference and without class change
- area without significant (< 25 cm) height difference but with class difference
- area with significant (> 25 cm) erosion but without class change
- area with significant (> 25 cm) erosion and with class change
- area with significant (> 25 cm) accumulation but without class change
- area with significant (> 25 cm) accumulation and with class change

Figure 4-7 illustrates the difference map for the Knokke-Zoute area (beach sections 233 till 243 on Figure 4-5 and Figure 4-6). Between March and May 1999 a beach nourishment with sea sand was performed from section 233 till section 243; the total amount of sand put on the backshore was 486 418 m³. On the seaward side of the nourishment area, there is an important erosion zone of 31 800 m³ (area 17); the mean height difference is -49 cm (in only one year). However, the type of sand remains the same which means that the erosion is still limited to the nourished volume. However, in area 16, class 7 is replaced by class 5 indicating that the erosion reached the underlying sand type. Class 5 is the most widely found type of sand on the dry part of the beach. In area 18, a small erosion strip replaced class 7 by classes 3 and 4; these are typical sand types of the wet beach which means that there is probably a landward regression of the nourishment area. Also the wet part of the beach is mainly prone to erosion; in zone 20 an erosion of 20 600 m³ (-16 cm in average) was measured but without class change (classes 3 and 4 occur here). Along the low water level a small area with class 7 can be seen; this is probably a temporary stock of nourishment sand. The arrows F indicate the resulting sand transport directions: erosion of the nourishment area especially at the seaward side (zones 16, 17 and 18), erosion of the wet beach (zone 20) and accumulation of a shallow layer of nourishment sand along the low water level. The thickness of the arrows is an indication of the amount of sand transported: thick arrows indicate more sand transport than fine arrows. Arrow G stands for the longshore transport of nourishment sand to the East (see also Figure 4-8

which is situated eastward from Figure 4-7). In the area of Figure 4-7 it is necessary to take an important transport of 40 000 to 50 000 m³ sand to the nearshore into account, i.e., sand which has been eroded but not deposited elsewhere on the backshore or foreshore.

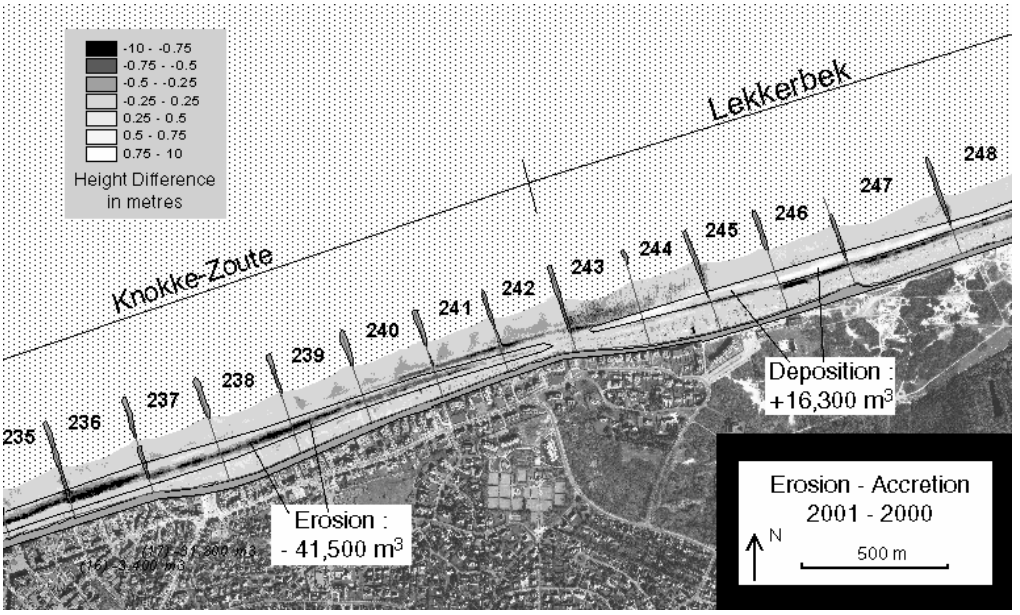

Figure 4-5: Erosion-accretion map of the area between Knokke-Heist and the Dutch border. The black zones were subject to erosion, the white zones were characterized by sedimentation, while in the grey zones no important erosion or accretion was measured. Note that the major erosion took place at the seaward side of the beach nourishment zone (polygon on the left side of the scene). The numbers ranging from 235 till 248 are beach survey sections.

Figure 4-8 shows the sand transport map in the Lekkerbek area which is situated eastward from Knokke-Zoute. Between 2000 and 2001 the total volume of sand in this area remained the same. However, some internal processes can be detected. Along the dune foot, a long narrow erosion zone can be seen (zone 21); seawards from this zone there is an accumulation zone (zone 22). The eroded volume is almost the same as the accumulated volume (16 800 m³), which gives the impression that there is a transport as indicated by arrow H. However, a lot of pixels changed from class, especially in zone 22 there is a change to class 7 which is the nourishment sand. This means that most probably there is transport from nourishment sand from Knokke-Zoute to the Lekkerbek (arrow G). A second indication of this can be found in zone 23 where a small accumulation of class 7 was measured. In section 251 there is a zone (24) where an erosion of -28 cm was measured in combination with a class change from 7 to 5. Probably, class 7 was an earlier sedimentation of nourishment sand originating from Knokke-Zoute which has been eroded between 2000 and 2001.

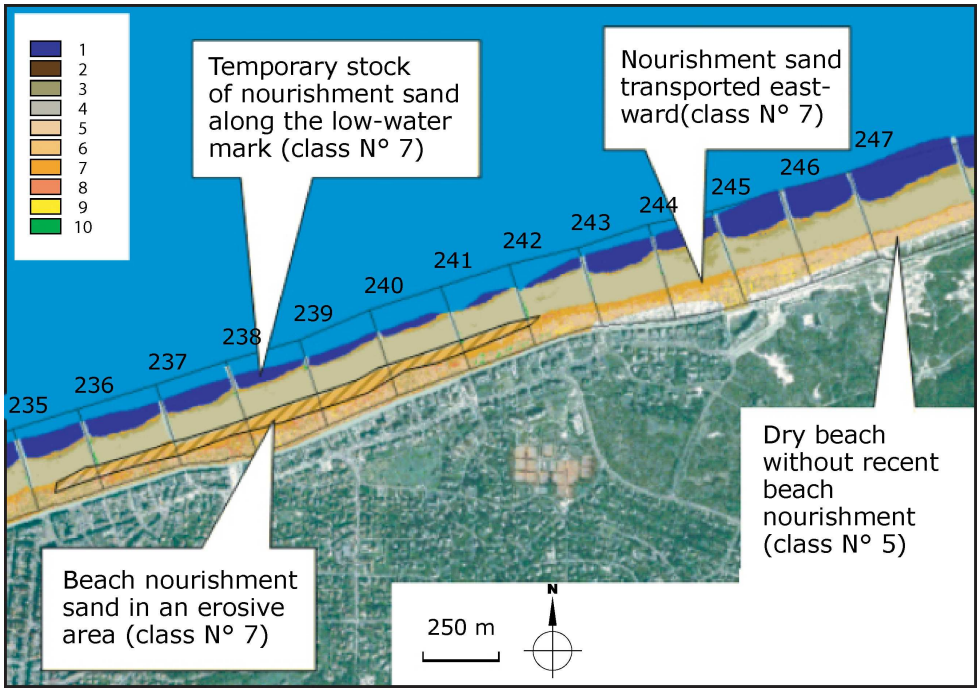

Figure 4-6: Classified image (2001 survey) of the beach near Knokke-Zoute derived by SAM classification. 8 different sand types can be distinguished (labelled 2 – 9 in the legend; class 1 is water and class 10 is vegetation). Classes 3, 5, and 7 are the most dominant classes in this area. Therefore each of them was highlighted separately. The numbers ranging from 235 till 247 are beach survey sections.

The processes seen in the Lekkerbek area show that this area is subject to transport of sand from the West to the East. The accumulation in some parts of the beach is temporarily. It is possible that the total cumulated transport is higher than the volume differences calculated from the two acquisitions since they represent only two morphological snapshots.

These two examples illustrate that the combination of both data types opens possibilities for experts to gain a better understanding of the transport processes along the beach. The erosion maps as such are not sufficient to understand the nature of the transport. Successive recordings in the years to come will reveal more of the complex dynamics of the beach environment. If the nourishment sand in Knokke-Heist is progressively transported towards the East, as is sometimes put forward, new surveys will unambiguously show this process, and will allow to quantify it.

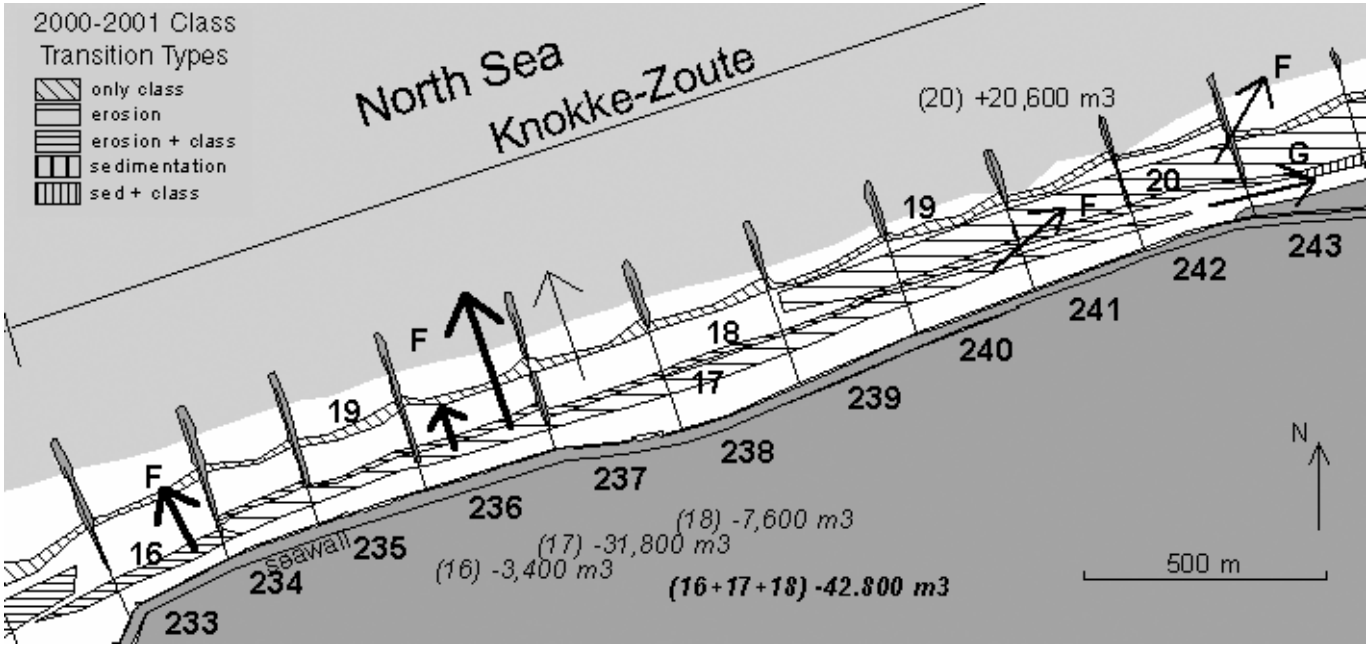

Figure 4-7: Schematical representation of the sand transport directions and volumes between 2000 and 2001 in Knokke-Zoute. The thickness of the arrows is an indication of the amount of sand transported: thick arrows indicate more sand transport than fine arrows.

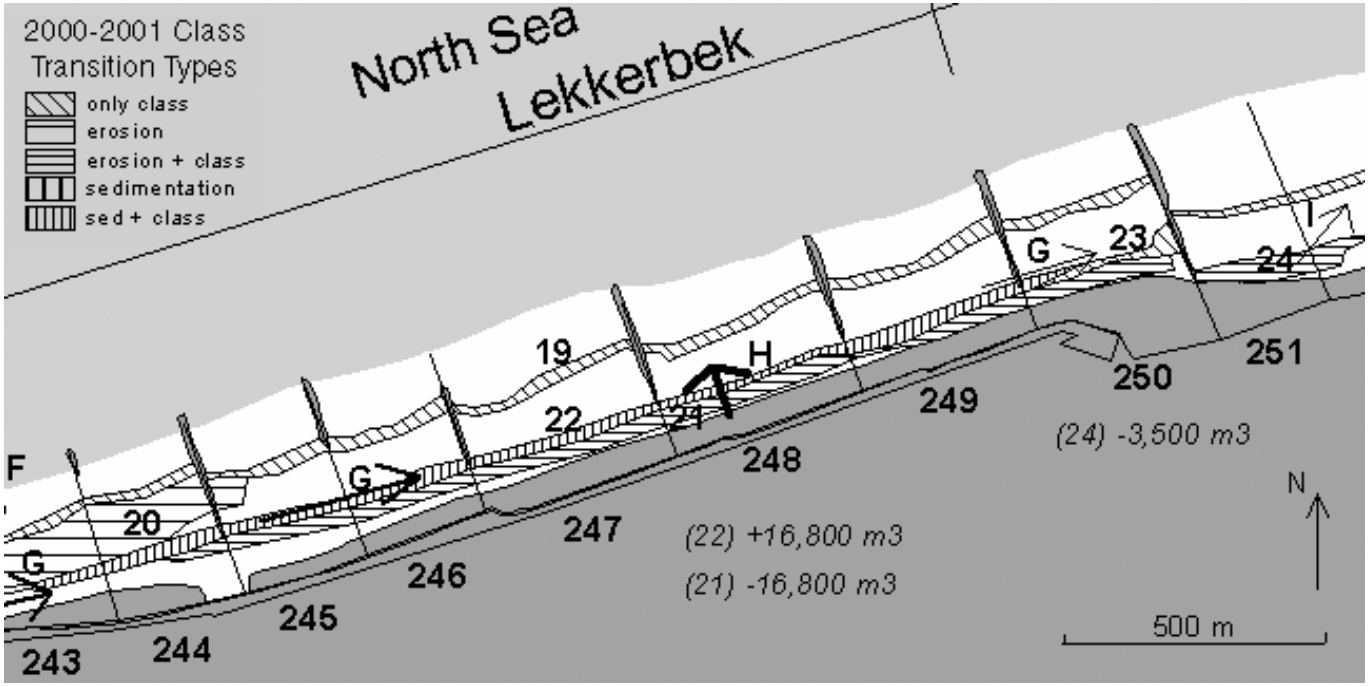

Figure 4-8: Schematical representation of the sand transport directions and volumes between 2000 and 2001 in the Lekkerbek area. The thickness of the arrows is an indication of the amount of sand transported: thick arrows indicate more sand transport than fine arrows.

4.7 Discussion

Geological and pedological studies using imaging spectroscopy often focus on reflectance data in the Short Wave InfraRed or SWIR region (i.e., 1 000-2 500 nm), since several minerals show well expressed absorption features in this wavelength range. In this paper, only VNIR data were used to thematically map the beach into 8 classes, which were previously defined in the field based on physical appearance. However, the potential of employing hyperspectral data in the SWIR range should not be overlooked. A new flight with a HyMap sensor covering the entire range between 450 and 2 500 nm was performed in the summer of 2004. These data will be used to study the possibilities of the reflectance in the SWIR range for classifying sandy beaches. Additionally, attention will be paid to band or feature selection since, according to the Hughes phenomenon, it is not always recommended to use as many bands or features as possible, especially when there is a limited number of training samples (Landgrebe, 2003).

Beach processes are characterised by significant transfers of sand between the beach and the nearshore. Because of this, it can be difficult to understand the processes of sand dynamics since the thematic information of the part of the system which is below the low water level is lacking. A new ambitious approach in which the monitoring of the sediment type on the seabed and in the water column is performed in combination with the airborne hyperspectral measurements over the dry beach is being considered. Tests to determine the sediment concentration and type in the water column with hyperspectral measurements have been undertaken. They make clear that this is not straightforward; in the case of very high sediment concentrations it is possible to detect the presence of sediment in the water column in general, but it appears to be very difficult to define accurately the concentration and sediment type. More research on this topic is needed and will be performed in the near future. On the other hand, monitoring of the seabed sediment type should be possible without too many problems with an acoustic mapping technique such as side-scan sonar. For the Belgian near- to foreshore, Van Lancker *et al*. (2003) could discriminate the variation from fine to medium sands from a detailed acoustic facies analysis. The combination of this information with the results from airborne hyperspectral surveys would allow to study sand transport processes over the continuum of the dunes, back- and foreshore to the nearshore. However, an innovative strategy will be needed to minimise the difference in time needed to carry out the shipborne acoustic and the airborne hyperspectral measurements.

4.8 Conclusions

A combined method to study beach morphodynamics was presented. The method consists of performing (quasi) simultaneous airborne hyperspectral and laserscanning recordings of the beach at low tide. After the radiometric, geometric and atmospheric corrections, and a few processing steps, the hyperspectral images could be classified into eight meaningful sand type classes. Laboratory analyses indicated that these classes contain sand with a different median grain size, different grain size sorting and different amount of shells. It is possible to assign an arbitrary sample to a class with a probability determined by the statistical distribution of the parameters in Table 4-1. The laserscan data were used to make DTMs with a vertical accuracy of approximately 5 cm. When subtracting the DTM of September 2000 and the one of September 2001 a map indicating the erosion and accretion zones was generated. The combination of the erosion/accretion map and the classifications derived from the hyperspectral data from 2000 and 2001, generated a product which is well suited to study beach morphodynamics. It was found that on the Belgian East Coast the major erosion took place at the seaward side of the beach nourishment zone of Knokke-Heist. Small quantities of the nourishment sand were found along the high water mark eastward of this zone, and in a small strip at the low water mark. Another important conclusion is that not all eroded sand is deposited elsewhere on the beach (in the same limited area). It was calculated that the beach strip of Knokke-Heist showed a net loss of 40 000 to 50 000 m³ sand to the nearshore.

Chapter 5

Linear discriminant classifier and feature selection in support of sediment ecotope mapping

This chapter is based on:

Deronde B., Kempeneers P., Forster R.M. and W. Debruyn, 2006, Imaging spectroscopy as a tool to study sediment characteristics on a tidal sand bank in the Westerschelde. Estuarine Coastal and Shelf Science, 69(3-4): 580-590.

5.1 Abstract

This paper focuses on the use of imaging spectroscopy for the mapping of sediment characteristics on a tidal sandbank in the Westerschelde, called the Molenplaat. On June 8, 2004, during low tide, a HyMap scanner recorded the Molenplaat at 4 m pixel resolution. The hyperspectral data were radiometrically calibrated, geometrically corrected, and atmospherically corrected to give apparent surface reflectance data. On the calibrated and corrected dataset, a supervised binary classification was performed, based on linear discriminant analysis. Simultaneous to the flight, 25 sediment samples were collected in the field and analysed in the lab to define the median grain size, the water content, the total organic matter content and the chlorophyll-a concentration. These four parameters play a crucial role in sediment stability and macrofaunal habitat definition. Prior to the classification, a feature selection, based on sequential floating forward search (SFFS), was performed. For each of the four parameters two to three bands were retained for the classification. These bands were most frequently selected

in the visible and near infrared parts of the spectrum, except for the organic matter content where also SWIR bands were used. The overall classification accuracy was highest for the water content (88%), the median grain size (88%) and the chlorophyll-a concentration (84%). The organic matter content, for which three instead of two classes were distinguished, scored somewhat lower but still reached 80%. The classifications were limited to a small number of classes in order to obtain reliable statistics with a small number of training samples. The spatial patterns in the classified images indicated that the four parameters under study are highly correlated. In most cases coarse sediment coincided with dry conditions, low organic matter and low concentrations of chlorophyll-a. The wet and muddy parts of the Molenplaat were in general characterised by a notably higher amount of organic matter and chlorophyll-a. The individual classification results for the median grain size, the water content and the chlorophyll-a concentration were combined to generate a sediment ecotope map. The presented study illustrates how airborne hyperspectral data can be used to achieve accurate classified maps of intertidal sediment ecotope types, applying feature selection and a binary classification approach.

5.2 Introduction

The Westerschelde is unique among the larger European estuaries. It is home for one of the largest wading bird populations in western Europe and contains several rare habitat types such as freshwater tidal marshes. These, together with a variety of other brackish and marine habitats, make the Scheldt estuary a site of international recognition and importance for nature. But the estuary is also a site of heavy industry, as well as an important commercial shipping transport route. Therefore, coastal zone managers must constantly balance the demands of many conflicting interest groups when making planning decisions which affect this complex system (Meire *et al.*, 2005). Decision making can be improved if better knowledge of ecological processes is available. Some of the most important bio-geochemical processes in the estuary occur on the large areas of soft sediments which are exposed at low tide, suggesting that these intertidal sandbanks and mudflats require detailed study. Photosynthesis by benthic micro-algae at the sediment surface fuels primary production, supporting many grazing animals and birds. Accumulations of algal cells in a surface biofilm also cause the sediment to become more stable, slowing down the rate of erosion, and allowing the deposition of fine sediments (Coles, 1979). In contrast, grazing and bioturbation of macro-fauna may enhance the erosion rate (de Deckere *et al.*, 2000).

However, obtaining accurate data on the basic biological, chemical and physical processes in sediments is expensive and difficult. Access to the sites is limited, and estuaries are characterised by a wide spatial heterogeneity, especially in intertidal areas. If used correctly, remote sensing methods can produce detailed information on habitats and ecological functioning in a cost-effective manner (Wulder *et al.*, 2004).

Hyperspectral airborne scanners such as HyMap can be used to identify important groups of inorganic and organic materials at a high spatial and spectral resolution (Kruse *et al*., 2000; Thiemann and Kaufman, 2002). Intertidal and saltmarsh habitats have previously been investigated by Thomson *et al*. (1998), who used the airborne CASI scanner in a mode with 14 spectral bands to classify the vegetation and sediments in the Wash embayment on the East Coast of England in 6 vegetation and 4 sediment classes. In the same study area, Yates *et al*. (1993) tried to classify sandy and muddy sediments with spaceborne Landsat TM data; the poorer spatial resolution inspired them to try a sub-pixel classification which was performed with success. Bryant *et al*. (1996) and Rainey *et al*. (2000 and 2003) explored the possibilities of sediment classification further by using the Daedalus 1268 Airborne Thematic Mapper (ATM) to map sandy and clayey sediments in the Ribble estuary (UK), focussing on the different grain sizes as one of the main parameters influencing the spectral reflectance. Finally, the work of Smith *et al*. (2003) should be mentioned; in this study the sediments on the Molenplaat were classified in an unsupervised way using DAIS-7915 data.

The work described in this paper builds on these earlier studies by using high-resolution, visible (VIS), near infrared (NIR) and shortwave infrared (SWIR) imaging spectroscopy for the mapping of sediment characteristics in the intertidal zone of the Molenplaat. A supervised classification approach based on linear discriminant analysis is adopted to classify not only the median grain size, but also the water content, the total organic matter content and the chlorophyll-a concentration. These four parameters provide a good basis for sediment stability studies as well as for the study of microphytobenthos and macrofaunal biotopes. Finally, an ecotope map of the intertidal site is made, as part of a sustained effort to gain more insight in the biological role of the intertidal sandbanks and mudflats of the Westerschelde.

5.3 Study area

The Westerschelde estuary in the Netherlands is western Europe's largest natural estuary. It has a special protected status according to Council Directive 92/43/EEC: "on the conservation of natural habitat and of wild fauna and flora", also large parts of the Scheldt estuary are designated as special protection areas or special areas of conservation under the European Bird (79/409/EEC) and Habitat Directive (92/43/EEC). From an ecological point of view the Westerschelde estuary is unique due to its high tidal range (up to 6 m), the complete transition from saline to fresh water environments and a freshwater tidal area almost 60 km long. However, due to human interventions the deep water areas are expanding at the expense of intertidal areas. Nevertheless, the latter are very important ecotypes for a more natural functioning of the estuary.

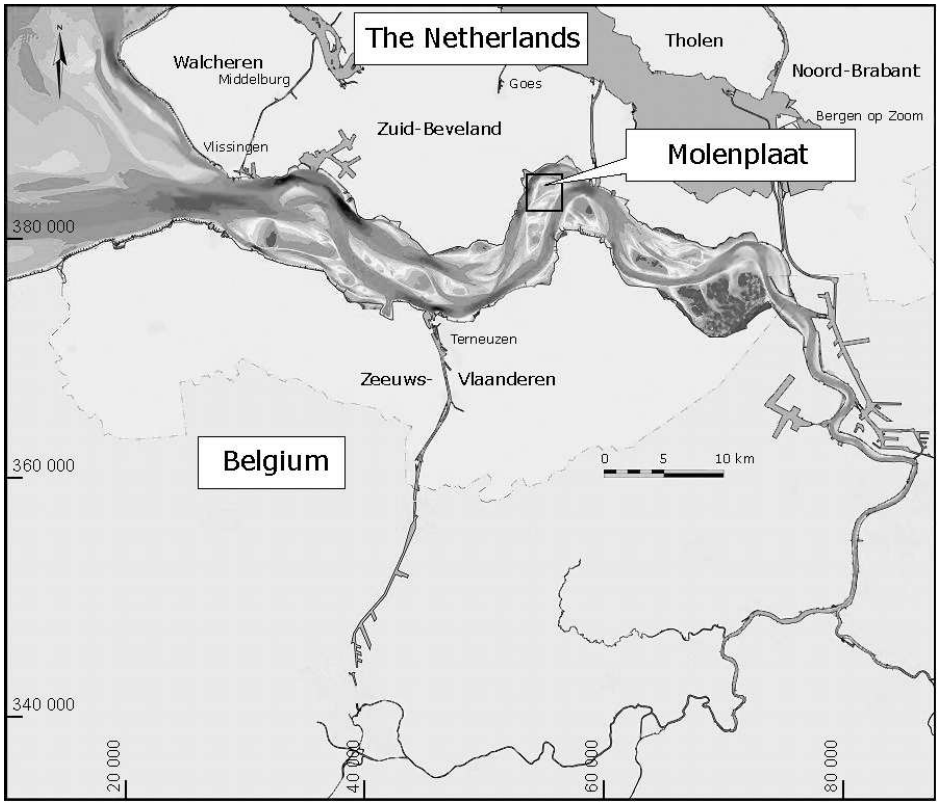

Figure 5-1: Location of the Molenplaat study area. (source: Ministerie van Verkeer en Waterstaat, The Netherlands).Coordinates are in the Dutch Rijksdriehoeksnet system (m).

The Westerschelde estuary (Figure 5-1) was formed by rapid landward expansion of a tidal channel in the early Middle ages, after which it became the major mouth of the river Scheldt. The estuary reached its largest extent in the 17th century after which it partly silted up. The tidal marshes along the estuary have been reduced strongly in surface area since then (Meire *et al.*, 2005). Simultaneously, the tidal range and the tidal celerity in the estuary have increased. The infilling of the estuary with predominantly sand is the consequence of the North Sea tide which rises faster than it falls, causing higher landward current velocities and consequently landward sediment transport. The large particles, i.e., sand, are transported during the rising tide but the current velocities during falling tide are too slow to transport the sand particles back to the open sea. However, recent studies pointed out that this process has reversed for unknown reasons; the estuary has now become a net sand-exporting system (Nederbragt and Liek, 2004). Hence, quantification of the relative amounts of muddy and sandy sediments in intertidal areas, and characterisation of the main intertidal ecotope types were among the aims of this study.

5.4 Methodology

5.4.1 Instrumentation and data collection

On June 8, 2004 between 12.41 and 13.22 local time a HyMap scanner on board a Dornier 228 recorded the Molenplaat in the Westerschelde. Prosperpolder, situated 25 km upstream from the Molenplaat, reported low tide at 14.42 local time. Hence, the acquisitions were performed approximately one and a half hour before low tide. The level of low tide was - 1.97 m NAP (the highest low tide in June 2004 was -1.75 m NAP and the lowest was -2.63 m NAP). The meteorological conditions were very good; the nearby station of Vlissingen recorded a daily maximum temperature of 30.2°C with a mean wind speed of 2 Bft from SSW. There were a few cirrus clouds (0-2 octas) and the mean daily relative humidity was 72%.
The operations were carried out by the Deutsches Zentrum für Luft- und Raumfahrt (DLR) in cooperation with VITO. The instrument was calibrated before the beginning of the flight campaign at DLR's home base in Oberpfaffenhofen using HyVista calibration gear. The HyMap, developed by HyVista Corp., is a whiskbroom scanner utilising diffraction gratings and four 32-element detector arrays (1 Si, 3 liquid-nitrogen-cooled InSb) to provide 126 spectral channels covering the 0.45 – 2.50 µm range over a 512-pixel swath (Kruse *et al.*, 2000). To minimise the image distortion caused by aircraft pitch, roll and yaw motions, the HyMap is mounted in a gyro-stabilised platform. While the platform minimises the effects of aircraft motion, small image distortions remain. These residual motions are monitored with a 3 axis gyro, 3 axis accelerometer system (IMU – Inertial Measurement Unit). The system currently used with the HyMap is a Boeing C-MIGITS II.

Figure 5-1 summarises the spectral characteristics of the HyMap sensor system. The reflected light is dispersed into 126 spectral bands: 32 for the VIS, SWIR1 and SWIR2 spectrometers and 30 for the NIR, (in the VNIR range the bands are contiguous).

The flight was conducted at 6 300 ft AGL (Above Ground Level), resulting in pixels of 4x4 m. The raw data were geometrically corrected and georeferenced using the software ORTHO (Müller *et al.*, 2002) while the radiometric calibration was performed with the standard software of HyVista (Cocks *et al.*, 1998). The geometrically corrected and radiometrically calibrated data were corrected for atmospheric influences using ATCOR-4 which is based on the radiometric transfer model MODTRAN-4 (Richter and Schläpfer, 2002). Simultaneously to the flight, sunphotometer measurements (with a SOLAR Microtops II) were performed to estimate the amount of water vapour and the aerosol concentration, needed for the atmospheric correction. The DTM illustrated in Figure 5-4 was not used in the atmospheric correction since the slopes present on the sandbank are too weak (in general 0-2°) to influence the reflectance significantly.

Table 5-1: Spectral configuration of the HyMap sensor system.

Spectral Configuration of HyMap			
Module	**Spectral range** (μm)	**Bandwidth across module** (nm)	**Average spectral sampling interval** (nm)
VIS	0.45 – 0.89	15 – 16	15
NIR	0.89 – 1.35	15 – 16	15
SWIR1	1.40 – 1.80	15 – 16	13
SWIR2	1.95 – 2.48	18 – 20	17

5.4.2 Image Analysis

The supervised classifier used is based on Linear Discriminant Analysis (LDA) (Fischer, 1936; Duda *et al*., 2001). For C classes, LDA projects the N-dimensional input vector onto a (C-1) dimensional vector with optimal class discrimination in mind. It minimises the ratio of the within class over the between class scatter matrices. For a two-class problem, the feature space is projected onto a 1-dimensional space, and the LDA technique immediately serves as a linear classifier. For this study, in which for each parameter 2 to 3 classes were to be distinguished, a multiple-binary approach was applied. This means that the outputs of several binary classifications were combined to obtain the final classification. Mostly, one-against-all or one-against-one approaches are used. With the one-against-all strategy, each classifier is trained to differentiate one class from all the others, which requires a number of classifiers equal to the number of classes. In the one-against-one approach, all possible pairs of classes are compared requiring
C(C-1)/2 classifiers. Generally, good results are obtained using the one-against-one approach with a maximum voting technique, as was also found by Kempeneers *et al*. (2004) using an AISA-Eagle dataset. Therefore the one-against-one approach was followed.
The multidimensional hyperspectral data showed frequent autocorrelation between adjacent bands in most parts of the spectrum. The performance of classifiers can therefore be improved by selecting a subset of bands, especially when dealing with a limited number of training samples (Kalayeh *et al*., 1983; Landgrebe, 2003). The selection procedure requires a criterion to evaluate the obtained subset of features. This criterion is a measure of separability of the classes, and can e.g., be the result of a classifier. In this work, we applied the overall accuracy of the LDA-classifier as the criterion. The search strategy followed was the sequential floating forward search (SFFS) (Pudil, 1994): one selects the best single band, then adds a second band to have the best combination of two bands, adds a third band to have the best combination of three bands and so on. But, after each forward step, SFFS performs one or more backward steps, i.e., it removes a previously selected feature to investigate if the score can be improved using another band. This floating aspect was used to minimise the

chance that one ends up in a so-called local minimum, i.e., a good combination of bands but not the best one, due to previously chosen bands which cannot be changed if one does not perform backward steps. After the feature selection procedure, a combination of n bands which are (sub)optimal for classification was obtained. The SFFS was run on the 120 quality-controlled HyMap bands (see Section 5.5 for bad band removal). The validation was performed with the leave-one-out method, i.e., all samples were used for training except one which was kept for validation (Landgrebe, 2003). This was repeated until every sample was left out once, after which the average classification accuracy was calculated. This cross-validation procedure generally gives good estimates of the classification accuracy, however, it is known that leave-one-out generates in general higher accuracy predictions than for instance a 50%–50% cross-validation procedure (Duda *et al.*, 2001). The predicted accuracy of a classifier is be proportional to the size of the training dataset (Azuaje, 2003).

The number of bands that has to be used in the classification was defined after testing the classification accuracy on the training samples with 1, 2, 3 and 4 bands. Using too many bands in relation to the number of training samples resulted in saturation and even a slight decrease of the classification accuracy; this effect is known as the Hughes phenomenon (Landgrebe, 2003). For each parameter, we selected the smallest number of bands within 1% of the maximum overall accuracy.

Accuracy was defined as the weighted overall accuracy (which takes into account the number of pixels used in the analysis), calculated using a confusion matrix (Kohavi and Provost, 1998).

5.4.3 Ground truthing

Field sampling took place on June 8, 2004, during the same low tide as the overflight. A grid of 25 stations with node intervals of 200 m was established using d-GPS (See Figure 5-6a). To account for geometric mismatches and to reduce variability, a square of 3x3 pixels was drawn around each sample point, so that each ground point corresponded to 9 image pixels. The spectra of the 9 image pixels were averaged so that each sample point corresponded to one averaged spectrum.

In order to control the accuracy of the airborne reflectance measurements, spectral reflectance of the sediment surface was measured at each grid node. A series of 9 spectra were recorded with portable diode-array spectroradiometers (a USB-2 000 from Ocean Optics, USA and a Ramses ARC from TRIOS, Germany) within a radius of 3 m around the GPS position: on a straight line the first spectrum was taken at 1 m from the centre, the second at 2 m from the centre and the third at 3 m from the centre; then moved round 120° and took another 3, then another 120° turn for the last 3 spectra. Spectra from all instruments were converted to reflectance and resampled to 1 nm intervals. In addition, the main surface features were described and also recorded by digital photography. Surface sediment samples were collected for analysis with a contact corer (Ford and Honeywill, 2002) from exactly the same position as the third,

sixth and ninth spectra (located at the end of the three converging lines). The contact corer freezes a layer of 2 mm, which includes all photosynthetically-active algal cells, as well as the bulk of sediment chlorophyll (Forster and Kromkamp, 2004). Thus, three samples were taken at each site to reduce the effect of non-representative samples.

Samples were stored in liquid nitrogen during transport to the laboratory, and then freeze-dried for 48 hours. The difference in weight before and after freeze-drying was used to calculate the water content. Algal biomass was estimated from measurement of chlorophyll-a (chl-a). Pigments were extracted from freeze-dried contact core samples with 95% methanol (Zapata *et al*., 2004). Methanol extracts were quantified using HPLC (High-Performance Liquid Chromatography) (Wright *et al*., 1991) to give chlorophyll concentration in units of mg/m². Grain size distribution was determined using a Coulter Counter LS100. The median grain size was prefered above the mean to minimise the effect of outliers in the grain size distribution. Samples were classified into 5 fractions according to the grain size distribution of Udden-Wentworth (Wentworth, 1922):

≤ 63 µm = mud (clay & silt)
63 – 125 µm = very fine sand
125 – 250 µm = fine sand
250 – 500 µm = medium sand
500 – 2 000 µm = coarse and very coarse sand

The percentage of organic matter was calculated by difference in weight after combustion at 550º C. The complete data set was quality-controlled and assembled in a relational database to enable correlations to be made with the remotely-sensed imagery. The three analytical results obtained for the three samples in each position were averaged for each parameter to give the average value per parameter for each position.

5.5 Results

Hyperspectral reflectance spectra collected from individual pixels of the image showed good agreement with spectra measured from the corresponding positions on the ground, indicating that geometric and atmospheric corrections were accurate. As expected, the individual reflectance spectra showed a large amount of variability depending on the nature of the sediment surface. Selected spectra from different sites varying in sediment composition, wetness and algal cover are shown in Figure 5-2. The spectral resolution is sufficiently detailed to see features like the characteristic absorption band of chlorophyll-a at 676 nm in three of the spectra. However, there were also some anomalies in the spectra that had to be corrected. First of all, the reflectance in the first blue band (band centre at 442 nm) was too low, probably due to a poor radiometric calibration of this band. Therefore the first band was excluded from further analysis. The last five bands of the SWIR2 sensor (2 420-2 482 nm) also

contained a lot of noise caused by the absorption of photons by water vapour between 2 400 and 2 500 nm. Moreover, the type of sensor used in the SWIR (InSb) is less sensitive than the Si sensor used in the VIS range. These five bands were also excluded from analysis, resulting in 120 bands that could be used in the feature selection procedure. Note that there were no bands between 1 342-1 405 nm and between 1 806-1 953 nm since these wavelengths are highly influenced by water vapour absorption.

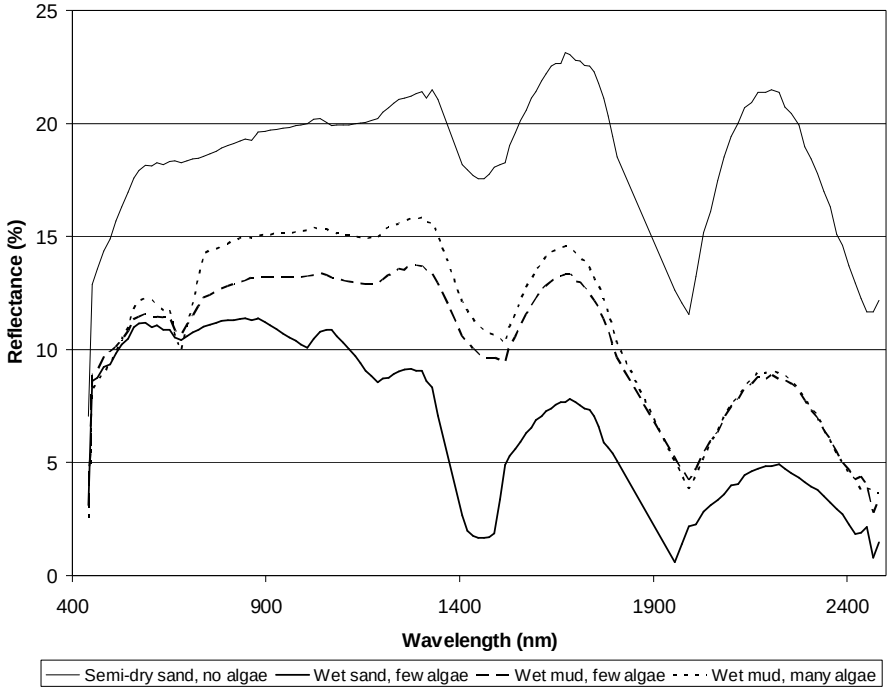

Figure 5-2: Four reflectance spectra measured with HyMap. The 1st blue band had to be eliminated because of poor radiometric calibration while the last 5 SWIR bands were too noisy because of absorption by water vapour.

5.5.1 Median grain size

Sediment grain size is a good predictor variable for the composition of benthic macrofauna (Ysebaert *et al.*, 2002), which in turn are among the most widely used indicators in ecological monitoring programmes. A histogram of the grain size distribution for the Molenplaat showes that two fractions appear to be dominant: a fine sand fraction and a silt & clay dominated fraction (Figure 5-3). Medium and especially coarse sand was almost absent, while very fine sand occurred in variable fractions of 0-35%.

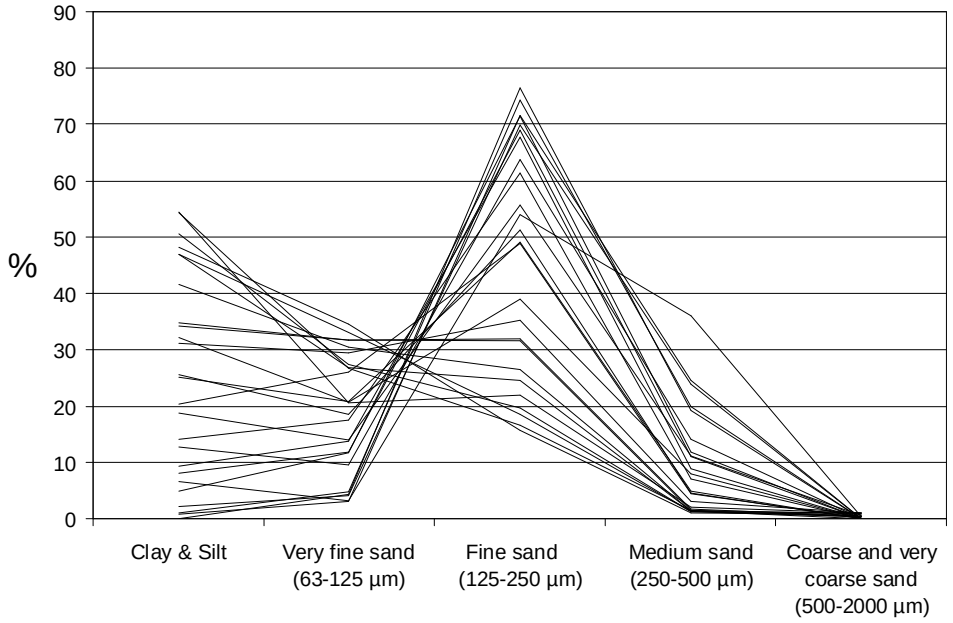

Figure 5-3: Grain size distribution of the 25 samples taken over the Molenplaat.

In order to label two ecologically relevant classes, the following rules were adopted:

If clay&silt > 30%, then the class is labelled as 'mud'

If clay&silt < 30%, then the class is labelled as 'sand'. This class is usually dominated by the fine fraction, followed by very fine then medium, with coarser fractions almost absent.

The overall accuracies, after LDA classification of the training samples, for each band set are shown in Table 5-2. Using more than 2 bands did not result in an important increase in the classification accuracy. Note also that with only one band a high accuracy could be obtained. The bands which were selected most are listed in Table 5-3. Bands in the VIS and NIR range gave the highest classification accuracies, which can be explained by the influence of particle size on the general brightness of the surface.

Table 5-2: Overall weighted accuracies after LDA classification for different band sets.

	Grain size	**Water content**	**Chlorophyll-a**	**Organic matter**
1 band	80	68	64	48
2 bands	**88**	84	**84**	76
3 bands	88	**88**	76	**80**
4 bands	84	88	68	80

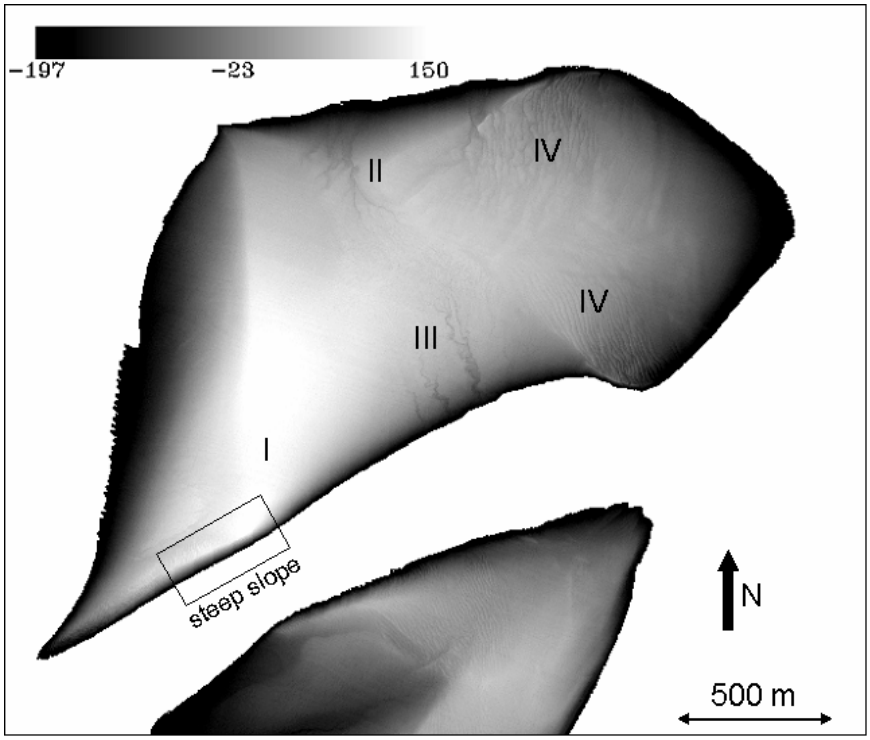

Figure 5-4: DTM of the Molenplaat, recorded by means of airborne laserscanning on April 25, 2004. The elevation is expressed in cm NAP. At the day of the HyMap flight the low water level was -1,97 m NAP.

The image classification was performed with two bands, and all samples were used for training. However, before describing the classification result, it is interesting to have a look at a DTM of the Molenplaat. On April 25, 2004 a DTM was acquired with an airborne laserscanner (Figure 5-4). Although it was not acquired at the same time as the HyMap data it provides valuable information to interpret the classification results. The highest parts of the bank are situated in the southern and western part of the bank (region I). The highest points are nearly 3,5 m above the low water level at the day of the flight = -1,97 m NAP. The central part of the bank runs off via channels to the North and to the South (region II and III). In the eastern part, one can see some mega-ripple structures (regions IV). In general, the relief of the bank is very flat with only in the Southwest a short steep slope.

The classified map is shown in Figure 5-5a. The sand class was found across a large area in the western part of the site (region I), on the elevated southwestern tip of the bank (region II), and in large areas in the eastern part of the bank (region III). The finer class, mud, was found in the large central part (region IV) and in an area near the western edge (region V). In the eastern part, the sand and mud class often occur mixed, in contrast with the western part where they form large more or less homogenous areas.

Note the mega-ripples or sandwaves in the eastern part of the scene (VI). The ripples are approximately 20 m apart and 50 cm high, with the top of the ripples characterised by sand while muddy sediments occurred in the troughs. The sand class was also found in the bed of small run-off channels in the North of the image (VII), while mud occurred around the channels. This can be explained by the higher current velocities and shear stress within the run-off channels. The southern part of the image shows the northern part of the neighbouring Ossenisse bank (VIII). Although this area was not part of the ground survey, it appears to contain a low valley with mud surrounded by coarser sandy sediments. The overall classification accuracy (88%) as well as the confusion matrix can be found in Table 5-4a. Both classes were classified with high accuracy.

5.5.2 Water content

The water content in the sediment database of the Molenplaat was highly correlated to sediment grain size and topography (Figure 5-4 and Figure 5-5a). This is mainly due to the better drainage capacity of coarse sediment, although areas of dry, muddy sediment were also detected. The weather on the sampling date was hot, with weak drying winds which could have evaporated surface water during the low tide period. The highest points of the sandbank were for 3 to 4 hours exposed to sun and wind before the overpass. The sediment samples were assigned to one of the two following water content classes (weight percentage):

0-30 % ‘low’
> 30 % ‘high’

When applying the SFFS feature selection procedure, three bands proved to be necessary to produce the highest accuracy (Table 5-2). Table 5-3 lists the bands which were most often selected, they are centred around 528 nm, 619 nm and 1069 nm. The classification of the Molenplaat into two water content classes is shown in Figure 5-5b. In general, areas covered by the sand class tend to be drier (see for instance points I and II) than the ones with muddy sediment (point III and IV). However, there are some exceptions where the muddy sand class appears to be rather dry (point V on Figure 5-5b). The opposite case, sand which was water-saturated, was seldom found. The confusion matrix for the water content classification is shown in Table 5-4b. The overall weighted accuracy was 88% with a class specific producer accuracy of 77% for the low water content class and a perfect (100%) classification result for the high water content class.

5.5.3 Chlorophyll-a concentration

The presence of microphytobenthos at the sediment surface was detectable by the presence of the characteristic dip in reflectance at around 675 nm, as well as low

reflectance throughout the 400-550 nm region where photosynthetic pigments result in strong absorption. An overview of absorption features caused by the main pigments in microphytobenthos is given by Stephens *et al*. (2003). Chlorophyll-a (chl-a) was the most abundant pigment in the Molenplaat samples, and its presence caused reflection of green light and absorption of red light. The presence of fucoxanthin as the most abundant accessory pigment indicated that the benthic microflora was dominated by diatoms. The chl-a concentration is expressed in mg/m². Initially, three classes were distinguished (low, medium and high chl-a). However, the middle class showed very high confusion with the two other classes. Therefore the classification was limited to two classes:

0 – 40 mg/m² 'low'
> 40 mg/m² 'high'

Table 5-3: List of bands which were most frequently used in the classifications. Note that the number of bands listed depends not only on the number of bands that results in the highest accuracy but also on the number of classes (cf. binary classifications).

	Bands selected for classification (nm of central wavelength)
Grain size	619, 862
Water content	528, 619, 1069
Chlorophyll-a	680, 1342
Organic Matter	604, 846, 1038, 1517, 1806, 2083, 2188, 2205

Two bands were needed to obtain the highest classification accuracy; as can be seen in Table 5-2; using more than two bands significantly lowers the accuracies. The bands which were by far most often selected are situated at 680 nm and 1 342 nm; See Table 5-3. These results show that the spectral calibration of the sensor was very good since the theoretical absorption maximum of chl-a is at 675 nm (the bandwidth was 15 nm). The classified image (Figure 5-5c) shows that in most places high chl-a concentration coincides with muddy sediment and wet conditions (see for instance points I and II). However, there are again some exceptions. In the South of the bank, a sand area with high chl-a was observed (Point III), while the chl-a concentration at the northern shore around point IV was low despite wet conditions and muddy sand. For both classes a high user and producer accuracy was obtained (Table 5-4c) with an overall accuracy of 84%.

Table 5-4: Confusion matrix and derived accuracy measures for each parameter. The total amount of pixels available for training and validation is shown next to the class name. All pixels have been used for training, applying a leave-one-out method.

(a: Median grain size)

	Mud	**Sand**
Mud (15 samples)	14	1
Sand (10 samples)	2	8
User acc.	*87,5*	*88,9*
Producer acc.	*93,3*	*80*
Kappa	*0,75*	

(b: Water content)

	Low	**High**
Low (13 samples)	10	3
High (12 samples)	0	12
User acc.	*100*	*80*
Producer acc.	*76,9*	*100*
Kappa	*0,76*	

(c: Chlorophyll-a)

	Low	**High**
Low (18 samples)	10	2
High (7 samples)	2	11
User acc.	*83,3*	*84,6*
Producer acc.	*83,3*	*84,6*
Kappa	*0,68*	

(d: Organic matter)

	Low	**Medium**	**High**
Low (11 samples)	8	3	0
Medium (8 samples)	1	6	1
High (6 samples)	0	0	6
User acc.	*88,9*	*66,7*	*85,7*
Producer acc.	*72,7*	*75*	*100*
Kappa		*0,69*	

5.5.4 Total organic matter content

The total organic matter (OM) was expressed as a weight percentage. In order to have more or less equal numbers of training samples in each class, the following three classes were distinguished:

0 – 2% ’low’
2 – 4% ’medium’
> 4% ’high’

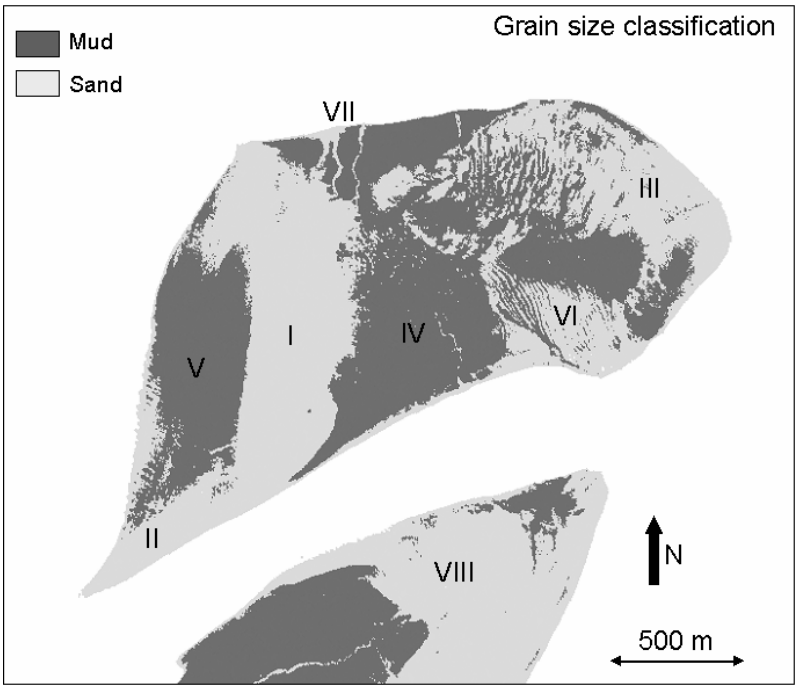

(a: median grain size)

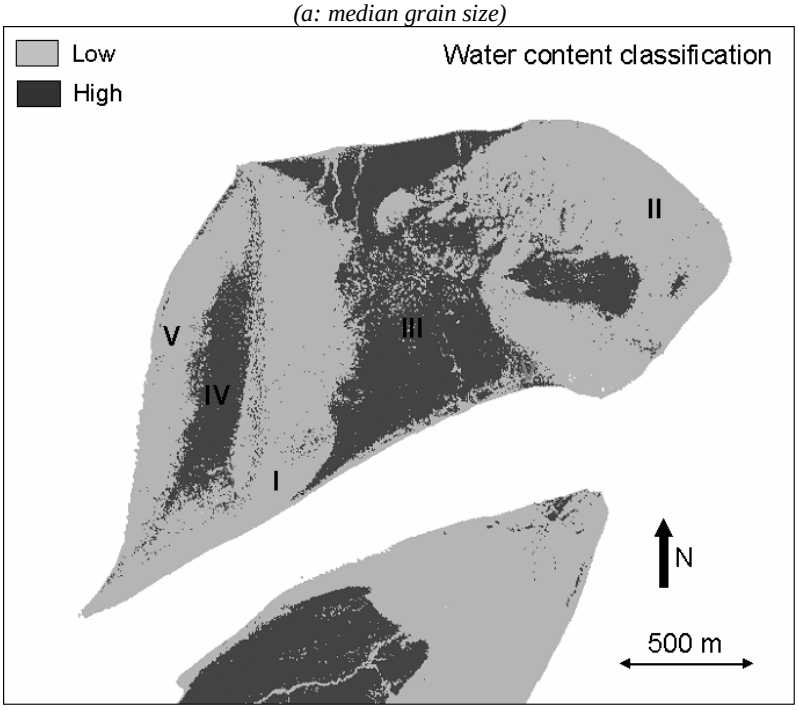

(b: water content)

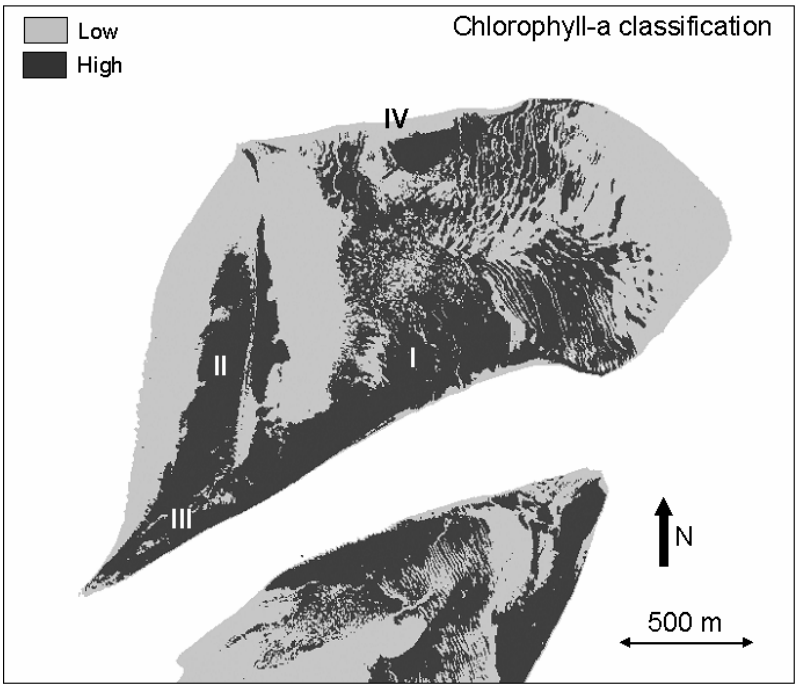

(c: chlorophyll-a concentration)

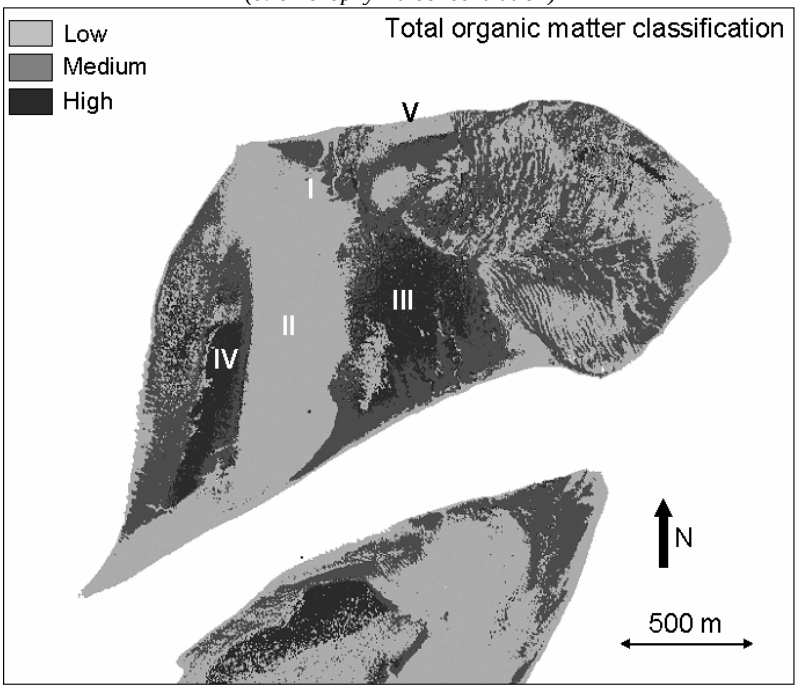

(d: organic matter content)

Figure 5-5: Classification results for the median grain size (a), water content (b), chlorophyll-a concentration (c) and organic matter content (d).

The amount and composition of organic matter can have a strong influence on terrestrial soil reflectance, especially when the OM content exceeds 2%. Several authors (see Baumgardner *et al.*, 1985 for a good overview) have concluded that OM correlates most highly with reflectance in the 0.5 – 1.2 µm range. This was only partly confirmed by the SFFS band selection procedure which selected as many bands in the VNIR part of the spectrum as in the SWIR part (Table 5-3). Since 604 nm was the most selected band, and living microphytobenthos absorb weakly at this wavelength, this OM was possibly derived from green plant detritus. As in the case of water content, three bands were needed to obtain the highest classification accuracy (Table 5-2). The classified image (Figure 5-5d) showed spatial patterns which are highly similar to those that were obtained with the three other parameters (Figure 5-5a-c). Even small details often coincided; for instance around the run-off channels in the North of the image (point I). The large sand areas contained few OM (point II), while the finer-grained sediments contained in general higher amounts of OM (points III and IV). An exception can be found at the northern shore of the bank where wet muddy sediments contain few organic matter (and few chl-a) (point V). The overall weighted accuracy for organic matter reached 80%; the class-specific accuracies can be found in Table 5-4d.

5.5.5 Ecotope map

The main goal of the HyMap campaign was to produce ecotope maps of the intertidal sediments. Ecotopes can be defined as small, ecologically-distinct features that support similar populations of flora and fauna (Hong *et al.*, 2004). Both abiotic and biotic factors can be recognised in the construction of ecotope maps, and one of the main uses of these maps has been in the selection of marine protected areas. However, maps based on abiotic factors alone (e.g., current speed, granulometry) have recently been criticised as inaccurate in their relationship to benthic macrofaunal distribution (Stevens and Connoly, 2004). Individual sediment parameters derived from the HyMap dataset were selected in order to create a macrofaunal ecotope map of the site. The layers featured in the map were chlorophyll – a biological parameter which indicates (from a faunal point of view) the potential abundance of a food source, grain size – an abiotic parameter of prime importance for macrofaunal colonisation, and water content – a sediment parameter which can be considered as a proxy for one of the main stress elements in the intertidal environment. Water content is closely related to the elevation; sites with higher elevation are exposed to longer emersion times, greater changes in salinity and temperature stress, and in the case of filter-feeders, reduced access to food.

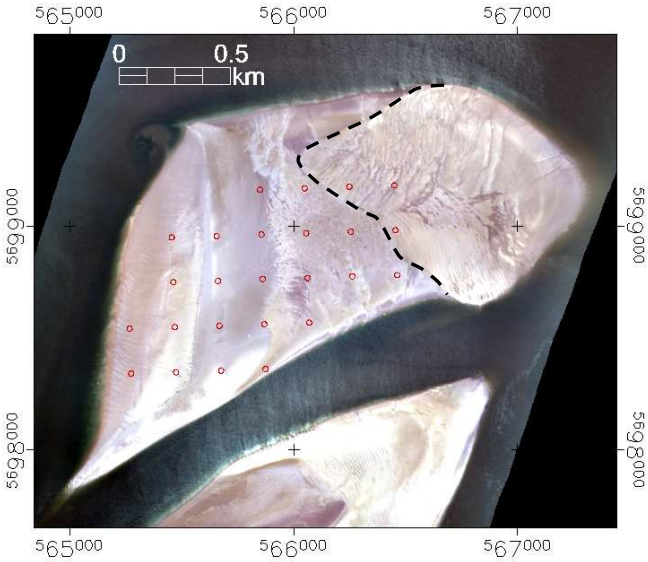

(a: True colour map)

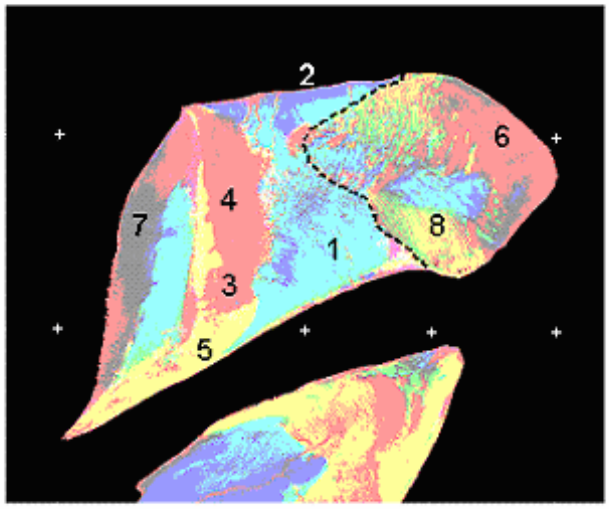

(b: Ecotope map)

Figure 5-6:

(a) True colour map of the Molenplaat (R=680 nm, G=573 nm, B=482 nm). In red the points where sediment samples were taken.The black dashed line indicates the border between the two parts of the bank. The image was linearly stretched.

(b) Map indicating the main sediment ecotope types. The black dashed line indicates the border between the two parts of the bank. This RGB composite was made of the median grain size in red, the chl-a concentration in green and the water content in blue.

Both maps are in UTM-WGS84 coordinates.

The resulting map (Figure 5-6b) shows that the western and central parts have a series of North-South oriented broad bands of different ecotope classes, whereas the eastern end had a more complex mosaic of small classes. This pattern is also reflected in the topography of the bank (Figure 5-4): in the West a sandy ridge stretches more or less North-South with finer sediments occurring on both sides. While in the eastern part, there is no distinct topography but rather a flat area with mega ripples in the South and the North. The large cyan area (see number 1 on Figure 5-6b), indicates wet areas with a high chl-a concentration and muddy sediment whereas dark purple (N° 2) represents wet, fine-grained sediment but with few chl-a. The little cyan dot at N° 3 is an artefact caused by the boat which was used to reach the bank. The other large entity is formed by the pale red (N° 4) and yellow areas (N° 5); they consist of sandy dry sediment with respectively few and high chl-a concentration. These ecotope types are found on the higher parts in the Southwest, on the large North-South oriented sand belt and on the eastern tip of the bank (N° 6). At location N° 7, a rather exceptional ecotope type is detected: muddy, dry sediment with few chl-a (grey colour). Note also the patterns formed by the mega ripples at N° 8; they consist of dry sediment with high chl-a concentration, muddy in the valleys and sandy at the top.

5.6 Discussion

As can be seen in Figure 5-5a-d the four classifications showed broadly similar spatial patterns. This is not surprising since the four parameters under study are, from an environmental point of view, closely corelated. The erosion and deposition of sediments of different grain sizes is controlled by local hydrographic factors. High current speeds and exposure to waves during submersion erode fine-grained sediments, leaving a bed of coarse-grained sediment. In contrast, fine-grained mud and clay deposits in areas of lower hydrodynamic energy. Sandy areas tend to dry faster than muddy areas, due to the difference in compactness of the sediment, and they are often characterised by a smaller amount of organic matter and chlorophyll. Muddy areas have in general higher organic matter contents and higher concentrations of chlorophyll. This can partially be explained by higher growth rates of benthic algae due to better nutrient availability and wetter conditions. In addition, resuspension of algal cells during flood is less likely, thus loss rates of benthic microalgae in muddy areas are lower. The higher algal concentration in muddy sediments supports in turn a greater concentration of other microorganisms such as bacteria, as well as a higher standing stock of macrofauna. There is also an interplay of biology with physics at the sediment-water interface, in that the presence of a microphytobenthic cell layer may facilitate the retention of fine sediments (Tolhurst *et al.*, 2003). Also, the production of mucus-like substances by bacteria, animals and algae in the sediment may aid in binding fine particles. Thus, the amount of living and dead organic material is highest in muddy sediments.

Hence, when training the classifier with a certain parameter it should be kept in mind that it is possible that the classification is not solely a classification based on that particular training parameter but also on parameters which are physically linked with this parameter. In extreme cases, it could be more influenced by another parameter than the one considered in training. However, since in nature these parameters are interrelated, it is not wrong to take them into account, but one should be aware of it.

A very remarkable feature on the ecotope map (Figure 5-6b) as well as on the classification results (Figure 5-5a-d) is the difference between the eastern and western part of the Molenplaat. The black dashed line indicates the border between both entities. eastwards of this border, one can see clearly mega-ripple structures (N° 10); the top of the ripples is formed by sandy dry sediment, while the troughs are covered with muddy, wet sediment. The amount of chlorophyll-a is quite high in both cases. The sedimentological differences make it likely that the current Molenplaat originated from two separate banks. This assumption is strengthened by the fact that recent shipping maps refer to the Brouwersplaat for the western part and to the Molenplaat for the eastern part of the current Molenplaat. The historical maps of the hydrographical unit of the "Agentschap voor Maritieme Dienstverlening en Kust" show clearly that between 1930 and 1935 the old Molenplaat and the Brouwersplaat merged into the current Molenplaat, although at that time there was still a tidal gully between both banks. In the forties the gully disappeared and both banks were joined. It is an remarkable finding that recent remote sensing images show signs of this history, even in this highly dynamic environment.

5.7 Conclusions

25 Samples, spread according to a regular grid, were taken over most of the Molenplaat. The sediment cores were analysed in the lab to define the median grain size, the water content, the total organic matter content and the chlorophyll-a concentration. By means of differential GPS measurements the samples could be accurately located on the HyMap images which contained 120 bands after bad bands removal. For each position, 9 image pixels (3x3 window) were averaged and used as input for the feature selection procedure and the classification algorithm. To calculate the accuracy of the different classifications, a leave-one-out approach was adopted on the samples. The images were classified with all sample spectra available. The number of bands needed to obtain the highest classification accuracy was defined after testing the accuracy for different numbers of bands. As little as two to three bands were required to classify each of the four parameters with the highest possible accuracy. Except for the organic matter parameter, these bands were most frequently selected in the VNIR part of the spectrum. The SWIR bands were barely used in the classification implying that for this application it is probably sufficient to use a more common VNIR

sensor. The overall weighted accuracy was highest for the water content (88%), the median grain size (88%) and the chlorophyll-a concentration (84%). The organic matter content scored somewhat lower with 80% but in this case three instead of two classes were retained.

The spatial patterns in the classified images indicate that the four parameters under study are highly correlated. In most cases, coarse sediments coincide with dry conditions, low organic matter and low chlorophyll-a. The wet and muddy parts of the Molenplaat are often characterised by a significant amount of organic matter and chlorophyll-a. However, there are exceptions where for instance chlorophyll-a coincides with rather dry and coarse sediments. These exceptions deserve some specific interest and will be investigated in a new project wherein the results presented here will serve as prior knowledge to guide the fieldwork. It was demonstrated that the classification of sediment parameters can reveal insight into the history of sandbanks. The spatial patterns in the classified images showed that the current Molenplaat resulted from two separate banks, the old Molenplaat and the Brouwersplaat. The results obtained provide valuable information for sediment stability studies since the parameters investigated play a key role in determining the erosion risk. Airborne hyperspectral remote sensing proves to be suited to determine certain parameters related to sediment stability. It is a valuable technique in remote and difficult to access tidal areas. The recent plans to deepen the Westerschelde place this kind of research in the spotlight; deepening will influence the bed topography, the sediment composition and the current velocities. With airborne hyperspectral remote sensing it will be possible to follow up the effects of the interventions planned.

Chapter 6

Sediment facies classification of a sandy shoreline by means of airborne imaging spectroscopy

This chapter is based on:

Deronde B., Kempeneers P., Houthuys R., Henriet J.-P. and V. Van Lancker, in press, Classification of a sandy shoreline by means of airborne imaging spectroscopy. International Journal of Remote Sensing.

6.1 Abstract

Airborne imaging spectroscopy (AISA Eagle and HyMap data) was applied to classify the sediments of a sandy beach in 7 sand type classes. On the AISA-Eagle data several classification methodologies were tried out and compared with each other. The best classification results were obtained applying a linear discriminant analysis (LDA) in combination with feature selection based on sequential floating forward search (SFFS). The statistical LDA was used in a multiple binary approach. In the first step, the original bands were used in the classification, but transformation of the bands to wavelet coefficients enhanced the accuracy obtained. The combination of LDA with

SFFS resulted in an overall accuracy of 82% (using 3 wavelets). Replacing the LDA with the non-statistical SAM algorithm reduces the overall accuracy to 74% (using all bands or wavelets). When applying LDA, the optimal number of bands/wavelet coefficients to be used was defined: using more than 2 bands or 3 wavelet coefficients did not result in a higher classification accuracy. Finally, the HyMap data, featuring 126 bands in the VNIR-SWIR range, were used to demonstrate that the VNIR range outperforms the SWIR range for this application.

6.2 Airborne datasets

6.2.1 AISA-Eagle

On July 6th 2004, during low tide, an AISA-Eagle scanner was flown over the entire Belgian coast. This pushbroom sensor, developed by Specim Ltd., covers the VNIR range between 400-900 nm and captured the reflected light in 32 contiguous bands with a spatial resolution of 1 m. However, since these data are also used to study dune vegetation, it was decided to apply narrow bandwidths (2.1 – 2.3 nm) in the green and red parts of the spectrum, at the cost of broader bandwidths in the blue and near infrared part of the spectrum. The absence of narrow absorption features in the spectral reflectance curve of beach sand (with the exception of red absorption in muddy sediments) allows for this band setting. Moreover, the broader bands in the blue compensate for the lower signal to noise ratio in this part of the spectrum. Table 6-1 summarises the band setting used for the AISA-Eagle.

Table 6-1: Band setting of the AISA-Eagle.

Spectral range (nm)	Band width (nm)	Number of bands
400 - 500	23.0 – 25.0	4
506 - 756	2.1 - 2.3	24
766 - 882	27.0 – 30.0	4

All images were corrected for atmospheric influences using ATCOR-4 (Richter *et al.*, 2002), based on the radiometric transfer model MODTRAN-4 by Berk *et al.* (1989). In support of this, sunphotometer measurements (with a SOLAR Microtops II) were performed to estimate the amount of water vapour and the aerosol concentration. For the geometric correction, an integrated GPS/INS system (Applanix POS-AV 510) was used, measuring the aircraft's position and attitude. Although state-of-the-art equipment was used, the geometric accuracy obtained was not very good. Errors of 2-5 pixels were common. Luckily the pixels were rather small (1 m) compared to the sediment patterns on the beach, and the ground truth (see Section 6.3) had been collected in such a way that the points were located in the middle of homogenous

areas. On top of that, squares of 3x3 pixels were used to derive the ground truth signatures.

6.2.2 HyMap

About one month before the AISA flight, on June 8th 2004 during low tide, the East Coast of Belgium (between the harbour of Zeebrugge and the Dutch border) was mapped with a HyMap sensor. The instrument was calibrated before the flight campaign using HyVista calibration gear. The HyMap is a whiskbroom scanner utilising diffraction gratings and four 32-element detector arrays to provide 126 spectral channels covering the 438 - 2491 nm range (Kruse *et al.*, 2000). However, the quality of the first blue band and the 5 last SWIR bands was too poor for further analysis; therefore the HyMap dataset was limited to 120 bands with a bandwidth (defined as the full width at half maximum) of 14 – 21 nm between 445 and 2414 nm. The spatial resolution of the pixels was 5x5 m and the raw data were geometrically corrected using the software ORTHO (Müller *et al.,* 2002) while the radiometric calibration was performed with the standard software of HyVista (Cocks *et al.,* 1998). The geometrically corrected and radiometrically calibrated data were, in the same way as the AISA data, corrected for atmospheric influences using ATCOR-4.

The acquisition area during the HyMap campaign was limited to the East Coast since the aim was to study the optimal spectral range for sediment mapping of sandy shorelines: "Is the VNIR range sufficient, or is it better to use the SWIR range or both?" The East Coast is characterised by quite narrow beaches (100-300 m wide at low tide) which are heavily prone to erosion. To compensate for the erosion, beach nourishments have been carried out since the 1960s and they continue up to the present day. The beach nourishments are the reason why the East Coast was selected for the HyMap flight, since this allowed to focus on the classification of the type of sand used for these soft defence works. The follow-up of the nourished areas is one of the most interesting applications of shoreline classification. The characteristic type of sand used for the nourishment can serve as a tracer in the study of the coastal dynamics (Deronde *et al.*, 2006a).

6.3 Ground truthing

In the same period as the airborne acquisitions, an extensive field survey was conducted to collect the necessary ground truth data for the supervised classifications. At well spread locations, 135 samples of the top layer of the beach were collected and their position was measured with differential GPS, resulting in a planimetric accuracy better than one pixel. After the data acquisition we saw that some ground truth locations were covered by water at the time of the acquisitions what forced us to

exclude these locations from further analysis. To compensate for this and to have enough training samples in each class a few additional locations were chosen on the images. These points were carefully located at well-known and stable areas (but no sample could be taken in these points). Finally, exactly 100 samples were used for training and validation of the classifications of the AISA data, while 48 samples were used during the HyMap classifications.

The field samples were analysed in the lab to obtain a physical description of each class (see Table 6-2). The following parameters were measured: grain size distribution (described by the median grain size = D50, and the sorting), organic matter content, carbonates content, total content of iron and percentage of shell fragments. The carbonates were removed with HCl, the organic matter was removed by heating the sample up to 300°C, and after these two steps the grain size distribution was determined by means of dry sieving. The iron content was determined using X-ray diffraction analysis (ED-XRF[9]) and the percentage of shell fragments was defined by manually counting a sub-sample under the microscope.

The classes were defined in order to obtain meaningful entities with respect to the monitoring of the morphological changes of the beach, i.e., changes in the spatial pattern of the classes help to gain insight in the dynamics of the system.

The classes 'Fine sand from the intertidal beach' and 'Coarser sand from the intertidal beach' are mainly found between the low and high water mark; they contain a fine-grained sand type which is well sorted and contains few shell fragments and iron. The 'Sand from the supratidal beach' is the class which corresponds to the type of sand that could be found above the high water mark before the largescale beach nourishment works took place. It is somewhat coarser, less well sorted, but it contains also few shell fragments and iron. The 'Sand used for beach nourishments' and the 'Sand with a lot of shells' are coarse-grained, poorly sorted and they contain a lot of shells and iron. As a result, the carbonates content is also significantly higher in these classes. The 'Fine dune sand' contains fine sand that is mainly transported by aeolian processes; hence, it is well sorted and contains few shell fragments. The organic matter content was low for all classes, except for the 'Muddy sand' class. However, it should be noted that the samples used to define this class were purely silt/mud samples, as can be seen from the results in Table 6-2. Finally, one can see that the number of samples in Table 6-2 does not sum to 100, which is explained by the fact that there are 7 samples for 'Mixed vegetation and sand', 8 for 'Vegetation' and 6 for 'Water'.

[9] Energy Dispersive X-Ray Fluorescence (Jenkins, 1999)

Table 6-2: Physical description of the 7 sand type classes that could be distinguished on the AISA data (w% = weight percentage, c% = a percentage obtained after counting a sub-sample of 500 grains).

	D50 (µm)	Sorting (phi)	Carbonates (w%)	Organic matter (w%)	Fe (w%)	Shell fragments (c%)	Number of training samples for AISA data
Muddy sand / pure mud	< 63	n/a	52.05	7.300	2.201	0.00	8
Fine sand from the intertidal beach	189	0.366	11.51	0.071	0.419	2.82	8
Medium sand from the intertidal beach	239	0.394	10.54	0.020	0.408	4.53	12
Original sand from the supratidal beach	244	0.428	10.22	0.076	0.432	4.56	20
Sand used for beach nourishments	300	0.573	20.43	0.055	0.618	5.31	18
Sand with a lot of shells	381	0.838	42.97	0.100	0.847	7.68	6
Fine dune sand	217	0.341	7.14	0.000	0.400	2.85	7

The effect of these different sediment components on the spectral reflectance is very well explained by Baumgardner *et al.* (1985). The work of Leu (1977) provides some specific spectral analysis of beach sands, focusing on the influence of soil water content, iron content and grain size. Table 6-2 lists the 7 sand type classes distinguished on the AISA data. On the HyMap data only 5 classes were distinguished due to the limited number of training samples and due to the coarser resolution of these data what makes it more difficult to distinguish between certain classes (see Section 6.4).

6.4 Methodology

Two classification algorithms were tried out: a statistical Linear Discriminant Classifier and a non-statistical Spectral Angle Mapper classifier. The first is applied in

combination with a feature selection approach. The following sections explain briefly the classification methodology adopted.

6.4.1 Linear Discriminant Analysis (LDA)

The first classification algorithm used is based on Linear Discriminant Analysis (LDA) (Fischer, 1936; Duda *et al.*, 2001). Briefly described, this algorithm performs as follows: for C classes and N bands, LDA projects the N-dimensional input vector onto a (C-1) dimensional vector with optimal class discrimination in mind. It minimises the ratio of the within class over the between class scatter matrices. Hence, for a two-class problem, the feature space is projected onto a 1-dimensional space, and the LDA technique immediately serves as a linear classifier. For this study, in which 7 classes were to be distinguished, a multiple-binary approach was adopted. This means that the outputs of several binary classifications were combined to come to a final class decision. Several studies pointed out that multiple binary classifiers outperform multiclass classifiers who consider all classes in one step (e.g., Kempeneers *et al.*, 2005a; among others). Mostly, one-against-all or one-against-one approaches are used. With the one-against-all strategy, each classifier is trained to differentiate one class from all the others, which requires a number of classifiers equal to the number of classes. In the one-against-one approach, all possible pairs of classes are compared requiring $C(C\text{-}1)/2$ classifiers. Generally, good results are obtained using the one-against-one approach in combination with a maximum voting technique to come to a final class decision (i.e., the class winning most in the binary classifications is the one finally assigned). Therefore the one-against-one approach was followed in this study. The validation was performed with the leave-one-out method, which implies that all 100 AISA samples and all 48 HyMap samples could be used for training.

6.4.2 SAM classifier

The second classification algorithm used is SAM (Spectral Angle Mapper). SAM considers each spectrum as an N-dimensional vector in an N-dimensional space, where N is the number of bands, and compares this vector with pre-defined library spectra (Kruse *et al.*, 1990). The angles between each pixel spectrum and the library spectra are calculated and the pixel is assigned to the class corresponding to the smallest angle.

6.4.3 Feature selection by means of sequential floating forward search (SFFS)

The multidimensional hyperspectral data cubes showed frequent autocorrelation between adjacent bands in most parts of the spectrum. This means that a lot of bands can be omitted without losing a lot of information. Moreover, the Hughes phenomenon

tells us that the accuracy decreases when too many bands are trained with a small amount of training samples, due to over-training of the classifier (Kalayeh *et al.*, 1983; Landgrebe, 2003). Therefore, LDA was combined with a feature selection approach, in this case a Sequential Floating Forward Search (SFFS) (Pudil, 1994). SFFS performs as follows: one selects the best single band, then adds a second band to have the best combination of two bands, adds a third band to have the best combination of three bands and so on. But, after each forward step, SFFS performs one or more backward steps, i.e., it removes a previously selected feature to investigate if the score can be increased using another band. This floating aspect was used to minimise the possibility to end up in a local minimum. After the feature selection procedure a combination of n bands which are (sub)optimal for classification was obtained.

Note that in the case of the SAM algorithm it was not necessary to apply a feature selection since SAM reduces all bands to one single angle.

6.5 Results

6.5.1 Linear Discriminant Classifier in combination with SFFS

In a first attempt, the original AISA bands were used for classification. Figure 6-1 shows clearly that one does not need a large number of bands to obtain high classification accuracy. Using only one band resulted in a Kappa of 0.51. The Kappa statistic was used as a measure for the accuracy, since this statistic excludes the accuracy due to chance. Note that for each binary classification, the ideal band was chosen. If the algorithm is allowed to choose two bands for each binary classification, a Kappa of 0.66 was obtained (corresponding to an overall accuracy of 70%). Using more than two bands did not improve the accuracy; on the contrary, a small decrease in accuracy was observed (cf. the Hughes phenomenon mentioned above).

The 95% confidence interval on the Kappa statistic was calculated as follows:

$$95\%\,\text{int}\,erval = +/-1.96\sqrt{\frac{Kappa.(1-Kappa)}{S}} \qquad \textit{Eq 6-1}$$

with S = number of samples used for training

Inspired by the work of Kempeneers *et al.* (2005a) and Bruce *et al.* (2002), we transformed the original bands to wavelet coefficients. The wavelet coefficients were obtained using discrete Haar type wavelets (Chui, 1992). Using the wavelet coefficients, the accuracy raised significantly (see Figure 6-1). For only one wavelet coefficient a Kappa of 0.77 was obtained. The highest accuracy (Kappa of 0.80 or 82% overall accuracy) could be reached using three wavelet coefficients; however, the 95%

confidence interval shows that there was no significant difference between the Kappas obtained with different amounts of wavelet coefficients. At least for this application, where we have rather featureless spectra, wavelets prove to be a powerful tool to reorganise the information available within the original bands over a new subset of features. Using one new feature or wavelet coefficient is in this case already sufficient to obtain a good accuracy. When the spectral information would be divided over many different bands, one probably would have to use more wavelet coefficients to obtain the same accuracy.

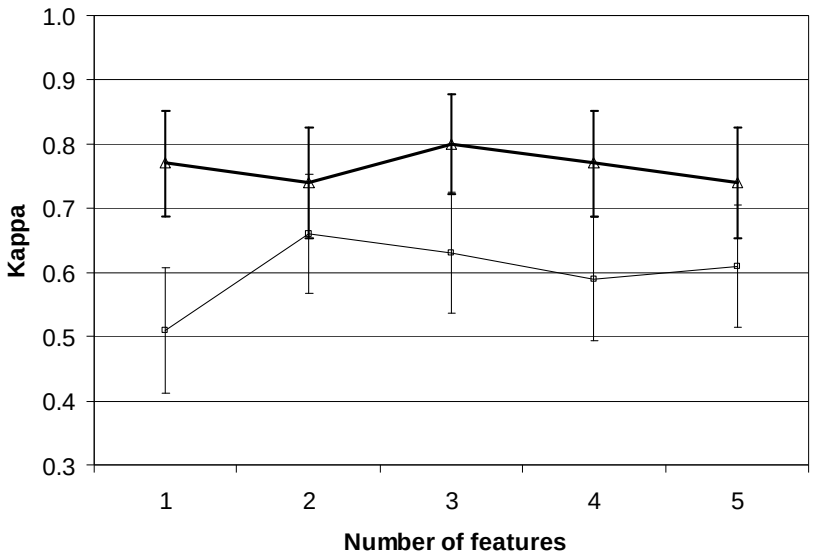

Figure 6-1: Kappa values and 95% confidence intervals obtained when using 1 to 5 bands (thin line with square markers) or wavelet coefficients (bold line with triangle markers). The classification algorithm used is a Linear Discriminant Classifier.

6.5.2 SAM classifier

In the methodology applied in Section 6.5.1. the LDA was replaced by the SAM algorithm. Since SAM uses one scalar value (an angle) to compare two bands, it was not necessary to apply a feature selection. Moreover, the use of all bands makes it unnecessary to transform the original bands into wavelets since all spectral information available in the data is used when applying all bands. The rest of the methodology, i.e., the multiple binary approach and the maximum voting remained the same. Hence, this test can be considered as a comparison of the LDA in combination with SFFS and the SAM classifier.

The Kappa was 0.71 and the overall accuracy 74%. Compared to the best accuracy obtained using LDA and a selection of 3 wavelets (Kappa: 0.80 or 82% overall accuracy), it is clear that LDA in this case performs better than SAM. However, when LDA is applied to the original bands, SAM performs slightly better. The results for LDA with an optimal subset of three wavelets and two bands, and SAM are summarised in Table 6-3.

Table 6-3: Kappa (with 95% confidence interval between brackets) and overall accuracy when applying the LDA algorithm with 2 bands or 3 wavelets, and when applying SAM on all original bands.

	LDA with 2 bands	**LDA with 3 wavelets**	**SAM with all bands**
Kappa	0.66	0.80	0.71
Overall accuracy	70%	82%	74%

6.5.3 Impact of the band width on the classification accuracy

Taking into account the featureless nature of the AISA spectra of the studied beach sands, the question arises whether we need the narrow bandwidth of the original data (see Table 6-1). This test was applied on the 24 central bands (range = 506 – 756 nm), all having an original FWHM (Full Width at Half of Maximum) of 2.2 nm. The bandwidths were stepwise widened starting with a FWHM of 22 nm, which is the double of the original sampling interval, and adding in each step 11 nm to the FWHM. To remove redundancy between adjacent bands, the number of bands was reduced accordingly: i.e., if the FWHM is twice the sampling interval, the number of bands retained is divided by two; if the FWHM is 4 times the sampling interval, the number of bands retained is divided by 4 etc. The largest FWHM used was 110 nm. The filter applied is a Gaussian filter. Figure 6-2 illustrates the principle of the Gaussian filter. In the first step the Gaussian is widened from 2.2 nm to 22 nm, hence integrating (part of) the reflectance in three neighbouring bands. Note that the filtering creates an artefact at the beginning and at the end of the spectrum caused by the position of the broad Gaussian (see Figure 6-2). To compensate for this, the spectral signature was mirrored around the first and last band. Since this artefact occurs in all spectra and in all classes, it has a negligible influence on the classification accuracy.

The results illustrated in Figure 6-3, show that the accuracy decreases when broader bands are used; after applying LDA in combination with SFFS. Roughly spoken, the Kappa decreases from 0.7 to 0.6 when the FWHM broadens from 2.2 nm to 110 nm. Hence, even with broad bands the accuracy remains high. This test proves clearly that for this application it is possible to configure the sensor with less and broader bands; bands of 30 – 50 nm seem to be sufficient to obtain a high classification accuracy. In the Section 6.6 we come back to this topic.

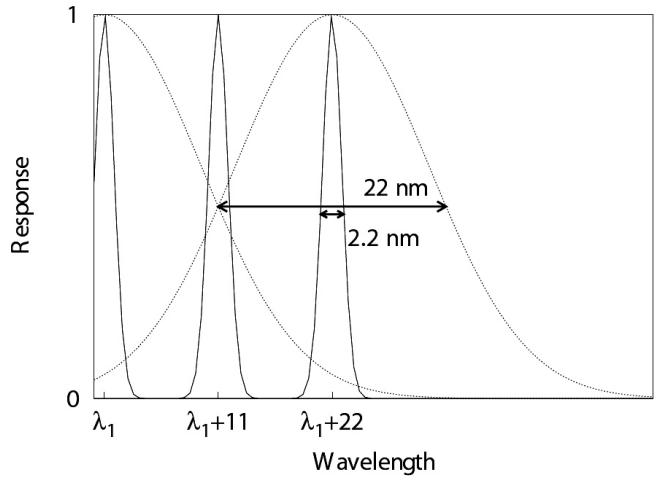

Figure 6-2: Schematic representation of the filtering of the original bands by a Gaussian filter. The original bands have a FWHM of 2.2 nm. The Gaussian filters have a FWHM of 22 till 110 nm. The response of the original bands and the response of the Gaussian with a FWHM of 22 nm are plotted.

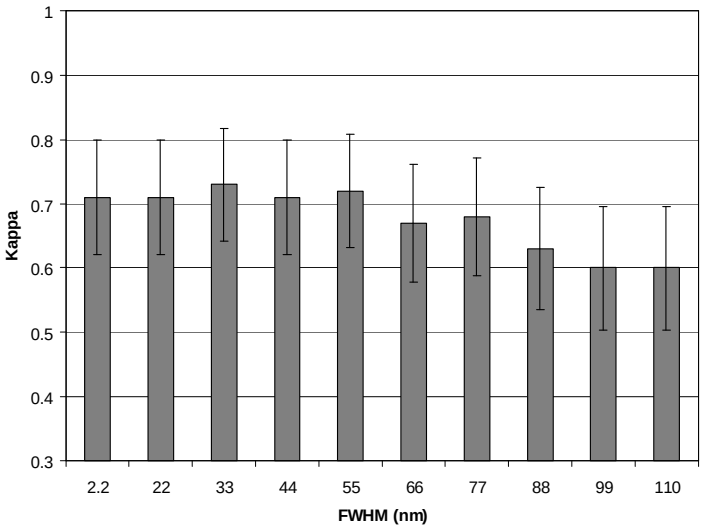

Figure 6-3: Kappa and 95% confidence interval when using bands with an increasing FWHM

6.5.4 Impact of the spectral range on the classification accuracy

In the last methodological section we consider the spectral range that is best suited to classify sandy shorelines. Since the AISA data cover only the VNIR part of the

spectrum, the HyMap dataset, covering the East Coast between the harbour of Zeebrugge and the Dutch border, was used for this purpose. However, the spatial resolution of the HyMap data is much lower (5 m) than that of the AISA data (1 m). As a consequence of this and because less training data were available for the coastal strip covered by the HyMap data, a smaller number of classes could be distinguished. Table 6-4 lists the classes that were retained. The classification algorithm used is the LDA in combination with SFFS, applied on the wavelet coefficients.

Table 6-4: Classes used in the classification of the HyMap data (with their corresponding number of samples).

Class	Number of samples
Sand from the supratidal beach	9
Fine sand from the intertidal beach	7
Fine-medium sand from the intertidal beach	8
Sand used for beach nourishments	8
Vegetation	8
Water	8

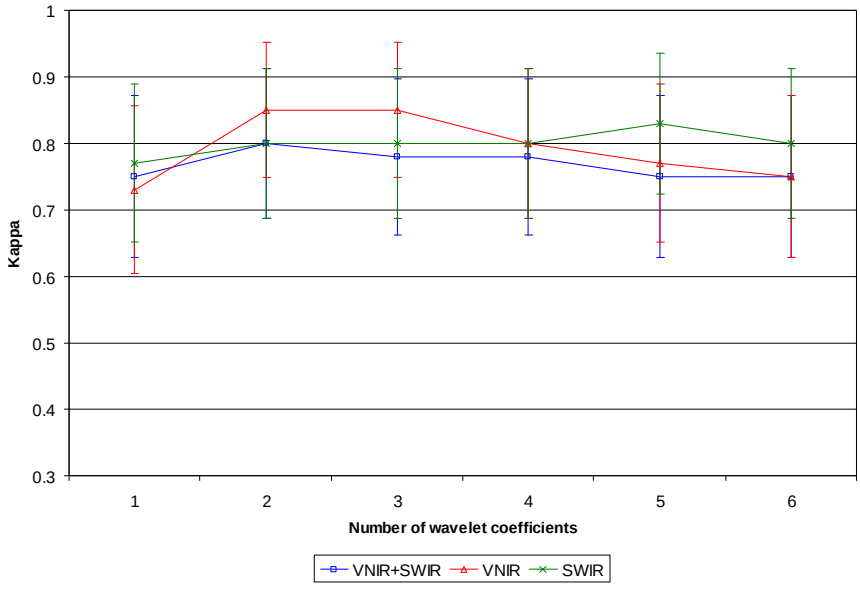

Figure 6-4: Kappa obtained when using only the VNIR range, only the SWIR range, or the full range. The X-axis shows the number of wavelet coefficients that was used in the Linear Discriminant Classifier.

The VNIR range covered the bands between 400 and 1 000 nm (i.e., bands 2 > 38), while the SWIR range ran from 1 000 up till 2 500 nm (i.e., bands 39 > 121). Figure 6-4 shows the Kappa obtained when only the VNIR range was used, when only the SWIR range was used and when the full range was used. The X-axis shows the number

of wavelet coefficients that was used. Taking into account the 95% confidence interval, calculated according to Eq 6-1, it can be concluded that both the VNIR range and the SWIR range result in high classification accuracies. For 2 or 3 wavelet coefficients the VNIR range scored the best results (Kappa of 0.85), but the differences are negligible. Hence, for this application and with a limited amount of training samples one could use both a VNIR or a SWIR sensor, but seen the slightly higher Kappas obtained with few (N° 2 or 3) wavelet coefficients and the logistic argument that VNIR sensors are much more common and less expensive, a VNIR sensor seems to be the best choice for this application.

6.6 Discussion

The methodological sections show that airborne hyperspectral remote sensing is a suited tool to classify sandy shorelines. Not less than 7 sand type classes could spectrally be distinguished with high accuracy. The technique proves also suited to map areas where artificial beach nourishment works took place and to follow up their dynamic behaviour. Figure 6-5 shows on top an RGB image (R=634 nm, G=545 nm, B=463 nm) and below the classification result for Knokke-Zoute; being the most easterly part of the Belgian coastline. As this area has always been prone to erosion, it is the scene of repeated large-scale nourishment works (1977-1979, 1986, 1999, 2004). The sand used for these defence works is borrowed from offshore banks. The coarser grain size, the bad sorting, and the high content of shell fragments and iron (see Table 6-2) allow to distinguish this type of sand spectrally from the original sand. In Deronde *et al*. (2006a) it is explained and demonstrated how this technique can be combined with airborne LIDAR data to study the morphodynamics of the shoreline.

The class with beach nourishment sand is mainly found on the higher parts of the beach, where it was originally deposited (N° 1). Seawards of these areas (N° 2), between the low and high water level, shell-rich sand is found. This indicates that the nourished sand has been reworked and that the shell fragments were washed out and temporarily stocked on the intertidal part of the beach. This could be explained by the high wave energy in the swash zone, leading to the uptake of coarse sediments and shells in the uprushing water flow. During the backwash (i.e., the flow of water seawards) the wave energy disappears and the heavy shells are deposited (Short, 2001). eastwards, less nourishment sand and more original supratidal beach sand was found on the dry part of the beach (N° 3), while the shells become sparser on the intertidal part of the beach (N° 4).

The muddy sand along the low water level (N° 5) may correspond to a temporary veneer of mud deposited on the lower part of the beach under quiet meteorological conditions (the offshore part of these beach sections is largely muddy). Although this could be a logical explanation, this class seems to be overestimated in this area. In the fore dunes, the class with fine dune sand is widespread (N° 6); this fraction is

transported by aeolian forces and deposited between the vegetation and the artificial fences on the fore dunes. In the extreme East, one sees the channel of the Zwin nature reserve (N° 7), being the last remnant of a tidal inlet. Indeed, the ancient shoreline was constituted of a discontinuous sandy beach barrier and a shallow lagoon between the land and the beach barrier. The Zwin was formed as a result of a heavy storm in 1134 (the 'Elisabethstorm'), causing a break-trough of the narrow beach barrier.

Without denying the possibilities of airborne imaging spectroscopy, the above sections showed that a high amount of small bands is not needed to obtain good classification accuracies. A few broad bands or wavelet coefficients proved to be sufficient. However, in the SFFS algorithm used, a feature selection is performed for each binary classification. Hence, in total more than 2 or 3 bands are used to obtain these good accuracies. However, it was observed that the bands selected are often the same bands, and on top of that it does not matter if a band is substituted for its neighbouring band, due to the high correlation between the bands. With these elements in mind, we would advise to use for this type of application a hyperspectral VNIR sensor, configured with only 10-20 bands, in favour of the spatial resolution. It is our conclusion that more useful and accurate beach sand classifications can be obtained with 10 bands and 1 m ground resolution than with 100 bands and 5 m ground resolution.

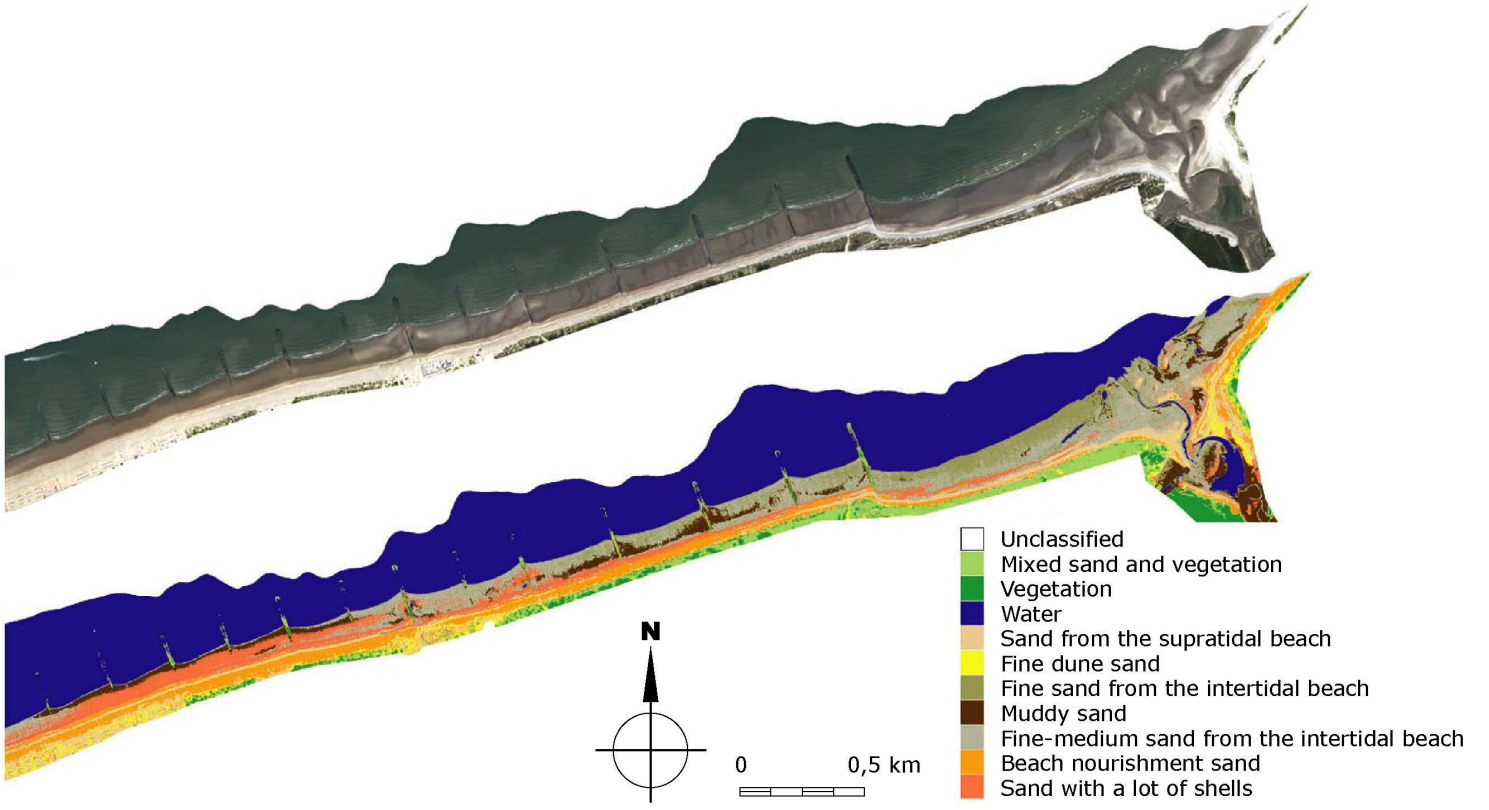

Figure 6-5: Classification of the shoreline in Knokke-Heist. 7 sand type classes could be distinguished, applying a Linear Discriminant Classifier and feature selection on wavelet transformed bands.

6.7 Conclusions

Airborne imaging spectroscopy data (AISA and HyMap) were used to classify the sandy sediments along the Belgian shoreline. The AISA data, featuring 32 bands and 1 m ground resolution, were used to test different classification strategies and to obtain classified maps that can be (and are) used by the administration responsible for the management of the coastal zone. Due to the type of sand used to perform the beach nourishment works, the technique proved to be especially suited to map beach nourishment areas and to follow-up their dynamic behaviour. The best classification results were obtained applying Linear Discriminant Analysis (LDA) in combination with feature selection by means of Sequential Floating Forward Search. Transformation of the original bands into wavelet coefficients significantly improved the accuracy. Using wavelet coefficients, a Kappa of 0.80 could be obtained for 7 sand type classes. The non-statistical SAM algorithm scored somewhat lower (Kappa of 0.71) than LDA. The LDA algorithm was also run on artificially broadened bands; this test showed that for this application narrow bands are not needed to obtain good classification accuracies: it was possible to broaden the bands from 2.2 nm up to 55.0 nm without losing classification accuracy. Finally, the HyMap data were used to test the hypothesis that a VNIR sensor is sufficient to classify sandy shorelines. It was shown that nearly the same classification accuracy could be obtained using the VNIR range than the SWIR range or the whole VNIR+SWIR range. To conclude, it is suggested to use for this application a hyperspectral VNIR sensor configured with a limited number of bands (10 to 20) but with a high spatial resolution. The trade-off between spectral and spatial information, due to the limited storage capacity of airborne systems, should in this case be handled in favour of the spatial resolution.

Chapter 7

Monitoring of the sediment dynamics along a sandy shoreline by means of airborne hyperspectral remote sensing and LIDAR, a case study in Belgium

This chapter is based on:

Deronde B., Houthuys R., Henriet J.-P. and V. Van Lancker, in press, Monitoring of the sediment dynamics along a sandy shoreline by means of airborne hyperspectral remote sensing and LIDAR, a case study in Belgium. Earth Surface Processes and Landforms.

7.1 Abstract

Airborne hyperspectral data and airborne laserscan or LIDAR data were applied to analyse the sediment transport and the beach morphodynamics along the Belgian shoreline. Between 2000 and 2004, four airborne acquisitions were performed with both types of sensors. The hyperspectral data were classified in seven sand type classes following a supervised classification approach in which feature selection served to reduce the number of bands in the hyperspectral data. The seven classes allowed to analyse the spatial dynamics of specific sediment volumes. The technique made it possible to distinguish the sand used for berm replenishment works or for beach nourishments from the sand naturally found on the backshore and the foreshore. Subtracting sequential DTMs (Digital Terrain Models) resulted in height difference

maps indicating the erosion and accretion zones. The combination of both data types, hyperspectral data and LIDAR data, provides a powerful tool, suited to analyse the dynamics of sandy shorelines. The technique was demonstrated on three sites along the Belgian shoreline: Koksijde, located at the West Coast and characterised by wide accretional beaches, influenced by dry berm replenishments and the construction of groynes. Zeebrugge, at the Middle Coast, where a beach nourishment was executed one year before the acquisitions started and where the dams of the harbour of Zeebrugge are responsible for the formation of a large accretional beach. The third site, Knokke-Heist, is located at the East Coast and is characterised by narrow, locally reflective, beaches, heavily influenced by nourishment activities. The methodology applied allowed retrieving the main sediment transport directions as well as the amount of sediment transported. It proved to be specifically suited to follow up the redistribution and the resorting of the fill in beach nourishment areas.

7.2 Methodology

Table 7-1 summarises the dates and sensors of the airborne hyperspectral and LIDAR acquisitions. Due to organisational constraints no recordings could be performed in 2003 and the LIDAR and hyperspectral acquisitions could not always be synchronised in time. In 2000 and 2001, both acquisitions were performed within one month, but in 2002 and in 2004 more time elapsed between the LIDAR and hyperspectral recordings. In 2000, 2001 and 2002 a hyperspectral CASI scanner was used. This instrument, developed by ITRES Ltd., measures the reflected sunlight in a 545 nm spectral range configured in the Visual and Near-InfraRed (VNIR) range. The 96 spectral bands were radiometrically calibrated, atmospherically corrected (Berk *et al.*, 1989; Richter and Schläpfer, 2002) and geometrically corrected.

Table 7-1: Sensors and dates of the airborne hyperspectral and LIDAR acquisitions in the period 2000 – 2004.

	2000	**2001**	**2002**	**2004**
Hyperspectral	CASI	CASI	CASI	AISA-Eagle
	23/08/2000	27/08/2001	11/10/2002	6/07/2004
LIDAR	ALTM 1225	ALTM 1225	ALTM 1225	ALTM 2050
	11/09/2000	28/09/2001	18/12/2002	2/09/2004

In 2004 an AISA-Eagle was used. This sensor, developed by Specim Ltd., covers the VNIR range between 400-900 nm and was configured to capture the reflected light in 32 spectral bands. The smaller number of bands proved to be sufficient to classify the sand with high accuracy. This is due to the featureless nature of the spectra causing a high inter-correlation between adjacent bands. The spatial resolution (i.e., the pixel

size) of all hyperspectral data was resampled to 2x2 m, using nearest neighbour resampling.

The hyperspectral data were used to classify the beach in 7 sand type classes; these sediment facies classes were defined in the field to correspond to the most common sand types found along the Belgian coast and are linked to the topography and geomorphology of the beach, i.e., certain topographical or geomorphological units of the beach can be characterised by a certain type of sand. Table 7-2 lists the sediment parameters for each of the 7 sand type classes used in the classification of the beach; the samples used to derive the parameters in this table are the ground truth samples that served as training and validation of the classifications of the AISA data of 2004. Note that these samples correspond to the upper millimeters of the sediment as the reflectance is only determined by this top layer. Each airborne hyperspectral campaign was accompanied by a field sampling campaign that served to collect field samples to train and validate the classifications. An important element during the field sampling was the collection of both dry and wet samples for those classes that occur both on the intertidal and the supratidal beach. As the wetness of the sand has an influence on the spectral reflectance: the reflectance lowers in a quasi homothetic way (i.e., without changing the shape of the spectrum) when the water content increases, it is important to take this variance into account when collecting the samples. The classification results pointed out that it is possible to group samples with a different water content in one class if the samples cover the entire variance present in the population of that particular class.

The hyperspectral data were classified with a Linear Discriminant Classifier (LDC) (Fischer, 1936; Duda *et al.*, 2001) in combination with feature or band selection based on a Sequential Floating Forward Search (SFFS) (Pudil *et al*., 1994). For a description of these techniques, the reader is refered to Section 6.4. For this study, in which 7 classes were to be distinguished, a multiple-binary approach was adopted. This means that the outputs of several binary classifications were combined to come to a final class decision. Kempeneers *et al.* (2005a) compared the multiple binary classification approach with the more common multiclass approach and concluded that the multiple binary approach outperforms the multiclass approach. The best classification results were obtained when the original spectral bands were transformed to wavelets (discrete Haar type wavelets). Using three wavelet coefficients, selected with SFFS, in each binary classification, resulted in an overall accuracy of 82% for the imagery of 2004. More information on the classification methodology used and the accuracy obtained can be found in Deronde *et al*. (2006b) and Kempeneers *et al.* (2005b).

Table 7-2: Sediment parameters for each of the 7 sand type classes used in the classification of the beach; based on the field sampling of 2004. (w% = weight percentage, c% = a percentage obtained after counting a sub-sample of 500 grains).

	D50 (mm)	Sorting (phi)	Carbonates (w%)	Organic matter (w%)	Fe (w%)	Shell fragments (c%)
Muddy sand / pure mud	< 63	n/a	52.05	7.3	2.2	0
Fine sand of the lower shoreface	189	0.37	11.51	0.07	0.42	2.82
Fine-medium sand of the lower shoreface	239	0.39	10.54	0.02	0.41	4.53
Original sand of the upper shoreface	244	0.43	10.22	0.08	0.43	4.56
Sand used for beach nourishments	300	0.57	20.43	0.06	0.62	5.31
Shell-rich sand	381	0.84	42.97	0.1	0.85	7.68
Fine dune sand	217	0.34	7.14	0	0.4	2.85

To reduce the amount of data (i.e., bands) to be used in the classification algorithm and to take into account the limited number of training samples, which from a statistical point of view limit the number of bands that can be used (Kalayeh *et al.*, 1983), a feature selection step was necessary. A straightforward method would be to try all possible band combinations. This will always yield the best subset of features, but it is a very exhaustive and time-consuming approach. Therefore, the Sequential Floating Forward Search (SFFS) was used. SFFS performs as follows: one selects the best single band, then adds a second band to have the best combination of two bands, adds a third band to have the best combination of three bands and so on. But, after each forward step, SFFS performs one or more backward steps, i.e., it removes a previously selected feature to investigate if the score can be increased using another band. This floating aspect was used to minimise the possibility to end up in a local minimum. After the feature selection procedure a combination of N bands which are (sub)optimal for classification is obtained.

The LIDAR data served to create maps indicating the erosion and accretion. These maps could easily be obtained by subtracting the successive DTMs from each other. The DTMs were obtained after morphological filtering of the DEMs, i.e., all elements which do not belong to the Earth's surface, e.g., beach cabins, were eliminated. After filtering, the point density was reduced to 1 point every 16 m². The vertical accuracy of the DTMs on flat reference surfaces, expressed as the mean absolute error (Su and Bork, 2006), was app. 5 cm, with a standard deviation of 7 cm. The errors on the gentle sloping beach are not exactly known, as there were no reference surfaces, but according to the investigations of Su and Bork (2006), the mean absolute error will not

significantly increase for slopes between 0 - 15%. The volume differences were calculated in two ways: per polygon, where the polygons delineate areas with major volume changes between two dates; and per coastal zone, where zones are larger areas of a few km long that integrate the beach between the low water mark and the dune foot.

The final analysis (see Section 7.3) is based on the combination of the DTMs, the erosion/accretion maps resulting from the subtracted DTMs and the classified hyperspectral images. The latter is the innovative aspect in this research. While DTMs only allow for a calculation of the amount of sediment eroded or deposited, the classified scenes allow for a qualitative interpretation in which the classes serve as tracer for the sediment dynamics. This is the fundamental reason why the hyperspectral images have to be classified in a number of sand type classes. Without these classes, it is not possible to derive any information on the direction of the sediment transport as the raw hyperspectral data only offer per pixel a reflectance spectrum. In order to use this reflectance data for sand dynamics studies, one has to classify the hyperspectral data into classes which spectrally can be distinguished and which are related (however not inextricably) to certain geomorphological units of the beach. E.g., the class 'Fine sand of the lower shoreface' is typically found on the lower shoreface, it features a mineralogical composition, a grain size and a sorting which are the result of the processes acting on the lower shoreface, but it is possible that this class is found elsewhere on the beach. Hence, the classified images reveal information on the nature and the geomorphology of the beach. By studying the spatial dynamics of the classes, one gains knowledge on the morphodynamics of the beach.

7.3 Results

Before focusing on the three case studies, it is worthwhile to have a look at the volumetric changes of the entire beach. Table 7-3 summarises these volumetric changes, the mean height difference and the total volume of nourished sand for the whole area considered. The latter was divided in five units which are bordered by harbour channels or dams. The reason to divide the coastline in this way is that the channels and harbour dams act as a barrier for the longshore transport. Hence, these units can be considered as entities without (or with a limited) input from the neighbouring units. This facilitates the analysis and interpretation.

The first and westernmost unit is characterised by minor nourishment activities in the form of beach berm replenishment works. The total volume difference on the beach largely exceeded the nourished volume, indicating that this is an accretional beach, bordered by dunes which also grew in the period 2000-2004.

In the second unit, moderate volumes were deposited by means of berm replenishment works between 2000 and the beginning of 2004. In April-June 2004, an important

beach nourishment took place in the centre of Oostende resulting in a net volume difference for this unit of app. + 450 000 m³ (foreshore) and + 125 000 m³ (backshore and foredunes) between 2000 and 2004. The 'emergency' nourishment in Oostende served to increase the safety level in the centre of Oostende; before the nourishment, there was no dry beach anymore at high tide. The sea dike was the only protection to the city.

The third unit features a net loss of sand in the studied time frame: app. 312 000 m³ of sand eroded in 4 years time, despite a total nourished volume of 84 000 m³. However, it should be noted that before the studied period large scale beach nourishments were executed: 3 200 000 m³ in 1992-1996 and 260 000 m in 1998-2000. The erosion in the following years can be interpreted as an adjustment of the beach towards a more natural profile. The foredunes grew with the same rate as in the first two units.

The fourth unit is rather small, but it is a unique unit due to the location at the western side of the harbour dams of Zeebrugge. These dams are more than 4 km long and act as a perfect sand trap (the net longshore sediment transport is from the West to the East), causing the wide accretional beach in Zeebrugge (See the case study "The Middle Coast in Zeebrugge"). The net volume difference between 2000 and 2004 (on foreshore, backshore and foredunes) was + 265 000 m³ without any nourishment carried out in the time lapse considered. Earlier, in 1998-1999, the backshore immediately West of Zeebrugge (at the Duinse Polders) was nourished with 490 000 m³.

The last and most eastward unit is situated between the eastern harbour dam and the Dutch border. Despite some berm replenishment works and a maintenance beach nourishment in 2004, the net volume difference of the foreshore was negative (- 8 300 m³). The foredunes grew, but less fast than in the 4 other units. This unit will also be elaborated in the case studies.

Table 7-3: Mean height difference, volume difference, and total volume of nourished sand for the entire Belgian coastline, divided in five units and with a distinction between the foreshore and the backshore + foredunes. The time window is 2000 till 2004.

	Time window	Foreshore mean height difference (cm)	Foreshore volume difference (m^3)	Backshore and foredunes mean height difference (cm)	Backshore and foredunes volume difference (m^3)	Nourished sand volume (m^3)
1. French border to channel of Nieuwpoort (14.3 km)	2001 - 2000	2.9	119 300	-2.8	-34 400	19 000
	2002 - 2000	6.7	273 200	11.6	143 600	38 000
	2004 - 2000	7.5	301 600	20.1	248 100	76 000
2. Channel of Nieuwpoort to the harbour of Oostende (16.6 km)	2001 - 2000	0.4	13 900	16.5	66 100	70 000
	2002 - 2000	1.5	49 809	26.7	107 200	140 000
	2004 - 2000	13.3	454 200	34.1	124 500	998 000
3. Harbour of Oostende to the harbour of Blankenberge (15.5 km)	2001 - 2000	0.7	23 400	11.2	81 400	21 000
	2002 - 2000	-6.6	-207 900	24.6	178 900	42 000
	2004 - 2000	-10.1	-312 800	32.9	236 600	84 000
4. Harbour of Blankenberge to the harbour of Zeebrugge (5.3 km)	2001 - 2000	0.3	4 800	5.5	18 500	0
	2002 - 2000	5.0	80 800	13.4	45 200	0
	2004 - 2000	13.5	207 500	17.2	57 800	0
5. Harbour of Zeebrugge to the Dutch border (10.1 km)	2001 - 2000	-7.8	-164 700	-2.2	-17 300	0
	2002 - 2000	-16.6	-351 700	1.4	10 700	0
	2004 - 2000	-0.4	-8 300	9.7	75 200	403 000

7.3.1 Case study: The West Coast in Koksijde

Figure 7-1 gives an overview of all thematic GIS layers used to analyse the coastal dynamics in a certain area. Note that the sand transport map (C) is an analysis product of the five base layers. The first striking pattern when looking at the height difference maps in Figure 7-1 are the parallel erosion and accretion areas on the intertidal beach (N° 1). These are caused by the cross-shore displacement of the ridges and runnels, characteristic for these wide dissipative beaches. The net resulting transport over a larger coastal section is close to zero. Note however that these images are snapshots taken at one moment in the year; the location of the ridges and runnels changes continuously, but these intra-year changes are not visible in our yearly observations. In Figure 7-1B, one can see that fine to medium sand is dominant on this intertidal beach. Unfortunately, the hyperspectral acquisition of 2004 was performed close to high tide, leaving only the supratidal beach dry (in Section 7.5 we come back to the operational limitations of this technique). However, the small strip observed in 2004 (Figure 7-1B-2) illustrates the accretion caused by the two groynes at N° 2. In 1987-1988 both groynes were constructed to counter the erosion which was taking place before. The area between and eastward (N° 3) of these groynes is now accretional and grew with 70 600 m³ on the intertidal beach and 60 000 m³ on the supratidal beach. Looking at the sand class map of 2000 (Figure 7-1B-1), one can see that there is coarse and shell-rich sea sand on the dry beach (N° 4) caused by berm replenishment works (in the four years studied, 48 000 m³ was deposited). Hence, the growth of the supratidal beach (N° 2) is a combination of man-made growth and natural accretion caused by the extended groynes. The sand class map suggests also longshore transport of (fractions of) the nourished sand in eastern direction (N° 5). However, one should be careful with this interpretation; the shell-rich sand found around N° 5 could also be the result of the lowering of the beach that occurred after the construction of the groynes. The latter caused a starvation of the supply of sand from the West. This lowering could have been responsible for the formation of a deflation floor on which the rough and coarse sediment fractions were concentrated. Hence, the type of sand in this area can be both the result of an erosion process and an eastward longshore transport of nourished sand. The shell-rich sand found at N° 6 is caused by a local nourishment with sea-sand. A last remarkable feature on this beach is the heavy erosion of the sea-boardering dunes at N° 7. Shortly after the construction of the groynes in Koksijde, the intertidal beach in front of the dunes lowered (see above). The lowering of the intertidal beach caused the dunes to be more exposed to storm surges. The erosion is clearly visible at N° 7. Locally, aeolian deflation adds to the dunefront erosion. The aeolian transport is directed landwards and deposition takes place at the lee-side of the eroded dune (N° 8). More recent surveys seem to indicate the intertidal beach around the groynes is attaining a new equilibrium state, allowing more transport eastward. This will most probably stop the lowering of the intertidal beach in front of N° 8 and the landward retreatment of the foredunes.

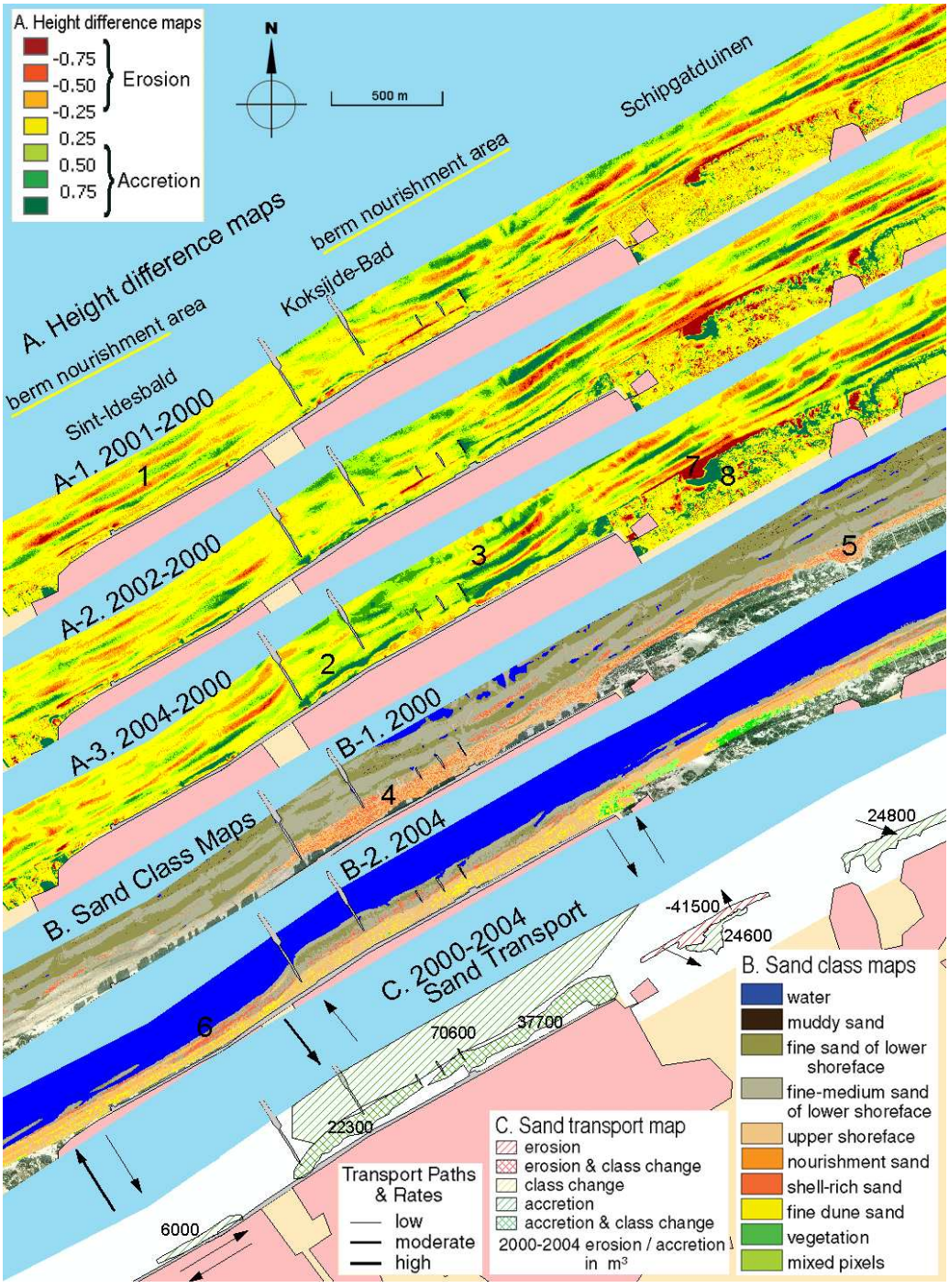

Figure 7-1: Different GIS layers used to analyse the sediment transport around the seaside resort of Koksijde. In top-down order, one can see the three height difference maps with the year 2000 as reference year. Then two classified hyperspectral scenes featuring the sand classes in 2000 and 2004. At the bottom, the resulting sand transport for the period 2000 – 2004 is given; the arrows indicate the direction and amound of the sand transport.

7.3.2 Case study: The Middle Coast in Zeebrugge

The most striking feature in this coastal strip is the large accretional beach at the western side of the harbour dam of Zeebrugge (Figure 7-2, N° 1). The net West-to-East transport resulted in the deposition of app. 265 000 m³ in the four years studied. West of this deposition area, the beach nourishment area of the Duinse Polders stands out (N° 2). The backshore berm created in 1998 - 1999 is clearly distinguishable on the classified hyperspectral scenes due to the type of sand used: it is somewhat coarser-grained and it contains more shells and iron than the sand naturally found on this part of the beach. The fill is eroded during high tide and storm events. The reason for the beach nourishment should be sought in the extension of three groynes in Blankenberge in 1985 – 1986 and 1991. They act as a sand trap in the longshore transport, resulting in accretion between the groynes. However, this beneficial effect led to a reduction in the supply of sand in the area of the Duinse Polders and hence, to a lowering of the foreshore and the backshore.

On the three height difference maps (Figure 7-2A) one can see clearly that the berm is gradually eroded year after year, causing a landward retreat of the seaward border of the nourished berm. Some of the nourishment sand is deposited on the lower parts of the beach (N° 3) and eastward along the high water mark (N° 4). It contributes to the accretion area mentioned above, but the total volume eroded on the intertidal and supratidal beach (app. 108 000 m³ at the nourishment site; see Figure 7-2C) is much lower than the amount deposited eastward, indicating that the deposited volume mainly consisted of natural, non-nourished sand that is supplied through longshore transport processes. This assumption is confirmed by the classified maps, indicating that the deposited sand mainly consisted of fine and medium sand of the intertidal beach. The yellow class found on the highest parts of the beach and in the foredunes (N° 5) is a fine quartz fraction transported and deposited by aeolian processes. The source area of this sand is the nourished berm but also the non-nourished supratidal beach westwards. The small area indicated as nourishment sand at N° 6 is not natural; it is the remnant of a man-made sand castle, built with a mixture of sand and cement.

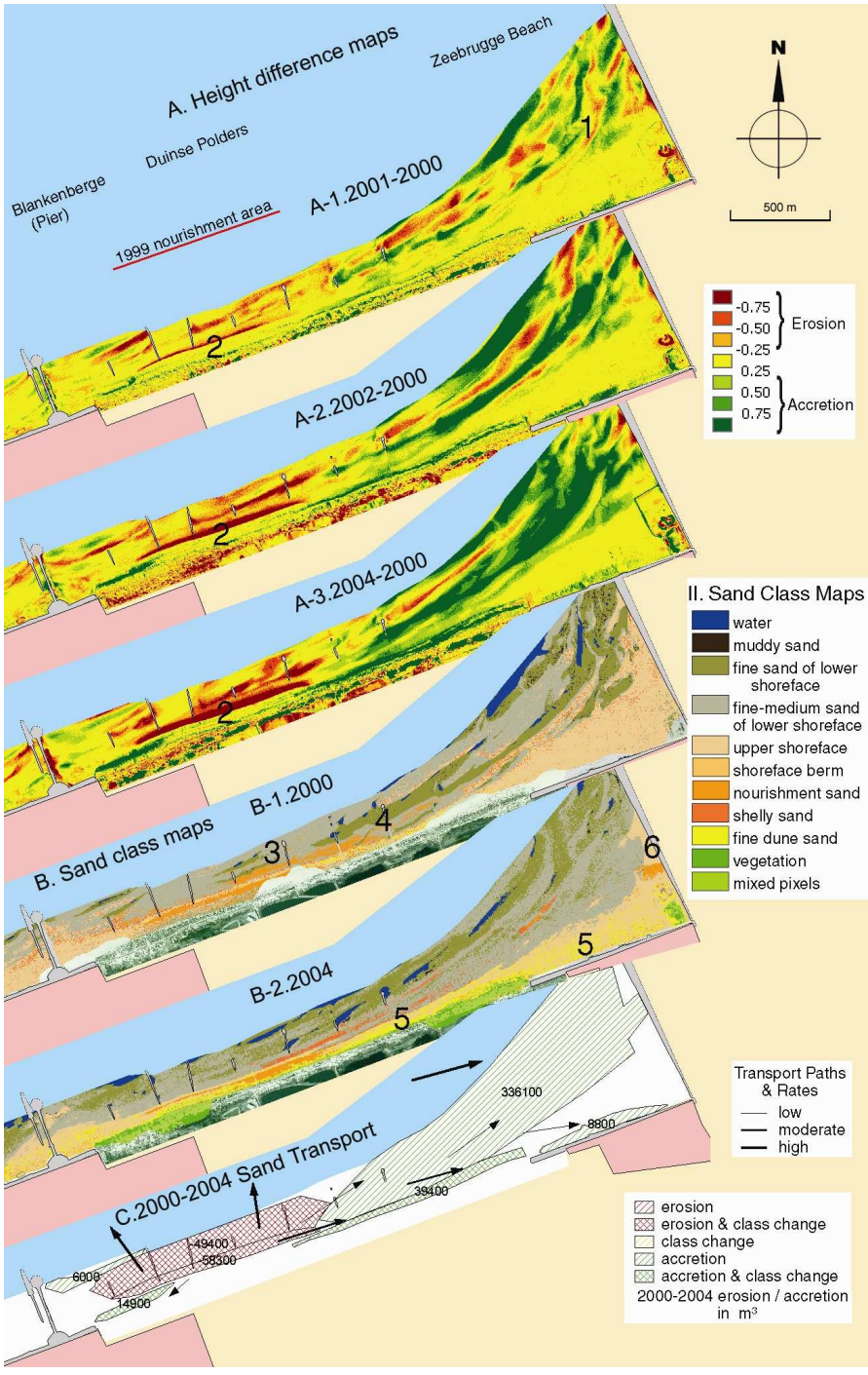

Figure 7-2: Different GIS layers used to analyse the sediment transport between the pier of Blankenberge and the harbour dam of Zeebrugge. In top-down order one can see the three height difference maps with the year 2000 as reference year. Then two classified hyperspectral scenes featuring the sand classes in 2000 and 2004. At the bottom, the resulting sand transport for the period 2000 – 2004 is given; the arrows indicate the direction and amount of the sand transport.

7.3.3 Case study: The East Coast in Knokke-Heist

The third case study concerns the beach in the centre of Knokke-Heist. As mentioned before, this unit has for many decades been prone to heavy erosion, causing it to be the first place along the Belgian coast where large-scale beach nourishments were executed (1978-1980; locally re-nourished in 1986, 1999 and 2004, see Figure 7-3 at the top). The effects of these interventions are clearly visible on the different layers in Figure 7-3: on Figure 7-3B one can see that the supratidal beach largely consisted of nourishment sand. The 1999 fill could spectrally be distinguished because it contains coarse-grained, poorly sorted sand containing a lot of shells, and even some gravel (N° 1). The reflectance is lower and the colour more reddish due to the iron-rich sand used (borrowed from banks offshore). The two first height difference maps (Figure 7-3A-1 and Figure 7-3A-2) show clearly the erosion of the nourished berm at the seaward side (N° 2) as well as the erosion of the lower parts of the intertidal beach (N° 3). A few weeks before the airborne campaigns of 2004 a maintenance nourishment was executed (N° 4 and 5). Once again, the fill was quickly eroded and reworked, i.e., the shells were washed out and temporarily stocked on the intertidal beach (N° 6). This can be explained by the high wave energy in the swash zone, leading to the uptake of coarse sediments and shells in the uprushing water flow. During the backwash there is no wave energy and the heavy shells are deposited (Short, 2001). The muddy sand along the low water level (N° 7) may correspond to a temporary veneer of mud deposited on the lower parts of the beach under quiet meteorological conditions (the offshore part of these beach sections is largely muddy). In the fore dunes, the class with fine dune sand is widespread (N° 8); it is deposited between the vegetation and the artificial fences on the foredunes.

Figure 7-3C, indicating the net sand transport, is rather difficult to interpret due to the extra nourishment between the two last acquisitions. However, it can be concluded that despite the recent nourishment, the intertidal and to a lesser extent also the supratidal beach are largely erosive. At N° 9, where the nourished volume was smaller and limited to a small strip (20 m wide), the net erosive character of the intertidal beach becomes clear, despite a net growth of the supratidal beach and the foredunes. The eroded sand is, after temporary stock of certain fractions on the intertidal beach, mainly transported nearshore, although also longshore transport to the East occurred. The latter is confirmed by Figure 7-3B-3 where nourished sand was found all along the high water mark eastwards of the nourished areas (N° 10); westwards almost no influence of the nourishment could be observed (N° 11).

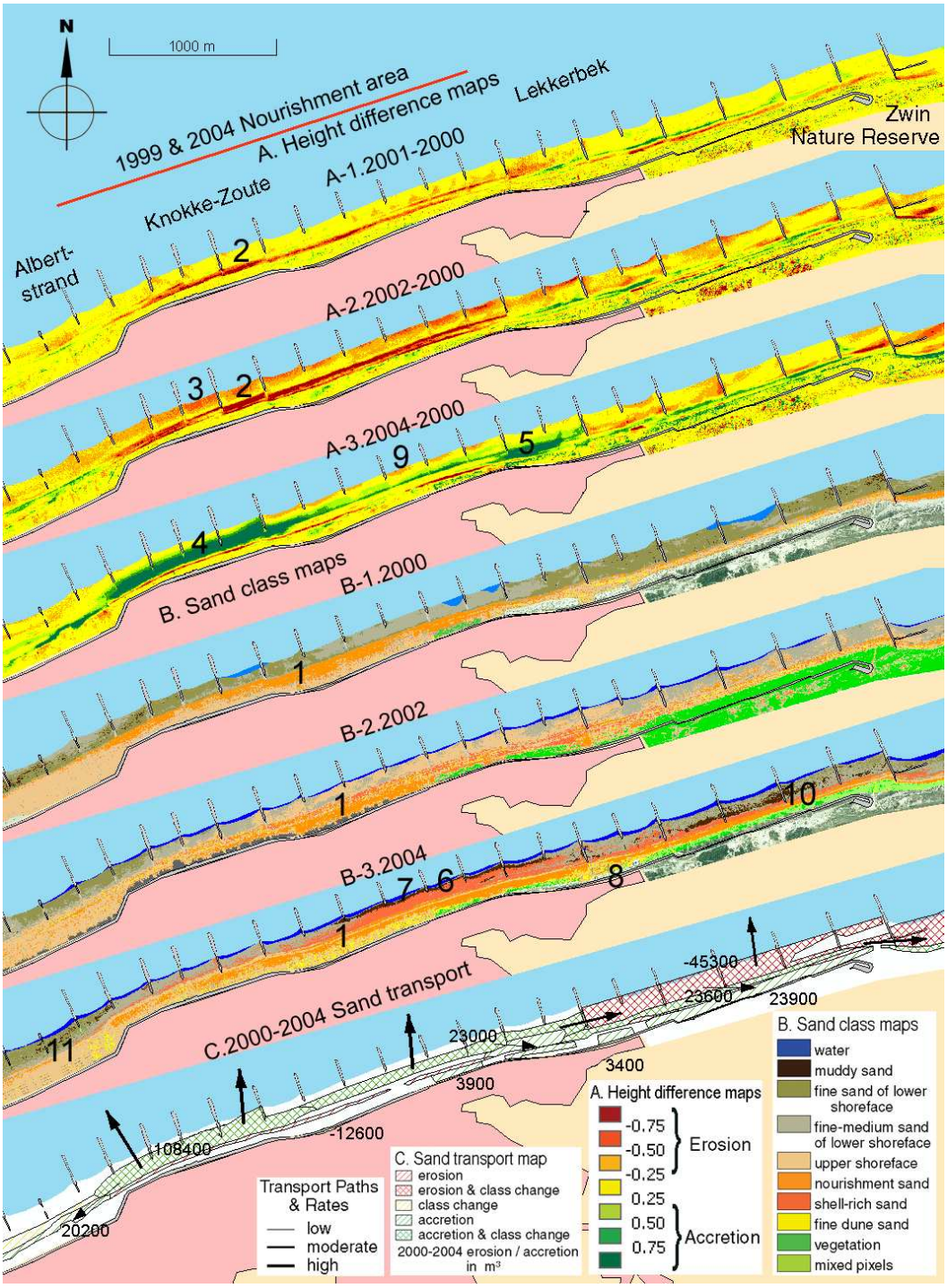

Figure 7-3: Different GIS layers used to analyse the sediment transport in the city of Knokke-Heist. In top-down order one can see the three height difference maps with the year 2000 as reference year. Then three classified hyperspectral scenes featuring the sand classes in 2000, 2002 and 2004. At the bottom, the resulting sand transport for the period 2000 – 2004 is given; the arrows indicate the direction and amount of the sand transport.

7.4 Discussion

The case studies presented above do not only demonstrate the capabilities of airborne hyperspectral remote sensing and LIDAR to map and monitor the transport of beach sediments, they also illustrate the response of a sandy beach to different protection measures. At the Belgian coast, three types of measures are currently in use: (beach) groyne fields, beach nourishments, and berm replenishments. In Koksijde, long groynes were combined with berm replenishments, the area of the Duinse Polders was subject to a backshore and dune front nourishment, whereas in Knokke-Heist the shoreline is protected by a groyne field. However, the latter did not keep the beach from eroding and subsequently, several large-scale beach nourishments, covering both the backshore and the foreshore, were carried out in Knokke-Heist. In the last two decades, preference is given to soft defence structures like beach nourishments and berm replenishments rather than hard structures like groynes. The main reason for this choice is that soft defence structures (i.e., adding sand to the system) have a smaller impact on the natural dynamics of the beach and provide a better barrier in case of heavy storms (Dean, 2002). Since dredging of harbour channels is a regular necessity, deposition of the dredged material on the beach (supplemented as needed by other deep water sources) has been seen by many as a win-win solution. However, though beach nourishments are generally considered as an environment-friendly and efficient option for coastal protection and beach restoration, it should be noted that this technique may have ecological impacts both in the short and the longer term (Speybroeck *et al*., 2006, for a review).

The second and third case studies showed varying degrees of beach nourishment efficiency. Clearly, the Duinse Polders backshore and dunefront nourishment has a larger retention period and it is inferred that the losses to the nearshore are probably intercepted at the nearby Zeebrugge harbour dam which is located downdrift with respect to the Duinse Polders site. The retention period of the 1999 and 2004 nourishment in Knokke-Zoute is in comparison much less, about 5 years. Between both nourishments, app. 55% of the 1999-fill was transported longshore and appeared to add to the, mostly downdrift, backshore and dunefront area. This conclusion can be drawn with the help of the classified hyperspectral data which indicate the presence of nourishment sand in this area. The option that this sand volume is still a remnant of the nourishments in 1978-1980 is not retained as it was observed (e.g., at the Duinse Polders) that a nourishment fill is subject to resorting, especially on the foreshore; hence, the 20-year old fill would not classify anymore as nourishment sand. The remainder of the losses were transported to the foreshore and further down to the nearshore, from where they were removed out of the area, as the foreshore and the neighbouring nearshore also continue to erode.

As hard structures perpendicular to the coastline, groynes act as a trap for the longshore transport and stimulate the sedimentation between them. The drawback of the latter is

that they seriously impede dynamic beach behaviour and that by intercepting sand from the longshore transport, they cause erosion downdrift. Hence, the beneficial effect between the groynes is often accompanied by a negative side effect a few kilometres further. The negative influence continues as long as a new equilibrium state between and around the new or extended groynes is not attained. A good example of the theory above was observed in Koksijde-Bad where the beach in front of the Schipgatduinen lowered due to the construction of two groynes in 1987-1988. The same process was the cause of the beach erosion at the Duinse Polders in the 1990s.

The main added value of the hyperspectral data is the ability to analyse the direction of the sediment transport. Although sediment volumes are subject to resorting processes, which sometimes hampers the analysis as this influences the classification results, the classified hyperspectral scenes offer insight in the directions of the sediment transport.

LIDAR, or topographical data in general, offer only local height information.

7.5 Considerations regarding future monitoring strategies

Although hyperspectral remote sensing is a very powerful technique on itself, its added value is best manifested when combined with other remote sensing data, in this case laserscan data. Despite the obvious potential of data fusion techniques, this methodology is still novel. Most remote sensing based research is based on one single type of data. An important reason for this is the logistical and financial aspect. Both hyperspectral and LIDAR data are today only available from airborne platforms. The CHRIS instrument on board the PROBA satellite and the Hyperion sensor on EO-1 offer spaceborne hyperspectral data, but the radiometric quality and the spatial resolution is much lower than the specifications we are used to when working with airborne data. Moreover, their fixed orbit is not compatible with observations bounded by meteorological and tidal constraints. Therefore, expensive airborne acquisitions are the only option left today. This is probably the main reason why the technique illustrated above is not widespread yet.

Currently, new platforms and sensors are being built; by 2009-2010 a new generation of hyperspectral satellite sensors should become operational. They will have an increased radiometric performance, but will still be limited from an operational point of view. To overcome this, entirely new platforms are being developed: Unmanned Aerial Vehicles (UAV) cruising in the stratosphere for several weeks or even months will drastically reduce the cost of airborne campaigns without losing the operational flexibility characteristic of airborne surveys (For more information see http://www.pegasus4europe.com). It is expected that these new platforms, which in a later stage will also be designed to carry active systems like laserscanners, will announce a new era of coastal surveys, allowing an almost continuous and cost-effective monitoring strategy. The latter will allow to study the sediment dynamics on a

much smaller time scale, revealing more insight in the transport processes. Today, the yearly observations only allow for a longer term analysis. The first operational UAV systems are expected in 2008.

7.6 Conclusions

Airborne hyperspectral data were classified in seven sand type classes following a multiple-binary classification approach based on Sequential Floating Forward Search and Linear Discriminant Analysis, while LIDAR data were morphologically filtered to obtain DTMs with a vertical accuracy (mean absolute error) of 5 cm. Subtracting sequential DTMs resulted in height difference maps indicating the erosion and accretion zones. The combined interpretation of both data types allowed analysis of the sediment dynamics along the Belgian shoreline. The technique was demonstrated at three sites: Koksijde, located at the West Coast and characterised by wide accretional beaches, bordered in the South-East by a high active dune barrier. Much of the accretion was triggered by the extension of two groynes and was supplemented by berm replenishment works. In Zeebrugge, at the Middle Coast, a beach nourishment was executed one year before the data acquisitions started. The hyperspectral data allowed to distinguish the nourished berm and to detect how the fill was eroded and how the nourished sand was redistributed. East of the nourished area, the dam of the harbour of Zeebrugge halts the longshore transport causing a wide accretional beach. The third site, Knokke-Heist, is situated at the East Coast and is characterised by narrow and rather steep beaches, heavily influenced by nourishment activities. The three sites allowed demonstrating the potential of the joint use of airborne hyperspectral data and LIDAR data. While LIDAR data only offer topographical information, hyperspectral data and especially the combination of both, allow for an analysis of the sediment transport directions. Despite the huge potential of the techniques demonstrated, the high cost of the data acquisition is today a major drawback. New unmanned platforms will hopefully reduce the cost of this type of acquisitions, heralding a new era in remote sensing based coastal studies.

Chapter 8

Analysis of the sediment transport along the Belgian shoreline in the period 2000 – 2006

8.1 Introduction to the methodology

Before analysing in detail the sediment transport in the period 2000 – 2006, it is worthwhile to mention the general transport processes acting along our sandy shoreline. They can briefly be divided as follows:

- Cross-shore processes: in general, it is considered that on dissipative beaches, the net cross-shore transport is directed offshore due to bed return currents (Short, 2001). However, along the Belgian shoreline it is observed that the net cross-shore transport is directed onshore under calm weather conditions and seaward in case of stormy weather.

- Longshore processes: these processes act along the shoreline and are mainly driven by (tide-induced) currents. They play an important role in coastal erosion as they transport the sediment which was eroded due to cross-shore processes downdrift. Calculated over the entire Belgian coast and in the long-term (more than one year), the net longshore transport is directed eastward, to The Netherlands. However, locally and temporarily, the longshore transport can be in the opposite direction. The groynes along our coastline are constructed to prevent serious beach erosion by the longshore transport.

- Aeolian processes: in addition to the processes linked to waves and currents (which may be at least partly generated by wind action), the beach and dunes may be shaped or modified by the wind. The sandy sediment on the Belgian

beach is transported via the process of saltation[10] (van der Wal, 1998; van der Wal, 2000a; van der Wal, 2000b).

Note that this division is a theoretical one, used to simplify the complex transport mechanisms acting on the beach and in the surf zone. In reality, these processes act as one complex process and it is the combination of these processes which is responsible for the shape and dynamics of our shoreline.

Via both airborne remote sensing techniques (hyperspectral remote sensing and LIDAR) we try to gain more insight in the dynamics of the Belgian shoreline. While LIDAR is a well-known technique to calculate the amount of sand eroded or deposited, the hyperspectral data are used to classify the beach in several sand types which we prefer to call sand facies types. The definition of these classes is based on two criteria:

- they should be spectrally distinguishable;

- they have to be representative for a certain geomorphological or landscape area on the beach. I.e., as the class changes from one class to another, this has to represent a certain geomorphological change of the beach. For example, a change from 'beach nourishment sand' towards 'original sand from the supratidal beach', in combination with a lowering of the surface, is often indicative for the erosion of the nourished fill till the level of the underlying sand volume. It shows that the positive sediment budget, caused by the nourishment, has been eliminated. Without the classified hyperspectral data, it would not be possible to interpret the volumetric changes. However, certain classes are closely linked to each other, e.g., the classes 'fine sand from the intertidal beach' and 'fine-medium sand from the intertidal beach' both occur typically on the intertidal beach where the first class is mainly found close to the low water mark or in the runnels parallel to the coastline and the second class on the higher parts of the intertidal beach. A change between these two classes represents minor and often temporarily changes on the intertidal beach which are not indicative for geomorphological changes in the longer term.

Probably the most important application of the methodology developed and applied is the follow-up of nourished areas (see further in this chapter).

It is important to realise that the methodology adopted in this chapter represents a powerful technique which allows the researcher to make assumptions on the amount and the directions of the sediment transport, but, the analysis can not be performed without detailed field knowledge and understanding of the prevailing processes and their possible effects on the classification results.

[10] Saltation is the primary process of sand movement. As wind moves over a sand deposit, it is able to pick up grains from the surface and give them a forward momentum, but the weight of the sand grains soon brings the grains back to the surface. The bouncing grains can move downwind at about half the speed of the wind (Bagnold, 1941).

The analysis is limited to the beach between the low water mark and the foredunes. However, these are not the natural boundaries of the system studied. In reality, sediment transport takes place in the whole continuum dunes – backshore – foreshore – nearshore (and even further offshore). Due to technical limitations of the airborne remote sensing techniques used[11], the analysis is limited to the dunefoot – backshore – foreshore area. The open boundaries explain why sometimes assumptions had to be made.

As only longer term data were available, no detailed analysis has been performed on the weather and hydrometeorological conditions that occurred between the surveys. Most remarkable fact for the longer term morphological behaviour of the beach is no doubt the absence of major storms, especially NW-storms, in the period under study.

8.2 Information on the maps produced

In Chapter 7, the capabilities of the methodology described above were demonstrated, focusing on three selected sites: Koksijde, the Duinse Polders (situated between the Pier of Blankenberge and the harbour dam of Zeebrugge) and the beach of Knokke-Heist, East of the Albertstrand. In this chapter, the methodology is applied to the entire shoreline; each section between the French and the Dutch border is systematically analysed. In Chapter 7, the analysis was limited to the time window 2000 – 2004; however, recently the DTM of 2006 (April 18) could be added. Although there was no hyperspectral recording in 2006, we chose to include the DTM of 2006 in the analysis since this allows for a trend analysis in the longer term. Nevertheless, the main focus remains on the period 2000 – 2004.

[11] Airborne hyperspectral remote sensing can not be applied to measure the reflectance of the nearshore, unless the water is very clear (which is not the case along the Belgian shoreline).

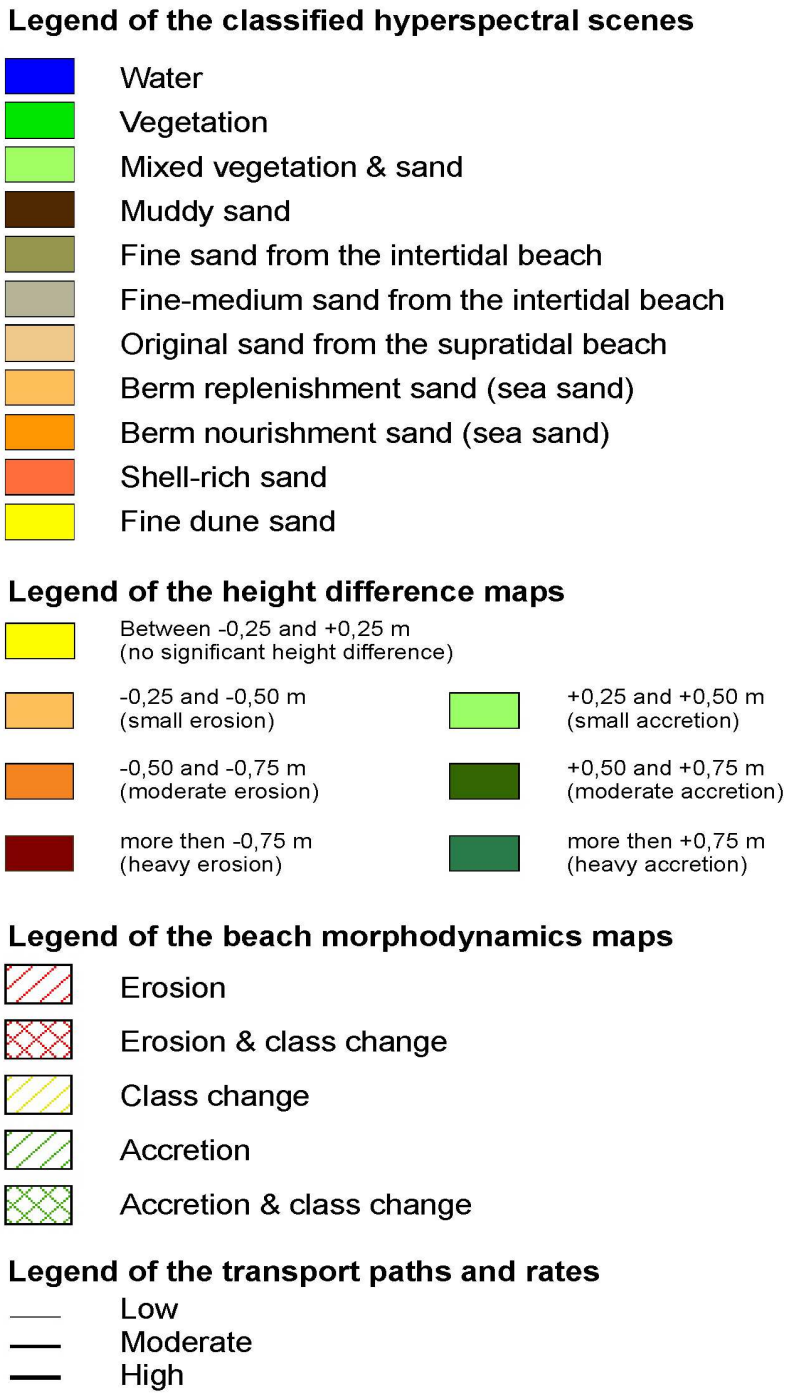

Figure 8-1: Legends of the classified hyperspectral images, of the height difference maps, of the beach morphodynamics maps and of the transport paths and rates.

For each coastal unit the following steps are walked through:

- Firstly, an overview is given of the man-made structures in the section under study (yellow = berm replenishment with sea sand, green = berm replenishment with sand from the foreshore, red = beach nourishment with sea sand). This is a prerequisite to understand any further analysis.

- Secondly, a general analysis is made of the volumetric changes per coastal section, i.e., spatial blocks covering the beach and the foredunes. A distinction is made between the beach and the foredunes as they often show a different dynamic behaviour.

- Thirdly, a detailed analysis is made, focusing on certain areas (polygons) on the beach or in the foredunes which feature remarkable changes. This analysis is not only based on the volumetric changes or the height difference maps, but also on the classified hyperspectral scenes. For the height difference maps and the classified hyperspectral images, the legends as shown in Figure 8-1 are used.

The polygons are manually digitised and labelled according to the following procedure: a polygon is drawn around each area with major volumetric change. A change is considered as 'major' when the absolute height difference is more than 25 cm. This limit is based on the errors inherent to LIDAR observations: on flat, hard surfaces, like the beach, a mean absolute error of 5 cm was attained during each of the four airborne acquisitions (See Chapter 4 and Chapter 7). As the height difference maps are calculated from two DTMs, the mean accuracy increases by a factor $\sqrt{2}$ and one should take possible errors of up to 10 cm (or locally even more) into account. Therefore, and in order to avoid erroneous interpretations, a threshold of 25 cm for major height changes was used in the maps. The volumetric accuracy furthermore depends on the position accuracy of the order of 2 m, which in the present application, where hectare-sized areas are considered, is negligible. The mean absolute error in sand volume differences is $\sqrt{2} \times 100 \times 100 \times 0.05$ m = 707 m³ per hectare. Therefore, volume differences are often rounded to multiples of 100 m³, as more precise figures are meaningless. The change can be either positive (i.e., accretion), negative (i.e., erosion), or neutral (i.e., between -0.25 m and + 0.25 m). Secondly, it was analysed whether the class changed between both acquisitions or whether it remained the same. Hence, there are two possibilities: 'class change' or 'no class change'. Finally, 5 types of polygons were drawn (Figure 8-1). In this third part, the reader always finds two maps:

- On top: a situation map indicating the place names, the position and official number of the coastal sections, as well as the position and numbering of the polygons in which a change in class or height was measured (numbers between 100 and 199 for the coastal strip between the French border and the harbour of Nieuwpoort, numbers between 200 and 299 for the coastal strip between the harbour of Nieuwpoort and the harbour of Oostende, numbers between 300 and 399 for the coastal strip between the

French border and the rotunda of Wenduine, and numbers between 400 and 499 for the coastal strip between the rotunda of Wenduine and the Dutch border.

- Below: a map indicating the type of change in each polygon (cf. Figure 8-1), the volumetric changes in each polygon between 2000 and 2004, and arrows indicating the main sediment transport directions. These arrows are the result of the interpretation of the integrated sediment transport. They were derived from the DTMs, the height difference maps and the successive classified hyperspectral data. In the latter, possible source to destination class changes are important to take into account. However, knowledge on the sediment transport processes acting (Short, 1999) and on the human interventions executed, as well as local field expertise remains necessary to make this interpretation. As a process of interpretation is necessarily individual, different operators might arrive at different conclusions. However, the temporal and spatial data density is more than sufficient to allow overall robust conclusions on the beach morphodynamics within the scope set at the start of this work.

Three dedicated terms are used to indicate certain parts of the coastline:

- A coastal unit: is a large area, often bordered by a harbour dam or another structure that acts as a barrier in the longshore transport. There are five units defined in this study:

  French border – Nieuwpoort
  Nieuwpoort – Oostende
  Oostende – Blankenberge
  Blankenberge – Zeebrugge
  Zeebrugge – Zwin channel

- A coastal zone: is a part of the beach (i.e., foreshore and backshore) or a part of the foredunes, mostly a few hundred meters to a few kilometers long

- A coastal section: is an official term used to indicate a small coastal area of a few hundred meters long (on average 250 m). It comprises the foreshore, the backshore and the foredunes. The Belgian coast has been divided in 280 sections, often coinciding with the area between two groynes. The coordinates of the sections are fixed and defined by the Coastal Division of the Agency for Maritime and Coastal Services (Flemish Government).

All maps are oriented northwards, unless otherwise indicated.

8.3 Analysis per coastal unit

8.3.1 French border – Nieuwpoort

Note: the morphodynamic evolution in the coastal area between Sint-Idesbald and the Schipgatduinen is also described in Section 7.3.1.

8.3.1.1 Human interventions

This section features the most natural beach along the Belgian shoreline. There are only a few groynes in Koksijde-Bad and in Nieuwpoort-Bad. The same places are the only ones with a sea dike. Between the seaside resorts one can still find large dune belts; in some of them the continuum sea-beach-dunes is still intact. The wide dissipative beaches have several parallel ridges and runnels. In the West, this section has no real border, it continues into France until the harbour of Dunkerque. In the East, it is bordered by the mouth of the river IJzer along which we find a marina and a fishing-harbour.

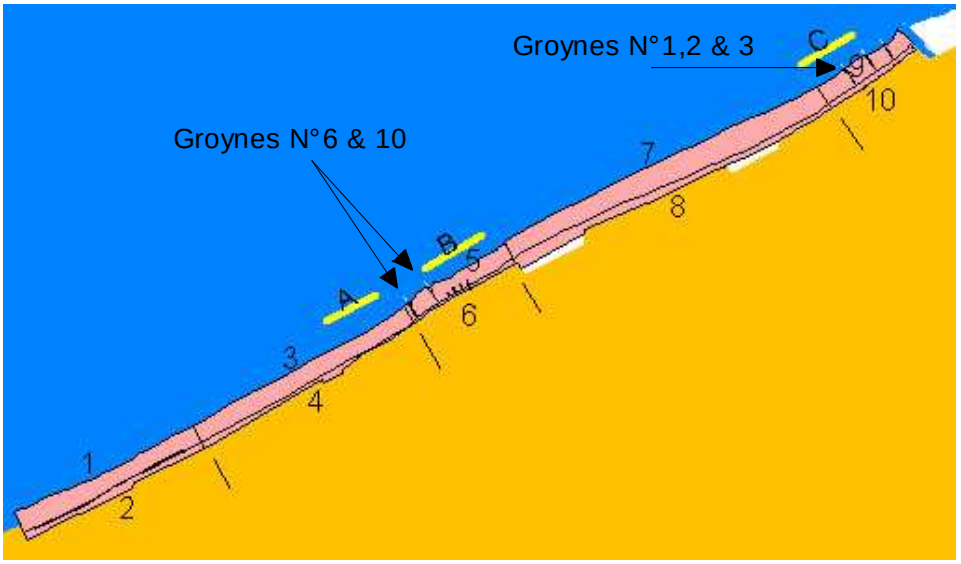

Figure 8-2: Coastal unit between the French border and the IJzer. The numbers (even for the dunes and odd for the beach) are the zones in which the volumetric changes were calculated. The corresponding changes can be found in Table 8-1. The letters (A, B, C) indicate the areas where berm replenishment works were executed.

In 1987 – 1988 groynes N° 6 and 10 in Koksijde-Bad were built to counter the erosion that was taking place before. In Nieuwpoort, groynes N° 1, 2 and 3 were extended for the same reason. In the same areas, berm replenishment works were executed as can be seen on Figure 8-2. Note that the berm replenishment works were mainly executed

with sand borrowed from banks offshore. The larger grain size, the high amount of shells and the presence of reddish iron allow to distinguish this type of sand from the sand naturally found on the beach.

8.3.1.2 General trends

Looking at the whole unit between the French border and Nieuwpoort, the volumetric changes are slightly positive. The natural accretional character of these beaches is in contrast with most of the other beaches along the Belgian shoreline where erosion is the natural trend. However, the amount of accretion is very small, only a few cm between 2000 and 2006, and it is not a continuous process: between 2000 and 2002 there was accretion, followed by a stable situation between 2002 and 2004 and erosion between 2004 and 2006. The beaches in Koksijde-Bad and Groenendijk-Bad were the most accretional while De Panne and Sint-Idesbald featured some erosion. Due to the wide beach, the foredunes grew steadily from Koksijde-Bad till Nieuwpoort. In De Panne and Sint-Idesbald, the growth of the foredunes was less pronounced.

Table 8-1: Volumetric changes and mean height differences for the areas indicated in Figure 8-2

Zone	Beach or foredunes	Zone N°	Year	Surface (ha)	Volume diff. (m^3)	Mean height diff. (cm)
Westhoek	beach	1	2001 - 2000	76.1	8 700	1.1
		1	2002 - 2000	76.1	33 600	4.4
		1	2004 - 2000	74.5	14 000	1.9
		1	2006 - 2000	71.2	-59 800	-8.4
Westhoek	foredunes	2	2001 - 2000	26.1	-40 000	-15.3
		2	2002 - 2000	26.1	1 900	0.7
		2	2004 - 2000	26.1	13 800	5.3
		2	2006 - 2000	10.9	8 500	7.9
De Panne-Centre and Sint-Idesbald	beach	3	2001 - 2000	90.7	-14 500	-1.6
		3	2002 - 2000	90.7	-22 000	-2.4
		3	2004 - 2000	90.6	-20 000	-2.2
		3	2006 - 2000	90.7	-109 400	-12.1
De Panne-Centre and Sint-Idesbald	foredunes	4	2001 - 2000	20.1	-14 500	-7.2
		4	2002 - 2000	20.1	17 800	8.9
		4	2004 - 2000	20.1	30 400	15.2
		4	2006 - 2000	18.5	26 300	14.2
Koksijde-Bad	beach	5	2001 - 2000	41.5	43 700	10.5
		5	2002 - 2000	41.3	70 600	17.1
		5	2004 - 2000	40.3	100 700	25.0
		5	2006 - 2000	41.5	121 100	29.2
Koksijde-Bad	foredunes	6	2001 - 2000	8.5	-6 500	-7.6
		6	2002 - 2000	8.5	19 100	22.4
		6	2004 - 2000	8.5	21 800	25.7
		6	2006 - 2000	8.5	31 000	36.4
Koksijde-East, Oostduinkerke and Groenendijk-Bad	beach	7	2001 - 2000	160.4	68 600	4.3
		7	2002 - 2000	160.4	147 300	9.2
		7	2004 - 2000	156.6	157 500	10.1
		7	2006 - 2000	160.4	121 300	7.6
Koksijde-East, Oostduinkerke and Groenendijk-Bad	foredunes	8	2001 - 2000	57.0	2 000	0.3
		8	2002 - 2000	57.0	69 100	12.1
		8	2004 - 2000	57.0	129 900	22.8
		8	2006 - 2000	33.1	142 600	43.1
Nieuwpoort-Bad	beach	9	2001 - 2000	39.2	12 800	3.3
		9	2002 - 2000	39.2	43 700	11.1
		9	2004 - 2000	38.6	49 400	12.8
		9	2006 - 2000	39.2	22 200	5.7
Nieuwpoort-Bad	foredunes	10	2001 - 2000	11.8	24 600	20.8
		10	2002 - 2000	11.8	35 700	30.2
		10	2004 - 2000	11.8	52 200	44.1
		10	2006 - 2000	11.8	78 900	66.6

Zone	Beach or foredunes	Zone N°	Year	Surface (ha)	Volume diff. (m^3)	Mean height diff. (cm)
French border – Nieuwpoort						
	beach		2001 - 2000	407.9	**119 300**	**2.9**
			2002 - 2000	407.7	**273 200**	**6.7**
			2004 - 2000	400.6	**301 600**	**7.5**
			2006 - 2000	403.0	**95 400**	**2.4**
	foredunes		2001 - 2000	123.6	**-34 400**	**-2.8**
			2002 - 2000	123.5	**143 600**	**11.6**
			2004 - 2000	123.5	**248 100**	**20.1**
			2006 - 2000	82.8	**287 300**	**34.7**

8.3.1.3 Detailed analysis of the morphodynamics

Between the French border and Sint-Idesbald, the morphology of the beach is characterised by parallel ridges and runnels. These structures move alternately seawards and landwards but the net displacement is rather small. At the Westhoek, the net cross-shore transport is landward oriented, while in De Panne and Sint-Idesbald, it is directed seaward.

The small accretional area (N° 104) is not natural; it is the result of yearly berm replenishments. The nourished volume compensates the small natural erosion. The classified map (Figure 8-4) shows clearly that the sand used is sea sand; this coarse, shell-rich sand is found eastward and westward along the high water mark, highlighting the processes of longshore transport.

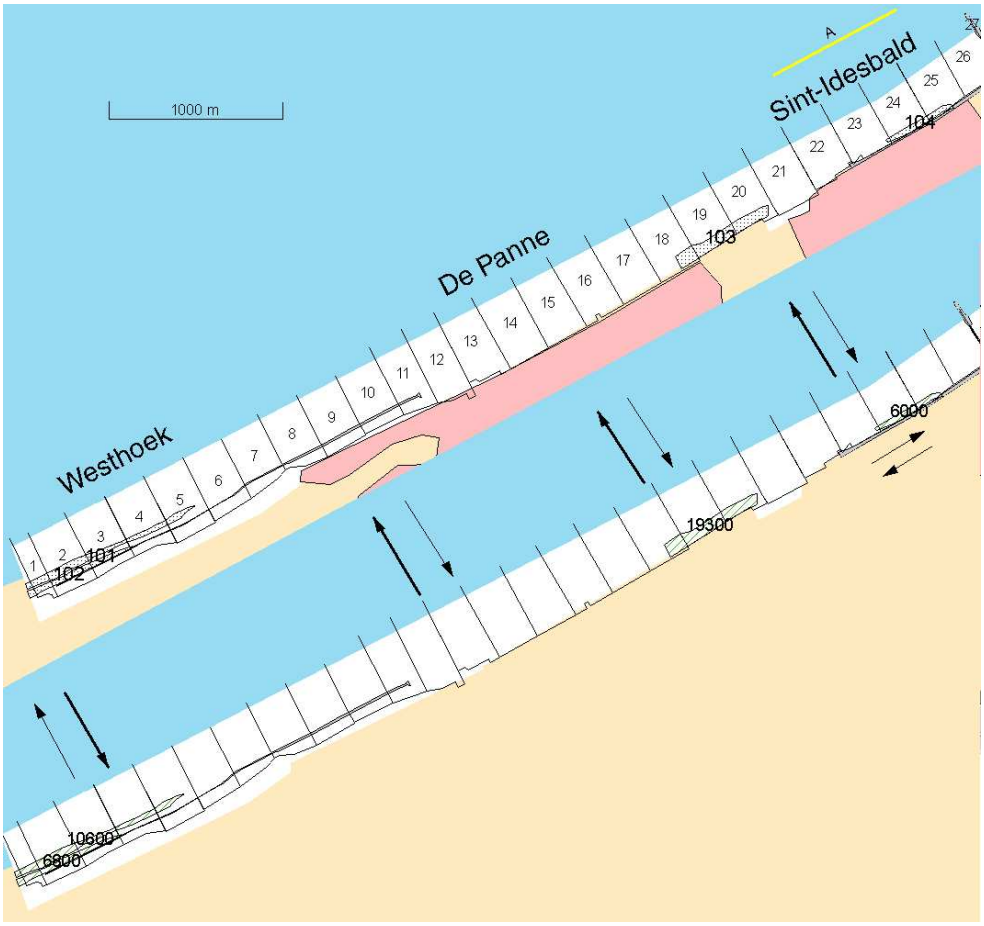

Figure 8-3: Map indicating the major morphodynamic changes between 2000 and 2004. In the upper map one finds the coastal sections with their corresponding number (bordered by lines perpendicular to the coast), the erosion/accretion polygons with their number, and the areas where artificial nourishment activities were executed, indicated with capital letters (yellow = berm replenishment with sea sand). On the lower map, one finds the amount (in m³) of sediment eroded or deposited in each polygon, as well as arrows indicating the direction and amount of the sediment transport. The pink area in the upper map indicates the built-up area.

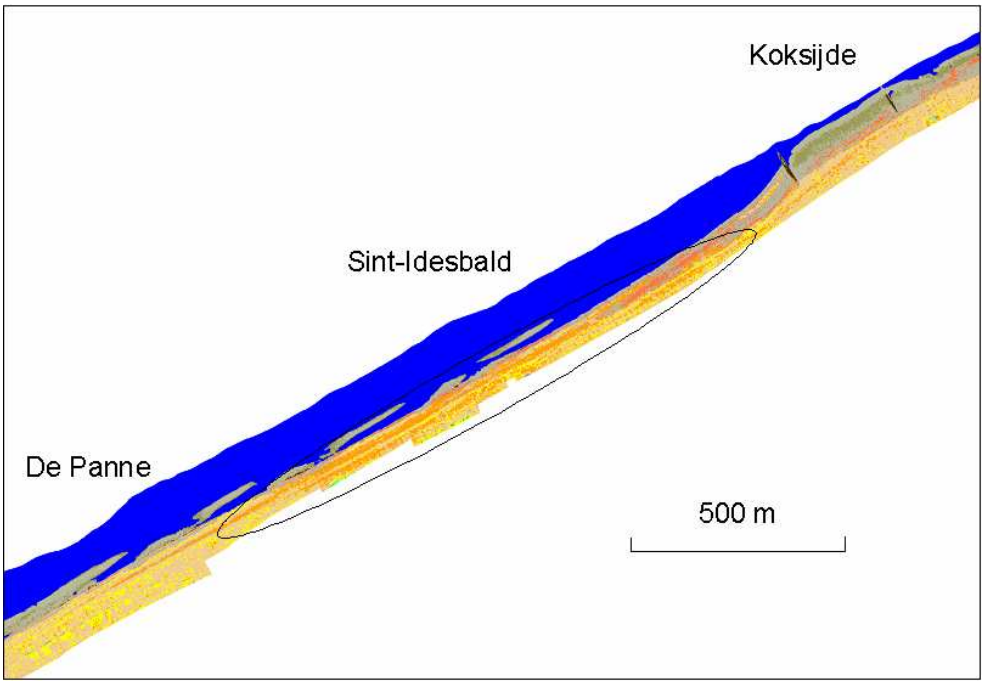

Figure 8-4: Detail of a classified AISA-Eagle image (July 6, 2004) between De Panne and Koksijde, focusing on the berm replenishment area in Sint-Idesbald. In the black polygon sea sand was deposited on the backshore. Via cross-shore and longshore processes the nourishment sand is transported eastward and westward across the foreshore.

In Koksijde-Bad, between and eastward of groynes N° 6 and 10, a clear accretion area stands out (visible as the wide beach in the East of Figure 8-4 and in polygons N° 105-107 in Figure 8-5). The accretion can be attributed to two human interventions: the construction of groynes N° 6 and 10, and the yearly berm replenishments. The volumetric change between 2000 and 2004 (+ 60 000 m³) exceeds the nourished volume (48 000 m³). Before the construction of the groynes, the beach in Koksijde-Bad was erosive; after the construction of the groynes in 1987-1988 accretion took place between the groynes and recently the major accretion takes place eastward of the groynes. This can probably be explained by the equilibrium state which is now attained around the groynes, allowing again longshore transport to the East. Thanks to the accretion, the nourished volumes in area B are not eroded, in contrast with the most nourished berms along the Belgian coast. The erosion of the dune front in area 108 can also be attributed to the extension of the groynes: before the equilibrium state was attained, longshore transport was hampered, causing a lowering of the beach in front of the Schipgatduinen. The erosion lead to the formation of a deflation pavement: small and light particles were eroded faster than the heavier particles (coarse sand and shells). Spectrally, the deflation pavement is very similar to the type of sand used for the nourishment activities. This explains why the classification algorithm classifies the

sand in front of area 108 as nourishment sand, although it could be that there is also a certain apply of nourished sand in this area. On the lee side of the high dune (+/- 21 m TAW) accretion took place (area 109), but the net volumes indicate that there has been erosion and not only a landward displacement of the dune. Probably, the new accretional character of the beach in front of the dune will cease the erosion of the dune foot.

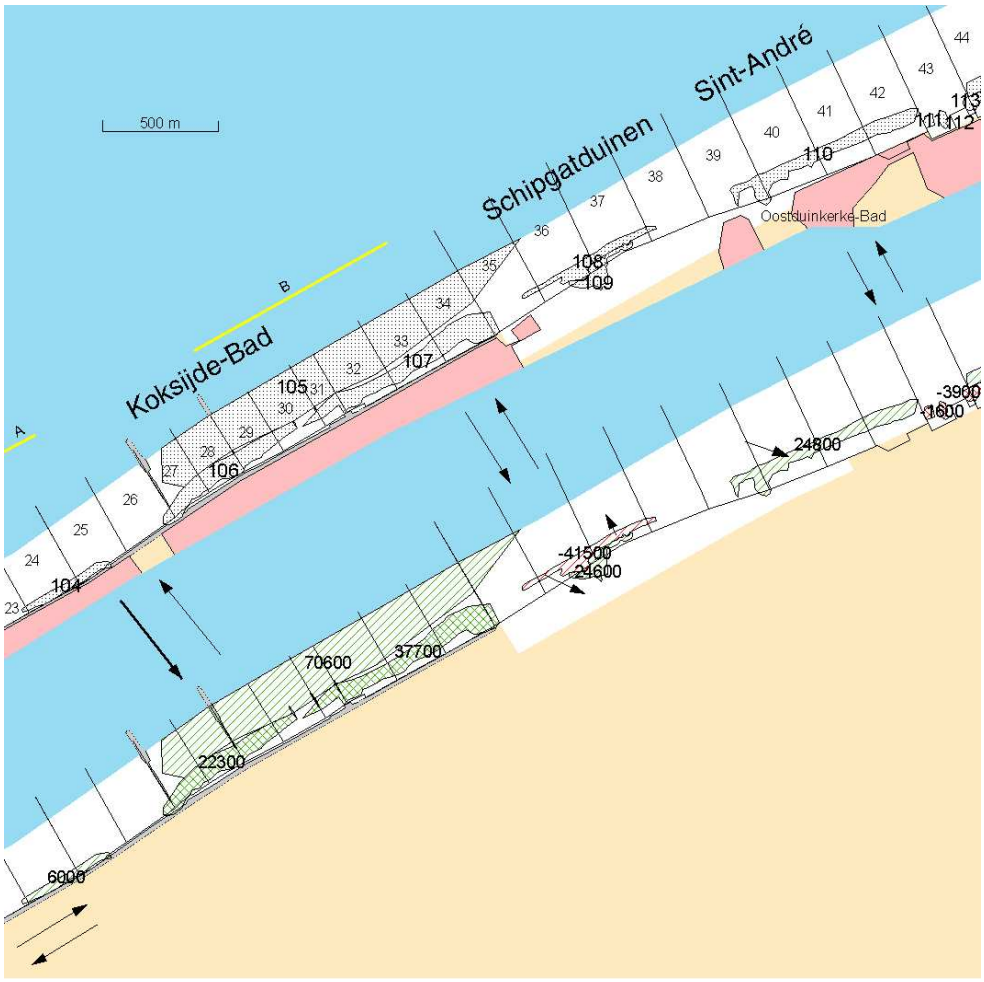

Figure 8-5: Map indicating the major morphodynamic changes between 2000 and 2004. In the upper map one finds the coastal sections with their corresponding number (bordered by lines perpendicular to the coast), the erosion/accretion polygons with their number, and the areas where artificial nourishment activities were executed, indicated with capital letters (yellow = berm replenishment with sea sand). On the lower map, one finds the amount (in m³) of sediment eroded or deposited in each polygon, as well as arrows indicating the direction and amount of the sediment transport. The pink area in the upper map indicates the built-up area.

Between the Schipgatduinen and Sint-André, the foredunes grew steadily (area 110). The same occured eastward between Oostduinkerke and Nieuwpoort (areas 114-117: total volume difference between 2000 and 2004: + 170 100 m³). The local erosive anomaly in areas 111 and 112 is artifical: the growing foredunes are flattened during the spring to keep a sea view from the walking promenade in Oostduinkerke. The growth of the foredunes is possibly due to the wide beach in Oostduinkerke and Groenendijk-Bad. Only in case of heavy storms the dune foot can be eroded, but in the period under study no heavy storms were recorded. In the meantime, the strength of the natural seawall increases. Local berm nourishment in Nieuwpoort-Bad reinforces the accretion of the backshore and the dune foot.

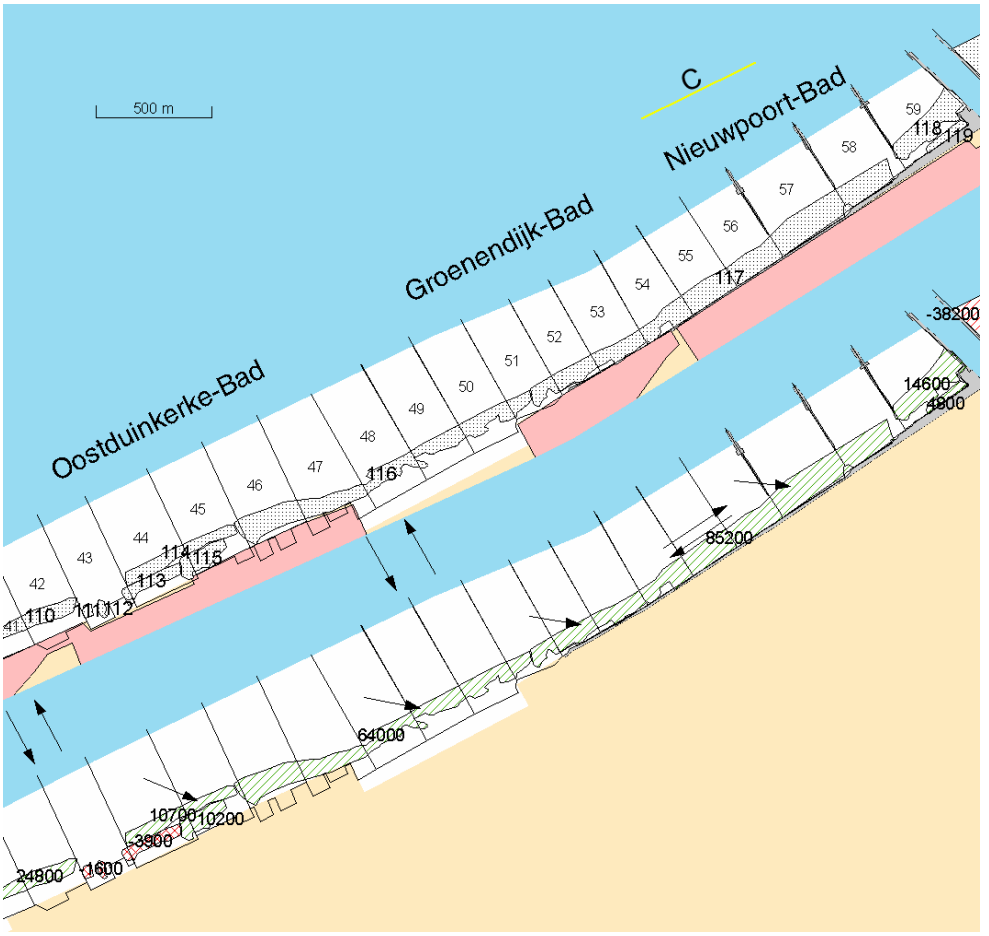

Figure 8-6: Map indicating the major morphodynamic changes between 2000 and 2004. In the upper map one finds the coastal sections with their corresponding number (bordered by lines perpendicular to the coast), the erosion/accretion polygons with their number, and the areas where artificial nourishment activities were executed, indicated with capital letters (yellow = berm replenishment with sea sand). On the lower map, one finds the amount (in m³) of sediment eroded or deposited in

each polygon, as well as arrows indicating the direction and amount of the sediment transport. The pink area in the upper map indicates the built-up area.

8.3.2 Nieuwpoort – Oostende

8.3.2.1 Human interventions

This coastal unit is bounded by two harbour channels, both protected by low dams. In the West, the harbour entry of Nieuwpoort acts as barrier against the longshore transport from the West to the East, while the harbour entry of Oostende acts as a similar barrier against the longshore transport in the opposite sense. This beach is composed of two morphological units; the first small one stretches from the harbour dam of Niewpoort to the first groyne West of Sint-Laureins. There are no groynes in this part; the beach is in a fairly natural state with several parallel ridges and runnels. The only artificial construction is a reinforced dune foot of ca. 780 m long. To protect its eastern end, a berm with sea sand was deposited (see letter D on Figure 8-7). The remaining part of this coastal unit features narrower beaches with many groynes (Figure 8-7). In the places indicated with letters E till J, regular berm replenishments are executed. These works take place in springtime and aim at maintaining a dry beach wide enough for the touristic exploitation during the summer months. Per m in the longshore direction about 5 – 15 m³ sea sand is deposited yearly.

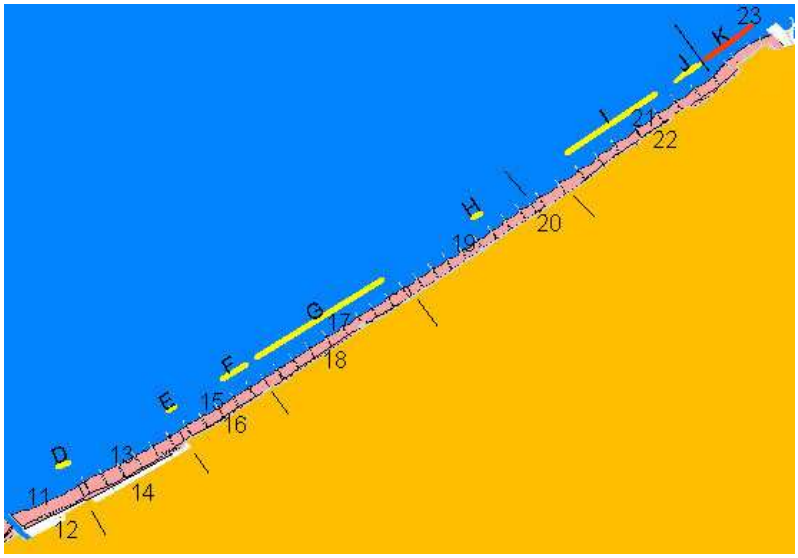

Figure 8-7: Coastal unit between the harbour of Nieuwpoort and the harbour of Oostende. The numbers (even for the dunes and odd for the beach) are the zones in which the volumetric changes were calculated. The corresponding changes can be found in Table 8-2. The letters (D till J) indicate the areas where berm replenishment works were executed. In area K, a beach nourishment was executed.

During the last decades, the centre of Oostende was characterised by the absence of a dry beach at high tide. Even at low tide, the beach became very narrow. As the centre of Oostende is situated several meters below storm high tide, a potentially dangerous situation was created. To counter this, a beach nourishment was executed in April-June 2004 (see letter K on Figure 8-7), just before the airborne acquisition of 2004. In total app. 575 000 m³ of sea sand was deposited on the backshore and foreshore, creating a dry berm at the level of 6 m TAW. The amount deposited was 533 m³ per m in the longshore direction. To protect the newly created berm, an offshore underwater berm was created (see Figure 8-8). The large western part of it consists of sea sand (115 700 m³ was deposited), in the East, in front of the 'Klein Strandje' a second berm was made of gravel (28 800 m³). For the design of the nourishment, the reader is referred to De Wolf *et al.* (2006).

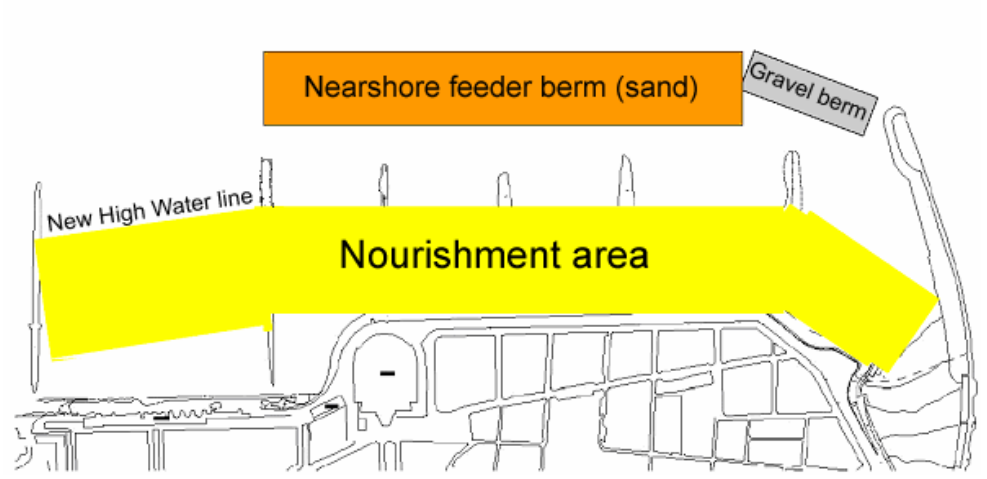

Figure 8-8: Schematic representation of the design of the 'new beach' in Oostende, constructed in April - June 2004 (De Wolf et al., 2006).

8.3.2.2 General trends

The general trends in this coastal unit can be summarised as follows: erosion of the beach at the military basis of Lombardsijde, limited accretion in Sint-Laureins, especially between 2000 and 2004, and erosion between Westende and Oostende; see Table 8-2. The large nourishment in Oostende causes a net positive volumetric change over the period 2000 – 2006, but without the nourishment the net volumetric change, calculated over the entire beach, is negative. The dunes tend to grow in all zones, but especially in Sint Laureins the growth is remarkable.

Table 8-2: Volumetric changes and mean height differences for the areas indicated in Figure 8-7.

Zone	Beach or foredunes	Zone N°	Year	Surface (ha)	Volume diff. (m^3)	Mean height diff. (cm)
Mil. base Lombardsijde	beach	11	2001 - 2000	29.9	11 900	4.0
		11	2002 - 2000	29.9	900	0.0
		11	2004 - 2000	29.8	-30 400	-10.2
		11	2006 - 2000	29.9	-60 700	-20.3
Mil. base Lombardsijde	foredunes	12	2001 - 2000	6.4	17 900	28.1
		12	2002 - 2000	6.4	11 300	17.8
		12	2004 - 2000	6.4	11 600	18.2
		12	2006 - 2000	4.2	9 300	22.0
Sint-Laureins	beach	13	2001 - 2000	53.7	58 000	10.8
		13	2002 - 2000	53.7	49 700	9.2
		13	2004 - 2000	53.6	51 200	9.5
		13	2006 - 2000	53.7	9 400	1.8
Sint-Laureins	foredunes	14	2001 - 2000	10.0	29 800	29.7
		14	2002 - 2000	10.1	41 200	41.0
		14	2004 - 2000	10.1	55 600	55.2
		14	2006 - 2000	9.6	80 200	83.7
Westende-Bad	beach	15	2001 - 2000	38.0	6 300	1.7
		15	2002 - 2000	38.0	4 900	1.3
		15	2004 - 2000	38.0	-2 400	-0.6
		15	2006 - 2000	38.0	-13 800	-3.6
Westende-Bad	foredunes	16	2001 - 2000	5.3	8 800	16.6
		16	2002 - 2000	5.3	13 900	26.3
		16	2004 - 2000	4.1	13 100	31.7
		16	2006 - 2000	5.3	8 000	15.2
Middelkerke-Bad	beach	17	2001 - 2000	59.6	-59 900	-10.1
		17	2002 - 2000	59.6	-21 700	-3.6
		17	2004 - 2000	59.0	-26 700	-4.5
		17	2006 - 2000	59.6	-33 700	-5.7
Middelkerke-Bad	foredunes	18	2001 - 2000	7.9	-300	-0.4
		18	2002 - 2000	7.9	15 900	20.0
		18	2004 - 2000	5.8	24 500	42.4
		18	2006 - 2000	7.9	25 800	32.5
Middelkerke-East - Raversijde	beach	19	2001 - 2000	50.7	-14 400	-2.8
		19	2002 - 2000	50.7	8 900	1.7
		19	2004 - 2000	50.5	1 700	0.3
		19	2006 - 2000	50.7	-25 400	-5.0

Zone	Beach or foredunes	Zone N°	Year	Surface (ha)	Volume diff. (m^3)	Mean height diff. (cm)
Raversijde	foredunes	20	2001 - 2000	0.5	600	14.1
		20	2002 - 2000	0.5	1 700	38.6
		20	2004 - 2000	0.4	1 800	44.6
		20	2006 - 2000	0.5	700	15.7
Mariakerke - Oostende groot strand	beach	21	2001 - 2000	80.6	-10 800	-1.3
		21	2002 - 2000	80.6	1 700	0.2
		21	2004 - 2000	80.5	-3 900	-0.5
		21	2006 - 2000	80.6	67 900	8.4
Mariakerke - Oostende groot strand	foredunes	22	2001 - 2000	10.0	9 300	9.3
		22	2002 - 2000	10.0	23 200	23.2
		22	2004 - 2000	9.8	17 900	18.3
		22	2006 - 2000	10.0	32 000	32.0
Oostende - Centre and klein strandje	beach	23	2001 - 2000	29.9	22 800	7.6
		23	2002 - 2000	29.9	6 300	2.1
		23	2004 - 2000	29.9	464 700	155.7
		23	2006 - 2000	29.9	464 400	155.6
Nieuwpoort – Oostende						
	beach		2001 - 2000	342.3	**13 900**	**0.4**
			2002 - 2000	342.4	**49 809**	**1.5**
			2004 - 2000	341.3	**454 200**	**13.3**
			2006 - 2000	342.3	**408 100**	**11.9**
	foredunes		2001 - 2000	40.1	**66 100**	**16.5**
			2002 - 2000	40.1	**107 200**	**26.7**
			2004 - 2000	36.5	**124 500**	**34.1**
			2006 - 2000	37.5	**156 000**	**41.6**

8.3.2.3 Detailed analysis of the morphodynamics

Figure 8-9 illustrates nicely the general trends described above. eastward of the mouth of the river IJzer the beach is eroded: between 2000 and 2004 38 200 m^3 was eroded (cf. polygon N° 201). In the 90s, this erosion was attributed to the extension of groynes N° 1, 2 and 3 in Nieuwpoort. The extended groynes formed a barrier for the longshore transport; but today a new equilibrium state is attained in Nieuwpoort allowing longshore transport as was formerly the case. Nevertheless, the erosion continues. This leads to the assumption that the longshore transport is hampered by the outflow at the mouth of the IJzer; hence the erosion in Lombardsijde is a natural and continuous process.

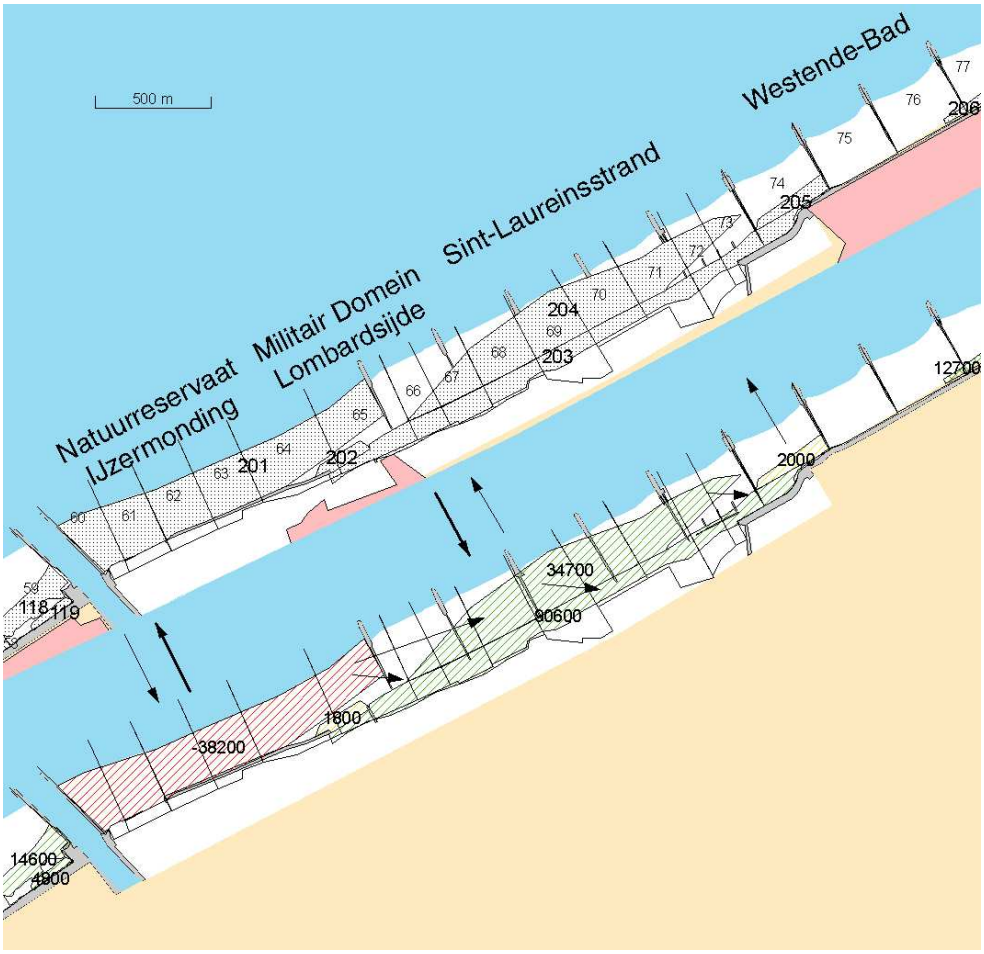

Figure 8-9: Map indicating the major morphodynamic changes between 2000 and 2004. In the upper map one finds the coastal sections with their corresponding number (bordered by lines perpendicular to the coast), the erosion/accretion polygons with their number. On the lower map, one finds the amount (in m³) of sediment eroded or deposited in each polygon, as well as arrows indicating the direction and amount of the sediment transport. The pink area in the upper map indicates the built-up area.

The small polygon N° 202 indicates the erosion of the small nourished volume that serves to protect the eastern end of the reinforced dune foot in Lombardsijde. Yearly, 4 000 m³ of sea sand is deposited here. Although this is a very small nourishment, the fill is clearly visible on the classified hyperspectral data (Figure 8-10).

Between the military base of Lombardsijde and Westende, the beach and the foredunes grew (polygons N° 203 and 204). In the beginning of the 90s, the groynes in this zone were extended. The observed accretion is probably a morphological response to this extension as the groynes act as a barrier in the longshore sediment transport. The

growth of the foredunes can be explained by the widening and the raising of the beach which leads to an efficient protection of the dune foot. The aeolian deposited sand at the dune foot is under normal conditions not eroded. This is a good example of the beneficial effect of the construction or the extension of groynes. Polygon N° 205 respresents a small berm replenishment area, also clearly distinguishable on the hyperspectral data.

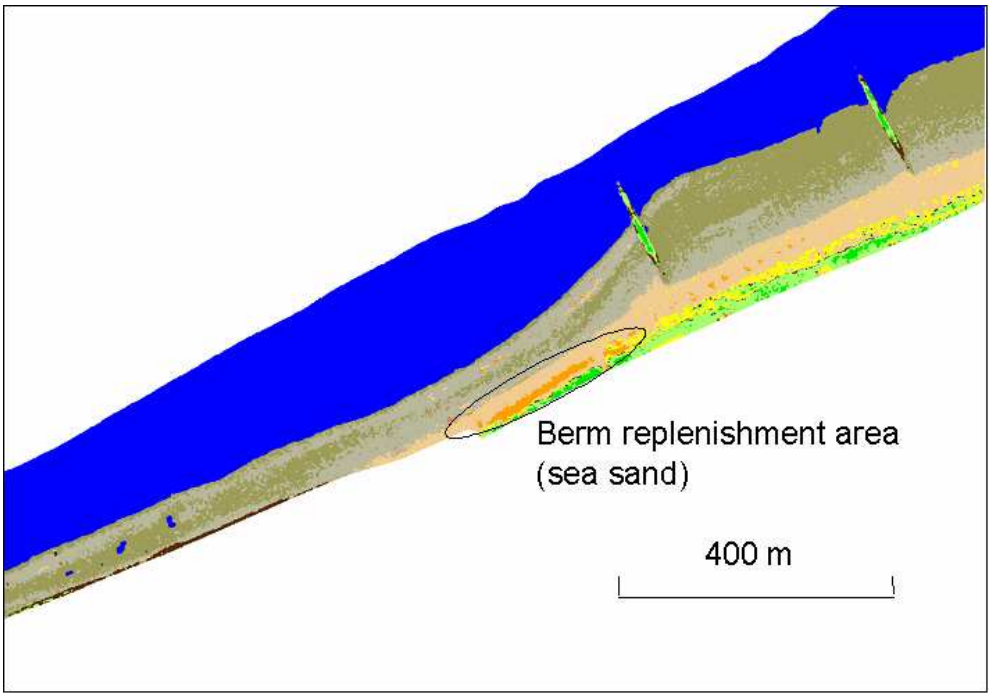

Figure 8-10: Classified AISA-Eagle image (July 6, 2004), focusing on a small berm replenishment area in Lombardsijde. The fill is visible as the orange class.

The beach around Westende-Bad and Middelkerke-Bad is erosive; yearly berm replenishments are executed to maintain a dry beach, but the net erosive character is confirmed by the difference between the nourished volume between 2000 and 2004 (125 000 m³) and the observed volumetric change in the corresponding polygons, N° 206-209 (+ 48 500 m³). The yearly nourishments compensate completely for the erosion. East of Middelkerke-Bad the beach is in a stable state; there is no supply of nourished sand from Middelkerke-Bad, neither erosion.

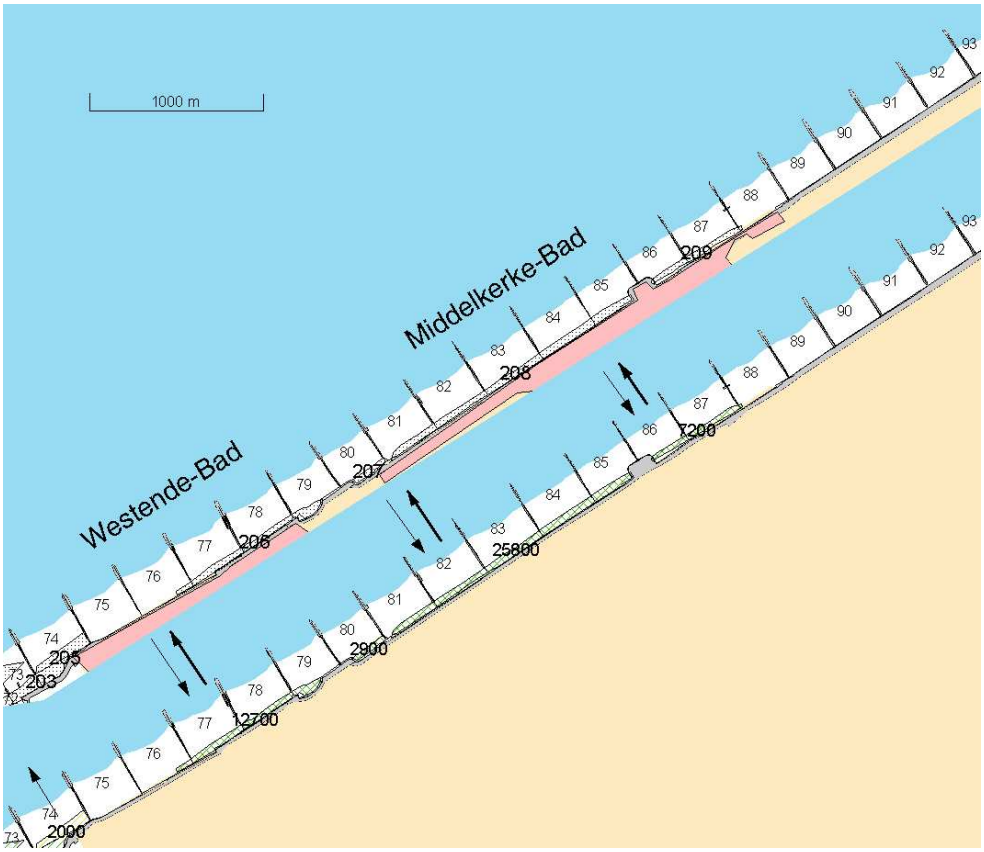

Figure 8-11: Map indicating the major morphodynamic changes between 2000 and 2004. In the upper map one finds the coastal sections with their corresponding number (bordered by lines perpendicular to the coast), the erosion/accretion polygons with their number. On the lower map, one finds the amount (in m³) of sediment eroded or deposited in each polygon, as well as arrows indicating the direction and amount of the sediment transport. The pink area in the upper map indicates the built-up area.

In Raversijde and Mariakerke, the same dynamics as in Middelkerke were observed: the natural trend is gentle erosion, but the latter is completely compensated by the yearly berm replenishments (see letters H and I on Figure 8-12), executed with sea sand. In Raversijde, the total supplied volume between 2000 and 2004 is 12 000 m³, while there was no accretion observed. In Mariakerke, the supplied volume in the same time window was 90 000 m³, resulting in a net accretion of app. 20 000 m³. The nourished areas are again easily detectable on the classified hyperspectral data, due to the coarse, shell-rich sand used for the nourishments.

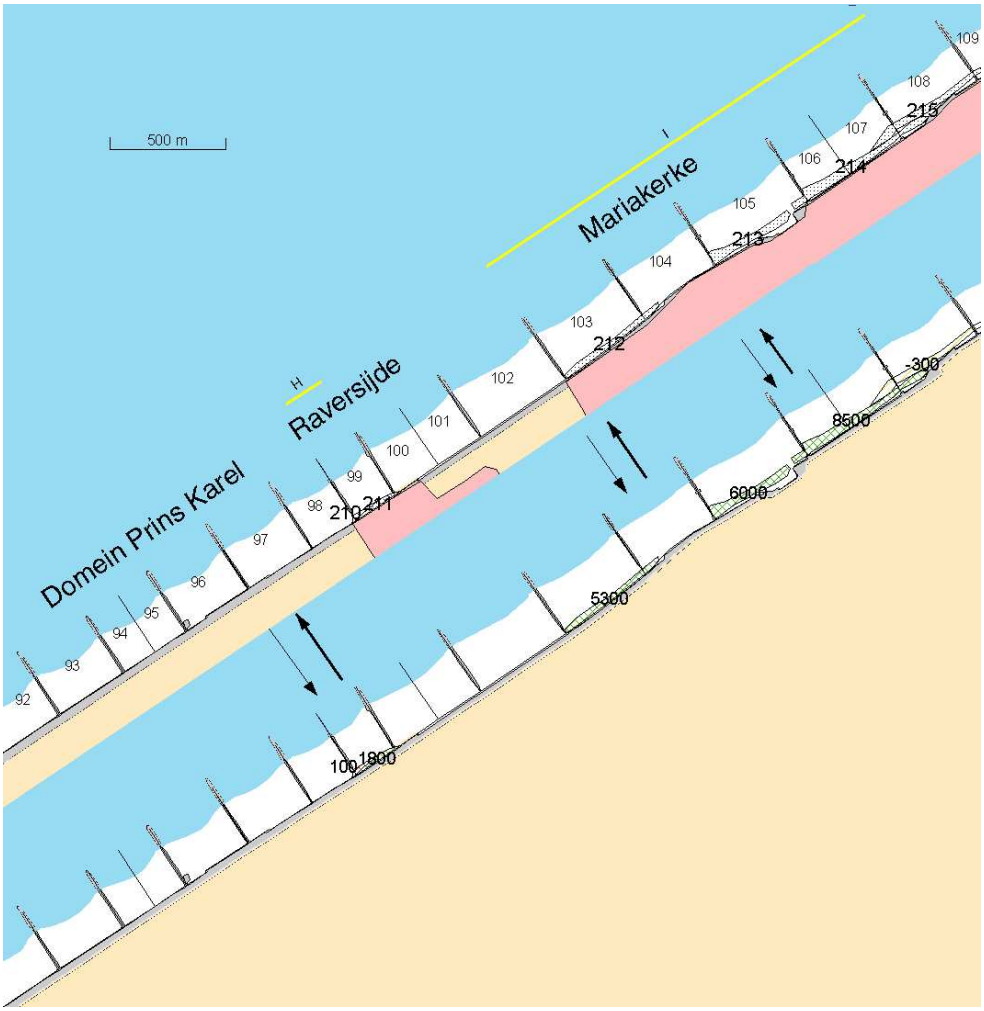

Figure 8-12: Map indicating the major morphodynamic changes between 2000 and 2004. In the upper map one finds the coastal sections with their corresponding number (bordered by lines perpendicular to the coast), the erosion/accretion polygons with their number, and the areas where artificial nourishment activities were executed, indicated with capital letters (yellow = berm replenishment with sea sand). On the lower map, one finds the amount (in m³) of sediment eroded or deposited in each polygon, as well as arrows indicating the direction and amount of the sediment transport. The pink area in the upper map indicates the built-up area.

Figure 8-13: Nourishment sand accumulates on the 'Klein Strandje' from where it is taken to compensate for the erosion at the 'Trappekes' (Photo: February 8, 2007).

Figure 8-14: Deposition of nourishment sand at the 'Trappekes'; the sand was borrowed from the 'Klein Strandje' (Photo: February 8, 2007).

In Oostende, an important beach nourishment took place in April – June 2004, see Section 8.3.2.1. The fill (polygon N° 217 on Figure 8-16) is clearly visible on the classified sand map of 2004 (Figure 8-15). However, though the airborne acquisition in 2004 took place one month after the nourishment, it can be seen that the fill has already been reworked. Instead of a homogeneous distribution of nourished sand, several bands parallel to the shoreline have been formed. On the newly created dry beach, the original nourished sand is still present (A on Figure 8-15), but on the same backshore a small band attributed to the class 'original sand of the supratidal beach' was formed (B). In this area, the shells were washed out and temporarily stocked on the foreshore (C). This process has also been observed in other nourished areas. The beach nourishment sand found on the 'Klein Strandje' indicates eastward transport and accretion on the eastern side of the nourished area (D). This is confirmed by the volume difference map where an accretion of 18 000 m³ was measured in polygon N° 218 between 2000 and 2004 (Figure 8-16). To compensate for the erosion at the letters B and C, and for the accretion at letter D, regular works are executed to redistribute the sand (Figure 8-13 and Figure 8-14).

On the western side, in polygon N° 216, an accretion of 7 400 m³ was measured between 2000 and 2004 but on Figure 8-15 (letter E) it can be seen that this accretion is not supplied with nourishment sand. It is merely fine dune sand which was deposited after aeolian transport. Hence, it can be concluded that there is little or no transport of nourished sand to the West. Most of the fill will be transported offshore and eastward to the 'Klein Strandje'.

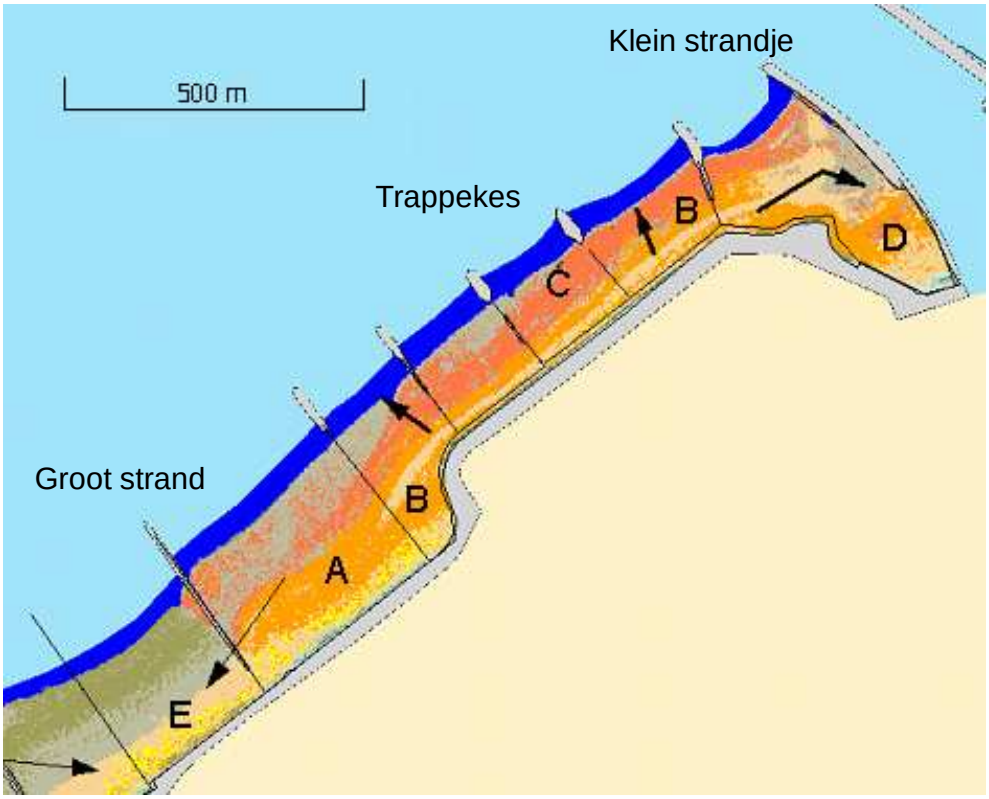

Figure 8-15: Sand class map of July 2004, focusing on the beach nourishment in the centre of Oostende.

The original volume deposited on the supratidal beach was app. 575 000 m³. The accretion measured between 2000 and 2004 was only 452 300 m³. Even if we take into account the loss during the nourishment works (on average 12% according to De Wolf *et al.*, 2006), the measured accretion should be around 506 000 m³. This shows clearly the erosion (app. 54 000 m³) that took place in the first three months after the nourishment. Consequently, we added the height difference map in Figure 8-16 to illustrate the morphological changes in the first two years after the nourishment (2004 – 2006). In the first winter after the nourishment, a storm occurred between 12 – 15 February 2005. The storm altered the artificial profile rapidly; a dry beach berm was formed immediately landwards from the low water mark and a lot of sand supplied in section 116 was transported to section 117, causing the formation of a dry beach berm in this section. The erosion in section 116 was app. 60 000 m³. After the winter of 2004 – 2005, a limited nourishment (159 500 m³) was performed in June 2005 to compensate for the losses. However, this volume is not traceable on the height difference map in Figure 8-16, indicating that the extra nourishment nicely compensated for the losses during the previous winter. The same map shows also accretion on the higher parts of the 'Groot Strand', i.e., on the western side of the

nourishment. As mentioned before, this can largely be attributed to aeolian deposition of sand originating from the West. After the relatively calm winter of 2005 – 2006, no new nourishment was needed in 2006.

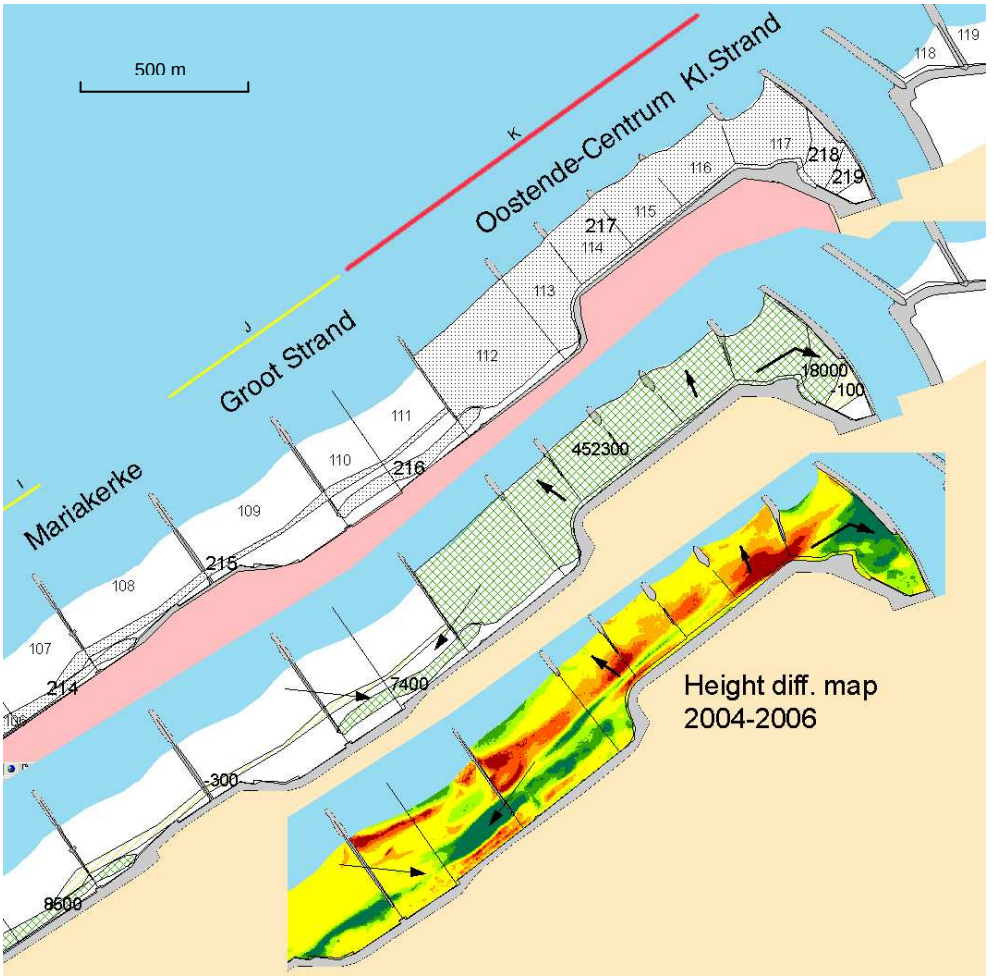

Figure 8-16: Map indicating the major morphodynamic changes between 2000 and 2004. In the upper map one finds the coastal sections with their corresponding number (bordered by lines perpendicular to the coast), the erosion/accretion polygons with their number, and the areas where artificial nourishment activities were executed, indicated with capital letters (yellow = berm replenishment with sea sand, red = beach nourishment with sea sand). On the middle map, one finds the amount (in m³) of sediment eroded or deposited in each polygon, as well as arrows indicating the direction and amount of the sediment transport. The lower map is the height difference map between 2004 and 2006. The pink area in the upper map indicates the built-up area.

8.3.3 Oostende – Blankenberge

8.3.3.1 Human interventions

This coastal unit is bounded by two harbour channels; in the West the harbour channel of Oostende and in the East the harbour channel of Blankenberge. Thanks to these structures the sand transport in this unit can be studied assuming little or no influence from the neighbouring beaches. At the rotunda of Wenduine, the Belgian coast forms a weak turn; the orientation of the coastline changes from 35° West of the rotunda to 30° East of it. Although this can be considered as a rather minor change in orientation, an influence on the sediment transport has been observed. The nourished sand found on the backshore West of the rotunda was not detected eastward of the rotunda (see Section 8.3.3.3), what could be expected in case of a straight coastline. On the foreshore and the nearshore there is probably more transport around the rotunda.

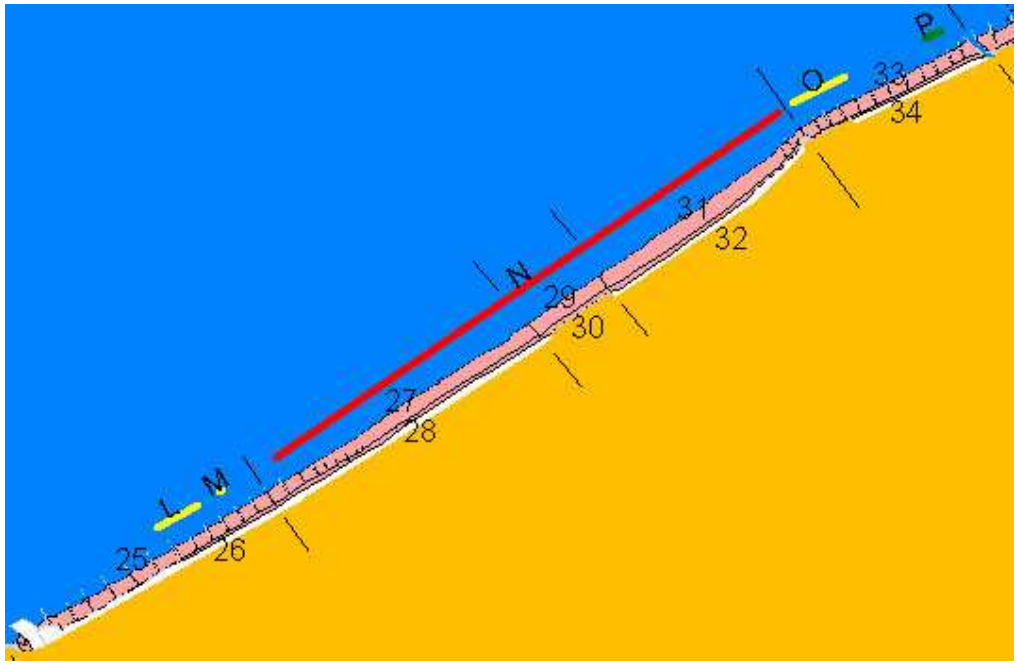

Figure 8-17: Coastal unit between the harbour of Oostende and the harbour of Blankenberge. The numbers (even for the dunes and odd for the beach) are the zones in which the volumetric changes were calculated. The corresponding changes can be found in

Table 8-3. The letters (L, M, O and P) indicate the areas where berm replenishment works were executed. In area N a beach nourishment was executed in combination with the construction of an offshore berm.

Eastward of Oostende the beach and especially the backshore becomes narrow and is protected by groynes. Between Bredene – Hippodroom and a few hundred meters West of the rotunda of Wenduine there are no groynes. From this point on, groynes protect the beach up to the harbour dam of Blankenberge. The areas with berm replenishments (L, M and O on Figure 8-17) are situated in Bredene and Wenduine. In P, small amounts of sand are deposited to protect the 'strandpaviljoen van Harendijke'.

Far more important than these small scale berm replenishments, is the beach nourishment and the nearshore nourishment that took place in the 90s around De Haan. Sustained erosion and a severe storm in 1990 reduced the safety level of this coastal strip dramatically. To counter this, an offshore berm of 8.7 km long was created between 1991 and 1998. The top of the berm was originally situated at 600 m from the dune foot. In combination with this, the backshore was nourished between 1992 and 1996. Per meter in the longshore direction 360 m³ sand was deposited. The sand used was coarse-grained sea sand with a D50 of 300 – 400 µm, easily detectable on the hyperspectral data. Between 1998 and 2000, the offshore berm was a few times renourished (in total 197 000 m³) and in May – June 2000, a few months before our first flight campaign, the backshore was renourished over a length of 1200 m, with 260 500 m³ sea sand.

8.3.3.2 General trends

Overall, the beach between Oostende and Blankenberge is erosive, especially in De Haan-West and in the centre of De Haan, significant erosion was measured between 2000 and 2006. In Bredene, the beach was rather stable, while in Wenduine limited accretion was measured. In contrast with the beach, the foredunes grew in the entire unit, except for the centre of De Haan. This illustrates nicely the concept that the foredunes can only grow when the beach in front of them is sufficiently large and stable (or accretional), which is not the case in the centre of De Haan. The total volume eroded on the beach between 2000 and 2006 (285 000 m³) is somewhat smaller than the accretion in the foredunes (375 500 m³) indicating that the safety level of the dune wall increases, while the height of the beach decreases. Hence, the profile of the continuum beach – dunes alters towards a steeper profile. In case of a heavy storm this could cause serious damage to the dune wall.

Table 8-3: Volumetric changes and mean height differences for the areas indicated in Figure 8-17.

Zone	Beach or foredunes	Zone N°	Year	Surface (ha)	Volume diff. (m^3)	Mean height diff. (cm)
Oostende East - Bredene	beach	25	2001 - 2000	70.4	-12 800	-1.8
		25	2002 - 2000	70.4	2 100	0.3
		25	2004 - 2000	70.3	-8 700	-1.2
		25	2006 - 2000	70.4	-3 600	-0.5
Bredene	foredunes	26	2001 - 2000	7.4	9 300	12.5
		26	2002 - 2000	7.4	12 500	16.8
		26	2004 - 2000	7.4	13 700	18.5
		26	2006 - 2000	6.6	35 900	54.4
Hippodroom - De Haan West	beach	27	2001 - 2000	88.1	-100	0.0
		27	2002 - 2000	88.1	-105 500	-12.0
		27	2004 - 2000	87.7	-159 000	-18.1
		27	2006 - 2000	88.1	-143 700	-16.3
Hippodroom - De Haan West	foredunes	28	2001 - 2000	26.7	-400	-0.1
		28	2002 - 2000	26.7	45 800	17.2
		28	2004 - 2000	26.6	46 300	17.4
		28	2006 - 2000	24.9	96 000	38.6
De Haan-Centre	beach	29	2001 - 2000	25.3	-25 400	-10.0
		29	2002 - 2000	25.3	-61 000	-24.1
		29	2004 - 2000	23.9	-73 800	-30.8
		29	2006 - 2000	25.3	-75 400	-29.8
De Haan-Centre	foredunes	30	2001 - 2000	8.2	700	0.9
		30	2002 - 2000	8.2	-9 200	-11.2
		30	2004 - 2000	7.4	-16 300	-22.0
		30	2006 - 2000	8.2	-6 300	-7.6
De Haan East - Wenduine	beach	31	2001 - 2000	77.9	24 400	3.1
		31	2002 - 2000	77.9	-45 500	-5.8
		31	2004 - 2000	77.9	-79 400	-10.2
		31	2006 - 2000	77.9	-79 900	-10.3
De Haan East - Wenduine	foredunes	32	2001 - 2000	20.4	47 500	23.3
		32	2002 - 2000	20.4	96 800	47.5
		32	2004 - 2000	20.4	141 800	69.7
		32	2006 - 2000	20.4	186 200	91.5
Wenduine Centre and East	beach	33	2001 - 2000	54.7	37 300	6.8
		33	2002 - 2000	54.7	2 000	0.4
		33	2004 - 2000	51.2	8 100	1.6
		33	2006 - 2000	54.7	17 900	3.3
Wenduine Centre and East	foredunes	34	2001 - 2000	10.1	24 300	23.9
		34	2002 - 2000	10.1	33 000	32.5
		34	2004 - 2000	10.1	51 100	50.5
		34	2006 - 2000	9.8	63 700	65.3

Zone	Beach or foredunes	Zone N°	Year	Surface (ha)	Volume diff. (m^3)	Mean height diff. (cm)
Oostende - Blankenberge						
	beach		2001 - 2000	316.3	**23 400**	**0.7**
			2002 - 2000	316.3	**-207 900**	**-6.6**
			2004 - 2000	311.0	**-312 800**	**-10.1**
			2006 - 2000	316.3	**-284 700**	**-9.0**
	foredunes		2001 - 2000	72.8	**81 400**	**11.2**
			2002 - 2000	72.8	**178 900**	**24.6**
			2004 - 2000	71.9	**236 600**	**32.9**
			2006 - 2000	69.8	**375 500**	**53.8**

8.3.3.3 Detailed analysis of the morphodynamics

Between the eastern harbour dam of Oostende and Bredene the beach is in a morphodynamic stable state; no major changes can be reported. In Bredene, the accretion in polygons N° 301 and 302 (Figure 8-18) corresponds to the berm replenishment works executed here. Between 2000 and 2004 app. 60 000 m^3 sea sand was deposited; in the same time frame the beach remained stable and the dunes grew with app. 30 000 m^3; hence, one can conclude that half of the volume nourished is transported to the dunes while the other half was transported offshore.

There seems to be no transport of nourished sand from the area East of Bredene towards Bredene. On Figure 8-19 one can see that in 2001 and 2002 nourishment sand was found in sections 129 – 131, but there was no height difference. Hence, it was only a shallow top layer which disappeared by 2004. One can conclude that the nourishment around De Haan has no influence on the beaches West of De Haan.

As described in Section 8.3.3.1 the nearshore part of the beach and the backshore around De Haan were subject to large scale nourishments in the 90s. Between 2000 and 2004 the backshore berm has been eroded at its seaward side. Fractions of the nourished sand were temporarily stocked on the foreshore and consequently transported offshore (Figure 8-20). The foredunes on the other hand grew due to aeolian transport across the new berm (see the arrows indicating the sand transport directions in Figure 8-20). The sand is trapped by artificial wooden fences placed on the berm in an orientation perpendicular to the coastline. The corresponding volumes can be found in

Table 8-3. Note that the total volume eroded (198 600 m³) in sections 131 till 147 is more than the double of the volume that was deposited in the foredunes (88 800 m³), pointing on the cross-shore transport seawards and indicating that the fill will have to be renourished regularly to maintain the safety level attained immediately after the large-scale nourishments. However, the rate of erosion (110 000 m³ over 4 years) is not alarming and the offshore berm allows for cross-shore transport landwards during calm weather conditions.

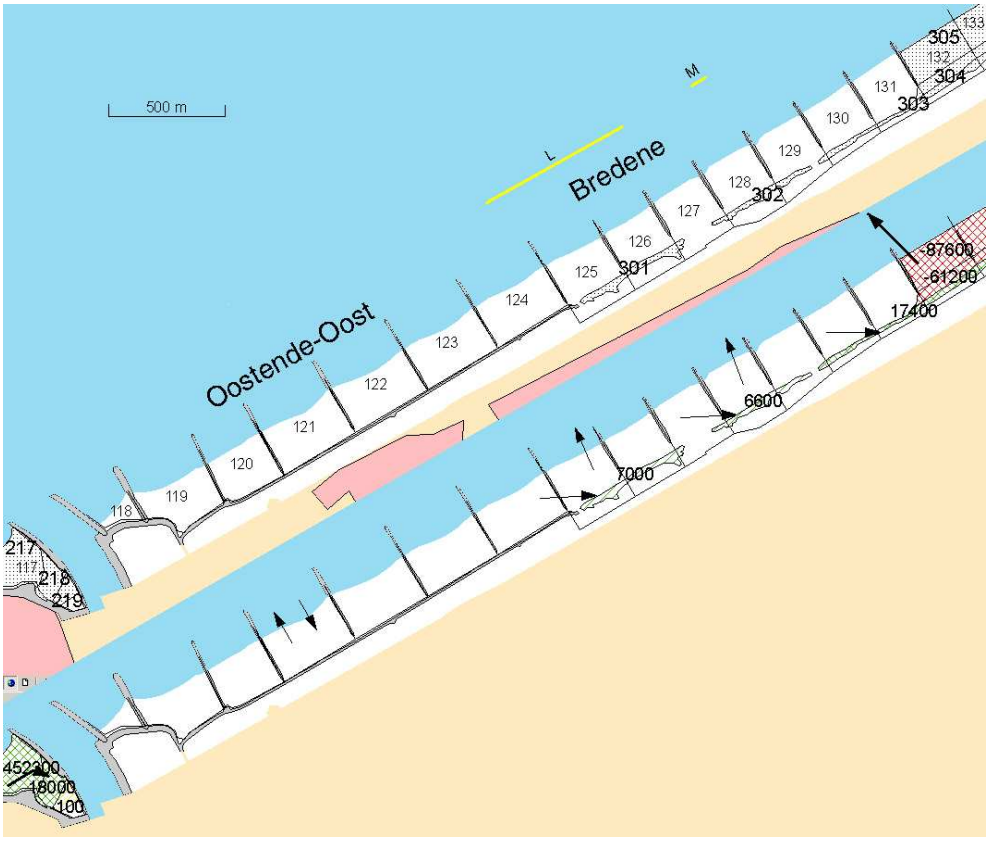

Figure 8-18: Map indicating the major morphodynamic changes between 2000 and 2004. In the upper map one finds the coastal sections with their corresponding number (bordered by lines perpendicular to the coast), the erosion/accretion polygons with their number, and the areas where artificial nourishment activities were executed, indicated with capital letters (yellow = berm replenishment with sea sand). On the lower map, one finds the amount (in m³) of sediment eroded or deposited in each polygon, as well as arrows indicating the direction and amount of the sediment transport. The pink area in the upper map indicates the built-up area.

Figure 8-21 illustrates the typical resorting that occurs on a nourished beach: originally, the berm consists of poorly sorted nourishment sand and the foreshore consists of fine to medium sand typical for the intertidal beach. After a few months to years, the fill is eroded by the waves and the wind. The smaller particles are

transported offshore but the coarser fractions, especially the shells are temporarily stocked on the foresfore. The berm itself becomes a mixture of nourishment sand, fine aeolian deposits and a type of sand that resembles the natural dry beach sand. The latter is actually the result of the resorting of the nourished sand. The different classes or fractions often appear in parallel bands on the dry beach.

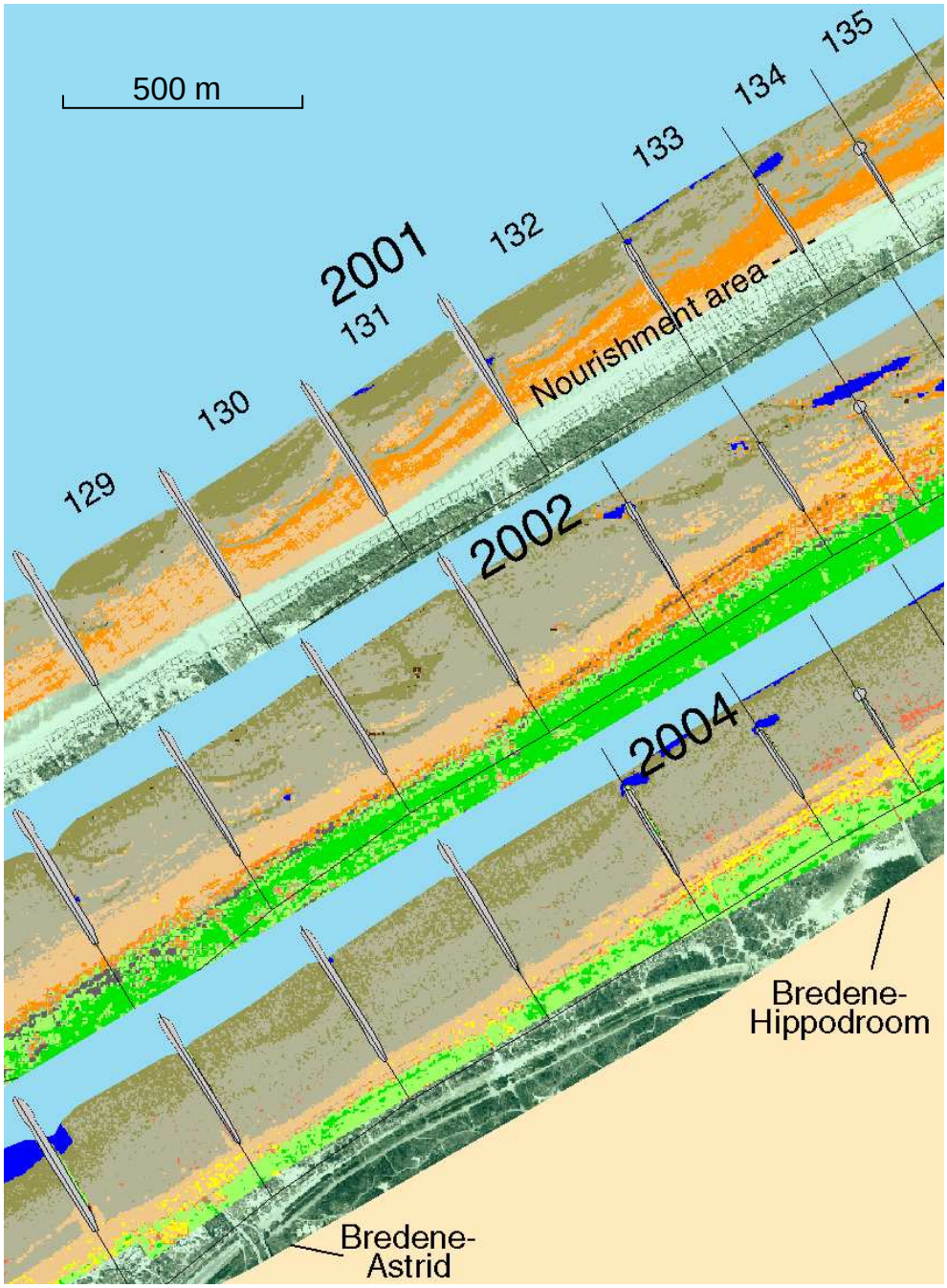

Figure 8-19: Sand class maps for 2001, 2002 and 2004 in the sections 129 – 135 (Bredene-Astrid tot Bredene-Hippodroom). The nourishment area starts from section 132.

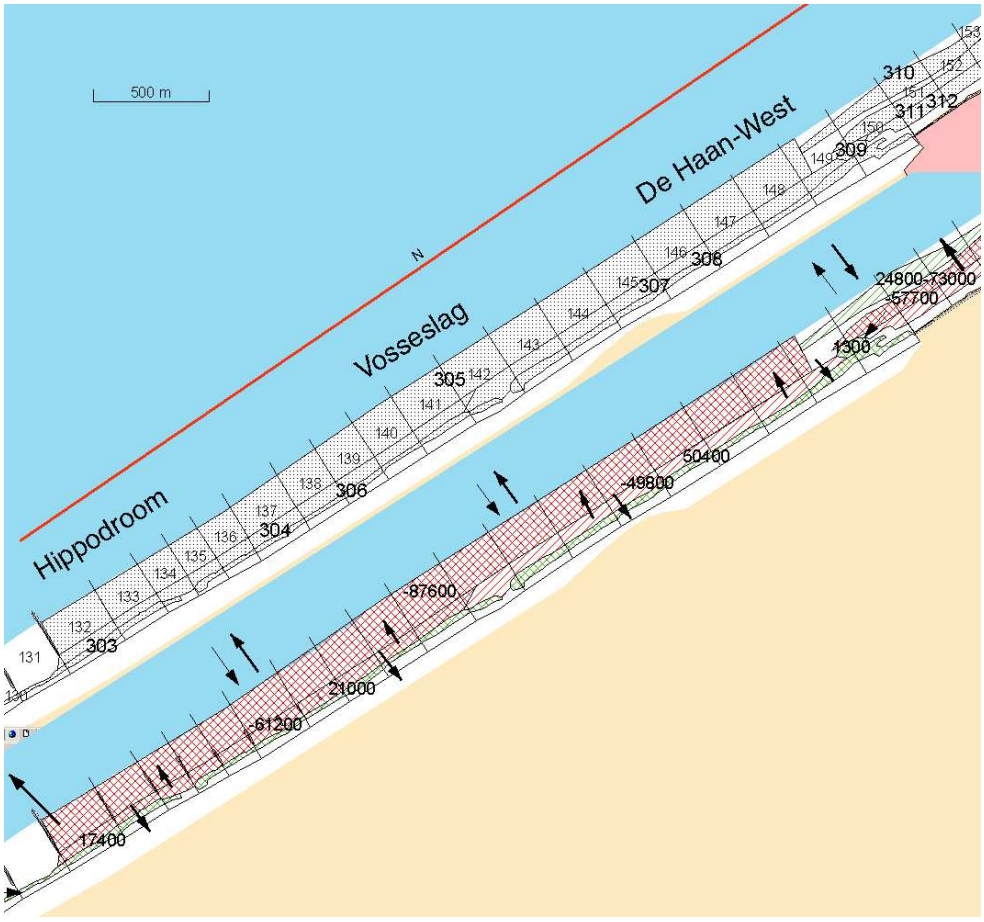

Figure 8-20: Map indicating the major morphodynamic changes between 2000 and 2004. In the upper map one finds the coastal sections with their corresponding number (bordered by lines perpendicular to the coast), the erosion/accretion polygons with their number, and the areas where artificial nourishment activities were executed, indicated with capital letters (red = beach nourishment with sea sand). On the lower map, one finds the amount (in m³) of sediment eroded or deposited in each polygon, as well as arrows indicating the direction and amount of the sediment transport. The pink area in the upper map indicates the built-up area.

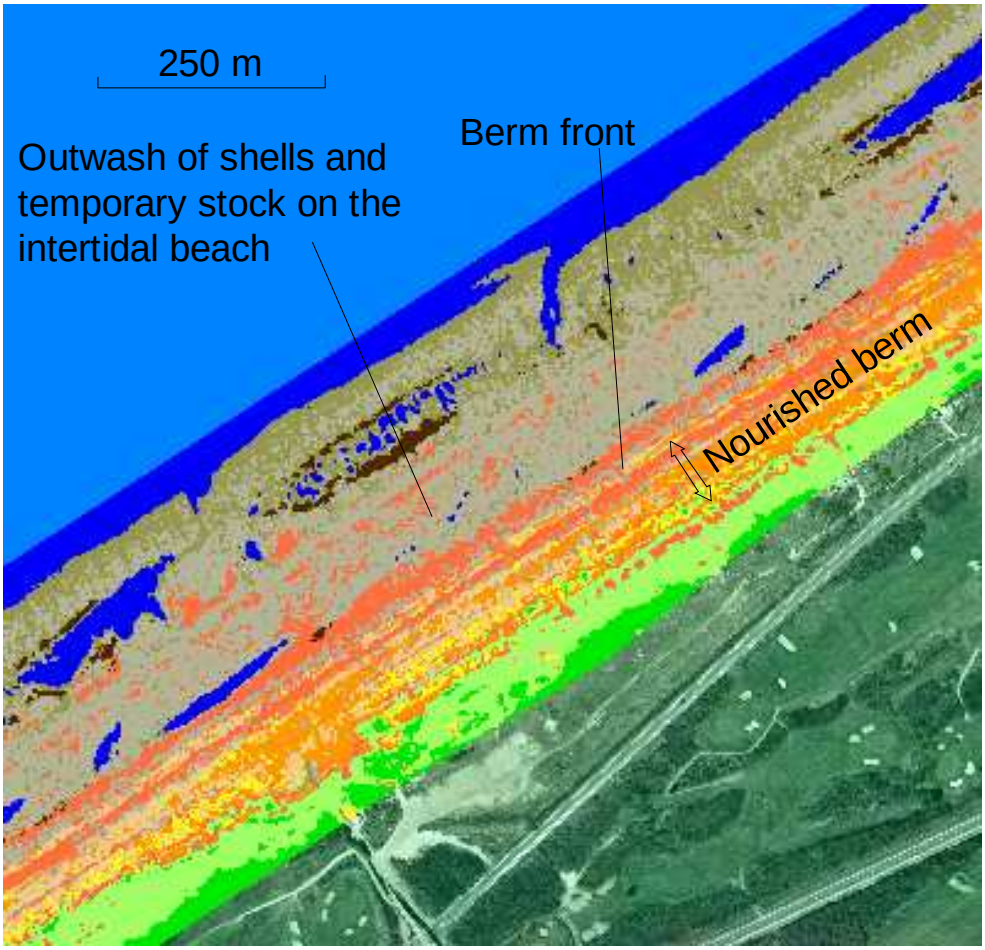

Figure 8-21: Sand class map of July 2004 at the Vosseslag (De Haan).

The morphological evolution in the eastern part of the nourished area around De Haan is similar to the evolution reported in the western part. However, the net volume difference measured here is positive since 2000; the intertidal beach is erosive (app. 80 000 m³ was eroded between 2000 and 2004 over a length of 3 km), but the foredunes grew in the same time frame with 140 000 m³. This growth is possible due to the wider dry beach. In this area, situated eastward of the large nourishment area, more nourishment sand is found on the intertidal beach than in the area West of De Haan, pointing on the net sediment transport from the West to the East.

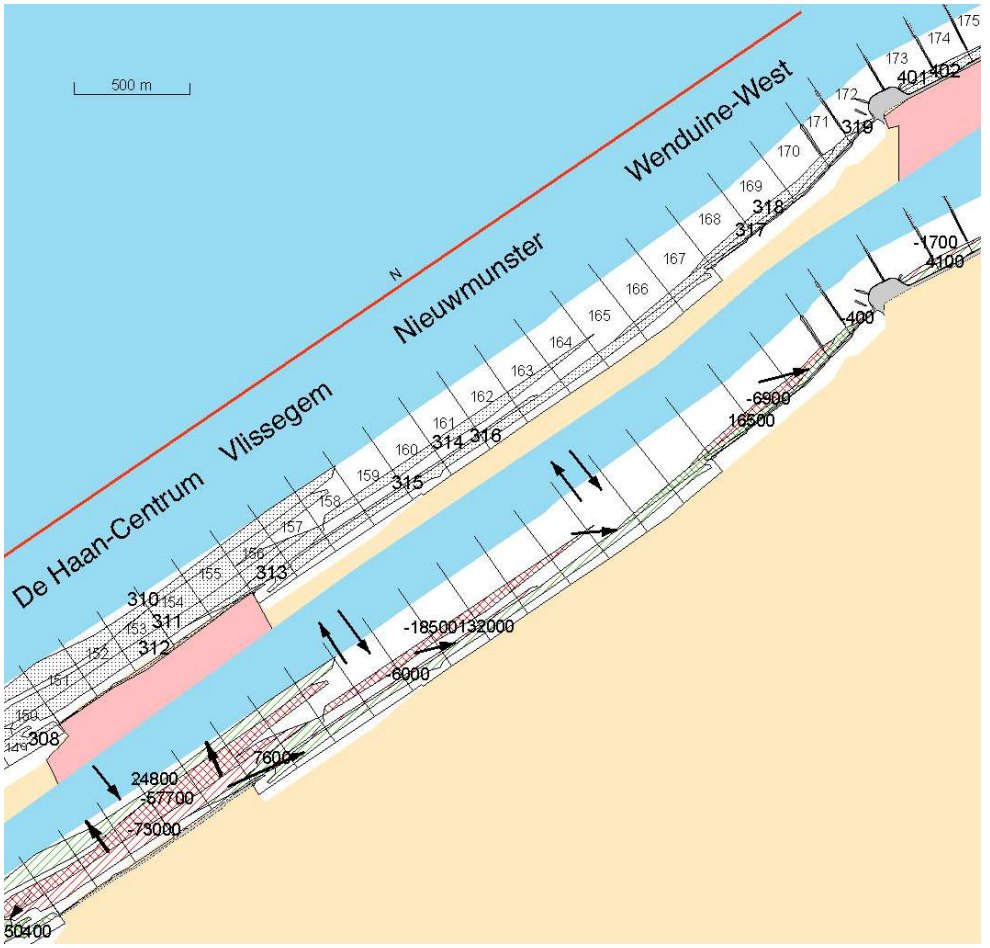

Figure 8-22 Map indicating the major morphodynamic changes between 2000 and 2004. In the upper map one finds the coastal sections with their corresponding number (bordered by lines perpendicular to the coast), the erosion/accretion polygons with their number, and the areas where artificial nourishment activities were executed, indicated with capital letters (red = beach nourishment with sea sand). On the lower map, one finds the amount (in m³) of sediment eroded or deposited in each polygon, as well as arrows indicating the direction and amount of the sediment transport. The pink area in the upper map indicates the built-up area.

The coastal zone between the rotunda of Wenduine and the harbour channel of Blankenberge experiences a morphological stable state. However, it is a dynamic equilibrium: in Wenduine (O on Figure 8-23) and in Harendijke (P on Figure 8-23) berm replenishments are executed yearly to compensate for the erosion of the backshore berm. Hence, the stable situation is the result of regular human interventions. The foredunes experience the same growth as we measured West of the rotunda. Remarkably, there is very few nourishment sand found on the intertidal beach

here. It is assumed that the fill of the nourishment of De Haan remains in De Haan and immediately East of it, but is not transported further East than the rotunda.

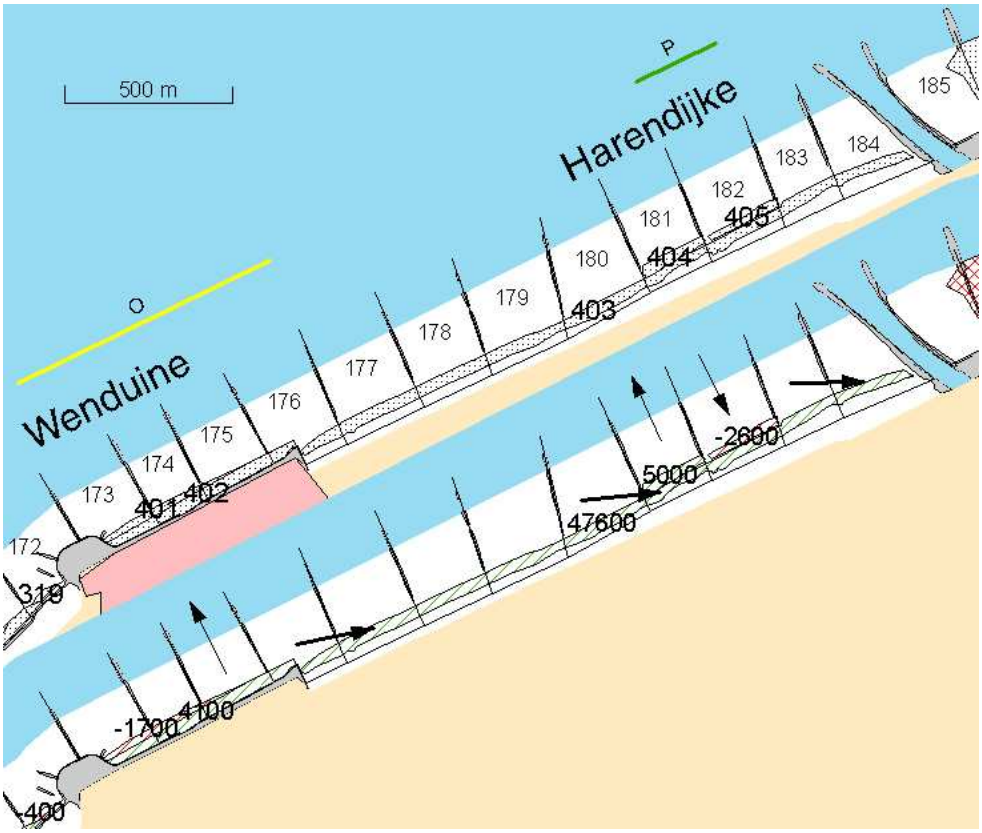

Figure 8-23 Map indicating the major morphodynamic changes between 2000 and 2004. In the upper map one finds the coastal sections with their corresponding number (bordered by lines perpendicular to the coast), the erosion/accretion polygons with their number, and the areas where artificial nourishment activities were executed, indicated with capital letters (yellow = berm replenishment with sea sand, green = berm replenishment with sand from the foreshore). On the lower map, one finds the amount (in m³) of sediment eroded or deposited in each polygon, as well as arrows indicating the direction and amount of the sediment transport. The pink area in the upper map indicates the built-up area.

8.3.4 Blankenberge – Zeebrugge

Note: the morphodynamic evolution in the coastal area between the pier of Blankenberge and the western harbour dam of Zeebrugge is also described in Section 7.3.2.

8.3.4.1 Human interventions

This small, 5 km-long unit is situated between the low dams of the harbour of Blankenberge in the West and the 4 km long western dam of the harbour of Zeebrugge in the East. The latter was constructed between 1979 and 1985 and forms an almost complete barrier for the longshore transport, resulting in a very wide accretional beach at its western side. With the exception of zone N° 39 in Zeebrugge (Figure 8-24), the beach in this coastal unit is everywhere protected with groynes. In section 194 (between zone 35 and 37 on Figure 8-24) the pier of Blankenberge forms one of the typical vistas at the Belgian coast.

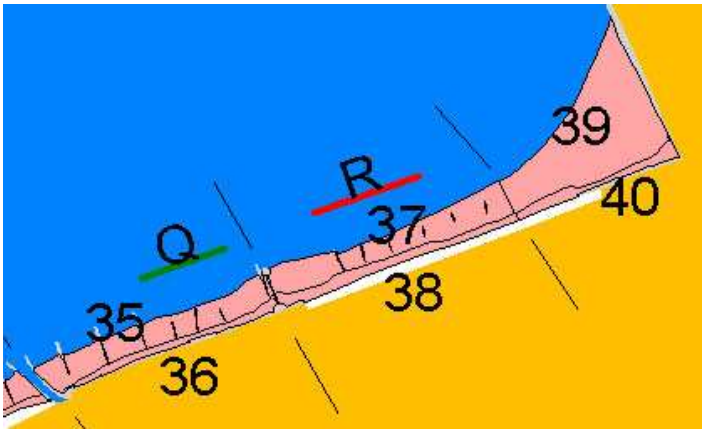

Figure 8-24: Coastal unit between the harbour of Blankenberge and the harbour of Zeebrugge. The numbers (even for the dunes and odd for the beach) are the zones in which the volumetric changes were calculated. The corresponding changes can be found in Table 8-4. The letters (Q and R) indicate the areas where respectively a berm replenishment and a backshore nourishment was executed.

In Blankenberge, westward of the pier, yearly berm replenishments are executed using sand from the intertidal beach (see letter Q in Figure 8-24). The volumes deposited are rather small, i.e., a few 1 000 m³ per year. At the Duinse Polders, a backshore nourishment was executed between October 1998 and April 1999 (see letter R in Figure 8-24). In contrast with the other nourishment areas (e.g., De Haan), the sand used was not particularly coarse-grained (D50: 250 – 300 µm), nor shell-rich. Over a length of 930 m, 486 300 m³ sand was deposited, i.e., 523 m³ per m in the longshore direction. It should be noted that the wet nourishment technique used, results typically in a loss of 5 – 20%, hence, the net volume change was app. 410 000 m³ (with a loss of app. 15%). The accretional beach of Zeebrugge has recently been used to capture sand which is used in the lock approach of Zeebrugge. The capture zone is located on the intertidal beach and covered in 2006 app. 30 ha. The following captures have recently been executed:- 1999: 450 000 m³

- 2000 - 2005: none
- 2006: 185 000 m³ in Febr. - April and 75 000 m³ in Sept. - Oct

8.3.4.2 General trends

In total, this coastal unit is accretional. There is a positive volume change for the beach of 206 900 m³ (+ 12.7 cm) between 2000 and 2006 and 100 600 m³ (+30.2 cm) for the foredunes. However, these figures are biased by the huge accretion taking place in Zeebrugge; see Table 8-4. In contrast with this, the beach in Blankenberge and at the Duinse Polders is erosive. In the next chapters each zone is described in detail.

Table 8-4: Volumetric changes and mean height differences for the areas indicated in Figure 8-24.

Zone	Beach or foredunes	Zone N°	Year	Surface (ha)	Volume diff. (m³)	Mean height diff. (cm)
Blankenberge	beach	35	2001 - 2000	40.6	-32 300	-7.9
		35	2002 - 2000	40.6	-37 100	-9.1
		35	2004 - 2000	40.0	-41 400	-10.3
		35	2006 - 2000	40.6	-78 300	-19.3
Blankenberge	foredunes	36	2001 - 2000	9.3	-7 600	-8.1
		36	2002 - 2000	9.3	-500	-0.5
		36	2004 - 2000	9.3	1 400	-1.5
		36	2006 - 2000	9.3	16 700	17.9
Duinse Polders	beach	37	2001 - 2000	42.0	-32 000	-7.6
		37	2002 - 2000	42.0	-60 900	-14.5
		37	2004 - 2000	40.5	-60 200	-14.9
		37	2006 - 2000	42.0	-23 000	-5.5
Duinse Polders	foredunes	38	2001 - 2000	14.7	21 400	14.5
		38	2002 - 2000	14.7	21 600	14.7
		38	2004 - 2000	14.7	30 400	20.7
		38	2006 - 2000	14.3	36 900	25.7
Zeebrugge	beach	39	2001 - 2000	73.6	69 100	9.4
		39	2002 - 2000	80.0	178 800	22.3
		39	2004 - 2000	72.6	309 100	42.6
		39	2006 - 2000	80.1	308 200	38.5
Zeebrugge	foredunes	40	2001 - 2000	9.7	4 700	4.9
		40	2002 - 2000	9.7	24 100	24.9
		40	2004 - 2000	9.5	28 800	30.3
		40	2006 - 2000	9.7	47 000	48.7
Blankenberge – Zeebrugge						
	beach		2001 - 2000	156.2	**4 800**	**0.3**
			2002 - 2000	162.6	**80 800**	**5.0**
			2004 - 2000	153.2	**207 500**	**13.5**
			2006 - 2000	162.7	**206 900**	**12.7**
	foredunes		2001 - 2000	33.7	**18 500**	**5.5**
			2002 - 2000	33.7	**45 200**	**13.4**
			2004 - 2000	33.5	**57 800**	**17.2**
			2006 - 2000	33.3	**100 600**	**30.2**

8.3.4.3 Detailed analysis of the morphodynamics

The beach of Blankenberge featured accretion in the 80s and in the beginning of the 90s. Three human interventions were at the basis of this: the extension of the groynes East of the harbour channel in 1985 – 1986 and 1991, the deposition of dredged material out of the harbour channel in the sections immediately East of the channel (app. 25 000 – 30 000 m³ was deposited yearly) and thirdly, the yearly berm replenishments. Recently, the accretion turned into erosion because the deposition of dredged material was stopped and because a new equilibrium state was attained after the extension of the groynes. The berm replenishments continue until today. Polygon N° 406 in Figure 8-25 illustrates the erosion taking place in the area where before the dredged material was deposited. Between 2000 and 2004, 31 400 m³ of sand was eroded here. Due to the lowering of the foreshore, the dry beach berm was also prone to erosion (cf. polygon N° 407): 10 900 m³ was eroded between 2000 and 2004. The other sections West of the pier (N° 189 – 193) are rather stable, while the small erosion and accretion zones around the pier are the result of recent human interventions.

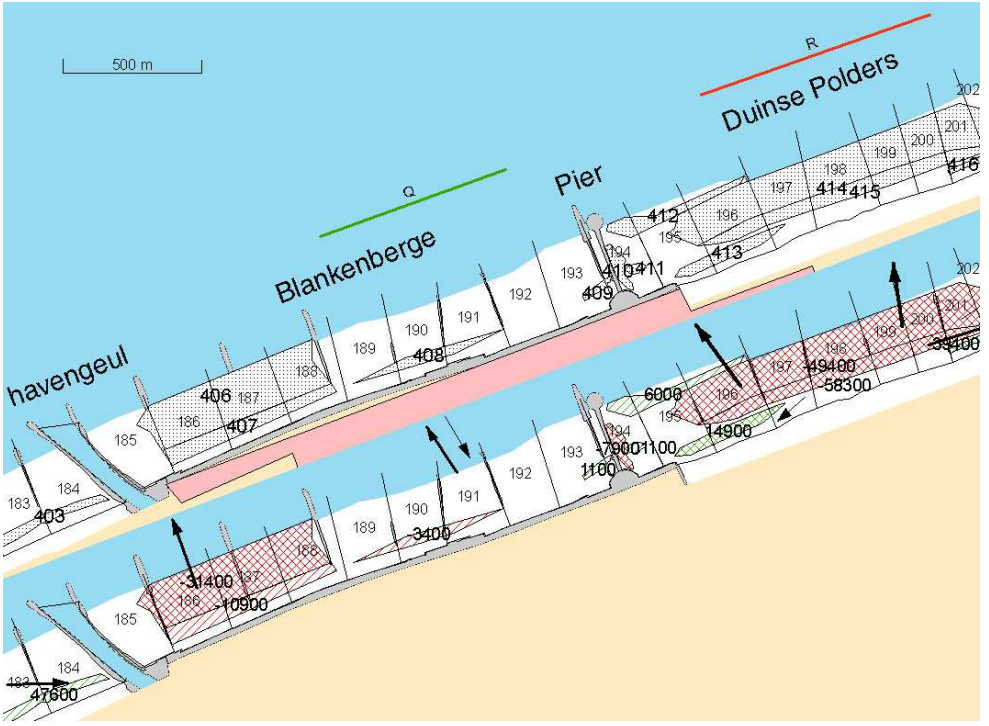

Figure 8-25: Map indicating the major morphodynamic changes between 2000 and 2004. In the upper map one finds the coastal sections with their corresponding number (bordered by lines perpendicular to the coast), the erosion/accretion polygons with their number, and the areas where artificial nourishment activities were executed, indicated with capital letters (green = berm replenishment with sand from the foreshore, red = beach nourishment with sea sand). On the lower map, one finds the amount (in m³) of sediment eroded or deposited in each polygon, as well as arrows

indicating the direction and amount of the sediment transport. The pink area in the upper map indicates the built-up area.

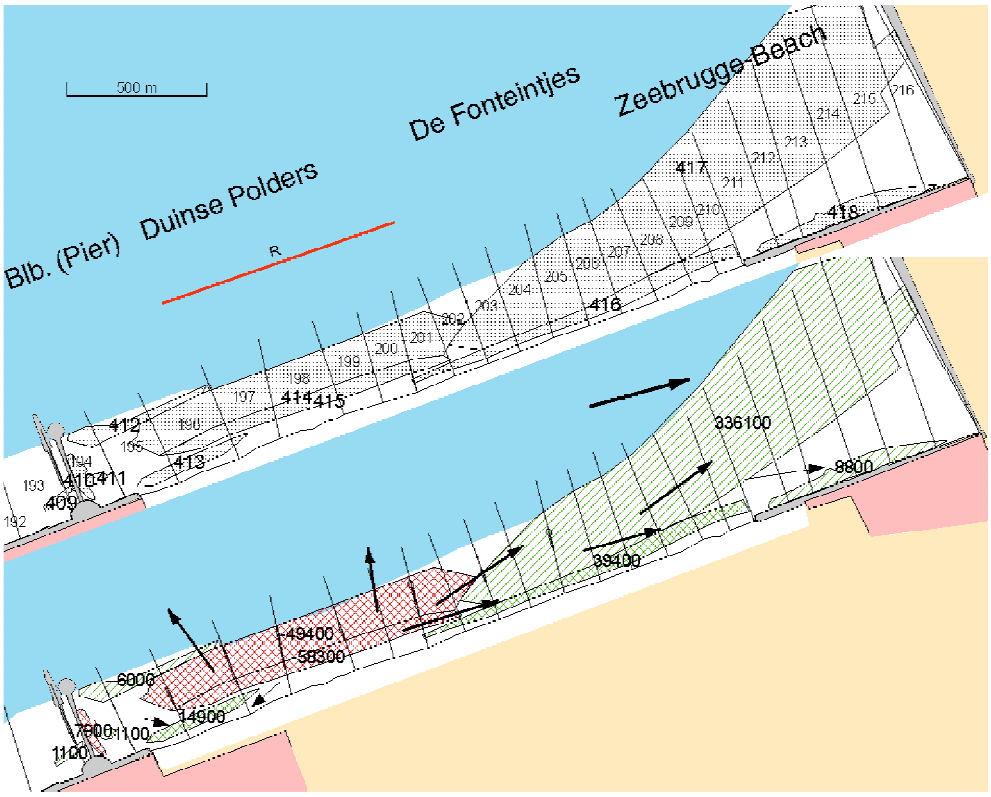

Figure 8-26: Map indicating the major morphodynamic changes between 2000 and 2004. In the upper map one finds the coastal sections with their corresponding number (bordered by lines perpendicular to the coast), the erosion/accretion polygons with their number, and the areas where artificial nourishment activities were executed, indicated with capital letters (red = beach nourishment with sea sand). On the lower map, one finds the amount (in m³) of sediment eroded or deposited in each polygon, as well as arrows indicating the direction and amount of the sediment transport. The pink area indicates the built-up area.

In the eastern part of Figure 8-25 and on Figure 8-26, one sees the area around the Duinse Polders where a backshore nourishment was executed in 1998 – 1999 in sections 196 - 201. The intervention was necessary because of the lowering of the intertidal beach, possibly linked to the extension of the groynes in Blankenberge. The latter reduced the longshore transport from Blankenberge to the Duinse Polders. This, in combination with the natural seaward oriented cross-shore transport, caused the lowering of the intertidal beach and the erosion of the dune foot. As the dune belt at the Duinse Polders is very narrow (only 30 – 40 m wide) a reinforcement of the beach and dunes became absolutely necessary in the second half of the 90s. In addition to the

classical backshore nourishment, the dune front was restored till a height of 14 m TAW.

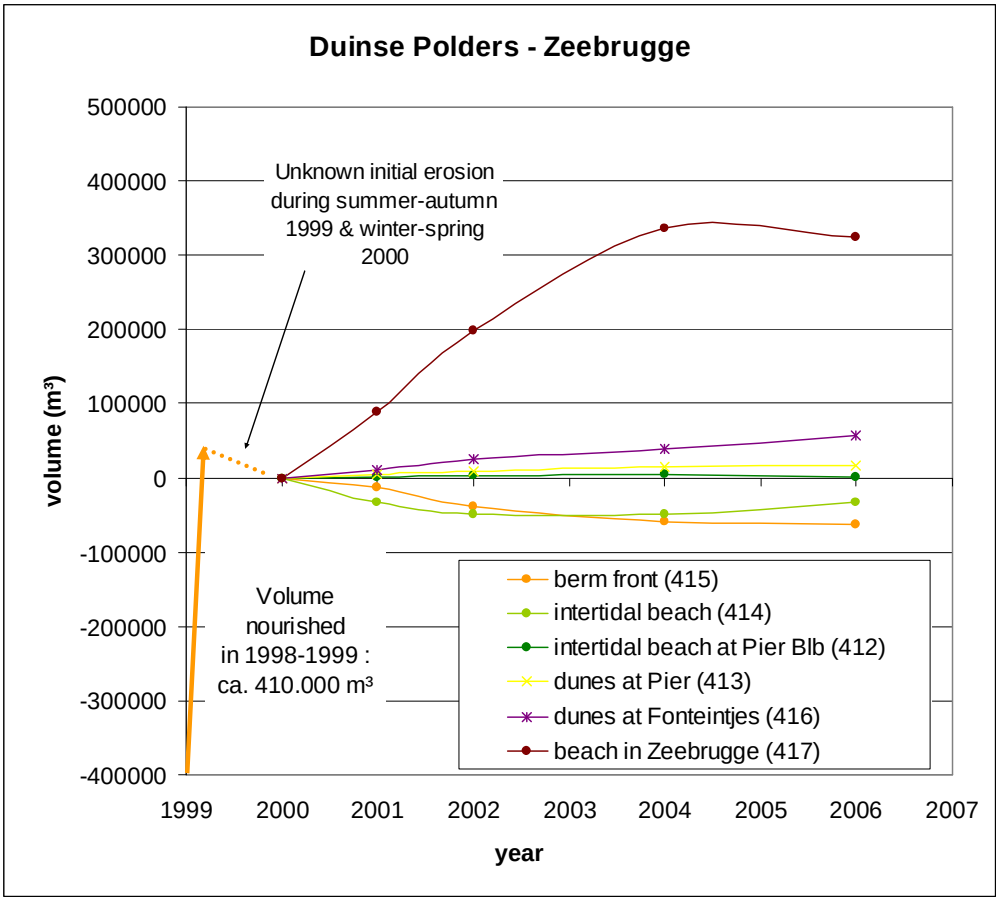

Figure 8-27: Evolution of the beach profile at and around the Duinse Polders between 1999 and 2006. The backshore nourishment was completed in April 1999; the first LIDAR observation was executed in September 2000.

After the nourishment, the backshore berm and the foreshore were eroded: between 2000 and 2004 the volume loss at the berm was 58 300 m³ and the foreshore lost 49 400 m³ (respectively polygons N° 415 and 414 in Figure 8-26). However, the fastest erosion always takes place immediately after a human intervention; hence, it can be assumed that between our first observation in August 2000 and the end of the nourishment works (April 1999) a significant amount had already been eroded. The eroded sand is mainly transported via cross-shore transport to the nearshore, where it enters into longshore transport processes, taking it to the accretional beach at the harbour dam. However, as a result of the sorting processes taking place during the transport, the sand deposited in Zeebrugge is not detectable as nourishment sand

anymore. The total volume deposited in polygon N° 417 (Figure 8-26) sums to 336 100 m³ between 2000 and 2004. In the foredunes smaller accretion of 39 400 m³ and 8 800 m³ was observed in polygons N° 416 and 418. The latter is the result of aeolian transport taking place over the wide dry beach.

Figure 8-27 illustrates the change in volume that was observed in the first years after the nourishment. The largest erosion took place at the berm front and on the foreshore in front of the berm. The foreshore in polygon N° 412 remained stable, while the dunes in polygon N° 413 and especially in polygon N° 416 grew. A remarkable fact is the sudden stop in accretion in polygon N° 417. This is an artificial trend caused by sand dredged in this area (see earlier in Section 8.3.4).

8.3.5 Heist – Zwin channel

8.3.5.1 Human interventions

The easternmost unit of the Belgian coast is bounded by the eastern harbour dam of Zeebrugge and the Zwin channel which is situated at the border between Belgium and The Netherlands. The total length of this coastal unit is 10 km. In Heist, a very wide beach hosts the only beach nature reserve along the Belgian shoreline (see Chapter 2). The extent of the beach in Heist is similar to the wide beach of Zeebrugge but its historical record is completely different. While the beach in Zeebrugge is formed 'naturally' (see Section 8.3.4), the beach in Heist is in the first place the result of several human interventions, coupled to the construction of the long harbour dams in 1979 - 1985. However, despite the human interventions, it is assumed that also natural forces add to the widening of the beach in Heist: the net West-to-East transport of sediments is interrupted by the harbour dams of Zeebrugge. At the eastern (lee) side of this construction, the current velocity, during rising tide, is lower causing sedimentation in the Bay of Heist. During the falling tide, the tidal current runs from the East to the West and the dams act as a sediment trap causing again accretion. The combination of both processes might lead to a widening of the beach in the Bay of Heist. The latter is expressed by the formation of a sand bank in the bay which is nowadays almost an island at low tide. However, in the remainder of this chapter it will be shown that locally also erosion occurs in the Bay of Heist. The sedimentation processes in this highly complex area have been studied and are reported by Waterbouwkundig Laboratorium (2006).

Before listing the human interventions that have been executed in this unit, it should be noted that the entire beach in zones 43, 45 and 47 (Figure 8-28) is protected by groynes. Only in Heist and in the last 1.3 km West of the Dutch border, there are no groynes.

During the last decades, the shoreline in Knokke-Heist has been prone to severe erosion. To counter this, several human interventions were needed:

- In 1977 – 1979 a major beach nourishment was executed over a length of 8.8 km (V in Figure 8-28). With the exception of zone 49, the entire shoreline of Knokke-Heist was nourished. In total, 8 500 000 m³ sand was used, corresponding to 965 m³/m. Before the nourishment, there was, in certain places, no dry beach anymore during high tide. It was expected that the construction of the harbour dams would result in an increase of the erosion rate in Knokke-Heist, due to the cut-off of sand supply from the West via longshore transport processes.
- In 1986, the foreshore and the nearshore immediately East of the harbour dam, in Heist, were nourished with 500 000 m³ of sand originating from dredging activities in the harbour of Zeebrugge (letter S in Figure 8-28). Afterwards, in 1992, an excavation zone in the Bay of Heist silted up with mud. The unstable mud layer had to be removed and the depression was filled with sand during two nourishment activities in 1993 and 1994.
- Also in 1986, a second nourishment was executed in zone W (Figure 8-28). Although 1 000 000 m³ of sand was deposited, the fill was almost completely eroded by 1991.
- Therefore, a third nourishment proved to be necessary and was executed in March - May 1999; 486 418 m³ of sand was deposited in zone U. This nourishment could be mapped with the hyperspectral data of August 2000.
- The fourth nourishment in zone U (390 000 m³) was executed in June 2004, only a few days before our fourth hyperspectral campaign.
- Some smaller berm replenishments have been executed in Duinbergen (zone T in Figure 8-28). Table 8-5 summarises the amounts and origin of the sand used in Duinbergen:

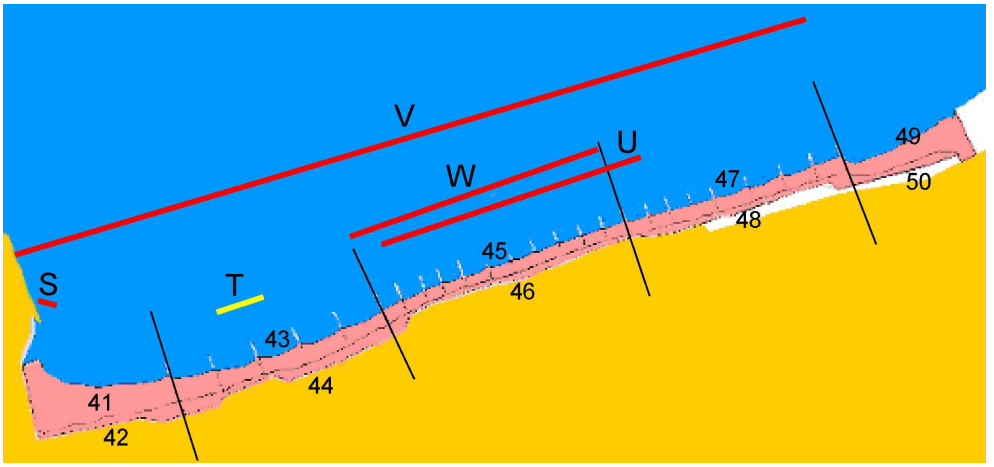

Figure 8-28: Coastal unit between the harbour of Zeebrugge and the Dutch border (Zwinmonding). The numbers (even for the dunes and odd for the beach) are the zones in which the volumetric changes were calculated. The corresponding changes can be found in Table 8-5. The letters (U, S and V) indicate the areas where beach nourishments were executed. In the area marked with letter T regular berm replenishments occur.

Table 8-5: Volumes of the yearly berm replenishments in Duinbergen (zone T on Figure 8-28).

Year	Sea sand (m³)	Intertidal beach sand (m³)
1997	-	7 049
1998	-	10 617
1999	-	12 411
2000	-	13 655
2001	-	13 692
2002	-	13 077
2003	4 855	13 597
2004	13 124	-
2005	18 146	-
2006	19 372	-

Finally, it is important to take into account the human interventions taking place on the eastern side of the Zwinmonding, i.e., in Cadzand (The Netherlands). Although the net transport along the Belgian coast takes place from the West to the East, East to West transport occurs during falling tide and during periods with northerly and easterly winds. The following nourishments have been executed in the coastal strip between the border and the channel of Cadzand:

- Autumn 1990: deposition of 346 000 m³ of sand, which resulted in a beach raising of 1 – 2 m (the sand was borrowed from the Sluise Hompels)
- Summer 1992: berm replenishment with sand originating from a sand trap in the Zwin channel (90 000 m³)
- Autumn 1995: 26 200 m³ of sand was deposited in a meander of the Zwin channel
- February 1997: construction of a dry beach berm on the eastern bank of the Zwin channel, using sand caught in the sand trap

8.3.5.2 General trends

Although the beach nourishment in 2004 hampers the analysis of the long term trends, one can conclude that the coastal unit between the beach of Heist and the Zwin channel is erosive. Between the acquisition of 2000 and 2002, 351 700 m³ sand eroded from the backshore and the foreshore. In the same time window, the foredunes remained stable. By the acquisition of July 2004, the volume difference on the beach was close to zero (-8 300 m³), but the volume nourished in 2004 was 390 000 m³. Hence, the erosion between 2002 and 2004 was only 46 600 m³. This implies that the erosion rate between 2002 and 2004 was much smaller than between 2000 and 2002. This fast erosion can be seen as the initial compensation for the nourishment of 1999. The same pattern was observed between 2004 and 2006: 216 000 m³ eroded in the first two years after the nourishment. It can be expected that in the next years the erosion rate will slow down to a few 10 000 m³ per year if the coast is not hit by heavy storms.

Table 8-6: Volumetric changes and mean height differences for the areas indicated in Figure 8-28.

Zone	Beach or foredunes	Zone N°	Year	Surface (ha)	Volume diff. (m^3)	Mean height diff. (cm)
Heist	beach	41	2001 - 2000	63.6	-30 800	-4.8
		41	2002 - 2000	63.6	-58 900	-9.3
		41	2004 - 2000	62.3	-43 900	-7.1
		41	2006 - 2000	63.6	-40 400	-6.4
Heist	foredunes	42	2001 - 2000	13.1	-13 000	-9.9
		42	2002 - 2000	13.1	-1 900	-1.4
		42	2004 - 2000	13.0	13 200	10.2
		42	2006 - 2000	13.1	31 300	23.9
Duinbergen - Albertstrand	beach	43	2001 - 2000	44.3	-22 700	-5.1
		43	2002 - 2000	44.3	-20 700	-4.7
		43	2004 - 2000	44.2	700	0.2
		43	2006 - 2000	44.4	-27 600	-6.2
Duinbergen - Albertstrand	foredunes	44	2001 - 2000	23.5	-18 000	-7.6
		44	2002 - 2000	23.5	-3 500	-1.5
		44	2004 - 2000	22.8	18 600	8.1
		44	2006 - 2000	23.5	54 600	23.2
Knokke-Zoute	beach	45	2001 - 2000	36.5	-66 200	-18.1
		45	2002 - 2000	36.5	-153 000	-41.9
		45	2004 - 2000	36.5	134 000	36.7
		45	2006 - 2000	36.5	-62 200	-17.0
Knokke-Zoute	foredunes	46	2001 - 2000	16.7	900	0.6
		46	2002 - 2000	16.7	-300	-0.2
		46	2004 - 2000	16.6	-12 100	-7.3
		46	2006 - 2000	16.7	19 000	11.4
Lekkerbek - Zwinbosjes	beach	47	2001 - 2000	34.8	-10 300	-3.0
		47	2002 - 2000	34.8	-30 000	-8.6
		47	2004 - 2000	34.7	9 300	2.7
		47	2006 - 2000	34.8	-23 300	-6.7
Lekkerbek - Zwinbosjes	foredunes	48	2001 - 2000	17.0	4 400	2.6
		48	2002 - 2000	17.0	9 000	5.3
		48	2004 - 2000	17.0	37 200	21.9
		48	2006 - 2000	16.9	77 800	46.2
Zwin	beach	49	2001 - 2000	32.7	-34 700	-10.6
		49	2002 - 2000	32.7	-89 100	-27.2
		49	2004 - 2000	32.7	-108 400	-33.1
		49	2006 - 2000	31.9	-62 500	-19.6
Zwin	foredunes	50	2001 - 2000	8.4	8 400	10.0
		50	2002 - 2000	8.4	7 400	8.9
		50	2004 - 2000	8.4	18 300	21.8
		50	2006 - 2000	7.7	30 300	39.2

Zone	Beach or foredunes	Zone N°	Year	Surface (ha)	Volume diff. (m^3)	Mean height diff. (cm)
Heist – Zwin channel						
	beach		2001 - 2000	212.0	**-164 700**	**-7.8**
			2002 - 2000	212.0	**-351 700**	**-16.6**
			2004 - 2000	210.4	**-8 300**	**-0.4**
			2006 - 2000	211.1	**-216 000**	**-10.2**
	foredunes		2001 - 2000	78.8	**-17 300**	**-2.2**
			2002 - 2000	78.8	**10 700**	**1.4**
			2004 - 2000	77.7	**75 200**	**9.7**
			2006 - 2000	78.0	**213 000**	**27.3**

The volume of the foredunes remained stable from 2000 till 2002, grew in the next two years with 64 500 m^3 and even with 137 800 m^3 between 2004 and 2006. Despite the general trend of erosion, the growth of the foredunes belt adds to the general strength of the sea wall.

8.3.5.3 Detailed analysis of the morphodynamics

The wide beach in Heist is characterised by parallel ridges and runnels, indicating the occurrence of cross-shore transport processes; see e.g., polygons N° 420 and 421 in Figure 8-31. However, the net erosion or accretion is small. In polygon N° 419 on the other hand, significant erosion takes place; between 2000 and 2004, 61 700 m^3 sand was eroded. This area is responsible for the net erosion in zone 41; see Table 8-6. The erosion in this area continues until 2006, but the rate of erosion slows down. The erosion is probably a result of the lack of sediment supply from the West as the harbour dams of Zeebrugge act as a sediment trap. The lack of longshore sediment supply from the West and the processes of cross-shore transport result in net erosion of the backshore. Despite the erosion of the backshore and the foreshore, the nearshore in Heist is accretional and a new sand bank has been developing since the construction of the harbour dams. The latter is caused by the low current velocities in the bay, both during rising tide and during falling tide, creating suited circumstances for sedimentation (Figure 8-29 and Figure 8-30).

In Waterbouwkundig Laboratorium (2006) the long term sediment transport in the Bay of Heist has been studied; the authors came to the conclusion that the entire beach in Heist (backshore-foreshore-nearshore) is accretional, but locally the trend can be different; while the nearshore is accretional, the foreshore is erosive. It is assumed that the erosion on the foreshore (polygon N° 419), as it was measured with the LIDAR observations, is due to a southward shift of the runnel which is situated South of the accretional sand bank.

This example illustrates the importance of an integrated approach in which not only the sediment balance on the backshore and the foreshore is studied, but also on the

nearshore. The continuum backshore-foreshore-nearshore forms one system. It is well possible that one of the sub-systems is erosive or accretional while the sediment balance of the entire system features the opposite trend. It is therefore recommended to combine the airborne acquisitions with sea-borne measurements that allow to calculate the sediment transport on the nearshore.

Higher on the backshore, one finds the nature reserve of the Bay of Heist. Here, the backshore is largely covered by halophytic vegetation (see Section 2.3 for a description of the vegetation in the Bay of Heist). Airborne hyperspectral remote sensing has recently been applied to classify the vegetation in the Bay of Heist (and in all dune nature reserves along the Belgian coast) in a number of vegetation type classes (Bertels *et al.*, 2005; Kempeneers *et al.*, 2004; Kempeneers *et al.*, 2005c; Kempeneers *et al.*, in press; Provoost *et al.* 2005). There has been little height difference in this area in the period studied. A central basin is at the seaside bordered by a sandy berm; the central basin is flooded during high tide and mud/sand deposition takes place. While in 2000 and 2001 the sediment in the basin was rather muddy, in 2004 it is covered by sand. The sanding is probably caused by a break-through in the berm causing faster flooding and draining of the basin. The shorter sedimentation time causes less mud particles to sediment in the basin.

At the Willemspark and in Duinbergen, the beach is in a dynamic equilibrium. In polygons N° 422 and 423 (located in the foredunes), accretion takes place, mainly due to aeolian transport and deposition. In polygon N° 423, the accretion is also influenced by the yearly berm replenishments, recently executed with sea sand (see Table 8-5). The accretion on the higher backshore continues in polygon N° 425, at the Albertstrand. At the eastern end of this area, the nourishments in Knokke-Zoute add to the accretion of the Albertstrand, however, the amount of nourished sand transported westward is rather small.

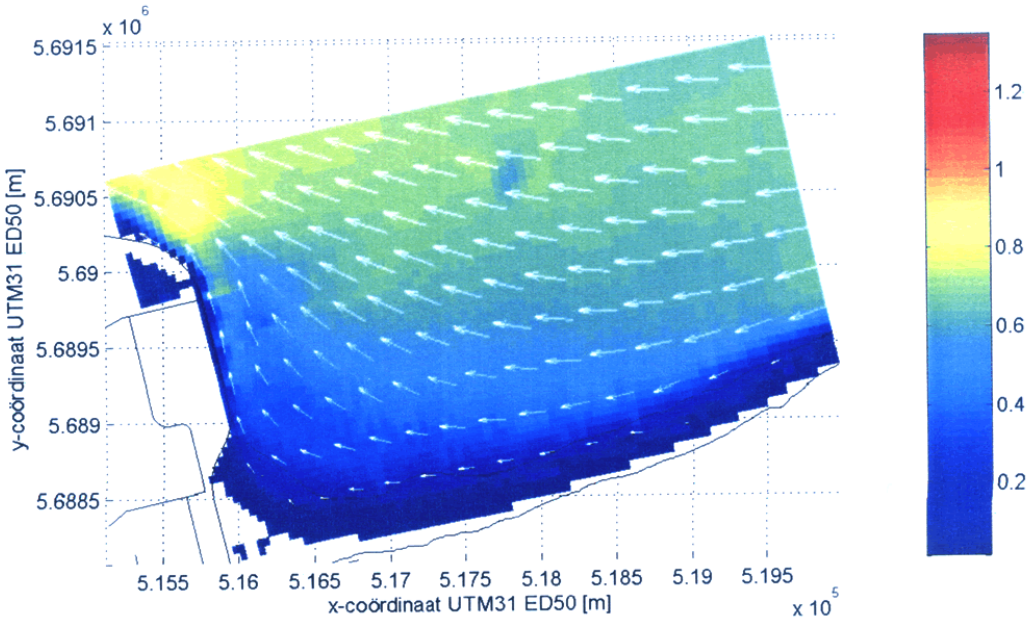

Figure 8-29: Modelled current velocity in the Bay of Heist (in m/s) during falling tide. (Waterbouwkundig Laboratorium, 2006)

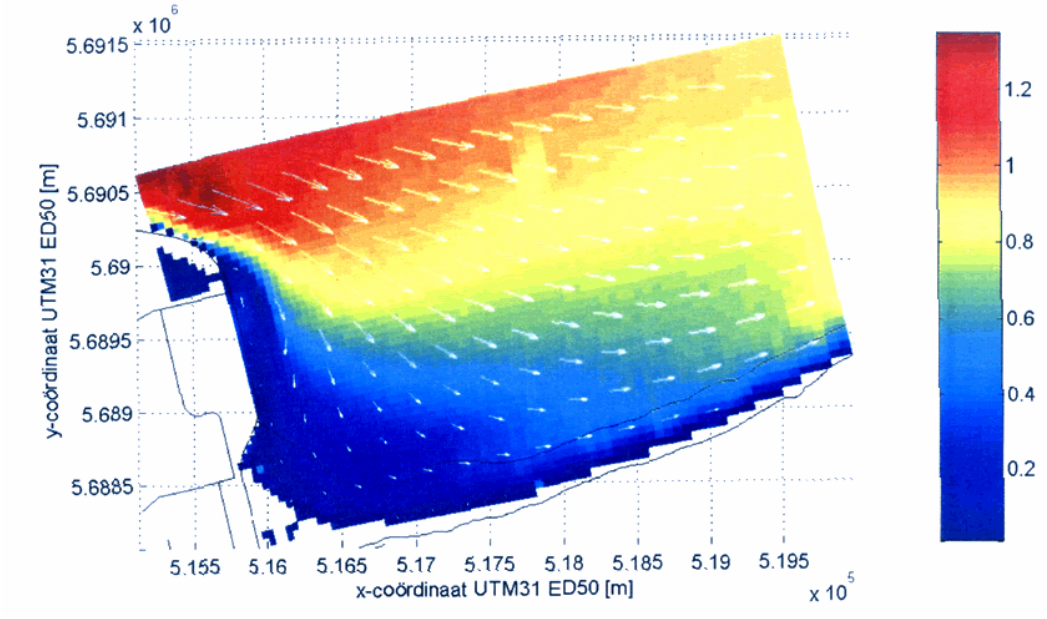

Figure 8-30: Modelled current velocity in the Bay of Heist (in m/s) during rising tide. (Waterbouwkundig Laboratorium, 2006)

To understand the morphological evolution of the beach in the area Knokke-Zoute – Lekkerbek – Zwin, it is indispensable to take into account the nourishment activities that have been executed here during and immediately before our airborne acquisitions. As mentioned earlier (Section 8.3.5.1), in March-May 1999, 486 418 m³ of sea sand was deposited in zone U (Figure 8-28). This nourishment could be mapped with the hyperspectral data of August 2000. In June 2004, the same area was subject to a new nourishment (390 000 m³ of sea sand). The latter took place a few days before the fourth hyperspectral campaign. On Figure 8-32 the effect of the last nourishment is clearly visible. In sections 232 – 236, a broad band (40 m wide) on the backshore and the foreshore was nourished. The top of the fill was brought to 6.2 m TAW. In sections 237 – 244 only a small strip of 20 m wide was nourished. The narrow erosive area landwards of the nourished area represents the natural evolution that took place between December 2002 and September 2004, without the compensating influence of the nourishment. The measured volume difference between both observations was 251 400 m³, while the total nourished volume in June 2004 was 390 000 m³. However, two elements are at the basis of this difference; first of all, when working with a classical pressure-pipeline, a mixture of sand and water is spout on the beach, a certain amount of sand and water runs back to sea. On average, a loss of 15% should be taken into account when applying this technique. Secondly, the LIDAR flight was in Sept. 2004 while the nourishment activities were completed in June 2004. It is well known that the fastest rate of erosion takes place immediately after the fill is brought on the beach.

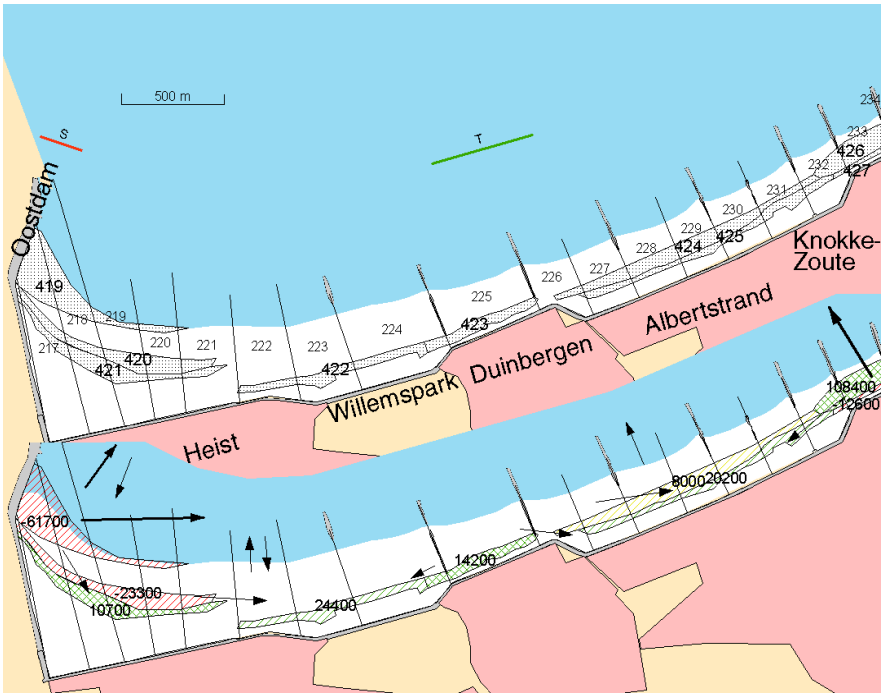

Figure 8-31: Map indicating the major morphodynamic changes between 2000 and 2004. In the upper map one finds the coastal sections with their corresponding number (bordered by lines perpendicular to the coast), the erosion/accretion polygons with their number, and the areas where artificial nourishment activities were executed, indicated with capital letters (green = berm replenishment with sand from the foreshore, red = beach nourishment with sea sand). On the lower map, one finds the amount (in m³) of sediment eroded or deposited in each polygon, as well as arrows indicating the direction and amount of the sediment transport. The pink area indicates the built-up area.

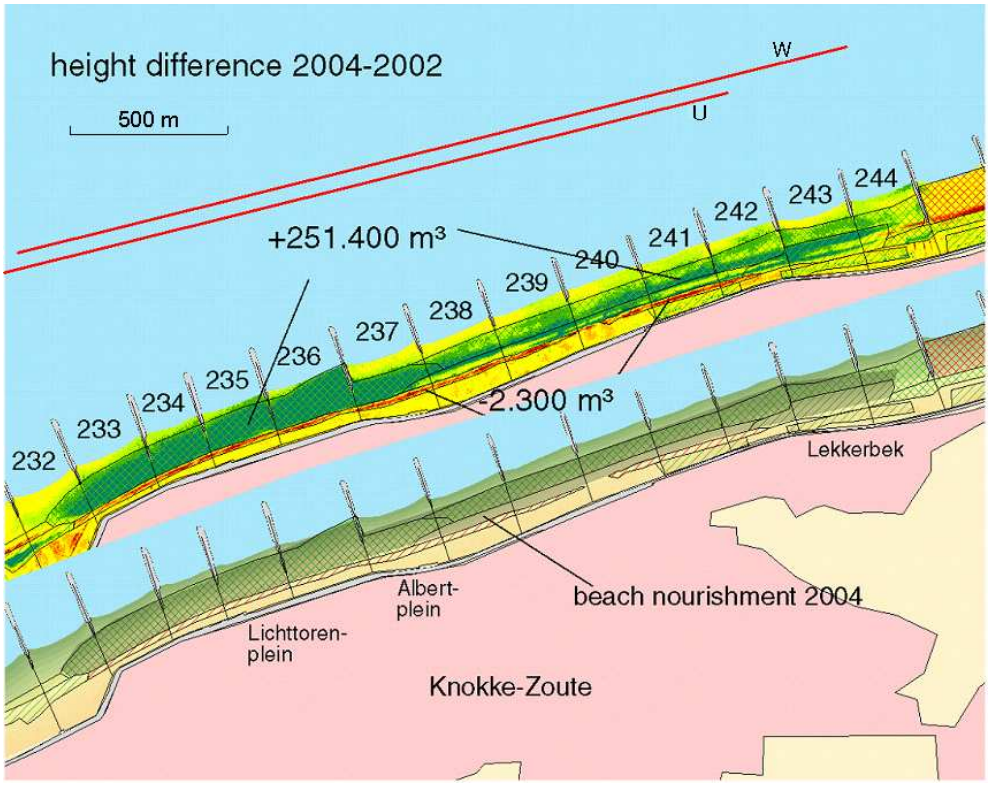

Figure 8-32: Height difference map between Dec. 2002 and Sept. 2004 (top) and height map of Sept. 2004 (bottom) in Knokke-Zoute. The pink area indicates the built-up area.

Figure 8-33 shows the areas with erosion and sedimentation between the observations in 2000 and 2004. The large black arrows indicate the seaward, cross-shore, transport of nourishment sand. Large amounts of the fill were transported to the nearshore, after which they enter in longshore transport processes. Part of it is brought back to the foreshore via cross-shore processes, especially during calm weather conditions. At the landward side, one notices the erosion that took place 'naturally', i.e., independent from the nourishment. In the most eastern sections of Figure 8-33 and Figure 8-34 (sections 245 till 250) the beach was not nourished in 2004 leading to a net loss of more than 45 000 m³ on the foreshore. While the foreshore eroded, the backshore and the dune foot grew with app. 50 000 m³, mainly due to aeolian transport and deposition.

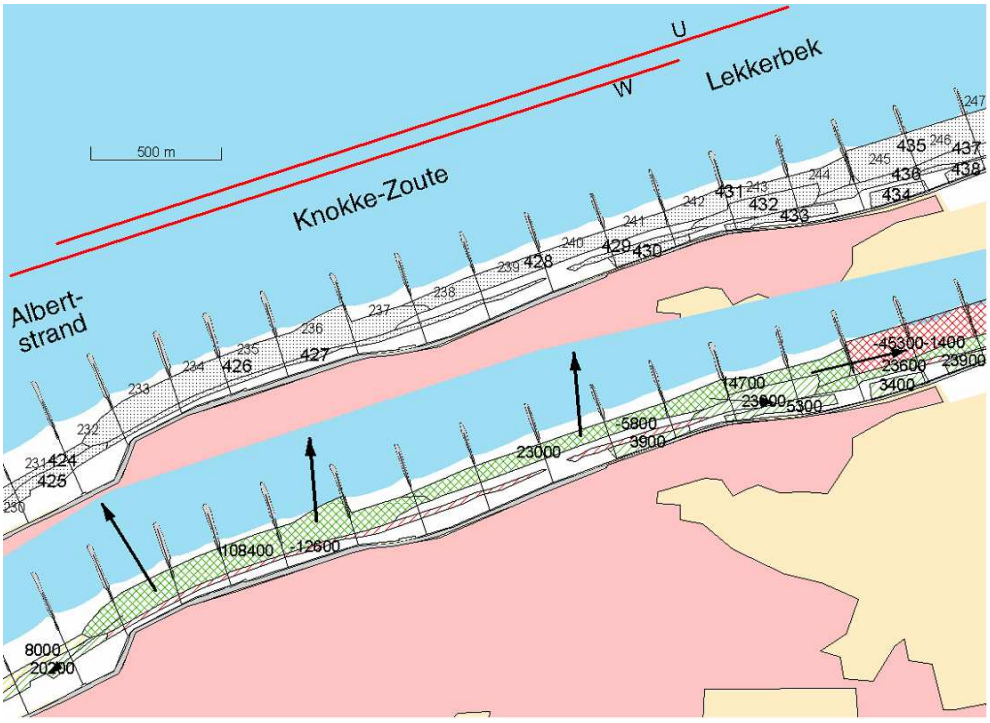

Figure 8-33: Map indicating the major morphodynamic changes between 2000 and 2004. In the upper map one finds the coastal sections with their corresponding number (bordered by lines perpendicular to the coast), the erosion/accretion polygons with their number, and the areas where artificial nourishment activities were executed, indicated with capital letters (red = beach nourishment with sea sand). On the lower map, one finds the amount (in m³) of sediment eroded or deposited in each polygon, as well as arrows indicating the direction and amount of the sediment transport. The pink area indicates the built-up area.

The most eastern sections of the Belgian coast (sections 251 – 257) feature a different beach morphology than the sections West of section 251. They are not protected by groynes and unlike the rest of the East Coast, they have never been nourished. An important reason for the latter is that in sections 255 – 257 the outlet of the Zwin nature reserve is situated. Nourishing this beach would influence and probably fasten the sanding up of the nature reserve, which is not desired. On Figure 8-34 one can see that between 2000 and 2004 the foreshore eroded with more than 100 000 m³, while the dune foot grew with 32 000 m³. The erosion in polygon N° 442 (-54 600 m³) is linked to displacements of the Zwin gully. Finally, it should be noted that the morphological evolution of the Zwin is not only influenced by the human interventions West of the Zwin, in Knokke-Zoute, but also by the works executed on the Dutch side of the border, in Cadzand.

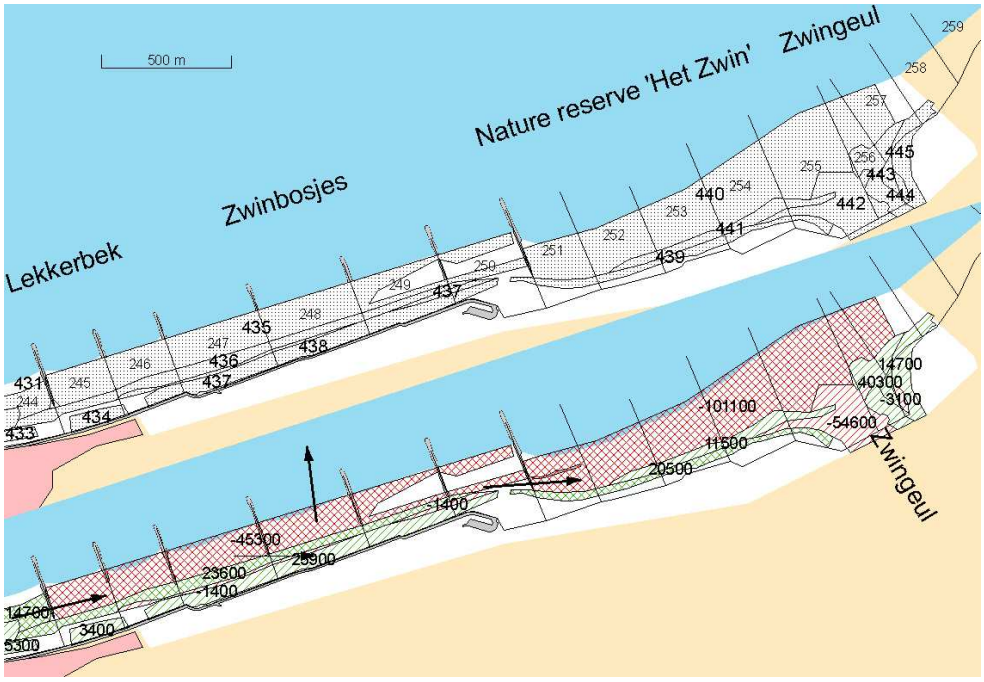

Figure 8-34: Map indicating the major morphodynamic changes between 2000 and 2004. In the upper map one finds the coastal sections with their corresponding number (bordered by lines perpendicular to the coast), the erosion/accretion polygons with their number. On the lower map, one finds the amount (in m³) of sediment eroded or deposited in each polygon, as well as arrows indicating the direction and amount of the sediment transport. The pink area indicates the built-up area.

8.4 Summary of the sediment transport in the period 2000-2006

In this section an overview is provided of the sediment transport as it was observed and calculated it each coastal unit.

French border – Nieuwpoort

Between the French border and Nieuwpoort, the coastline showed accretion between 2000 and 2006. Major accretion took place in Koksijde-Bad, Oostduinkerke-Bad and in Groenendijk-Bad, especially on the backshore and in the foredunes. The accretion continues for over more than 10 years now, but the last LIDAR observation in 2006 indicates that the accretion is halted. Especially between the Westhoek and Sint-Idesbald the beach featured erosion in the period 2004 – 2006. The volume added during the yearly berm replenishments is much smaller than the natural accretion. The

wide intertidal beach forms a very effective seawall and is therefore responsible for the accretion on the backshore and in the foredunes.

Nieuwpoort – Oostende

The coastal unit between the IJzermonding and the harbour channel of Oostende is erosive, but in most places berm replenishments and beach nourishments compensate for the natural erosion. Between the IJzermonding and the military base of Lombardsijde erosion continues; it was expected that the erosion would stop once an equilibrium state was attained around the extended groynes in Nieuwpoort. However, despite the new equilibrium state in Nieuwpoort, the erosion in Lombardsijde continued. The conclusion could be that the mouth of the river IJzer is an effective barrier for the longshore transport from the West and hence hampers the supply of sediment via longshore transport in Lombardsijde. The erosion, mainly due to cross-shore transport directed seawards, is not only reported in Lombardsijde, but is seen in the entire coastal unit between Nieuwpoort and Oostende. However, the yearly berm replenishments compensate for the natural losses; there is a small net positive balance. An exception is the beach in Sint-Laureins (Westende); this beach tends to grow slowly, probably as a result of the groynes which were extended in the beginning of the 90s. The last observation in 2006 indicates that the accretional trend might be halted in the next years. Thanks to the relative wide, accretional beach, the foredunes grew steadily in Sint-Laureins.

The centre of Oostende was in April-June 2004 subject to an important beach nourishment. Before the nourishment, there was no dry beach anymore in Oostende, i.e., at high tide the sea dike immediately served as seawall. The fill was easily detectable on the hyperspectral data. However, already in July 2004, it was clear that the fill was being reworked. Shells were washed out and temporarily stocked on the foreshore, while on the backshore a 'white band' was formed, parallel to the coastline. The bright colour is mainly due to the absence of shells in this band. The eroded sediment supplied the 'Klein Strandje', located East of the nourishment area, and to a lesser extent also the 'Groot strand', located West of the nourishment area. In 2005, a first 'maintenance nourishment' was executed in order to compensate for the initial erosion during the first year after the nourishment. In 2006, no extra nourishment was necessary.

Oostende – Blankenberge

Between the harbour channels of Oostende and Blankenberge, the beach was in a morphodynamic equilibrium state. In Bredene, half of the amount, supplied via berm replenishments (app. 45 000 m^3), remained in or was transported to the foredunes, while the other half was transported seaward. The beach of Bredene does not benefit from the large-scale nourishments in De Haan. In the nourishment area around De Haan, the seaward side of the dry beach berm is eroded. The eroded material is temporarily stocked on the foreshore after which it is transported to the nearshore. On the dry beach berm, aeolian transport occurs; the sand is transported towards the

foredunes and deposited between artificial wooden fences ('rijshouthagen'). The resulting sediment balance of the foredunes is positive. The amount deposited in the foredunes is approximately half of the amount eroded on the backshore and foreshore. The intensity of the erosion decreases from the West to the East: in the period 2000-2006, the total net erosion between Hippodroom and De Haan-Centre was app. 140 000 m³. Between De Haan-centre and Wenduine-Rotonde, there was in the same period a positive balance (+ 106 000 m³). The sand class maps indicate that the main sand transport directions are cross-shore; few nourishment sand is transported longshore, outside the nourished area.

Note however that the amounts of sand eroded in De Haan are rather small; this can probably be attributed to the nearshore berm which was created simultaneously to the backshore nourishment works. The berm acts as an underwater barrier, preserving the beach from fast cross-shore erosion.

In Wenduine, the backshore is yearly nourished via berm replenishments. The seaward side of the berm is eroded and needs yearly maintenance to remain at the same location. The foredunes between Wenduine and the harbour channel of Blankenberge grew, but less fast than the foredunes immediately West of Wenduine. The beach between Wenduine and Blankenberge is in a dynamic equilibrium. There is no significant influence or supply from the nourished area around De Haan.

Blankenberge – Zeebrugge

Between 1980 and 1990 the beach in Blankenberge was clearly accretional. The reasons hitherto where threefold: the extension of the groynes in Blankenberge (in 1985 – 1986 and 1991), the deposition of dredged material out of the harbour channel in the sections immediately East of the channel and thirdly, the yearly berm replenishments. Recently, the accretion turned into erosion because the deposition of dredged material was stopped and because a new equilibrium state was attained after the extension of the groynes. The berm replenishments continue until today. In 2000, the level of the foreshore was app. 20 cm lower than in 2006. The backshore remained stable thanks to berm replenishments (often with sand from the intertidal beach). The nourished berm at the Duinse Polders eroded, especially at its seaward side. The classified hyperspectral scenes indicate that the backshore East and West from the nourished berm was fed with nourishment sand. However, the main erosion was directed seaward; fractions of the fill were found on the foreshore seaward of the nourished berm, but also eastward on the foreshore in Zeebrugge. In Zeebrugge, longshore transport processes were responsible for the formation of a wide accretional beach, clearly illustrating that the net longshore transport at the Belgian coast is directed from the West to the East. Between 2000 and 2006, the beach in Zeebrugge grew yearly with 85 000 m³ and the foredunes with another 9 000 m³. The beach in Zeebrugge is therefore suited (and already used) as sand dredging area, but the sand sedimented on the foreshore is rather fine-grained and hence not ideally suited for nourishment works.

Zeebrugge – Zwin channel

In contrast with the beach in Zeebrugge, the wide beach in Heist is not natural. It was formed during several nourishment activities in order to compensate for the erosion that was expected to occur after the construction of the harbour dams. Between 2000 and 2006, the total erosion was 112 000 m³ or app. 19 000 m³ per year. The morphological evolution indicates both cross-shore transport to the nearshore and longshore transport to the East. The top sediments in the nature reserve of the Bay of Heist shifted from muddy to mainly sandy, probably as a result of the faster drainage of the basin in the nature reserve. The beach of Knokke-Zoute is one of the most erosive units along the Belgian coast. After the 'mother nourishment' of 1977 – 1979, three maintenance nourishments were needed: in 1986, 1999 and 2004. Between the consecutive nourishments, major erosion was measured, not only at the seaward berm of the nourished berm, but also on the foreshore. The latter is triggered by the Appelzak, a tidal gully situated immediately offshore from Knokke-Zoute and the Lekkerbek. While in 1900, the gully was located 1 km from the sea dike, in 1930 it was already at 300 m from the sea dike (Huygens, 2001). Later on, groynes were constructed which prevented a further landward shift, but a deepening (and a westward extension) of the Appelzak could not be prevented. The Appelzak is the main reason for the fast erosion in Knokke-Heist. Sand eroded on the back- and foreshore, and transported to the nearshore, enters in the tidal gully after which it is transported longshore by tidal currents. Hence, the eroded sand does not form a barrier on the nearshore from where it nourishes the beach during calm weather conditions. As a result, the beach remains rather narrow and is steeper than at the Middle and West Coast. A narrow, steep beach provides less efficient protection than a wide beach across which spilling breakers dissipate their energy. The result of all this is that the life-time of nourishments in Knokke-Heist is significantly shorter than elsewhere.

A detailed analysis of the erosion problematics in Knokke-Heist can be found in Huygens (2001) who focused on the nourishment of 1986 and compared field measurements with laboratory simulations and a mathematical modeling approach.

Although the main transport is directed seaward, the sand class maps indicate also the occurrence of longshore transport processes along the high water mark. The above mentioned fast erosion in Knokke-Zoute necessitates a renourishment of the beach at least every 5 years, in case no heavy storms occur. In 2006, 55% of the fill of the nourishment of 2004 was already eroded. This implies an average erosion rate of 100 000 m³ in the first two years after the nourishment. Between 2000 and 2004, an average erosion rate of 45 000 m³ per year was measured.

Finally, it should be noted that the foredunes in Knokke-Zoute grew in the period studied. Despite the erosive backshore and foreshore, the accretional foredunes add to the general strength of the seawall.

Chapter 9

Discussion

9.1 The beach dynamic behaviour in the period 2000 – 2006

If one integrates all volume differences between 2000 and 2006 for the entire beach and foredunes, it can be concluded that the beach grew with 209 700 m³ and the foredunes with 1 132 400 m³. I.e., a net positive balance. Taking into account the surface of the beach and the foredunes, this comes down to a raising of the beach with 1,5 cm and a raising of the foredunes with 37,6 cm. Hence, the foredunes grew significantly while the beach level didn't change at all. However, these numbers include all nourishment activities. Looking back to large beach nourishments executed in Oostende (575 000 m³ in 2004 on the backshore and the foreshore) and in Knokke-Zoute (390 000 m³ in 2004 on the backshore and the foreshore), it becomes clear that the positive balance was only achieved due to large-scale human interventions. It is difficult to estimate the exact volume differences without the nourishment activities, as the latter influence the dynamic behaviour of the beach, but there would probably be a loss between 1 000 000 m³ and 1 500 000 m³ for the beach. For the foredunes, the calculation is even more difficult as the nourished beaches protect the foredunes and hence stimulate their growth (see below). However, it can be assumed with high certainty that also the growth of the foredunes would be much smaller without the nourishments. The positive conclusion is that the measures taken prove to be sufficient to maintain the safety level of our sea wall, under the conditions observed between 2000 and 2006. The somewhat more troublesome conclusion is that the measures were and probably will remain necessary. Without these interventions the Belgian coastline would feature severe erosion, even in a period without severe storms.

The beaches which were most affected by erosion are mainly situated along the Middle and East Coast, amongst which the beaches of Knokke-Zoute, the Duinse Polders, and

a large area around De Haan, being the large-scale beach nourishment areas, featured the most severe erosion. The only accretional beaches were found in Zeebrugge, Sint-Laureins and the centre of Koksijde. These results confirm to a large extent previous research conducted by De Wolf *et al.* (1993), although some small differences were observed: in De Wolf *et al.* (1993) the beach of Nieuwpoort was strongly accretional due to the construction of new groynes in 1978 – 1979. In our study, this beach was still accretional (due to an extension of the groynes in the 90s) but the rate of accretion slowed down especially in the last two years of observation (between 2004 and 2006). The latter can probably be attributed to the new equilibrium state which is being attained around the new groynes in Nieuwpoort. Another difference was observed in Blankenberge, where the beach featured accretion in the 80s and in the beginning of the 90s, turning to erosion between 2000 and 2006. This recent erosive trend can probably be attributed to the stopping of the deposition of dredged material on the back- and foreshore, and to the fact that a new equilibrium state was attained after the extension of the groynes. A last remarkable difference between the observations made in the 80s and 90s and our recent observations is the erosive trend of the beach in the Bay of Heist. However, the accretion in the 80s and 90s was due to nourishments that had to counter the erosion after the construction of the harbour dams of Zeebrugge. The erosion we observed between 2000 and 2006 represents the 'expected' evolution of this beach.

As stated above, the foredunes grew in many places. This is remarkable as many beaches in front of the foredunes were erosive and as a prerequisite for dune growth is a stable or accretional beach. In theory, if the beach is erosive, it is unlikely that the foredunes grow. However, the observation of growing dunes can probably be attributed to the artificial nourishment of many beaches, creating wide fore- and backshores. Following the nourishment, the foreshore part suffers erosion while the wide backshore continues to feed the dunefronts. Another explanation for the growing dunes are the meteorological conditions in the period studied; no major storms were recorded in these years. It is very likely that a severe storm could drastically alter the accretional trend of the dunes as the erosive beach does not provide an effective barrier.

Looking back to the analysis made in the previous chapters, it was observed that the sediment dynamics along the Belgian shoreline seem to operate in separated shore stretches. The boundaries of these stretches appear to be natural or man-made structures. E.g., in Lombardsijde, the erosion continued even after a morphological equilibrium was attained around the extended groynes in Nieuwpoort, while it would be expected that once an equilibrium state was attained, the supply from the West would stop or slow down the erosion in Lombardsijde. The latter was not the case, indicating that the IJzermonding is an effective barrier against the longshore transport. A similar conclusion could be drawn in Oostende where the recent nourishment does not feed the beach eastward of the harbour channel (in Bredene). Even without large structures, it was observed that most of the sediment remained in a limited area and was not transported over large distances along the coastline. This is the case around De Haan; the nourished sand remained largely in the nourishment area instead of being

transported eastward or westward. Also the small change in orientation of the coastline at the rotunda of Wenduine appeared to be sufficient to limit the longshore transport (or to redirect it seawards). These observations call to mind to the principle of coastal cells[12] as defined by Motyka and Brampton (1993). It remains an open question whether these cells would also exist without the structures limiting the longshore drift, but there are at least indications that this would be the case.

The indications of coastal cells contradict other overwhelming evidence for longer-term, net longshore transport from the West to the East. Accretion of the beach in Zeebrugge goes on linearly with time, ever since the construction of the harbour dams in the 1980s. The present study points to the importance of nearshore transport in the longshore processes, as the direct contribution via the foreshore and backshore, indicated by the evolution in the Duinse Polders nourishment area, involves insufficient net volumes of sand to account for the large-scale accretion in Zeebrugge.

As mentioned, the Belgian shoreline is far from natural. Almost the entire coastline is protected by man-made structures. In general, it was observed that these structures have the desired effect on the beach dynamics: they weaken the erosive forces and stimulate accretion. However, a remark should be made regarding the construction or extension of groynes. It was observed that groynes have a beneficiary effect on the beach situated in between and immediately around the groynes, but the beach situated downdrift (mostly eastward) of the groynes experiences a negative effect, at least in the first years (up to 15 years) after the construction. This has very well been observed in Koksijde-Bad where the construction of two groynes resulted in accretion around the groynes, whereas 1.5 km eastward (at the Schipgat duinen), the foreshore and backshore lowered, giving the secondary effect of dune foot erosion. Only now, more than 15 years after the construction of the groynes, an equilibrium state seems to be attained and the erosion is halted. To prevent this adverse effects of groynes, it should be considered to limit the length of the groynes. Even short groynes constitute a barrier to the longshore transport but the negative effects downdrift would be limited. Obviously, the negative and positive effects are inextricably connected, hence, a compromise will always have to be made.

Another example of the influence of man on the Belgian coast is found around the harbour of Zeebrugge. While the western dam acts as an almost absolute barrier to the longshore transport from the West to the East, the effect of the eastern dam is rather complex. During the falling of the tide, a westward drift causes accretion at the eastern dam. But also during the rising tide, accretion is measured as a result of the currents entering the bay. The sheltered position of the bay causes sedimentation in the bay (Waterbouwkundig Laboratorium, 2006). The latter is manifested by the raising of a shoal (locally nicknamed ‘Verwilghen-bankje’) on the nearshore. Despite this, our observations revealed foreshore erosion. This seems contradictory to the accretion on

[12] A coastal cell is a compartment of coastline, divided from neighbouring sections of coast in terms of longshore drift, current flow, and wave convergence and divergence.

the foreshore, but it may be explained by a landward shift of a runnel situated at the low water mark. The net volume change of the whole continuum of backshore-foreshore-nearshore appears to show accretion. This observation supports the need for an integrated approach in which airborne observations are coupled with seaborne measurements (see further).

9.2 Hyperspectral remote sensing for beach monitoring

It is beyond dispute that airborne imaging spectroscopy opens new possibilities for sediment transport studies along sandy beaches. The classical approach, using only LIDAR data, does not allow to make a qualitative analysis of the sediment transport. The novel aspect in this research was the classification of the beach in sand type classes that are spectrally distinguishable and are linked to the geomorphology of the beach. These classes are used as a tracer to monitor the sediment dynamics. An important element in the classification methodology is the 'reproducibility' of the classifications, i.e., applying the same classification strategy and the same training data, the researcher will always obtain the same results. Moreover, the methodology remains unchanged, i.e. there is no need to 'tune' the classifier in an interactive way for each airborne data set. The only new input needed for each airborne data set are the corresponding ground truth data.

However, some remarks have to be made regarding the technique used and the methodology applied. As mentioned, the hyperspectral data can only distinguish classes that feature a unique spectral signature. An important class that we wanted to monitor was beach nourishment sand. As most nourishments along the Belgian shoreline make use of sea-sand (dredged on offshore banks) and as this type of sand differs in grain size, shell content and mineralogical composition from the sand naturally found on the beach, it was possible to classify beach nourishment sand as a separate class. However, beach nourishments or beach scrapings, executed with sand borrowed from the beach itself (cf. re-profiling) are much more difficult to detect. Although dry beach scrapings have an important geomorphological impact on the beach, it proved difficult to distinguish the areas involved. Hence, the mapping of geomorphological units is limited to those units that feature a different spectral behaviour. To some extent, the combination of the hyperspectral data with the LIDAR data can overcome this limitation, e.g., the LIDAR data allows to delineate areas with an anomalous topography even if the spectral characteristics of the sediment are the same. Another example of the limitations of a technique based on spectral discrimination, is the detection of shell-rich sand. Areas nourished with sea-sand are often (not always) shell-rich, but there are also concentrations of shells, often in linear strips along the margins of banks, that are not linked to nourishments. Hence, the classes 'shell-rich sand' and 'beach nourishment sand' are often mixed in nourishment

areas, while it could be that shell-rich areas are wrongly interpreted as nourishment sand.

Another difficulty, inherent to the spectral technique applied, we had to cope with, was the reworking of the fill in nourished areas. Immediately after a nourishment, the fill starts to be reworked due to the action of wind and water. Fine particles are blown away or washed out, while coarser particles remain in situ. It was also observed that at the high water mark (in case of dry beach nourishments), the fill was eroded during high tide (or storm events) leading to a relative concentration of shells which are deposited on the lower parts of the beach during the backwash. Another remarkable feature in nourished areas that are subject to reworking, was the formation of a 'white band' at the high water mark. The latter could very well be observed in the fill of Oostende (A on Figure 9-1) where a hyperspectral image was taken in July 2004, i.e., a few weeks after the nourishment activities. Note also the concentration of shells on the intertidal beach (B on Figure 9-1); this is a temporary stock after which the shells are transported offshore or longshore. In conclusion, the reworking of the fill may render the interpretation of the classified hyperspectral data difficult as the reworked sediment does not always correspond to the sediment types used as training for the classifications.

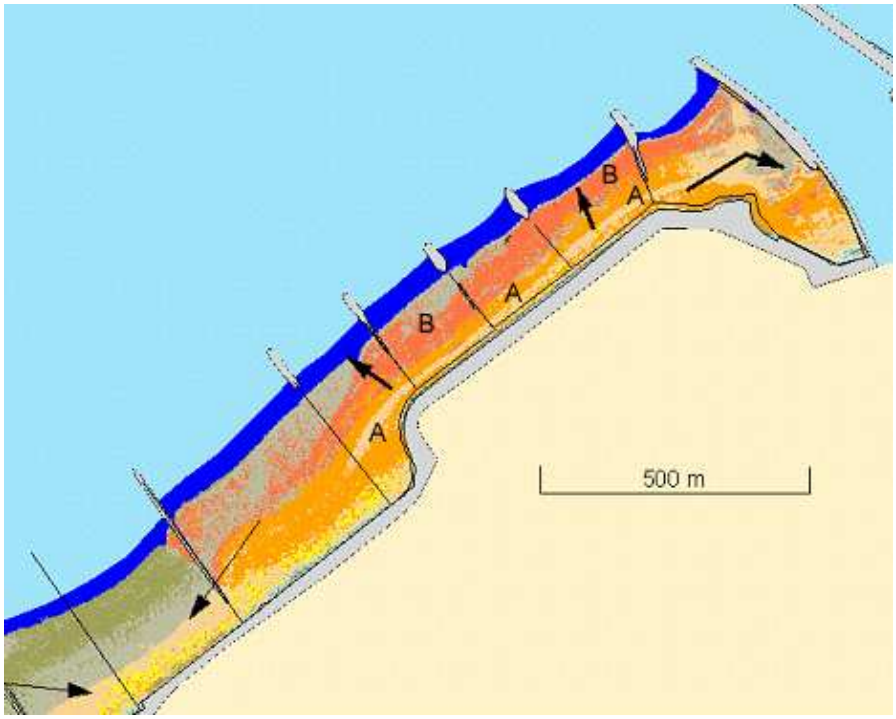

Figure 9-1: Sand class map of July 2004, focusing on the beach nourishment in the centre of Oostende. The arrows indicate the main sediment transport directions.

An important remark that should further be made when applying imaging spectroscopy to beach monitoring is that this technique maps only the very surface, i.e. the upper millimeters of the substrate. The electromagnetic radiation is either reflected at the top of the surface or absorbed; the amount of radiation that is reflected by deeper substrate layers is negligible. Hence, one can only derive information from the top layer. Conclusions on the deeper layers can only be made indirectly. This is an important element that had to be taken into account throughout the whole of this research. Field knowledge of the longer term processes is needed to interpret the top layer in connection with the deeper layers. One top layer class may be the result of different processes, e.g., a shell-rich coarse-grained top layer is often found in nourished areas where the deeper layers contain the same type of sediment, but the same top layer can also be observed as a deflation pavement where it is caused by beach lowering processes that result in a concentration of the heavier and coarse-grained fractions. There is no straightforward methodology to judge on the composition of the deeper layers, but sound field knowledge helps to extrapolate the observations, made at the surface, to the deeper layers.

Finally, it should be mentioned that, without denying the possibilities of airborne imaging spectroscopy, a high number of small spectral bands is not always needed to obtain good classification accuracies (see Chapter 6). A few broad bands proved to be sufficient to obtain the desired classification accuracy. However, in the SFFS algorithm used, a feature selection is performed for each binary classification. Hence, in total more than 2 or 3 bands are used to obtain the high accuracies. However, it was observed that the bands selected are often the same bands, and on top of that it does not matter if a band is substituted for its neighbouring band, due to the high correlation between adjacent bands. With these elements in mind, we would advise to use for this type of application a hyperspectral sensor covering only the VNIR part of the spectrum and configured with only 10-20 bands, in favour of the spatial resolution. It is our conclusion that more useful and equally accurate beach sand classifications can be obtained by trading spectral for spatial resolution (especially when the number of training samples is restricted). This is also in favour of the costs of an airborne hyperspectral campaign since the deployment of a SWIR sensor is more expensive than a VNIR sensor.

9.3 Future monitoring strategy

The previous paragraph brings us to the topic of monitoring strategies. It is evident that it would be interesting to have many more frequent airborne acquisitions (e.g., monthly acquisitions). This would allow for an analysis of the short-term beach dynamics. For example, the effect of seasonal weather conditions could be analysed. Although very interesting, these short term variations were beyond the scope of this research. We intended to focus on the longer term dynamics as these longer time scales are more

relevant for erosion and beach management issues. Therefore, we are convinced that one yearly observation is sufficient to study the sediment dynamics in the longer term; but, to exclude seasonal variations in the data set, this observation should preferably be taken in the same season.

Today, it is not possible to set up a monitoring strategy with frequent acquisitions at a short time interval as this would be extremely expensive. Both hyperspectral and LIDAR data are nowadays only available from airborne platforms. There are currently two hyperspectral satellites in orbit, but the radiometric quality (and the spatial resolution) is rather poor. Moreover, their fixed orbit is not compatible with observations bounded by meteorological and tidal constraints. Therefore, expensive airborne acquisitions are the only option left today. However, new platforms and sensors are being built; by 2009-2010 a new generation of hyperspectral satellite sensors should become operational. They will have an increased radiometric performance, but will still be limited from an operational point of view. To overcome this, entirely new platforms are being developed: Unmanned Aerial Vehicles (UAV) cruising in the stratosphere for several weeks or even months will drastically reduce the cost of airborne campaigns without losing the operational flexibility characteristic of airborne surveys (For more information see http://www.pegasus4europe.com). It is expected that these new platforms, which in a later stage will also be designed to carry active systems like LIDARs, will announce a new era of coastal surveys, allowing an almost continuous and cost-effective monitoring strategy.

A final remark that we want to stress is the need for an integrated approach covering the morphological continuum dunes-beach-nearshore. Similar studies as the one we conducted are being executed on the nearshore, applying seaborne remote sensing techniques (e.g., sonar and single/multibeam). These studies also aim at delivering sediment maps and the area they focus on is physically connected to the beach system we studied. We both have to cope with an open boundary as a result of the practical limitations of the observation techniques applied. To be able to study the sediment transport to its full extent, it is an absolute requirement to couple airborne or spaceborne measurements with seaborne measurements. While writing this, the first steps are being taken to start up a joint research project in this direction.

Conclusions

Airborne hyperspectral data and airborne LIDAR data were used to study the sediment dynamics along the Belgian shoreline in the period between 2000 and 2006. Prior to the geomorphologic analysis, tests were performed to compare different classification strategies, applied on the hyperspectral data. AISA data, featuring 32 bands and 1 m ground resolution, were used to test the different classification strategies. Due to the type of sand used to perform the beach nourishments, the technique proved to be especially suited to map beach nourishment areas and to follow-up their dynamic behaviour. The best classification results were obtained applying a Linear Discriminant Analysis (LDA) in combination with feature selection by means of Sequential Floating Forward Search (SFFS). Transformation of the original bands into wavelet coefficients significantly improved the accuracy. Using a small number (two to three) of wavelet coefficients, a Kappa of 0.80 could be obtained for 7 sand type classes. The non-statistical SAM algorithm was also tested and scored somewhat lower (Kappa of 0.71) than LDA. Consequently, the LDA algorithm was run on artificially broadened bands; this test showed that, for this application, narrow bands are not needed to obtain good classification accuracies: it was possible to broaden the bands from 2.2 nm up to 55.0 nm without losing classification accuracy. Hence, a limited number of broad bands proved to be sufficient to obtain good classification accuracies in this application. HyMap data were used to test the hypothesis that a VNIR sensor is sufficient to classify sandy shorelines. It was shown that nearly the same classification accuracy could be obtained using the VNIR range than the SWIR range or the whole VNIR+SWIR range, which leads to the recommendation to deploy a common VNIR sensor for this type of applications.

The LDA classification algorithm, in combination with SFFS, was also applied to classify the sandy and muddy sediments on the Molenplaat in the Westerschelde into sediment habitat classes. The overall weighted accuracy was highest for the water content (88%), the median grain size (88%) and the chlorophyll-a concentration (84%). The organic matter content scored somewhat lower with 80%. These four parameters

were used to define sediment habitat types which can serve as input for more detailed biological or sedimentological studies.

The ultimate goal of this thesis was the analysis of the sediment dynamics along the Belgian shoreline, making use of the classified hyperspectral data and LIDAR derived DTMs over the period 2000 - 2006. Subtracting sequential DTMs resulted in height difference maps indicating the erosion and accretion zones. While LIDAR data only offer topographical information, the classified hyperspectral data were used as tracer for the sediment transport. The combination of all data layers allowed analysing the sediment transport directions. The methodology was applied in five distinct units, most of them limited by harbour dams or harbour channels, which allowed to treat each unit as a more or less closed system. In summary, it could be concluded that the beach in the period studied was in most places stable (i.e., less that 25 cm accretion or erosion) or erosive. The beaches which were most affected by erosion are mainly situated along the Middle and East Coast, among which the beaches of Knokke-Zoute, the Duinse Polders, and a large area around De Haan featured the most severe erosion. The only accretional beaches were found in Zeebrugge, Sint-Laureins and the centre of Koksijde. However, each of these accretional beaches could be linked to human interventions. The overall natural tendency was erosive. Unlike the beach, the foredunes, i.e., the dunes immediately landward of the beach, grew or remained stable in most places. Only at the Middle Coast, between Westende and Oostende, the foredunes were erosive. A detailed analysis was performed for each unit separately and particular attention was paid to the sediment transport directions; hereto all available data layers originating from the LIDAR and hyperspectral data were combined in a GIS and an integrated analysis was performed.

The following paragraphs resume the most important conclusions drawn for each coastal unit:

Between the French border and Nieuwpoort, the coastline showed accretion between 2000 and 2006. However, the LIDAR observation of 2006 indicates that the accretion is halted. Especially between the Westhoek and Sint-Idesbald the beach featured erosion in the period 2004 – 2006. The wide intertidal beaches at the West Coast form an effective seawall and are therefore responsible for the accretion on the backshore and in the foredunes.

Unlike the westernmost part of the Belgian shoreline, the coastal unit **between the IJzermonding and the harbour channel of Oostende** was erosive. However, in most places berm replenishments (or beach scrapings) and beach nourishments compensated for the natural erosion. The only accretional beach in this unit, is the beach of Sint-Laureins (Westende). The accretion was probably the result of the extension of the groynes, executed in the beginning of the 90s. The last LIDAR observation in 2006 indicated that the accretional trend might be halted in the next years. The centre of Oostende was in April-June 2004 subject to an important beach nourishment. The fill could easily be detected on the hyperspectral data. However, already in July 2004, it was clear that the fill was being reworked and eroded. The eroded sediment supplied

the 'Klein strandje', located East of the nourishment area, and to a lesser extent also the 'Groot strand', located West of the nourishment area. With the available data, the influence of the underwater gravel berm and the possible sink function of the harbour access channel could not be assessed. Hereto, a coupling with nearshore data is needed.

Between the harbour channels of Oostende and Blankenberge, the beach was in a morphodynamic equilibrium. In the nourished area around De Haan, the seaward side of the dry beach berm was eroded. The eroded material was temporarily stocked on the foreshore after which it was transported to the nearshore. On the dry beach berm, aeolian transport occurred; the sand was transported towards the foredunes and deposited between artificial wooden fences ('rijshouthagen'). The resulting sediment balance of the foredunes was positive. The sand class maps indicated that the main sand transport directions were cross-shore; few nourishment sand was transported alongshore outside the nourished area. Despite the erosion of the nourished berm, the amount of sand eroded in De Haan was rather small compared with the volumes supplied: this may be due to a beneficiary effect of the nearshore berm. The beach between Wenduine and Blankenberge was in a dynamic equilibrium. There was no significant influence or supply from the nourished area around De Haan.

The small unit **between Blankenberge and Zeebrugge** was clearly accretional between 1980 and 1990. The reasons were threefold: the extension of some groynes in Blankenberge (in 1985 – 1986 and 1991), the deposition of dredged material out of the harbour channel in the sections immediately East of the channel and thirdly, the yearly berm replenishments. Recently, the accretion turned into erosion probably because the deposition of dredged material was halted and because a new morphological equilibrium state was attained after the extension of the groynes. The nourished berm at the Duinse Polders eroded, especially at its seaward side. The classified hyperspectral scenes indicated that the backshore East and West of the nourished berm was fed with nourishment sand. However, the main erosion was directed seaward; fractions of the fill were found on the foreshore seaward of the nourished berm, but also eastward on the foreshore in Zeebrugge. In Zeebrugge, longshore transport processes were responsible for the formation of a large accretional beach. This process has been going on ever since the new harbour dams were constructed around 1980. Between 2000 and 2006, the beach in Zeebrugge grew yearly with 85 000 m³ and the foredunes with another 9 000 m³.

In contrast with the beach in Zeebrugge, the wide beach in **Heist** is not accretional. Between 2000 and 2006, 112 000 m³ of sand (or app. 19 000 m³ per year) was eroded here. The morphological evolution indicated both cross-shore transport to the nearshore and longshore transport to the East. The beach of **Knokke-Zoute** confirmed to be one of the most erosive units along the Belgian coast. Although the main transport was directed seaward, the sand class maps indicated also the occurrence of longshore transport processes along the high water mark. The fast erosion in Knokke-Zoute necessitates a renourishment of the beach approximately every 5 years, in case no heavy storms occur. In 2006, 55% of the fill of the nourishment of 2004 was already

eroded. This implies an average erosion rate of 100 000 m³ in the first two years after the nourishment. Between 2000 and 2004, an average erosion rate of 45 000 m³ per year was measured. Finally, it should be noted that the foredunes in Knokke-Zoute grew in the period studied. Despite the erosive backshore and foreshore, the accretional foredunes add to the general strength of the seawall.

To conclude, we would like to highlight the potential of the airborne data collected for modelling studies. The spatially continuous data sets, covering six years, can be used to calibrate and validate morphodynamic models. The latter are -among others- used by the Flanders Hydraulics Research Laboratory (http:// watlab.lin.vlaanderen.be/) to study the dynamic behaviour of the Belgian coastline and to judge on the hard and soft defence structures needed to maintain the desired safety level at our coastline. While the LIDAR data are very suited in these morphodynamic models, the hyperspectral data can be used in ecological habitat studies, as it was demonstrated on the Molenplaat.

References

Armitage R.P., Kent M. and R.E. Weaver, 2004, Identification of the spectral characteristics of British semi-natural upland vegetation using direct ordination: a case study from Dartmoor, UK. *International Journal of Remote Sensing*, 25(17): 3369-3388.

Azuaje F., 2003, Genomic data sampling and its effect on classification performance assessment, *BMC Bioinformatics*, 4:5.

Baeteman C., 1981, De Holocene ontwikkeling van de Westelijke Kustvlakte (België). PhD Thesis, VUB, Brussel (Belgium), 297 pp.

Baeteman C., 1991, Chronology of coastal plain development during the Holocene in West Belgium. *Quaternaire*, 2: 116-125.

Baeteman C., 1999, The Holocene depositional history of the IJzer palaeovalley (Western Belgian coastal plain) with reference to the factors controlling the formation of intercalated peat beds. *Geologica Belgica*, 2: 39-72.

Baeteman C., 2007, De ontstaansgeschiedenis van onze kustvlakte. *De Grote Rede*, 18: 2-10.

Baeteman C. and P.Y. Declercq, 2002, A synthesis of early and middle Holocene coastal changes in the Western Belgian lowlands. *Belgisch Tijdschrift voor Geografie*, 2: 7-107.

Bagnold R.A., 1941, *The Physics of Blown Sand and Desert Dunes*. Chapman and Hall: London (UK), 265 pp.

Baltsavias E.P., 1999, Airborne laser scanning: basic relations and formulas. *ISPRS Journal of Photogrammetry and Remote Sensing*, 54: 199-214.

Bastin A., 1974, Regionale sedimentologie en morfologie van de zuidelijke Noordzee en van het Schelde estuarium. Onuitgegeven PhD thesis, Katholieke Universiteit Leuven, Leuven (Belgium), 91 pp.

Baumgardner M.F., Silva L.F., Biehl L.L. and E.R. Stoner, 1985, Reflectance properties of soils. *Advances in agronomy*, 38:1-44.

Bedidi A., Cervelle B., Madeira J. and M. Pouget, 1992, Moisture effects on visible spectral characteristics of lateritic soils. *Soil Science*, 153(2): 129-141.

Beets D.J. and A.J.F. Van Der Spek, 2000, The Holocene evolution of the barrier and the back-barrier basins of Belgium and the Netherlands as a function of late Weichselian morphology, relative sea-level rise and sediment supply. *Geologie en Mijnbouw*, 79 (1): 3-16.

Belpaire A., 1855, *Etude de la formation de la pleine maritime depuis Boulogne jusqu'au Danemark*. Schotmans: Antwerpen (Belgium), 26 pp.

Ben-Dor E. and A. Banin, 1994, Visible and Near-Infrared (0,4-1,1µm) analysis of arid and semiarid soils. *Remote Sensing of Environment*, 48: 261-274.

Ben-Dor E., Goldshleger N., Braun O., Kindel B., Goetz A.F.H., Bonfil D., Margalit N., Binaymini Y., Karnieli A. and M. Agassi, 2004, Monitoring infiltration rates in semiarid soils using airborne hyperspectral technology. *International Journal of Remote Sensing*, 25(13): 2607-2624.

Ben-Dor E., Patkin K., Banin A. and A. Karnieli, 2002, Mapping of several soil properties using DAIS-7915 hyperspectral scanner data - a case study over clayey soils in Israel. *International Journal of Remote Sensing*, 23(6): 1043-1062.

Berk A., Bernstein L.S. and D.C. Robertson, 1989, MODTRAN: A Moderate Resolution Model for LOWTRAN7. Rep. GL-TR-890122, Air Force Geophysics Lab: Bedford-Massachusetts (USA).

Bertels L., 2005, Hyperspectrale remote sensing van vegetatie in dynamische duingebieden. Master's thesis, Open University, The Netherlands.

Bertels L., Deronde B., Kempeneers P., Provoost S. and E. Tortelboom, 2005, Potentials of airborne hyperspectral remote sensing for vegetation mapping of spatially heterogeneous dynamic dunes, a case study along the Belgian coastline. *In*: Herrier J.-L., Mees J., Salman A., Seys J., Van Nieuwenhuyse H. and I. Dobbelaere (Eds.),

Proceedings of 'Dunes and Estuaries' – International Conference on Nature Restoration Practices in European Coastal Habitats, Koksijde (Belgium), 685 pp.

Bird E.C.F., 2000, *Coastal geomorphology, an introduction*. John Wiley & Sons LTD: Chichester (UK), 340 pp.

Bowers S.A. and R.J. Hanks, 1964, Reflection of radiant energy from soils. *Soil Science*, 100(2): 130-138.

Briquet A., 1930, *Le littoral du Nord de la France et son évolution morphologique*. Orléans (France), 439 pp.

Brock J.C., Wright C.W., Sallenger A.H., Krabill W.B. and R.N. Swift, 2002, Basis and methods of NASA airborne topographic mapper LIDAR surveys for coastal studies. *Journal of Coastal Research*, 18(1): 1-13.

Bruce L.M., Roger C.H. and J. Li, 2002, Dimensionality reduction of hyperspectral data using discrete wavelet transform feature extraction. *IEEE Transactions on Geoscience and Remote Sensing*, 40(10): 2331–2338.

Bryant R., Tyler A., Gilvear D., McDonald P., Teasdale I., Brown J. and G. Ferrier, 1996, A preliminary investigation into the spectral characteristics of inter-tidal estuarine sediments. *International Journal of Remote Sensing*, 17(2): 405-412.

Bufton J.L., 1989, Laser altimetry measurements from aircraft and spacecraft. *In*: Proceedings IEEE, 77(3): 463-477.

Burns R.G., 1970, *Mineralogical application to crystal field theory*, Cambridge University Press: Cambridge (UK), 224 pp.

Campbell J.B., 1996, *Introduction to remote sensing* (2nd edition). Taylor & Francis: London (UK), 622 pp.

Chabrillat S., Kaufmann H., Palacios-Orueta A., Escribano P. and A. Mueller, 2004, Development of land degradation spectral indices in a semiarid Mediterranean ecosystem. Proceedings of SPIE, 235-243.

Charlier R.H., Decroo D., De Meyer C.P., and B. Lahousse, 1998, To feed or not to feed, that is often the question. *International Journal of Environmental Studies*, 55: 1-23.

Charlier R.H. and C.P. De Meyer, 1995, New developments on coastal protection along the Belgian coast. *Journal of Coastal Research*, 11(4): 1287-1293.

Charlier R.H. and C.P. De Meyer, 2000, Ask nature to protect and build-up beaches. *Journal of Coastal Research*, 16(2): 385-390.

Chui C.K., 1992, *An Introduction to Wavelets*. Academic Press: San Diego (USA), 266 pp.

Clark R.N., King T.V.V., Klejwa M. and G.A. Swayze, 1990, High spectral resolution reflectance spectroscopy of minerals. *Journal of Geophysical Research*, 95(B8): 12653-12680.

Cocks T., Jenssen R., Stewart A., Wilson I. and T. Shields, 1998, The HyMap Airborne Hyperspectral Sensor: The System, Calibration and Performance. *In:* Schaepman M., Schläpfer D. and K. Itten (Eds.), Proceedings of the 1st EARSeL Workshop on Imaging Spectroscopy, Zurich (Switzerland), 6-8 October 1998.

Coles S.M., 1979, Benthic microalgal populations on intertidal sediments and their role as precursors to saltmarsh development. *In*: Jefferies R.L. and A.J. Davy (Eds.), Ecological processes in coastal environments: The 1st European Ecological Symposium and 19th Symposium of the British Ecological Society, Norwich, 12-16 September 1977, Blackwell: Oxford (UK), 684 pp.

Collins W., Chang S.H., Raines G., Canney F. and R. Ashley, 1983, Airborne biogeochemical mapping of hidden mineral deposits. *Economic Geology*, 78: 737-749.

COMRISK, 2004, Subproject 1: Evaluation of policies and strategies for coastal risk management. Final Report, 111 pp.

Cracknell A.P., 1999, Remote sensing techniques in estuaries and coastal zones - an update. *International Journal of Remote Sensing*, 19(3): 485-496.

Cracknell A.P. and L.W.B. Hayes, 1991, *Introduction to remote sensing*. Taylor & Francis: London (UK), 293 pp.

De Batist M., 1989, Seismo-stratigrafie en struktuur van het Paleogeen in de zuidelijke Noordzee. PhD Thesis, Rijksuniversiteit Gent, Gent (Belgium), 107 pp.

De Batist M., De Bruyne H., Henriet J.P. and F. Mostaert, 1989, Stratigraphic analysis of the Ypresian off the Belgian coast. *In*: Henriet J.P. and G. De Moor (Eds.), *The Quaternary and Tertiary Geology of the southern Bight*, North Sea. Belgian Geological Survey, 75-88.

De Batist M. and J.P. Henriet, 1995, Seismic sequence stratigraphy of the Palaeogene offshore of Belgium, southern North Sea. *Journal of the Geological Society of London*, 152: 27-40.

De Ceunynck R., 1985, The evolution of the coastal dunes in the Western Belgian coastal plain. *Eiszeitalter und Gegenwart*, 35: 33-41.

de Deckere E.M.G.T., Van de Koppel J. and C.H.R. Heip, 2000, The influence of Corophium volutator abundance on resuspension. *Hydrobiologia*, 426: 37-42.

De Moor G, 2006, *Het Vlaamse strand, geomorfologie en dynamiek*. VLIZ: Oostende (Belgium), 154 pp.

De Moor G. and W. De Breuck, 1973, Sedimentology and stratigraphy of Pleistocene deposits in the Belgian coastal plain. *Natuurwetenschappelijk Tijdschr*ift, 55: 3-96.

De Moor G., Mostaert P., Libeer L., Moerdijk F. and V. Van Den Abeele, 1992, Geomorfologische kaart van België. kaartblad Oostende, Nationaal Centrum voor Geomorfologisch Onderzoek.

De Moor G. and A. Pissart, 1992, Het reliëf. *In*: *Geografie van België*, Nationaal Comité voor Geografie, Gemeentekrediet: Brussel (Belgium), 129-215.

De Wolf P., Fransaer D., van Sieleghem J. and R. Houthuys, 1993, Morphological trends of the Belgian coast shown by 10 years of remote sensing based surveying. *In*: Hillen R. and J. Verhagen (Eds.), *Coastlines of the Southern North Sea*. American Society of Civil Engineers: New York (USA), 245-257.

De Wolf P. and R. Houthuys, 1997, Evaluation of a beach nourishment combined with a nearshore feeder berm realized at the Belgian coast. *In:* Proceedings of the Coastal Zone 97 conference, Boston, Massachusetts (USA), 20-26 July.

De Wolf P., Verwaest T., Gysens S., Trouw K., Martens C. and J. De Rouck, 2006, Beach Nourishment at Ostend, Belgium: Design and Monitoring. *In*: Mckee Smith J. (Ed.), Proceedings of the 30th International Conference on Coastal Engineering, San Diego (USA), 5696 pp.

Dean R.G., 2002, *Beach nourishment: theory and practice*. Advanced Series on Ocean Engineering, 18. World Scientific: New Jersey, NJ (USA), 399 pp.

Dekker A.G., Brando V.E., Anstee J.M., Pinnel N., Kutser T., Hoogenboom E.J., Peters S., Pasterkamp R., Vos R., Olbert C. and T.J.M. Malthus, 2001, Imaging spectrometry of Water. *In:* Van der Meer F.D. and S.M. de Jong (Eds.), 2001, *Imaging Spectroscopy: Basic Principles and Prospective Applications*. Kluwer Academic Publishers: Dordrecht (The Netherlands), 307-359.

Depuydt F., 1972, De Belgische strand- en duinformaties in het kader van de geomorfologie der zuidoostelijke Noordzeekust. Verhandelingen van de Kon. Ac. voor Wet., Lett. en Sch. Kunsten van België, Klasse der Wetenschappen, Jg. 34, N° 122, 228 pp.

Deronde B., Houthuys R., Debruyn W., Fransaer D., Van Lancker V. and J.-P. Henriet, 2006a, Using airborne hyperspectral data and laserscan data to study beach morphodynamics along the Belgian coast. *Journal of Coastal Research*, 22(5): 1108-1118.

Deronde B., Houthuys R., Henriet J.-P. and V. Van Lancker, in press, Monitoring of the sediment dynamics along a sandy shoreline by means of airborne hyperspectral remote sensing and LIDAR, a case study in Belgium. *Earth Surface Processes and Landforms*.

Deronde B., Houthuys R., Sterckx S., Debruyn W. and D. Fransaer, 2004, Sand dynamics along the Belgian coast based on airborne hyperspectral data and LIDAR data. *EARSel eProceedings*, 3(1).

Deronde B., Kempeneers P., Forster R.M. and W. Debruyn, 2006b, Imaging spectroscopy as a tool to study sediment characteristics on a tidal sand bank in the Westerschelde. *Estuarine Coastal and Shelf Science*, 69(3-4): 580-590.

Deronde B., Kempeneers P., Houthuys R., Henriet J.-P. and V. Van Lancker, submitted, Classification of a sandy shoreline by means of airborne imaging spectroscopy. *International Journal of Remote Sensing*.

Dubois G., 1924, *Recherches sur les terrains quaternaires du Nord de la France*. Mémoires de la Société Géologique du Nord, VIII, 356 pp.

Duda R.O., Hart P.E. and D.G. Stork, 2001, *Pattern classification* (2nd edition). Wiley: New York (USA), 654 pp.

Eisma D., 1980, *De Noordzee*. Spectrum: Utrecht (The Netherlands), 128 pp.

Eisma D., Jansen J.H.F. and T.C.E. Van Weering, 1979, Sea-floor morphology and recent sediment movement in the North Sea. *In*: Oele E., Schüttenhelm R.T.E. and A.J. Wiggers (Eds.), *The Quaternary history of the North Sea*, ActaUniv. Ups. Symp. Univ. Ups. Annum Quingentesimum Celebrantis, Uppsala (Sweden), 217-232.

Eleveld M.A., 1999, Exploring coastal morphodynamics of Ameland (the Netherlands) with remote sensing monitoring techniques and dynamic modelling in GIS. PhD thesis, Universiteit van Amsterdam, ITC Publication N° 70, 225 pp.

Eleveld M.A., Blok S.T. and J.P.G. Bakx, 2000, Deriving relief of a coastal landscape with aerial video camera. *International Journal of Remote Sensing*, 21(1) : 189-195.

Esteves L.S. and C.W. Finkl, 1998, The problem of Critically Eroded Areas (CEA): an evaluation of Florida beaches. *Journal of Coastal Research*, 26: 11-18.

Fisher R., 1936, The use of multiple measures in taxonomic problems. *Annals of Eugenics*, 7: 179-188.

Ford R.B. and C. Honeywill, 2002, Grazing on intertidal microphytobenthos by macrofauna: is pheophorbide a useful marker?. *Marine Ecology-Progress Series*, 229: 33-42.

Forster R.M. and J.C. Kromkamp, 2004. Modelling the effects of chlorophyll fluorescence from subsurface layers on photosynthetic efficiency measurements in microphytobenthic algae. *Marine Ecology-Progress Series*, 284: 9-22.

Gares P.A., Wang Y. and S.A. White, 2006, Using LIDAR to monitor a beach nourishment project at Wrightsville beach, North Carolina, USA. *Journal of Coastal Research*, 22(5): 1206-1219.

Goetz A.F.H., 1992a, Imaging spectroscopy for earth remote sensing. *In:* F. Toselli & J. Bodechtel (Eds.), *Imaging Spectroscopy: Fundamentals and Prospective Applications*. Kluwer Academic Publishers: Dordrecht (The Netherlands), 1-19.

Goetz A.F.H., 1992b, Principles of narrow band spectrometry in the visible and IR: instruments and data analysis. *In:* F. Toselli & J. Bodechtel (Eds.), *Imaging Spectroscopy: Fundamentals and Prospective Applications*. Kluwer Academic Publishers: Dordrecht (The Netherlands), 21-32.

Goetz A.F.H. and C.O. Davis, 1991, The high resolution imaging spectrometer (HIRIS): science and instrument. *Journal of Imaging Systems and Technology*, 3: 131-143.

Goetz A.F.H., Rowan L.C. and M.J. Kingston, 1982, Mineral identification from orbit: Initial results from the Shuttle Multispectral Infrared Radiometer. *Science*, 218, 1020.

Goldshleger N., Ben-Dor E., Benyamini Y., Blumberg D. and M. Agassi, 2002, Spectral properties and hydraulic conductance of soil crusts formed by raindrop impact. *International Journal of Remote Sensing*, 23(19): 3909-3920.

Halet F., 1931, Contribution à l'étude du Quaternaire de la pleine maritime Belge. *Bulletin de la Société Belge de Géologie*, 41: 141-166.

Henriet J.-P., De Batist M., De Bruyne H., Heldens P., Huylebroek J.P., Mostaert F., Sevens E., Auffret J.P. and B. D'Olier, 1989a, Preliminary seismic-stratigraphic maps and type sections of the Palaeogene deposits in the southern Bight of the North Sea. *In*: Henriet J.-P. and G. De Moor (Eds.), *The Quaternary and Tertiary Geology of the southern Bight*, North Sea. Belgian Geological Survey, 29-44.

Henriet J.-P., De Batist M., D'Olier B. and J.P. Auffret, 1989b, A Northeast trending structural deformation zone near North Hinder. *In*: Henriet J.-P. and G. De Moor (Eds.), *The Quaternary and Tertiary Geology of the southern Bight, North Sea*. Belgian Geological Survey, 9-16.

Hillen R. and H.J.Verhagen, 1993, *Coastlines of the Southern North Sea*. *In:* Magoon, O.T. (Ed.), Coastlines of the World. American Society of Civil Engineers: New York (USA), 363 pp.

Hong S.K., Kim S., Cho K.H., Kim J.E., Kang S. and D. Lee, 2004, Ecotope mapping for landscape ecological assessment of habitat and ecosystem. *Ecological Research*, 19(1): 130-139.

Houbolt J.J.H.C, 1968, Recent sediments in the southern Bight of the North Sea. *Geologie en Mijnbouw*, 47: 245-273.

Houthuys R, De Moor G and J. Somme, 1993, The shaping of the French-Belgian North Sea Coast throughout recent geology and history. *In*: Hillen R. and J. Verhagen (Eds.), *Coastlines of the Southern North Sea*, American Society of Civil Engineers: New York (USA), 27-40.

Hunt G.R., 1977, Spectral signatures of particulate minerals in the visible and near-infrared. *Geophysics*, 42: 501-513.

Hunt G.R., 1980, Electromagnetic radiation: the communication link in remote sensing. *In*: Siegal B.S. and A.R. Gillespie (Eds.), *Remote Sensing in Geology*. John Wiley: New York (USA), 5-45.

Hunt G.R. and J.W. Salisbury, 1970, Visible and near infrared spectra of minerals and rocks, I. Silicate minerals. *Modern Geology*, 1: 283-300.

Huygens M., 2001, Een geïntegreerd onderzoek van zandsuppleties als kustverdediging – toepassing voor de Belgische Oostkust. PhD Thesis, Universiteit Gent, Gent (Belgium).

Inman D.L., 1952, Measures for describing the size distribution of sediments. *Journal of Sedimentary Petrology*, 22(3): 125-245.

IPCC, 2001, *Climate Change 2001: Synthesis Report*. IPCC, Geneva (Switzerland), 397 pp.

Jenkins R., 1999, *X-ray Fluorescence Spectroscopy* (2nd edition). John Wiley: Chichester (UK), 207 pp.

Jensen J.R. and F. Qiu, 2001, A neural network image interpretation system to extract rural and urban land use and land cover information from remote sensor data. *Geocarto International*, 16: 1-10.

Johnson S.C., 1967, Hierarchical clustering schemes. *Psychometrika*, 2: 241-254.

Kalayeh H.M., Muasher M.J. and D.A. Landgrebe, 1983, Feature selection with limited training samples. *IEEE Transactions on Geoscience and Remote Sensing*, 21(4): 434-438.

Kelleher G., 1999, *Guidelines for Marine Protected Areas*. IUCN, Gland (Switzerland), 107 pp.

Kempeneers P., 2007, Information extraction from hyperspectral data – Applied to vegetation. PhD Thesis, Universiteit Antwerpen, Antwerpen (Belgium), 152 pp.

Kempeneers P., De Backer S., Debruyn W., Coppin P. and P. Scheunders, 2005a, Generic Wavelet-Based Hyperspectral Classification Applied to Vegetation Stress Detection. *IEEE Transactions on Geoscience and Remote Sensing*, 43: 610-614.

Kempeneers P., De Backer S., Deronde B., Bertels L., Provoost S., Debruyn W. and P. Scheunders, 2005b, Coupling posterior probabilities for classification and unmixing of vegetation along the Belgian coastline. *In:* Proceedings of the SPIE conference, Bruges (Belgium).

Kempeneers P., De Backer S., Provoost S., Debruyn W. and P. Scheunders, 2005c, Hyperspectral classification applied to the Belgian coastline. *In:* Proceedings of the SPIE International Symposium on Remote Sensing, 144-152.

Kempeneers P., Deronde B., Bertels L., Debruyn W., De Backer S. and P. Scheunders, 2004, Classifying hyperspectral airborne imagery for vegetation survey along coastlines. *In*: Proceedings of the International Geoscience and Remote Sensing Symposium (IGARSS), Anchorage, Alaska (USA).

Kempeneers P., Provoost S., De Backer S., Van Gompel W., Deronde B. and P. Scheunders, in press, Surveillance of dune vegetation along the Belgian coast using Hyperspectral Remote Sensing. *International Journal of Remote Sensing*.

Kidner D.B., Thomas M., Leigh C., Oliver J.R. and C.G. Morgan, 2004, Coastal monitoring with LIDAR: challenges, problems and pitfalls. *In:* Proceedings of the SPIE conference Remote Sensing for Environmental Monitoring, GIS Applications and Geology IV, vol. 5574: 80-89.

Kohavi R. and F. Provost, 1998, Special Issue on Applications of Machine Learning and the Knowledge Discovery Process. *Machine Learning*, 271-274.

Köhn W., 1989, The Holocene transgression of the North Sea as exemplified by the southern Jade bay and the Belgian coastline. *Essener geographische Arbeiten*, 17: 109-152.

Krumbein W.C., 1936, Application of logarithmic moments to size frequency distribution of sediments. *Journal of Sedimentary Petrology*, 6(1): 35-47.

Kruse F.A., Boardman J.W., Lefkoff A.B., Young J.M., Kierein-Young K.S., Cocks T.D., Jenssen R. and P.A. Cocks, 2000, HyMap: An Australian Hyperspectral Sensor Solving Global Problems – Results from USA HyMap Data Acquisitions. *In:* Proceedings of the 10th Australasian Remote Sensing and Photogrammetry Conference, Adelaide (Australia), 21-25 August 2000.

Kruse F.A., Keirein-Young K.S. and J.W. Boardman, 1990, Mineral mapping at Cuprite, Nevada with a 63-channel Imaging Spectrometer. *Photogrammetric Engineering and Remote Sensing*, 56: 83-92.

Laga P., Louwye S. and S. Geets, 2001, Palaeogene and Neogene lithostratigraphic units (Belgium). *In*: Bultynck P. and L. Dejonghe (Eds.), Lithostratigraphic scale of Belgium. *Geologica Belgica*, Special Issue, 135-152.

Landgrebe D.A., 2003, *Signal theory methods in multispectral remote sensing*. Wiley: New Yersey (USA), 508 pp.

Le Bot S., Van Lancker V., Deleu S., De Batist M. and J.-P. Henriet, 2003, Tertiary and Quaternary geology of the Belgian continental shelf. Scientific Report of SPSD II, Belgian Science Policy, 75 pp.

Lee D.S. and J. Shan, 2003, Combining LIDAR Elevation Data and IKONOS Multispectral Imagery for Coastal Classification Mapping. *Marine Geodesy*, 26: 117-127.

Leu D.J.,1977, Visible and Near-Infrared reflectance of beach sands: a study on the spectral reflectance / grain size relationship. *Remote Sensing of Environment*, 6: 169-182.

Loeppert R.H. and D.L. Suarez, 1996, Carbonate and gypsum. *In*: Sparks D.L. *et al.* (Ed.), *Methods of soil analysis: Part 3—Chemical methods*. SSSA Book Ser. No. 5: 437–475. SSSA and ASA: Madison, WI (USA).

Malthus T.J. and P.J. Mumby, 2003, Remote sensing of the coastal zone: an overview and priorities for future research. *International Journal of Remote Sensing*, 24(13): 2805-2815.

Maréchal R., 1992, De geologische structuur. *In*: *Geografie van België*. Nationaal Comité voor Geografie, Gemeentekrediet: Brussel (Belgium), 37-86.

McCloy K.R., 2006, *Resource management Information Systems: Remote Sensing, GIS and Modelling* (2nd edition), Taylor & Francis: New York (USA), 575 pp.

McLachlan A., Jaramillo E., Donn T.E. and F. Wessels, 1993, Sand beach macrofauna communities: a geographical comparison. *Journal of Coastal Research*, 15: 27-38.

Meire P., Ysebaert T., Van Damme S., Van den Bergh E., Maris T. and E. Struyf, 2005, The Scheldt estuary: a description of a changing ecosystem. *Hydrobiologia*, 540: 1-11.

Mills E., 2005, Insurers in a climate of change. *Science*, 308: 1040-1044.

Mitchum R.M.J., Vail P.R. and J.B. Sangree, 1977, Stratigraphic interpretations of seismic reflection patterns in depositional sequences. *In*: C.E. Payton, Seismic stratigraphy – Application to hydrocarbon exploration, 26. American Association of Petroleum Geologists, Memoir, 117-134.

Mostaert F., 1985, Bijdrage tot de kennis van de Kwartairgeologie van de oostelijke kustvlakte op basis van sedimentologisch lithostratigrafisch onderzoek. PhD thesis, Universiteit Gent, Gent (Belgium), 588 pp.

Motyka J.M. and A.H. Brampton, 1993, Coastal management, mapping of littoral cells. Unpublished report to the Ministry of Agriculture, Fisheries and Food, Report N° SR 328.

Müller R., Lehner M., Reinartz P., Schroeder M. and B. Vollmer, 2002, A program for direct georeferencing of airborne and spaceborne line scanner images. *In:* Proceeedings of the ISPRS symposium on Integrated Remote Sensing at the Global, Regional and Local Scale, Denver (USA).

Mumby P.J. and A.J. Edwards, 2002, Mapping marine environments with IKONOS imagery: enhanced spatial resolution can deliver greater thematic accuracy. *Remote Sensing of Environment*, 82: 248-257.

Mumby P.J., Chisholm J.R.M., Clark C.D., Hedley J.D. and J. Jaubert, 2001, A bird's-eye view of the health of coral reefs. *Nature*, 481: 36-36.

Myers J.S. and R.L. Miller, 2005, Optical airborne remote sensing. *In*: Miller *et al*. (Eds.), 2005, *Remote Sensing of Coastal Aquatic Environments*, 51-67.

Nederbragt G. and G.A. Liek, 2004, Beschrijving zandbalans Westerschelde en monding. Rapport RIKZ/2004.020. Rijkswaterstaat, Rijksinstituut voor Kust en Zee/RIKZ.

Okin G.S., Roberts D.A., Murray B. and W.J. Okin, 2001, Practical limits on hyperspectral vegetation discrimination in arid and semiarid environments. *Remote Sensing of Environment*, 77: 212-225.

O'Neill M. and S.L. Ustin, 2000, Mapping the distribution of leafy spurge at Theodore Roosevelt National Park using AVIRIS. *In:* Proceedings of the ninth JPL airborne earth science workshop, 339-343.

Peterson C.H., Hickerson D.H.M. and G.G. Johnson, 2000, Short-term consequences of nourishment and bulldozing on the dominant large invertebrates of a sandy beach. *Journal of Coastal Research*, 16(2): 368-378.

Peterson D.L., Brass J.A., Smith W.H., Langford G., Wegener S., Dunagan S., Hammer P. and K. Snook, 2003, Platform options of free flying satellites, UAVs or the

international space station for remote sensing assessment of the littoral zone. *International Journal of Remote Sensing*, 24(13): 2785-2804.

Post J.C. and C.G. Lundin (Eds.), 1996, *Guidelines for integrated coastal zone management*. Environmentally Sustainable Development Studies and Monograph Series, N° 9, World Bank, Washington DC (USA), 16 pp.

Provoost S., van Til M., Deronde B. and A. Knotters, 2005, Remote sensing of coastal vegetation in The Netherlands and Belgium. *In*: Herrier J.-L., Mees J., Salman A., Seys J., Van Nieuwenhuyse H. and I. Dobbelaere (Eds.), Proceedings of 'Dunes and Estuaries' – International Conference on Nature Restoration Practices in European Coastal Habitats, Koksijde (Belgium), 685 pp.

Pudil P., Novovièová J., and J. Kittler, 1994, Floating search methods in feature selection. *Pattern Recognition Letters*, 15(1): 1119–1125.

Rainey M.P., Tyler A.N., Bryant R.G., Gilvear D.J. and P. McDonald, 2000, The influence of surface and interstitial moisture on the spectral characteristics of intertidal sediments: implications for airborne image acquisition and processing. *International Journal of Remote Sensing*, 21(16): 3025-3038.

Rainey M.P., Tyler A.N., Gilvear D.J., Bryant R.G. and P. Mcdonald, 2003, Mapping intertidal estuarine sediment grain size distributions through airborne remote sensing. *Remote Sensing of Environment*, 86: 480-490.

Read R. and R. Graham, 2002, *Manual of Aerial Survey: Primary Data cquisition*. Whittles Publishing: Boca Raton (USA), 408 pp.

Rees W.G., 2001, *Physical principles of remote sensing* (2nd edition). Cambridge University Press: Cambridge (UK), 343 pp.

Revell D.L., Komar P.D. and A.H. Sallenger, 2002, An application of LIDAR to analyses of El Niño erosion in the Netarts littoral cell, Oregon. *Journal of Coastal Research*, 18(4): 792-801.

Richter R. and D. Schläpfer, 2002, Geo-atmospheric processing of airborne imaging spectrometry data. Part 2: Atmospheric/Topographic Correction. *International Journal of Remote Sensing*, 23(13): 2631-2649.

Rottier H. and H. Arnoldus, 1984. *De Vlaamse kustvlakte van Calais tot Saeftinge*. Lannoo: Tielt (Belgium), 208 pp.

Rutot A., 1897, Les origines du Quaternaire de la Belgique. *Bulletin de la Société Belge de Géologie*, 11, 140 pp.

Sallenger A.H., Krabill W.B., Swift R.N., Arens J., List J.H., Hansen M., Holman R.A., Manizade S., Sontag J., Meredith A., Morgan K., Yunkel J.K., Frederick E.B.

and H. Stockdon, 2003, Evaluation of airborne topographic LIDAR for quantifying beach changes. *Journal of Coastal research* 19(1): 125-133.

Scholte K.H., 2005, Hyperspectral remote sensing and mud volcanism in Azerbaijan. PhD Thesis, Technische Universiteit Delft, Delft (The Netherlands), 147 pp.

Short A.D. (Ed.), 2001, *Handbook of beach and shoreface morphodynamics*. Wiley and Sons: Chichester (UK), 379 pp.

Smith G., Thomson A., Möller I. and J. Kromkamp, 2003, Hyperspectral imaging for mapping sediment characteristics. *In*: Proceedings of the third EARSeL workshop on imaging spectroscopy, Herrsching (Germany), 13-16 may 2003.

Sommé J., 1988, La plaine maritime Française de la mer du Nord: Evolution holocène et héritage pléistocène. *In*: *Campagnes et littoraux d'Europe*, Mélanges P. Flatrès, Hommes et Terre du Nord, Lille (France), 273-281.

Speybroeck J., Bonte D., Courtens W., Gheskiere T., Grootaert P., Maelfait J.P., Mathys M., Provoost S., Sabbe K., Stienen E.W.M., Van Lancker V., Vincx M. and S. Degraer, 2006, Beach nourishment: an ecologically sound coastal defence alternative? A review. *Aquatic Conservation: Marine and Freshwater Ecosystems*, 16(4): 419-435.

Stephens F.C., Louchard E.M., Reid R.P. and R.A. Maffione, 2003, Effects of microalgal communities on reflectance spectra of carbonate sediments in subtidal optically shallow marine environments. *Limnology and Oceanography*, 48(1, part2): 535-546.

Stevens T. and R.M. Connolly, 2004, Testing the utility of abiotic surrogates for marine habitat mapping at scales relevant to management. *Biological Conservation*, 119: 351-362.

Stockdon H.F., Sallenger A.H., List J.H. and R.A. Holman, 2002, Estimation of shoreline position and change using airborne topographic LIDAR data. *Journal of Coastal Research*, 18(2): 502-513.

Su J. and E. Bork, 2006, Influence of vegetation, slope, and LIDAR sampling angle on DEM accuracy. *Photogrammetric Engineering & Remote Sensing*, 72(11): 1265-1274.

Tavernier R., 1947, L'évolution de la plaine maritime belge, *Bulletin de la Société Belge de Géologie*, 56: 332-343.

Tavernier R., Ameryckx J., Snacken F. and D. Farasyn, 1970, *Kust, duinen, polders*. Brussel, Nationaal Comité voor Geografie, Atlas van België, Blad 17, 32 pp.

Tavernier R. and F. Moorman, 1954, Les changements du niveau de la mer dans la plaine maritime Flamande pendant l'Holocène. *Geologie en Mijnbouw*, 16: 201-206.

Thiemann S. and H. Kaufmann, 2002, Lake water quality monitoring using hyperspectral airborne data - a semi-empirical multisensor and multitemporal approach for the Mecklenburg Lake District, Germany. *Remote Sensing of Environment*, 81: 228-237.

Thomson A.G., Fuller R.M., Sparks T.H., Yates M.G. and J.A. Eastwood, 1998, Ground and airborne radiometry over intertidal surfaces: waveband selection for cover classification. *International Journal of Remote Sensing*, 19(6): 1189-1205.

Tolhurst T.J., Jesus B., Brotas V. and D.M. Paterson, 2003, Diatom migration and sediment armouring - an example from the Tagus Estuary, Portugal. *Hydrobiologia*, 503: 183-193.

Toselli F. and J. Bodechtel (Eds.), 1992, *Imaging Spectroscopy: Fundamentals and Prospective applications*. Kluwer Academic Publishers: Dordrecht (The Netherlands), 266 pp.

Van der Meer F.D. and S.M. de Jong (Eds.), 2001, *Imaging Spectroscopy: Basic Principles and Prospective Applications*. Kluwer Academic Publishers: Dordrecht (The Netherlands), 403 pp.

Van der Meer F.D., Yang H., Kroonenberg S., Lang H., Van Dijk P., Scholte K. and H. Van Der Werff, 2001, Imaging spectroscopy and petroleum geology. *In:* Van der Meer F.D. and S.M. de Jong (Eds.), 2001, *Imaging Spectroscopy: Basic Principles and Prospective Applications*. Kluwer Academic Publishers: Dordrecht (The Netherlands), 219-241.

van der Wal D., 1998, The impact of the grain-size distribution of nourishment sand on aeolian sand transport. *Journal of Coastal Research*, 14(2): 620-631.

van der Wal D., 2000a, Grain-size-selective aeolian sand transport on a nourished beach. *Journal of Coastal Research*, 16(3): 896-908.

van der Wal D., 2000b, Modelling aeolian sand transport and morphological development in two beach nourishment areas. *Earth Surface Processes and Landforms*, 25: 77-92.

Van Lancker V.R.M., Moerkerke G., Vanstaen K., Degraer S. and G. Van Hoey, 2003, Development of a multidisciplinary side-scan sonar-based environmental assessment tool applicable for shallow marine waters. *In*: Proceedings of the International Conference on Coastal Sediments 2003, Corpus Christi, Texas(USA), 1-10.

Van Lancker V., 1999, Sediment and morphodynamics of a siliciclastic near coastal area, in relation to hydrodynamical and meteorological conditions: Belgian Continental Shelf. PhD Thesis, Universiteit Gent, Gent (Belgium), 194 pp.

Van Staalduinen C.J., 1979, Toelichtingen bij de geologische kaart van Nederland 1:50.000, blad Rotterdam West (37 W), Haarlem (The Netherlands).

Van Zuidam R.A., Farifteh J., Eleveld M.A. and T. Cheng, 1998, Developments in remote sensing, dynamic modelling and GIS applications for integrated coastal zone management. *Journal of Coastal Conservation*, 4: 191-202.

Vanderstraete T., 2007, The use of remote sensing for coral reef mapping in support of integrated coastal zone management – A case study in the NW Red Sea. PhD Thesis, Universiteit Gent, Gent (Belgium), 426 pp.

Verhulst A., 1959, Historische geografie van de Vlaamse kustvlakte tot 1200. *In*: *Bijdragen tot de geschiedenis der Nederlanden*, 14, 's Gravenhage (The Netherlands), 27 pp.

Verwaest T., Viaene P., Verstraeten J. and F. Mostaert, 2005, De zeespiegelstijging meten, begrijpen en afblokken. *De Grote Rede*, 15:15-25.

Waterbouwkundig Laboratorium, 2006, Oostkust-Baai van Heist, Langjarige Sedimentatie, Project N° 005_0139, 23 pp.

Wehr A. and U. Lohr, 1999, Airborne laser scanning – An introduction and overview. *ISPRS Journal of Photogrammetry and Remote Sensing*, 54: 68-82.

Wentworth C.K., 1922, A scale of grade and class terms for clastic sediments. *Journal of Geology*, 30: 377-392.

White S.A. and Y. Wang, 2003, Utilizing DEM's derived from LIDAR data to analyze morphologic change in the North Carolina coastline. *Remote Sensing of Environment*, 85: 39-47.

Wright L.D. and B.G. Thom, 1977, Coastal depositional landforms, a morphodynamic approach. *Progress in physical geography*, 1: 412-459.

Wright S.W., Jeffrey S.W., Mantoura R.F.C., Llewellyn C.A., Bjornland T., Repeat D. and N. Welshmeyer, 1991, Improved HPLC method for the analysis of chlorophylls and carotenoids from marine phytoplankton. *Marine Ecology Progress Series*, 77: 183-196.

Wulder M.A., Hall R.J., Coops N.C. and S.E. Franklin, 2004, High spatial resolution remotely sensed data for ecosystem characterization. *BioScience*, 54: 511-521.

Yates M.G., Jones A.R., Mcgrorty S. and J.D. Goss-Custard, 1993, The use of satellite imagery to determine the distribution of inter-tidal surface sediments of the Wash, England. *Estuarine Coastal and Shelf Science*, 36: 333-344.

Ysebaert T., Meire P., Herman P.M.J. and H. Verbeek, 2002, Macrobenthic species response surfaces along estuarine gradients: prediction by logistic regression. *Marine Ecology-Progress Series*, 225: 79-95.

Zapata M., Jeffrey S.W., Wright S.W., Rodriguez F., Garrido J.L. and L. Clementson, 2004, Photosynthetic pigments in 37 species (65 strains) of Haptophyta: implications for oceanography and chemotaxonomy. *Marine Ecology-Progress Series*, 270: 83-102.

List of publications

Peer reviewed publications

Bertels L., Vanderstraete T., Van Coillie S., Knaeps E., Sterckx S., Goossens R. and **B. Deronde**, in press, Mapping of coral reefs using hyperspectral CASI data; A case study: Fordata, Tanimbar, Indonesia. *International Journal of Remote Sensing*.

Deronde B., Houthuys R., Debruyn W., Fransaer D., Van Lancker V. and J.-P. Henriet, 2006a, Using airborne hyperspectral data and laserscan data to study beach morphodynamics along the Belgian coast. *Journal of Coastal Research*, 22(5): 1108-1118.

Deronde B., Houthuys R., Henriet J.-P. and V. Van Lancker, in press, Monitoring of the sediment dynamics along a sandy shoreline by means of airborne hyperspectral remote sensing and LIDAR, a case study in Belgium. *Earth Surface Processes and Landforms*.

Deronde B., Houthuys R., Sterckx S., Debruyn W. and D. Fransaer, 2004, Sand dynamics along the Belgian coast based on airborne hyperspectral data and LIDAR data. *EARSel eProceedings*, 3(1): 26-33.

Deronde B., Kempeneers P., Forster R.M. and W. Debruyn, 2006b, Imaging spectroscopy as a tool to study sediment characteristics on a tidal sand bank in the Westerschelde. *Estuarine Coastal and Shelf Science*, 69(3-4): 580-590.

Deronde B., Kempeneers P., Houthuys R., Henriet J.-P. and V. Van Lancker, in press, Classification of a sandy shoreline by means of airborne imaging spectroscopy. *International Journal of Remote Sensing*.

Deronde B., Sterckx S., Bertels L., Knaeps E. and P. Kempeneers, 2006, Imaging spectroscopy and integrated coastal zone management, a promising marriage. *In*: Brebbia C.A. (Ed.), Proceedings of the Wessex Coastal Environment 2006 workshop, Rhodos, Greece, 470 pp.

Kempeneers P., Provoost S., De Backer S., Van Gompel W., **Deronde B**. and P. Scheunders, in press, Surveillance of dune vegetation along the Belgian coast using Hyperspectral Remote Sensing. *International Journal of remote Sensing*.

Proceedings

Bertels L., **Deronde B**., Kempeneers P., Provoost S. and E. Tortelboom, 2005, Potentials of airborne hyperspectral remote sensing for vegetation mapping of spatially heterogeneous dynamic dunes, a case study along the Belgian coastline. *In*: Herrier J.-L., Mees J., Salman A., Seys J., Van Nieuwenhuyse H. and I. Dobbelaere (Eds.), Proceedings of 'Dunes and Estuaries' – International Conference on Nature Restoration Practices in European Coastal Habitats, Koksijde (Belgium), 685 pp.

Biesemans J., Sterckx S., Knaeps E., Vreys K., Adriaensen S., Hooyberghs J., Meuleman K., Kempeneers P., **Deronde B**., Everaerts J., Schläpfer D., and J. Nieke, 2007, Image processing workflows for airborne remote sensing. *In*: Proceedings 5th Earsel workshop on imaging spectroscopy, Bruges - Belgium, 23-25 April 2007.

Debruyn W., Reusen I., Kempeneers P. and **B. Deronde**, 2003, The Airborne Imaging Spectrometer APEX (Airborne Prism EXperiment): Overview and Status Questions. *In*: Proceedings of the EARSel General Assembly, Ghent (Belgium).

Eerens, H., **Deronde B**., Van Rensbergen J., and M. Badji, 2000, A new vegetation map of Central Africa, Update of the JRC-TREES map of 1992 with SPOT-VEGETATION imagery of 1998. *In*: Proceedings of the VEGETATION-2000 conference JRC, Ispra (Italy).

Kempeneers P., De Backer S., **Deronde B**., Bertels L., Provoost S., Debruyn W. and P. Scheunders, 2005, Coupling posterior probabilities for classification and unmixing of vegetation along the Belgian coastline. *In*: Proceedings of the SPIE conference, Bruges (Belgium).

Kempeneers P., **Deronde B**., Bertels L., Debruyn W., De Backer S. and P. Scheunders, 2004, Classifying hyperspectral airborne imagery for vegetation survey along

coastlines. *In*: Proceedings of the International Geoscience and Remote Sensing Symposium (Igarss), Anchorage, Alaska (USA).

Provoost .S, van Til M., **Deronde B**. and A. Knotters, 2005, Remote sensing of coastal vegetation in The Netherlands and Belgium. *In*: Herrier J.-L., Mees J., Salman A., Seys J., Van Nieuwenhuyse H. and I. Dobbelaere (Eds.), Proceedings of 'Dunes and Estuaries' – International Conference on Nature Restoration Practices in European Coastal Habitats, Koksijde (Belgium), 685 pp.

Reusen I., Bertels L., Debruyn W., **Deronde B**., Fransaer D. and S. Sterckx, 2003, Species Identification and Stress Detection of Heavy-Metal Contaminated Trees. *In*: Proceedings of the 'Spectral Remote Sensing of Vegetation" conference, Las Vegas, Nevada (USA).

Other

Deronde B., Houthuys R. and P. De Wolf, 2007, Het zandtransport langs de Vlaamse kust, opgevolgd vanuit de lucht. *De Grote Rede*, 19: 7-12.